

A Bird's-Eye View
on
Evolution of Seasonal Migration

Dissertation

in fulfillment of the requirements for the degree
Doctor rerum naturalium
of the Faculty of Mathematics and Natural Sciences
at the Christian Albrechts University of Kiel

Submitted by
Jun Ishigohoka

Max Planck Institute for Evolutionary Biology
Plön, Germany
May 2024

First referee:	Prof Dr Miriam Liedvogel
Second referee:	Prof Dr Hinrich Schulenburg
Examiner:	Prof Dr Julien Yann Dutheil
Chairperson:	Prof Dr Frank Kempken
Date of oral examination:	2024-06-07 (Fri)

Summary

What makes animals special is that they can actively move at a geographic scale, which allows them to relocate themselves from an adverse environment to other places in more favourable conditions to survive and reproduce. Seasonal migration is a type of animal movement typically between breeding and wintering sites with regularity in timing and orientation. Seasonal migration is both ecologically and evolutionarily important, because it is a behavioural adaptation to seasonal changes in environment, and it defines the distribution of animals when they mate and reproduce. Since the dawn of ethology, mechanism, development, ecological function and evolution of seasonal migration have been heavily studied in birds.

In this thesis, I address how seasonal migration evolves at a microevolutionary time scale. To this end, I study the Eurasian blackcap *Sylvia atricapilla*, or “blackcap”. Blackcaps are a common songbird species breeding widely in Europe and north Africa, ranging from Iberia to Caucasus and Scandinavia, as well as on Macaronesian and Mediterranean islands. The blackcap is a perfect species to study microevolution of migration because they have heritable variation in population-typical migratory behaviour in propensity, distance, orientation and timing. Using population genomics and epigenomics, I investigate the evolutionary history and molecular mechanisms of diversification of seasonal migration.

The aims of application of population genomics on the blackcap system are to identify possible genomic targets of selection associated with divergence of migratory behaviour and to understand the history of populations with different migratory phenotypes. I start with assessing the effects of recombination rate, instead of selection and true demographic events, on these two types of population genomics analyses using simulation and empirical analysis on blackcap genomes. I find that genomic regions with low recombination rates tend to have distinct patterns of genetic variation because the variance in underlying genetic ancestry reduces, instead of by selective processes. I also find that the presence of high-recombining genomic regions affects demography inference using methods based on the ancestral recombination graph, a structure representing genetic ancestries along recombining chromosomes, because underlying genealogies are not represented by sufficiently many mutations in high-recombining regions.

Through empirical validation of genome scans and demography inference using blackcap genome data, I found one polymorphic inversion with a gradient in frequency among populations with different migratory phenotypes and between continent and islands, which is unlikely to happen neutrally under the estimated demography of blackcap populations. By comparing population genetic simulations under the blackcap demography and the observed inversion frequencies, I find that the inversion is under negative frequency-dependent selection with different optimal inversion frequencies between continent and island.

I also determined how blackcap populations split in history. I find that the blackcap populations split in two phases. An ancestral migrant population split into Caucasus (eastern) and western refugia populations during one of the Pleistocene glacial cycles. The population expanded and split after the last glacial maximum, and there were at least four independent transition events from migrants to residents.

Focusing on one pair of migrant and resident populations, I investigate differential

epigenetic regulation between seasons and populations in the hypothalamus, a strong candidate brain region underlying the evolutionary transition. By combining a common garden experiment and quantification of single cell chromatin accessibility, I find that the amount of seasonal change in chromatin accessibility is reduced in some genomic regions in residents compared to migrants.

Finally, I synthesise the population genomic and single cell epigenomic insights in the light of phylogeography and evolution of phenotypic plasticity. This thesis therefore provides a step forward to the holistic understanding of how animal behaviour may evolve by historic changes in environment via modification of differential epigenetic regulation.

Zusammenfassung

Eine Besonderheit von Tieren ist, dass sie sich aktiv auf einer großflächigen geografischen Skala bewegen können. Dies ermöglicht es ihnen, sich aus einer ungünstigen Umgebung an andere Orte mit günstigeren Bedingungen zu begeben, um zu überleben und sich fortzupflanzen. Dieses saisonale Wander- oder Zugverhalten (Migration) ist eine Art der Tierbewegung, die typischerweise zwischen Brut- und Überwinterungsgebieten mit einer gewissen Regelmäßigkeit in Bezug auf Zeitpunkt und Ausrichtung stattfindet. Saisonale Wanderungen sind sowohl ökologisch als auch evolutionär sehr bedeutsam, da sie eine Verhaltensanpassung an die jahreszeitlichen Veränderungen der Umwelt darstellen und die Verteilung der Tiere bei der Paarung und Fortpflanzung bestimmen. Seit den Anfängen der Verhaltensforschung wurden Mechanismus, Entwicklung, ökologische Funktion und Evolution der saisonalen Migration bei Vögeln eingehend untersucht.

In dieser Arbeit befasse ich mich mit der Frage, wie sich saisonales Zugverhalten auf einer mikroevolutionären Zeitskala entwickeln kann. Meine Untersuchungen fokussieren sich hierbei auf die Eurasische Mönchsgrasmücke *Sylvia atricapilla*. Die Mönchsgrasmücke ist eine in Europa und Nordafrika weit verbreitete Singvogelart, deren Brutgebiet sich von der Iberischen Halbinsel über den Kaukasus und Skandinavien bis hin zu den makaronesischen und mediterranen Inseln erstreckt. Die Mönchsgrasmücke ist eine ideale Art, um die Mikroevolution des Zugverhaltens zu untersuchen, da sie entlang ihres Verbreitungsgebietes eine vererbte Variation im populations-typischen Zugverhalten in Bezug auf Zugneigung, Entfernung, Orientierung und Zeitpunkt aufweist. Mithilfe von Populationsgenomik und Epigenomik untersuche ich die Evolutionsgeschichte, sowie die molekularen Mechanismen der Diversifizierung der saisonalen Zugmuster.

Die Anwendung der Populationsgenomik auf das System der Mönchsgrasmücke zielt darauf ab, mögliche Angriffspunkte genomischer Selektion im Zusammenhang mit der Divergenz des Wanderverhaltens zu identifizieren und die Geschichte von Populationen mit unterschiedlichen Zugstrategien zu verstehen. Ich beginne damit, die Auswirkungen der Rekombinationsrate anstelle von Selektion und echten demografischen Ereignissen auf diese unterschiedlichen Ansätze populationsgenomischer Analysen zu bewerten, indem ich sowohl Simulationen, als auch empirische Analysen von Mönchsgrasmückengenomen verwende. Ich stelle fest, dass genomische Regionen mit niedrigen Rekombinationsraten dazu neigen, unterschiedliche Muster der genetischen Variation aufzuweisen, weil die Varianz der zugrundeliegenden genetischen Abstammung abnimmt, und dies nicht durch selektive Prozesse bedingt ist. Ich stelle auch fest, dass das Vorhandensein von Genomregionen mit hoher Rekombinationsrate die Demografie-Inferenz mit Methoden beeinflusst, die auf dem Abstammungskombinationsgraphen basieren, einer Struktur, die die genetische Abstammung entlang rekombinierender Chromosomen aufzeigt, weil die zugrunde liegenden Genealogien nicht durch ausreichend viele Mutationen in stark rekombinierenden Regionen repräsentiert werden können.

Durch empirische Validierung von Genom-Scans und Demografie-Inferenz unter Verwendung von Mönchsgrasmücken-Genomdaten fand ich eine polymorphe Inversion mit variablem Frequenzgradienten zwischen Populationen mit unterschiedlichen Zugverhaltens, sowie zwischen kontinentalen und Inseln Populationen, die bei der angenommenen Evolutionsgeschichte der Mönchsgrasmücken-Populationen wahrscheinlich nicht neutral

ist. Durch den Vergleich populationsgenetischer Simulationen mit der Demografie der Mönchsgrasmücke und den beobachteten Inversionshäufigkeiten stelle ich fest, dass die Inversion einer negativen frequenzabhängigen Selektion unterliegt, wobei sich die optimalen Inversionshäufigkeiten zwischen Kontinent und Insel unterscheiden.

Außerdem habe ich untersucht, wie verschiedene Mönchsgrasmückenpopulationen evolutionsgeschichtlich entstanden sind. Ich stelle fest, dass sich die Evolutionsgeschichte der Mönchsgrasmückenpopulationen in zwei Phasen aufteilen. Eine angestammte Ursprungspopulation ziehender Mönchsgrasnücken spaltete sich während eines der pleistozänen Gletscherzyklen in eine Kaukasus- (östliche) und eine westliche Refugienpopulation auf. Die Population expandierte und spalten sich nach dem letzten glazialen Maximum auf. Wir beobachten mindestens vier unabhängige Übergangsereignisse von Zug- zu Standvogelpopulationen.

Ich konzentriere mich auf ein Paar von Zug- und Standvogelpopulationen und untersuche die unterschiedliche epigenetische Regulierung zwischen den Jahreszeiten und Populationen im Hypothalamus, einer Hirnregion, die für den im Fokus stehenden evolutionären Übergang vom Zug zum Standvogel in Frage kommt. Durch die Kombination eines "Common Garden" Experimentes und der Quantifizierung der Chromatinzugänglichkeit einzelner Zellen stelle ich fest, dass das Ausmaß der saisonalen Veränderung der Chromatinzugänglichkeit in einigen genomischen Regionen bei Standvögeln im Vergleich zu Zugvögeln geringer ist.

Abschließend fasse ich die Erkenntnisse aus der Populationsgenomik und der Einzelzell-Epigenomik im Hinblick auf die Phylogeographie und die Evolution der phänotypischen Plastizität zusammen. Diese Arbeit stellt daher einen Fortschritt im ganzheitlichen Verständnis der Frage dar, wie sich das Verhalten von Tieren durch historische Veränderungen der Umwelt über die Modifikation der differentiellen epigenetischen Regulation entwickeln kann.

Acknowledgements

First and foremost, I would like to thank my supervisor, Miriam Liedvogel, for her mentoring. I learned what it means to be a good mentor and a good scientist from you, with a lot of characteristics which I had not thought this important before. You will forever be my reference point and bible of how to communicate professionally without losing personality. I could not thank you more for the trust and freedom you gave me and generous support on my scientific communication and networking. I always felt safe when I had to disagree with you, which assured my psychological security at work, and you motivated me to jump into new things. Continuing my PhD was never a question thanks to you. You helped me realise that I like doing science.

I would also like to thank Julien Dutheil for being in my thesis advisory and examination committees and for his scientific feedback on my project. I decided not to move to Wilhelmshaven following Miriam largely because of your presence in Plön, and you proved my decision was right. On top of that, thank you for offering to share the 10x Chromium machine, which was a big turning point of my epigenomics project.

I would like to thank Hinrich Schulenburg for being in my thesis advisory and examination committees. I felt honoured when you offered to be in my PhD TAC after my master's defense. Also, I learned from you the importance of expressing gratitude to people organising events when you did it to me in the IMPRS retreat I co-organised during the inter-lockdown phase.

I would like to thank Linda Odenthal-Hesse, Anja Guenther, Markéta Kaucká, Andrea Patricia Murillo Rincon, Diethard Tautz, Bernhard Haubold, Tobias Kaiser, Nicole Thomsen and Kerstin Schäfer for scientific and technical discussion, and support on my experiments and career. Linda, I really liked that you are committed to be accessible for communication with students from not only your own group but also from other groups by participating in most of the IMPRS retreats and Aquavits. Anja, thank you for exposing me to mixed effects modelling in the early phase of my PhD, which was used in different places of my projects. And thank you both for inviting me to the mouse Christmas party despite my toothless study system. Markéta and Andrea, thank you for generous materialistic and technical support on 10x scATAC, without your help it would not have been possible. Diethard, thank you for your generous support on consumables for my scATAC experiment (which you may not be even aware of) when the concept of budget disappeared from my perception, and of course, for scientific and career discussion and feedback. Bernhard, thank you for always being available for my algorithmic and bioinformatic questions, and making me an AWK lover. Tobias, thank you for including me in the Clunio meeting even after I became the last one from the Behavioural Genomics Group in Plön. Nicole and Kerstin, thank you for helping me navigate in the lab. You were always available and helpful. I would love to work with technicians in the future who are as into science as you are.

Many thanks to all current and past members of Behavioural Genomics Group in Plön and Wilhelmshaven. Corinna, thanks a lot for letting me be involved in the robin fieldwork. I admire your hard work and your attitude towards science on top of being a bird lover. Georg, I enjoy discussing with you, and watching you quickly learn biology from a different background was very inspiring. Karen, thanks for letting me be involved in the recombination project and spending time in the office for discussion. Juan and Andrea, I appreciate that you were approachable for questions and discussion in the early phase of my PhD. Matthias, thanks for a lot of discussion despite the distance, and making me feel we met many more times than we actually did. Joe and Robert, I admire your proactiveness and you are my models of good postdocs.

Many thanks to Carolina for exciting (and depressing... they can coexist) discussion on inversions. I admire your hard work and I really liked dropping by at your office when you were in for a random chat, and I would love to be as approachable and likeable as you are. Jule, you brought me enthusiasm in science and helped me with my internal peace and the community feeling outside science. I admire your hard work, active commitment and empathy. Alec and Demetris, thanks a lot for letting me interrupt you so frequently for discussion, and inviting me for barbecue, dinner and canoeing. You are the most important discussion partners in my PhD and a major drive for me to go out.

Christin and Mayo, you made Plön my home. I am not the most expressive person but here I secretly thank you two for making my personal life here colourful, tasteful, game-ful and Joey-ful.

Nikhil, thanks for a lot of discussion on concepts and phenomena of biology. I admire your sincere attitude towards science with your open-mindedness and how you are (or at least you behave) always so laid-back. Fernanda, thank you for making our office 164 (without my name on the plate until the end) lively by bringing plants, installing the whiteboard, and initiating conversations. Louk and Stella, thanks for the discussion on my scATAC analysis and making me slightly home-sick when each of you travelled in Japan. Thank you, Ian and Jinyang, for joining our PopClub to discuss population genetics including the ARG. Special thanks to Angela Donner for helping me with non-scientific troubles, and the IT team for making my analyses possible. I thank the IMPRS for Evolutionary Biology for generous funding.

My scientific activity was also supported by scientists outside the institute. I thank Kira Delmore for generously letting me work on demography inference as my first ever project for her big paper even before meeting in person. This project opened the door to population genetics including theoretical parts and eventually destined my whole project. I thank Javier Pérez-Tris and Juan Carlos Illera for providing me with feedback. A paper with many authors is not the easiest task, and I am so grateful that they always read the manuscript and gave me feedback. I thank Sean Stankowski, Daria Shipilina, Konrad Lohse and Jochen Wolf for being supportive and critical about my theory-oriented empirical population genomic projects which we discussed in different places from an online conference to Lucca, London, (near) Vienna, Wilhelmshaven and Plön. I thank Hirohisa Ebina for occasionally discussing diverse topics of science and career. I thank Masakazu Hoshino for cheering me up on my project and sharing his interesting data. I thank Nao Ota for sharing her experience of lab visits at Max Planck Institute for Ornithology during my bachelor's. This was when I started thinking of going out of Japan for a post-grad study. I thank Kazuhiro Wada for priming my journey on behavioural evolution and showing me his philosophy of doing unique science.

Finally I thank my family, especially my parents, for not being an obstacle to my decision to follow the non-canonical path of becoming a scientist. It might sound awkward to thank them for not doing something, but I am aware through anecdotes that this actually could have been a problem, arguably to a different extent between genders. I am grateful that they gave me the liberty to pursue my interest, and I believe they would have treated me the same way even if I were another gender. I thank my grandparents for always being cheerful and affirmative of my decision, mostly via Zoom, on which they struggle to set up the audio by forgetting to unplug the headphones.

Contents

Summary	4
Zusammenfassung	6
Acknowledgements	8
Contents	10
1 Introduction	11
2 Distinct patterns of genetic variation at low-recombining genomic regions represent haplotype structure	32
3 High-recombining genomic regions affect demography inference	131
4 Shifting balancing selection on a chromosomal inversion in island populations	171
5 Differential epigenetic regulation underlies evolutionary transition of seasonal migration	197
6 Discussion	232
List of Manuscripts	245
Author Contributions	246
Declaration / Affidavit	247

1

Introduction

Luria said something that seemed to him to be extremely important, although Benzer could not follow it at the time. “He said, ‘Everyone keeps going down, down, down, trying to be more reductionist, trying to see finer and finer, to find the basis of structure and function.’ And he said ‘I think it’s time to start going up again—going in the opposite direction’”

– Jonathan Weiner, *Time, Love, Memory: A Great Biologist and His Quest for the Origins of Behavior* (1999)

Definition and history

What makes animals special is that they can actively move, which allows them to avoid adverse environments — biotic and abiotic — and to relocate themselves to more favourable environments to survive and reproduce. Animals move at different scales in space and time with different types and levels of regularity (Dingle, 2014; Lovette & Fitzpatrick, 2016; Newton, 2010). Seasonal migration is one type of movement which is characterised with longer distance than other types of movement and high regularity in orientation, destination and seasonality (Dingle, 2014; Hansson & Åkesson, 2014; Newton, 2010). Seasonal migration involves movement between breeding and wintering areas in certain times of the year (Dingle, 2014; Hansson & Åkesson, 2014; Newton, 2010). The distance of seasonal migration is longer than local movement and dispersal when compared within species (Dingle, 2014; Newton, 2010). Unlike dispersal and nomadism, which lack directionality, animals migrate towards certain orientations and to specific destinations and they return to the same area (“philopatry”. Newton, 2010; Dingle, 2014; Lovette & Fitzpatrick, 2016). Seasonal migration is ubiquitous in animals, from insects and fish to mammals and birds (Dingle, 2014; Hansson & Åkesson, 2014; Liedvogel et al., 2011). Among these, birds are arguably the best studied and the most iconic migrants, and a large body of our current understanding of seasonal migration was obtained in birds (Hansson & Åkesson, 2014; Newton, 2010; Newton & Brockie, 2008).

The first recognition of bird migration dates back to Holy Roman Emperor Frederick II in the 13th century, who postulated in *De arte venandi cum avibus* that birds come and go following external conditions such as food supply and heat (Berthold, 1993, 1996). In the 18th century, von Pernau conceptualised the innate urge of seasonal migration as opposed to fully environmentally driven escape, and Johann Andreas Naumann observed nocturnal migratory restlessness in caged migratory birds (Berthold, 1993, 1996). In the 20th century, two types of experimental study on bird migration started. The first is ringing. Ringing provides more information compared to studies based on field observation and shooting as individuals’ movement can be tracked. Following the first use of rings for tagging birds by Mortensen in 1899 (Preuss, 2011), ringing was institutionalised in 1903 at the Bird Observatory of Rossitten (Vogelwarte Rossitten) in Prussia (now Rybachy in Kaliningrad Oblast, Russia),

led by Johannes Thienemann (Berthold, 1996; Berthold et al., 2003, 2003). Ringing revealed the prevalence and huge diversity of bird migration soon after the beginning: the first atlas of bird migration (Fig. 1. Schüz & Weigold (1931)) shows huge variation in the distance and direction of movement among and within more than 150 species of birds. With expansion of new bird observatories, ringing has since become a successful tool utilised worldwide to study seasonal migratory behaviour (Berthold, 1993). The second is experimental manipulation. By extending day length using artificial light, Rowan examined the photoperiodism of sexual maturation and seasonal migration in the dark-eyed junco (*Junco hyemalis*) and the American crow (*Corvus brachyrhynchos*) (Rowan, 1925, 1930, 1932). These two approaches founded the basis of our current understanding of bird migration side by side and contributed to the development of ethology.

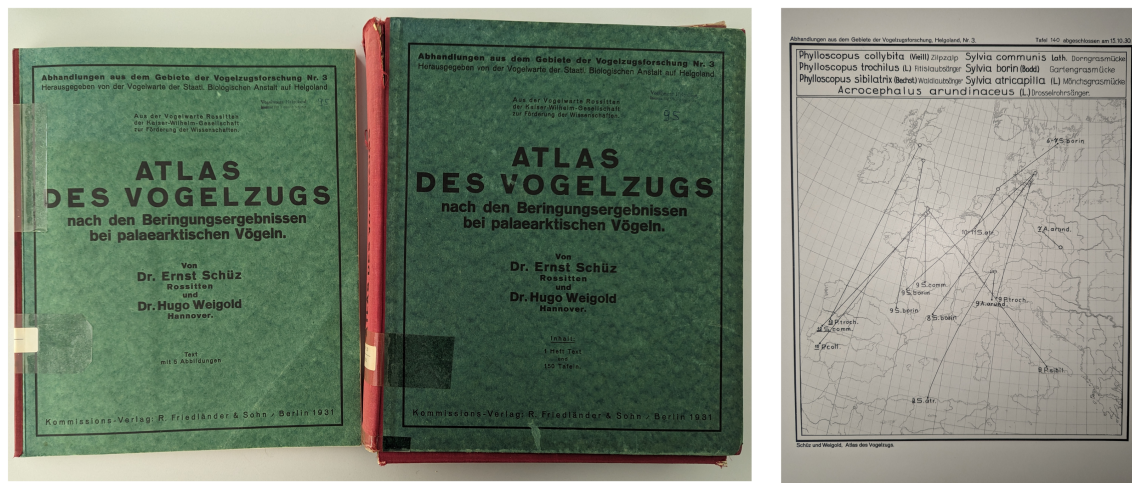


Figure 1: Migration atlas. Photographed at Institute of Avian Research, Wilhelmshaven.

Fundamental questions

Why do birds migrate? This simple question needs further clarification of what exactly to be answered. There are four kinds of fundamental *whys* to understand animal behaviour: mechanisms, development, adaptation, and evolution, collectively referred to as the Tinbergen's four questions (Alcock, 2013; Bateson & Laland, 2013; Tinbergen, 1963).

1. **Mechanisms.** Questions on mechanisms aim to understand what *is happening* in individ-

ual animals that makes them express the behaviour. The scale is within each individual and can go from physiology and metabolism at tissues to cells and molecules: How can they migrate? How do they know when to leave and where to go? What is happening in their brain specifically during migration? Which cells in what tissues regulate migration? Answering these questions is fundamental because control mechanisms are an integral part of holistic understanding of behaviour, allowing us to extend questions to different axes: how does the control mechanism change over developmental and evolutionary time? Which mechanisms are under natural selection?

2. **Development.** Questions on development concern how an individual *becomes* to express the behaviour. This question is of particular importance because this is where endogenous and exogenous factors, in time windows within individuals' lifetime, are integrated to control behaviour. Is migration urge and migratory orientation innate? Is there a critical period within which birds need to be exposed to environmental stimuli for them to express migration behaviour later in life? Do all migrants migrate every year, and do they follow the same path?
3. **Adaptation (ecological function).** Questions on adaptation (or ecological function) aim to understand the current utility of the behaviour. Questions of this type can be tricky because 1. not all observable traits have functional adaptation and 2. one should consider not only fitness benefits but also fitness costs. Still, they can also seed robust theories formulated and analysed with mathematics, which are often extendable to broader contexts, and the expectations can be directly tested by observation and experiments. What are the costs and benefits of migration? What would they lose by migrating earlier or later? Are migrants sexier than residents for other migrants and *vice versa*?
4. **Evolution.** Questions on evolution aim to understand changes in behaviour and emergence of new behaviour at a time scale longer than individuals' life. Despite the importance of this type of questions to understand the diversity of behaviour and underlying generality/commonality and uniqueness, ethology literatures tend to be relatively descriptive on this aspect, mostly focusing on discussing the evolutionary origin

and the ancestral states at the phylogenetic scale. Here, I list two fundamental (but not the only) questions to understand seasonal migration, stemming from the context of evolutionary biology. First, what is the genetic architecture of seasonal migration? By treating behaviour (migration) as complex traits, the number of underlying genes and the distribution of effect size are addressed. This question itself can be regarded as a question on mechanism and/or development, but the response to selection on phenotype substantially varies by the genetic architecture of the trait. Second, are evolutionary gain, loss, and change of seasonal migration repeatable? By understanding repeatability of the evolution of migration and the underlying change in the mechanism across phylogenies, we can understand the general principle of evolution of migration.

Methodologies to answer the fundamental questions of migration

To answer these fundamental questions, studies on migration today combine extensions of the aforementioned classical approaches and new methods: 1. recording migration in nature stemming from ringing, 2. field experiments, 3. experiments in captivity and 4. and laboratory experiments and sequencing.

Recording of natural migration

Ringing is still a very powerful tool to study the pattern of migration and its costs and benefits in nature, which requires phenotyping of individuals and measuring survival and reproductive success. For example, by intensive resighting of colour-ringed individuals of European shags *Phalacrocorax aristotelis* in a population consisting of migrants and residents (partial migrant population), Grist et al. (2017) found that residents have higher breeding success than migrants.

There are two major limitations of classical capture-mark-recapture based on ringing. First, the same bird has to be caught both in the location of departure and destination to directly confirm long distance movement. Despite the spread of bird observatories throughout the world and the success of ringing as citizen science, it is impossible to recapture ringed birds at all destinations. Second, ringing data reveals the origin, destination, and timing of

migration, but how the migratory journey is carried out (e.g. trajectory, elevation, stopovers) cannot be measured. These limitations are dealt with by newer systems described in the following paragraphs. Overall, there is a trade-off between resolution and scalability among these methods.

At a local scale, **radio telemetry** can be utilised to monitor presence/absence of tagged birds. This is particularly useful to phenotype migrants and residents in a partial migrant population. For example, by phenotyping migrant and resident individuals in a partial migrant population of European blackbirds *Turdus merula*, Zúñiga et al. (2017) found that migrants had higher probability of winter survival than residents, which complements the resighting-based results by Grist et al. (2017), collectively capturing costs in reproduction and benefits in survival of migration.

Light level geolocators are small electronic archival tracking devices, which can be fit to birds (Fig. 2) to record the time and light level (Croxall et al., 2005; Delmore et al., 2020a; Van Doren et al., 2021). Based on retrieved times of sunrise and sunset, the latitude and longitude can be calculated. In addition to geolocators, loggers with multiple sensors (a light sensor (as in geolocators), accelerometer (behavioural activity) and temperature-compensated barometric pressure sensor (altitude)) can be used to record migratory and other behaviour with local environmental conditions (Bäckman et al., 2017; Sjöberg et al., 2018, 2021). Being light weighted, these loggers allow measurement of long-distance migration behaviour of small birds including songbirds. Yet, retrieval of recorded data from these loggers requires recapturing. Hence possible causes of lack of data (e.g. complete return migration to different destinations, failure of migration, and death unrelated to migration) cannot be distinguished.



Figure 2: Light level geolocators. A geolocator is fitted to a Eurasian blackcap *Sylvia atricapilla*.

Satellite telemetry, including global positioning system (GPS) and Argos transmitters, allows to track movement of individual animals without recapturing (Aikens et al., 2024; Kays et al., 2015). Currently these transmitters are still too heavy (e.g. an ICARUS transmitter weighs 5 g) for many animals, including small songbirds, and too costly for tracking at population, species, and community levels.

Finally, use of military and weather **surveillance radars** (Hilgerloh, 1989; Van Doren et al., 2015) allows measurement of the time, speed, and direction of migration of a large number of birds in nature without tagging — hence without capturing. Yet the resolution of bird identification is limited to groups of birds with similar body size (e.g. passerines and waders), and observations at different locations cannot be directly compared due to the lack of tags.

Field experiments

The experimental manipulation and field work was already combined in one of the first experimental studies by Rowan (1930). To test the effect of photoperiodism on orientation of seasonal migration, crows were treated with longer day lengths and released in the field. The orientation of migration was measured by recapturing:

[T]he birds were surreptitiously released on the morning of the 9th [of November 1924] and the fact announced in the evening newspapers and over the radios, with an

appeal for anyone and everyone to hunt crows on Thanksgiving Day (and thereafter) and to mail the birds in to the Department of Zoology at the University. (Rowan, 1930).

Other types of field experiments include **displacement**. For example, to investigate development of migratory orientation, Perdeck (1958) caught and ringed more than 11,000 starlings (*Sturnus vulgaris*) in the Netherlands and released them in Switzerland. While adults were recaptured within their typical wintering range in northwestern Europe, juveniles on their first migration were recaptured in southwestern Europe including southern France and Spain following the direction which would have led to normal wintering sites, demonstrating that migratory orientation involves both innate vector orientation and learned goal orientation. Combining state-of-the-art tracking and these field experiments is informative of the mechanisms and development of migration in nature, yet interpretation is often challenging as the environmental factors are not controlled.

Experiments in captivity

Since the presumably first observation by Naumann in the 18th century, it has been recognised that captive birds exhibit behavioural activity during migratory season, characterised with hopping and fluttering wings (Berthold, 1993). As a proxy of migratory behaviour, this elevated activity called **Zugunruhe** (migratory restlessness) is recorded in **measurement cages** equipped with microswitches or infrared motion sensors with an event recording system (Bartell & Gwinner, 2005; Berthold, 1993, 1996; Berthold et al., 2000; Wiltschko, 1968). Proxy of orientation of seasonal migration can be measured in specific measurement cages called **Emlen funnels** (Emlen & Emlen, 1966. Fig. 3) and **circular cages** (Wiltschko, 1968). In the Emlen funnel setup, individual birds are placed in a funnel lined with correction paper, and the amount of oriented hopping is recorded as scratches on the paper (Berthold, 1993). In circular cages, behavioural activity is recorded at each perch arranged in the cage (Berthold, 1993).

These recording systems have been utilised as standard methods for quantifying migratory behaviour in controlled conditions, which is required to test potential environmental

(e.g. reference cues of compass systems for orientation, nutrition and photoperiodism for induction) and endogenous (e.g. neural basis of compass, biological clock, neuroendocrine basis of migration onset and offset, and genetic basis of migration) factors regulating seasonal migration. For example, Emlen (1967) and Wiltschko (1968) studied respectively the star and magnetic compasses as potential mechanisms of migratory orientation by measuring orientation of Zugunruhe using the Emlen funnel in a planetarium (Fig. 3C) and using the circular cage in magnetic coils (Fig. 3D). The neural entity of the magnetic compass underlying nocturnal migratory orientation was tested by Zapka et al. (2009), where the amount and orientation of Zugunruhe were measured using European robins *Erithacus rubecula* which received lesion at a candidate brain region, the cluster N. This revealed that the cluster N is essential for magnetic compass orientation but not for the sun compass or the urge to migrate. To understand how the timing of migration is regulated, Gwinner (1990) conducted experiments similar to the Rowan's study on photoperiodism (Rowan, 1925, 1930, 1932) but over much longer durations under systematically controlled light-dark cycles and with recording of Zugunruhe in captivity, which revealed that the timing of migration is regulated by an endogenous circannual clock entrained by exogenous photoperiod. Finally, the genetic basis of seasonal migration was studied by measuring Zugunruhe of Eurasian blackcaps *Sylvia atricapilla* from a partial migrant population (Pulido et al., 1996) or hybrids between migrant and resident blackcaps (Berthold, 1993, 1996; Berthold & Querner, 1981), revealing the polygenic basis of variation in migratory behaviour by standing genetic variation.

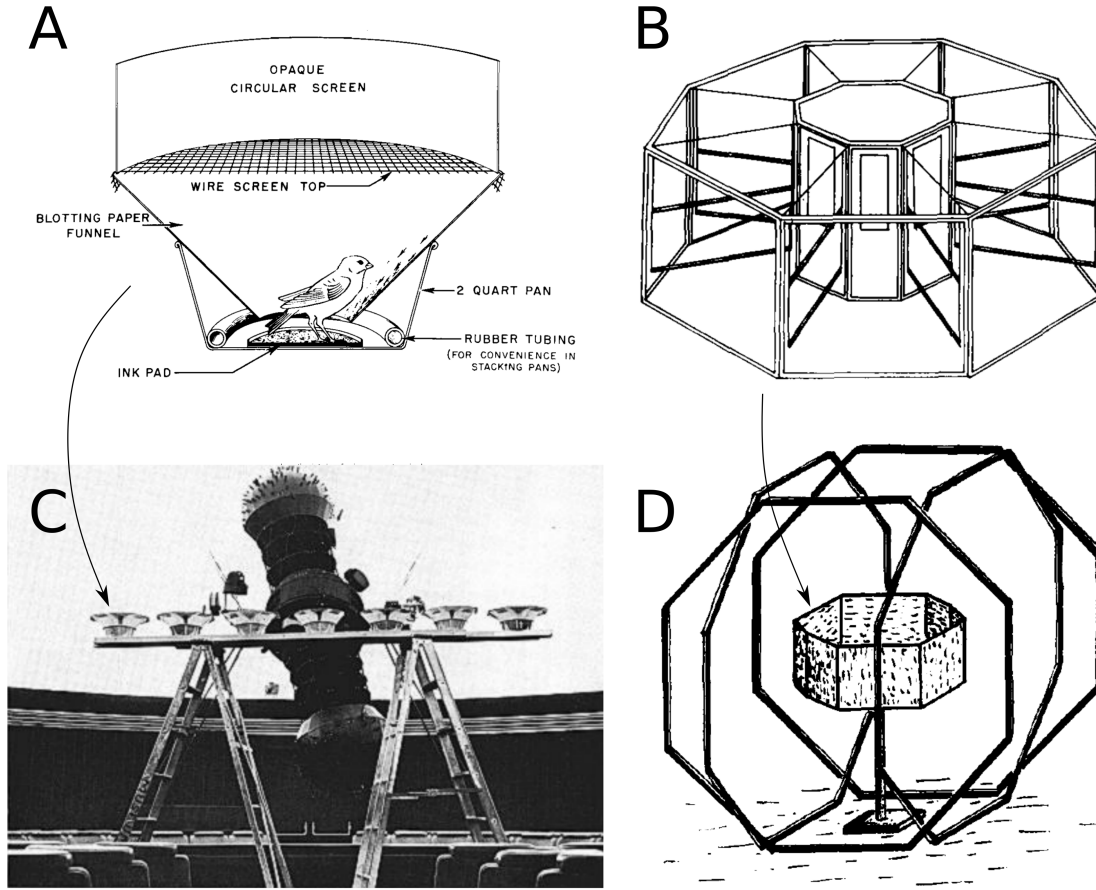


Figure 3: Orientation cages. **A.** Emlen funnel (Emlen & Emlen, 1966). **B.** Circular cage (Wiltschko, 1968). **C.** Emlen funnels with a planetarium projector. **D.** Circular cage in magnetic coils. A from Emlen & Emlen (1966); B and D from Wiltschko (1968); C from Emlen (1967).

Laboratory methods, genome sequencing, and more

In the field sites and in captivity, biological samples such as blood, gonads and brains, can be collected for physiological (Wingfield et al., 1990), histological and molecular (Rastogi et al., 2013) analyses. On top of these, a new set of methods have been applied to answer mechanisms and evolution of migration since the development of high-throughput genome sequencing. First, genome sequencing of multiple individuals allows population genomic analyses to investigate the structure and history of populations, potential targets of selection, and association between genotype and phenotype and/or environment (Dutheil, 2010). These methods enable us to address the evolutionary questions (genetic architecture and repeatability). Second, transcriptomics and epigenetics are used to quantify transcription activity and epigenetic

states (DNA methylation, histone tail modifications, and chromatin remodelling) as a measure of gene expression and regulation, often comparing between tissues, ages, seasons, conditions, populations, or species (Bakken et al., 2021; Bendesky et al., 2017; Colquitt et al., 2021; Hu et al., 2022; Jhanwar et al., 2021; Merritt et al., 2020). These approaches aim to integrate our understanding of how molecular mechanisms in the cell are regulated differently by endogenous and exogenous factors by seasons, conditions, or evolutionary time.

There are established and state-of-the-art methods which have not been fully applied in bird migration studies. First, compared to other behavioural and physiological adaptations to seasons, such as hibernation (Drew et al., 2007; Junkins et al., 2022), there are limited studies on the neural regulation controlling seasonal migration. Neural correlates of migration has been investigated through histological assay of immediate early genes (IEGs) using *in situ* hybridisation (Mouritsen et al., 2005; Rastogi et al., 2013; Zapka et al., 2010), yet recoding of neural activity with electrophysiology (Takahashi et al., 2022) is limited and recording in behaving animals (Hoffmann et al., 2019) and manipulation of local neural activity with infusion (Benichov & Vallentin, 2020; Warren et al., 2011), cell type-specific molecular genetic manipulation (Sánchez-Valpuesta et al., 2019), or optogenetics (Singh Alvarado et al., 2021; Tanaka et al., 2018) have not been applied for avian migration. Second, current development of single cell transcriptomics and epigenomics (Bakken et al., 2021; Mickelsen et al., 2019; Moffitt et al., 2018; Shafer et al., 2022) have not been applied. These approaches are particularly important to understand the mechanism of migration, because different cells likely contribute differently to seasonal migration (Rastogi et al., 2013). Finally, approaches of evolutionary developmental biology (evo-devo) (Carroll, 2005; Gilbert, 2015) have been limited in studies of bird migration. In evo-devo, the core question is the molecular mechanisms of development underlying different phenotypes expressed between species using a common genetic toolkit. The scarce application of evo-devo in bird migration has to do with the difficulty in molecular genetic manipulation in birds, and the likely polygenic nature of the control of seasonal migration (Pulido et al., 1996; Pulido, 2007).

Summary

Mechanisms, development, function, and evolution of migration are studied by combining ringing, tracking, experimental manipulation of endogenous and exogenous factors, standardised recording of behaviour in captivity, laboratory, and computational methods. Same methods can be used to answer different types of questions of seasonal migration. Conversely, the same question of migration can be approached using different types of methods.

The study system: Eurasian blackcaps

In my thesis, I address two of the four fundamental questions: evolution and mechanisms. Specifically, I aim to understand the evolutionary transition of migratory phenotypes and its molecular mechanisms at a micro-evolutionary time scale.

The Eurasian blackcap *Sylvia atricapilla* is an ideal system to address these questions. The blackcaps is a songbird species commonly breeding throughout Europe, northern Africa and Macaronesian and Mediterranean islands (Shirihai et al., 2010). Although the blackcap was one of many species shown to be migrants in the first decades of ringing (Fig. 1), this species is iconic in studies on differential control of migratory orientation and propensity between populations, because they exhibit large variation in seasonal migration among populations. Most of the continental populations are solitary nocturnal migrants (Shirihai et al., 2010). The distance of migration varies latitudinally, long to short distance migrants from northern to southern breeding populations (Berthold, 1988; Shirihai et al., 2010). The orientation of autumn migration (from the breeding ground to wintering area) are split longitudinally at a migratory divide in central Europe: western breeding populations migrate southwest, whereas eastern populations migrate southeast (Helbig, 1991a, 1991b, 1996). There are migrants with a novel migratory orientation to northwest wintering in the British Isles (Berthold et al., 1992; Helbig, 1991b; Langslow, 1979), which originate from a wide range of the continental Europe (Delmore et al., 2020a; Langslow, 1979). In addition to this large variation in migratory phenotypes among migrant populations, there are multiple resident populations in southern Iberia and northern Africa and on Macaronesian and Mediterranean islands. Phenotypic variation in migratory orientation, distance, timing, and propensity are heritable with polygenic

basis (Pulido et al., 1996).

Problems addressed in this thesis

To understand evolutionary transition of population-typical migratory phenotypes and its molecular mechanisms in blackcaps, I use population genomics and brain epigenetics.

Chapters 2, 3: How does recombination rate affect population genomics methods?

The general aims of population genomics are to understand what roles neutral and selective processes play in shaping patterns of genetic variation in a population of genomes, and to characterise how these processes operate in natural populations based on observed patterns of genomic variation (Dutheil, 2010; Hahn, 2018; Wakeley, 2008). Genome scans of genetic variation and demography inference are two of common population genomic methods to identify targets of selective processes in the genome and to reconstruct population history (Dutheil, 2010). These methods have been widely applied in various study systems including birds to answer evolutionary questions (Burri et al., 2015; Delmore et al., 2020b; Nadachowska-Brzyska et al., 2016; Vijay et al., 2017). However, through my empirical analyses in blackcaps, it became evident that these two approaches are both affected by a common factor: recombination rate.

Recombination rate depicts the expected number of crossover events occurring in a given segment of the genome per meiosis (i.e. per generation) (Hudson & Kaplan, 1985). Two mutations on a chromosome with no recombination would be inherited together: thus the pattern of their inheritance in a population would be perfectly correlated. Inheritance of two mutations on a recombining chromosome are not as correlated, because recombination *can* happen between the two loci, and if it does, the two mutations are not on the same chromosome in the offspring that inherit the recombined chromosome. In a population of a fixed size, the genotypes at the two loci become less correlated as the expected number of recombinations between the loci per generation increases. This is the case as the physical distance between the loci in base pairs (to be considered) become longer. In other words, genotypes of loci in a population are correlated if they are close to each other, and less so as they are further

apart. Some population genomics methods make use of this correlation of genotypes between loci along a recombining chromosome to model the ancestral process along the chromosome, whereas (interpretation of) other methods assume that the unit of the genome scan is large enough to assume genotypes between most combinations of loci are independent. Importantly, how rapidly this decay occurs along the chromosome (i.e. the local recombination rate) varies along chromosomes and among organisms.

In chapter 2, I address how genomic regions with reduced recombination rate can cause distinct patterns of genetic variation, which is often interpreted as a signature of selective processes, using population genetic simulation and empirical population genomic analysis in blackcaps. In chapter 3, I address how the presence of high-recombining genomic regions affects demography inference methods which use locally correlated genotypes along the chromosome to model the ancestral process, with population genomic simulation and empirical analysis in blackcaps.

Chapter 4: How did selection on a balanced inversion shift upon population split?

Within chapter 2, I identify a chromosomal inversion in blackcaps with a gradient in frequency across populations (cline). Inversion clines are commonly interpreted as the effect of locally varying selection and balancing selection. However, the mode of selection and parameter values of the type of selection operating have been rarely measured. In chapter 4, I extend the empirical population genomic analyses in chapters 2 and 3 to evaluate and measure the selective process acting on a polymorphic inversion, using a framework for estimating evolutionary models and parameter values based on extensive simulation.

Chapter 5: What is the epigenetic basis underlying evolutionary transition from migrant to resident?

Through demography inference conducted in chapters 3 and 4, I found that there were multiple independent and simultaneous transitions from migrants to residents in blackcaps. To understand the cellular and molecular mechanisms of differential regulation underlying this

transition, I evaluate single cell chromatin accessibility of the hypothalamus of migrant and resident blackcaps in migratory and non-migratory seasons.

Chapter 6: How does seasonal migration evolve?

Finally, I synthesise the preceding chapters. I discuss the pattern and cause of blackcap population history, and how migratory behaviour evolves.

References

- Aikens, E. O., Nourani, E., Fiedler, W., Wikelski, M., & Flack, A. (2024). Learning shapes the development of migratory behavior. *Proceedings of the National Academy of Sciences*, 121(12), e2306389121. <https://doi.org/10.1073/pnas.2306389121>
- Alcock, J. (2013). *Animal Behavior: An Evolutionary Approach*. Sinauer.
- Bäckman, J., Andersson, A., Alerstam, T., Pedersen, L., Sjöberg, S., Thorup, K., & Tøttrup, A. P. (2017). Activity and migratory flights of individual free-flying songbirds throughout the annual cycle: Method and first case study. *Journal of Avian Biology*, 48(2), 309–319. <https://doi.org/10.1111/jav.01068>
- Bakken, T. E., Jorstad, N. L., Hu, Q., Lake, B. B., Tian, W., Kalmbach, B. E., Crow, M., Hodge, R. D., Krienen, F. M., Sorensen, S. A., Eggermont, J., Yao, Z., Aeversmann, B. D., Aldridge, A. I., Bartlett, A., Bertagnolli, D., Casper, T., Castanon, R. G., Crichton, K., et al. (2021). Comparative cellular analysis of motor cortex in human, marmoset and mouse. *Nature*, 598(7879, 7879), 111–119. <https://doi.org/10.1038/s41586-021-03465-8>
- Bartell, P. A., & Gwinner, E. (2005). A Separate Circadian Oscillator Controls Nocturnal Migratory Restlessness in the Songbird *Sylvia borin*. *Journal of Biological Rhythms*, 20(6), 538–549. <https://doi.org/10.1177/0748730405281826>
- Bateson, P., & Laland, K. N. (2013). Tinbergen’s four questions: An appreciation and an update. *Trends in Ecology & Evolution*, 28(12), 712–718. <https://doi.org/10.1016/j.tree.2013.09.013>
- Bendesky, A., Kwon, Y. M., Lassance, J. M., Lewarch, C. L., Yao, S., Peterson, B. K., He, M. X., Dulac, C., & Hoekstra, H. E. (2017). The genetic basis of parental care evolution in monogamous mice. *Nature*, 544(7651), 434–439. <https://doi.org/10.1038/nature22074>
- Benichov, J. I., & Vallentin, D. (2020). Inhibition within a premotor circuit controls the timing of vocal turn-taking in zebra finches. *Nature Communications*, 11(1, 1), 221. <https://doi.org/10.1038/s41467-019-13938-0>
- Berthold, P. (1988). Evolutionary aspects of migratory behavior in European warblers. *Journal of Evolutionary Biology*, 1(3), 195–209. <https://doi.org/10.1046/j.1420-9101.1998.1030195.x>
- Berthold, P. (1993). *Bird Migration: A General Survey* (1st ed.). Oxford University Press.
- Berthold, P. (1996). *Control of Bird Migration*. Chapman & Hall.
- Berthold, P., Fiedler, W., & Querner, U. (2000). Die Zugunruhe bei Vögeln — eine Darstellung nach Videoaufnahmen bei Infrarotlichtbeleuchtung. *Journal für Ornithologie*, 141(3), 285–299. <https://doi.org/10.1007/BF02462238>
- Berthold, P., Gwinner, E., & Sonnenschein, E. (Eds.). (2003). *Avian Migration*. Springer-Verlag.
- Berthold, P., Helbig, A. J., Mohr, G., & Querner, U. (1992). Rapid microevolution of migratory behaviour in a wild bird species. *Nature*, 360(6405, 6405), 668–670.

<https://doi.org/10.1038/360668a0>

- Berthold, P., & Querner, U. (1981). Genetic Basis of Migratory Behavior in European Warblers. *Science*, 212(4490), 77–79. <https://doi.org/10.1126/science.212.4490.77>
- Burri, R., Nater, A., Kawakami, T., Mugal, C. F., Olason, P. I., Smeds, L., Suh, A., Dutoit, L., Bureš, S., Garamszegi, L. Z., Hogner, S., Moreno, J., Qvarnström, A., Ružić, M., Sæther, S.-A., Sætre, G.-P., Török, J., & Ellegren, H. (2015). Linked selection and recombination rate variation drive the evolution of the genomic landscape of differentiation across the speciation continuum of Ficedula flycatchers. *Genome Research*, 25(11), 1656–1665. <https://doi.org/10.1101/gr.196485.115>
- Carroll, S. B. (2005). *Endless Forms Most Beautiful: The New Science of Evo Devo*. W. W. Norton & Company.
- Colquitt, B. M., Merullo, D. P., Konopka, G., Roberts, T. F., & Brainard, M. S. (2021). Cellular transcriptomics reveals evolutionary identities of songbird vocal circuits. *Science*, 371(6530), eabd9704. <https://doi.org/10.1126/science.abd9704>
- Croxall, J. P., Silk, J. R. D., Phillips, R. A., Afanasyev, V., & Briggs, D. R. (2005). Global Circumnavigations: Tracking Year-Round Ranges of Nonbreeding Albatrosses. *Science*, 307(5707), 249–250. <https://doi.org/10.1126/science.1106042>
- Delmore, K. E., Van Doren, B. M., Conway, G. J., Curk, T., Garrido-Garduño, T., Germain, R. R., Hasselmann, T., Hiemer, D., van der Jeugd, H., Justen, H., Lugo Ramos, J. S., Maggini, I., Meyer, B. S., Phillips, R. J., Remisiewicz, M., Roberts, G. C. M., Sheldon, B. C., Vogl, W., & Liedvogel, M. (2020a). Individual variability and versatility in an eco-evolutionary model of avian migration. *Proceedings of the Royal Society B: Biological Sciences*, 287(1938), 20201339. <https://doi.org/10.1098/rspb.2020.1339>
- Delmore, K., Illera, J. C., Pérez-Tris, J., Segelbacher, G., Lugo Ramos, J. S., Durieux, G., Ishigohoka, J., & Liedvogel, M. (2020b). The evolutionary history and genomics of European blackcap migration. *eLife*, 9, e54462. <https://doi.org/10.7554/eLife.54462>
- Dingle, H. (2014). *Migration: The Biology of Life on the Move* (2nd ed.). Oxford University Press.
- Drew, K. L., Buck, C. L., Barnes, B. M., Christian, S. L., Rasley, B. T., & Harris, M. B. (2007). Central nervous system regulation of mammalian hibernation: Implications for metabolic suppression and ischemia tolerance. *Journal of Neurochemistry*, 102(6), 1713–1726. <https://doi.org/10.1111/j.1471-4159.2007.04675.x>
- Dutheil, J. Y. (Ed.). (2010). *Statistical Population Genomics* (1st ed., Vol. 2090).
- Emlen, S. T. (1967). Migratory Orientation in the Indigo Bunting, *Passerina cyanea*: Part I: Evidence for Use of Celestial Cues. *The Auk*, 84(3), 309–342. <https://doi.org/10.2307/4083084>
- Emlen, S. T., & Emlen, J. T. (1966). A Technique for Recording Migratory Orientation of Captive Birds. *The Auk*, 83(3), 361–367. <https://doi.org/10.2307/4083048>
- Gilbert, S. F. (2015). *Ecological developmental biology* (2nd ed.). Sinauer.

- Grist, H., Daunt, F., Wanless, S., Burthe, S. J., Newell, M. A., Harris, M. P., & Reid, J. M. (2017). Reproductive performance of resident and migrant males, females and pairs in a partially migratory bird. *Journal of Animal Ecology*, 86(5), 1010–1021. <https://doi.org/10.1111/1365-2656.12691>
- Gwinner, E. (1990). Circannual Rhythms in Bird Migration: Control of Temoral Patterns and Interactions with Photoperiod. In *Bird Migration: Physiology and Ecophysiology*. Springer-Verlag.
- Hahn, M. W. (2018). *Molecular Population Genetics*. Oxford Press.
- Hansson, L. A., & Åkesson, S. (Eds.). (2014). *Animal Movement Across Scales*. Oxford University Press.
- Helbig, A. J. (1991a). Inheritance of migratory direction in a bird species: A cross-breeding experiment with SE- and SW-migrating blackcaps (*Sylvia Atricapilla*). *Behavioral Ecology and Sociobiology*, 28(1), 9–12. <https://doi.org/10.1007/BF00172133>
- Helbig, A. J. (1991b). SE- and SW-migrating Blackcap (*Sylvia Atricapilla*) populations in Central Europe: Orientation of birds in the contact zone. *Journal of Evolutionary Biology*, 4(4), 657–670. <https://doi.org/10.1046/j.1420-9101.1991.4040657.x>
- Helbig, A. J. (1996). Genetic Basis, Mode of Inheritance and Evolutionary Changes of Migratory Directions in Palearctic Warblers (Aves: Sylviidae). *The Journal of Experimental Biology*, 199, 49–55. <https://doi.org/10.1007/s11892-016-0766-y>
- Hilgerloh, G. (1989). Autumn Migration of Trans-Saharan Migrating Passerines in the Straits of Gibraltar. *The Auk*, 106(2), 233–239. <https://doi.org/10.1093/auk/106.2.233>
- Hoffmann, S., Trost, L., Voigt, C., Leitner, S., Lemazina, A., Sagunsky, H., Abels, M., Kollmansperger, S., Maat, A. T., & Gahr, M. (2019). Duets recorded in the wild reveal that interindividually coordinated motor control enables cooperative behavior. *Nature Communications*, 10(1), 2577. <https://doi.org/10.1038/s41467-019-10593-3>
- Hu, C. K., York, R. A., Metz, H. C., Bedford, N. L., Fraser, H. B., & Hoekstra, H. E. (2022). Cis-Regulatory changes in locomotor genes are associated with the evolution of burrowing behavior. *Cell Reports*, 38(7). <https://doi.org/10.1016/j.celrep.2022.110360>
- Hudson, R. R., & Kaplan, N. L. (1985). Statistical properties of the number of recombination events in the history of a sample of DNA sequences. *Genetics*, 111(1), 147–164. <https://doi.org/10.1093/genetics/111.1.147>
- Jhanwar, S., Malkmus, J., Stolte, J., Romashkina, O., Zuniga, A., & Zeller, R. (2021). Conserved and species-specific chromatin remodeling and regulatory dynamics during mouse and chicken limb bud development. *Nature Communications*, 12(1, 1), 5685. <https://doi.org/10.1038/s41467-021-25935-3>
- Junkins, M. S., Bagriantsev, S. N., & Gracheva, E. O. (2022). Towards understanding the neural origins of hibernation. *Journal of Experimental Biology*, 225(1), jeb229542. <https://doi.org/10.1242/jeb.229542>
- Kays, R., Crofoot, M. C., Jetz, W., & Wikelski, M. (2015). Terrestrial animal tracking as an eye on life and planet. *Science*, 348(6240), aaa2478. <https://doi.org/10.1126/science>

- Langslow, D. R. (1979). Movements of Blackcaps ringed in Britain and Ireland. *Bird Study*, 26(4), 239–252. <https://doi.org/10.1080/00063657909476644>
- Liedvogel, M., Åkesson, S., & Bensch, S. (2011). The genetics of migration on the move. *Trends in Ecology and Evolution*, 26(11), 561–569. <https://doi.org/10.1016/j.tree.2011.07.009>
- Lovette, I. J., & Fitzpatrick, J. W. (2016). *Handbook of Bird Biology*. Wiley.
- Merritt, J. R., Grogan, K. E., Zinzow-Kramer, W. M., Sun, D., Ortlund, E. A., Yi, S. V., & Maney, D. L. (2020). A supergene-linked estrogen receptor drives alternative phenotypes in a polymorphic songbird. *Proceedings of the National Academy of Sciences*, 117(35), 21673–21680. <https://doi.org/10.1073/pnas.2011347117>
- Mickelsen, L. E., Bolisetty, M., Chimileski, B. R., Fujita, A., Beltrami, E. J., Costanzo, J. T., Naparstek, J. R., Robson, P., & Jackson, A. C. (2019). Single-cell transcriptomic analysis of the lateral hypothalamic area reveals molecularly distinct populations of inhibitory and excitatory neurons. *Nature Neuroscience*, 22(4, 4), 642–656. <https://doi.org/10.1038/s41593-019-0349-8>
- Moffitt, J. R., Bambah-Mukku, D., Eichhorn, S. W., Vaughn, E., Shekhar, K., Perez, J. D., Rubinstein, N. D., Hao, J., Regev, A., Dulac, C., & Zhuang, X. (2018). Molecular, spatial, and functional single-cell profiling of the hypothalamic preoptic region. *Science*, 362(6416), eaau5324. <https://doi.org/10.1126/science.aau5324>
- Mouritsen, H., Feenders, G., Liedvogel, M., Wada, K., & Jarvis, E. D. (2005). Night-vision brain area in migratory songbirds. *Proceedings of the National Academy of Sciences*, 102(23), 8339–8344. <https://doi.org/10.1073/pnas.0409575102>
- Nadachowska-Brzyska, K., Burri, R., Smeds, L., & Ellegren, H. (2016). PSMC analysis of effective population sizes in molecular ecology and its application to black-and-white Ficedula flycatchers. *Molecular Ecology*, 25(5), 1058–1072. <https://doi.org/10.1111/mec.13540>
- Newton, I. (2010). *Bird Migration* (3rd ed.). Collins.
- Newton, I., & Brockie, K. (2008). *The Migration Ecology of Birds*. Academic Press.
- Perdeck, A. C. (1958). Two Types of Orientation in Migrating Starlings, *Sturnus vulgaris* L., And Chaffinches, *Fringilla coelebs* L., As Revealed by Displacement Experiments. *Ardea*, 55(1–2), 1–2. <https://doi.org/10.5253/arde.v1i2.p1>
- Preuss, N. (2011). Hans Christian Cornelius Mortensen: Aspects of his Life and of the History of Bird Ringing. *Ardea*, 89(1), 1–10.
- Pulido, F. (2007). The Genetics and Evolution of Avian Migration. *BioScience*, 57(2), 165–174. <https://doi.org/10.1641/B570211>
- Pulido, F., Berthold, P., & van Noordwijk, A. (1996). Frequency of migrants and migratory activity are genetically correlated in a bird population: Evolutionary implications. *Proceedings of the National Academy of Sciences*, 93(25), 14642–14647. <https://doi.org/>

- Rastogi, A., Kumari, Y., Rani, S., & Kumar, V. (2013). Neural Correlates of Migration: Activation of Hypothalamic Clock(s) in and out of Migratory State in the Blackheaded Bunting (*Emberiza melanocephala*). *PLoS ONE*, 8(10), 1–12. <https://doi.org/10.1371/journal.pone.0070065>
- Rowan, W. (1925). Relation of Light to Bird Migration and Developmental Changes. *Nature*, 115(2892), 494–495. <https://doi.org/10.1038/115494b0>
- Rowan, W. (1930). Experiments in bird migration. II. Reversed Migration. *Proceedings of the National Academy of Sciences*, 16(7), 520–525. <https://doi.org/10.1073/pnas.16.7.520>
- Rowan, W. (1932). Experiments in Bird Migration. III. The Effects of Artificial Light, Castration and Certain Extracts on the Autumn Movements of the American Crow (*Corvus brachyrhynchos*). *Proceedings of the National Academy of Sciences*, 18(11), 639–654. <https://doi.org/10.1073/pnas.18.11.639>
- Sánchez-Valpuesta, M., Suzuki, Y., Shibata, Y., Toji, N., Ji, Y., Afrin, N., Asogwa, C. N., Kojima, I., Mizuguchi, D., Kojima, S., Okanoya, K., Okado, H., Kobayashi, K., & Wada, K. (2019). Corticobasal ganglia projecting neurons are required for juvenile vocal learning but not for adult vocal plasticity in songbirds. *Proceedings of the National Academy of Sciences of the United States of America*, 116(45), 22833–22843. <https://doi.org/10.1073/pnas.1913575116>
- Schüz, E., & Weigold, H. (1931). *Atlas des Vogelzugs nach den Beringungsergebnissen bei palaearktischen Vögeln*. Friedlander & Sohn.
- Shafer, M. E. R., Sawh, A. N., & Schier, A. F. (2022). Gene family evolution underlies cell-type diversification in the hypothalamus of teleosts. *Nature Ecology & Evolution*, 6(1, 1), 63–76. <https://doi.org/10.1038/s41559-021-01580-3>
- Shirihai, H., Gargallo, G., & Helbig, A. (2010). *Sylvia Warblers: Identification, taxonomy and phylogeny of the genus Sylvia*. Bloomsbury Publishing.
- Singh Alvarado, J., Goffinet, J., Michael, V., Liberti, W., Hatfield, J., Gardner, T., Pearson, J., & Mooney, R. (2021). Neural dynamics underlying birdsong practice and performance. *Nature*, 1–5. <https://doi.org/10.1038/s41586-021-04004-1>
- Sjöberg, S., Malmiga, G., Nord, A., Andersson, A., Bäckman, J., Tarka, M., Willemoes, M., Thorup, K., Hansson, B., Alerstam, T., & Hasselquist, D. (2021). Extreme altitudes during diurnal flights in a nocturnal songbird migrant. *Science*, 372(6542), 646–648. <https://doi.org/10.1126/science.abe7291>
- Sjöberg, S., Pedersen, L., Malmiga, G., Alerstam, T., Hansson, B., Hasselquist, D., Thorup, K., Tøttrup, A. P., Andersson, A., & Bäckman, J. (2018). Barometer logging reveals new dimensions of individual songbird migration. *Journal of Avian Biology*, 49(9), e01821. <https://doi.org/10.1111/jav.01821>
- Takahashi, S., Hombe, T., Matsumoto, S., Ide, K., & Yoda, K. (2022). Head direction cells in a migratory bird prefer north. *Science Advances*, 8(5), eabl6848. <https://doi.org/10.1126/sciadv.abl6848>

- Tanaka, M., Sun, F., Li, Y., & Mooney, R. (2018). A mesocortical dopamine circuit enables the cultural transmission of vocal behaviour. *Nature*, 563(7729), 117–120. <https://doi.org/10.1038/s41586-018-0636-7>
- Tinbergen, N. (1963). On aims and methods of Ethology. *Zeitschrift Für Tierpsychologie*, 20(4), 410–433. <https://doi.org/10.1111/j.1439-0310.1963.tb01161.x>
- Van Doren, B. M., Conway, G. J., Phillips, R. J., Evans, G. C., Roberts, G. C. M., Liedvogel, M., & Sheldon, B. C. (2021). Human activity shapes the wintering ecology of a migratory bird. *Global Change Biology*, 27(12), 2715–2727. <https://doi.org/10.1111/gcb.15597>
- Van Doren, B. M., Sheldon, D., Geevarghese, J., Hochachka, W. M., & Farnsworth, A. (2015). Autumn morning flights of migrant songbirds in the northeastern United States are linked to nocturnal migration and winds aloft. *The Auk*, 132(1), 105–118. <https://doi.org/10.1642/AUK-13-260.1>
- Vijay, N., Weissensteiner, M., Burri, R., Kawakami, T., Ellegren, H., & Wolf, J. B. W. (2017). Genomewide patterns of variation in genetic diversity are shared among populations, species and higher-order taxa. *Molecular Ecology*, 26(16), 4284–4295. <https://doi.org/10.1111/mec.14195>
- Wakeley, J. (2008). *Coalescent Theory: An Introduction* (1st ed.). W. H. Freeman.
- Warren, T. L., Tumer, E. C., Charlesworth, J. D., & Brainard, M. S. (2011). Mechanisms and time course of vocal learning and consolidation in the adult songbird. *Journal of Neurophysiology*, 106(4), 1806–1821. <https://doi.org/10.1152/jn.00311.2011>
- Wiltschko, W. (1968). Über den Einfluß statischer Magnetfelder auf die Zugorientierung der Rotkehlchen (*Erithacus rubecula*). *Zeitschrift Für Tierpsychologie*, 25(5), 537–558. <https://doi.org/10.1111/j.1439-0310.1968.tb00028.x>
- Wingfield, J. C., Schwabl, H., & Mattocks, P. W. (1990). Endocrine Mechanisms of Migration. In E. Gwinner (Ed.), *Bird Migration* (pp. 232–256). Springer. https://doi.org/10.1007/978-3-642-74542-3_16
- Zapka, M., Heyers, D., Hein, C. M., Engels, S., Schneider, N.-L., Hans, J., Weiler, S., Dreyer, D., Kishkinev, D., Wild, J. M., & Mouritsen, H. (2009). Visual but not trigeminal mediation of magnetic compass information in a migratory bird. *Nature*, 461(7268, 7268), 1274–1277. <https://doi.org/10.1038/nature08528>
- Zapka, M., Heyers, D., Liedvogel, M., Jarvis, E. D., & Mouritsen, H. (2010). Night-time neuronal activation of Cluster N in a day- and night-migrating songbird. *European Journal of Neuroscience*, 32(4), 619–624. <https://doi.org/10.1111/j.1460-9568.2010.07311.x>
- Zúñiga, D., Gager, Y., Kokko, H., Fudickar, A. M., Schmidt, A., Naef-Daenzer, B., Wikelski, M., & Partecke, J. (2017). Migration confers winter survival benefits in a partially migratory songbird. *eLife*, 6, e28123. <https://doi.org/10.7554/eLife.28123>

2

Distinct Patterns of Genetic Variation at Low-Recombining Genomic Regions Represent Haplotype Structure

“God grant me the serenity to accept the things I cannot change, courage to change the things I can, and wisdom always to tell the difference.” Among the things Billy Pilgrim could not change were the past, the present, and the future.

– Kurt Vonnegut, Slaughterhouse-Five (1969)

Distinct patterns of genetic variation at low-recombining genomic regions represent haplotype structure

Jun Ishigohoka^{1,*} Karen Bascón-Cardozo¹ Andrea Bours¹ Janina Fuß²
 Arang Rhie³ Jacquelyn Mountcastle⁴ Bettina Haase⁴ William Chow⁵
 Joanna Collins⁵ Kerstin Howe⁵ Marcela Uliano-Silva⁵ Olivier Fedrigo⁴
 Erich D. Jarvis^{4,6,7} Javier Pérez-Tris⁸ Juan Carlos Illera⁹
 Miriam Liedvogel^{1,10,*}

¹Max Planck Institute for Evolutionary Biology, Plön, Germany

²Institute of Clinical Molecular Biology (IKMB), Kiel University, Kiel, Germany

³Genome Informatics Section, Computational and Statistical Genomics Branch, National Human Genome Research Institute, National Institutes of Health, Bethesda, MD, USA

⁴The Vertebrate Genome Lab, Rockefeller University, New York, NY, USA

⁵Wellcome Sanger Institute, Cambridge, UK

⁶Laboratory of Neurogenetics of Language, Rockefeller University, New York, NY, USA

⁷The Howards Hughes Medical Institute, Chevy Chase, MD, USA

⁸Department of Biodiversity, Ecology and Evolution, Complutense University of Madrid, Madrid, Spain

⁹Biodiversity Research Institute (CSIC-Oviedo University-Principality of Asturias), Oviedo University, Mieres, Spain

¹⁰Institute of Avian Research, Wilhelmshaven, Germany

* Correspondence: [Jun Ishigohoka <ishigohoka@evolbio.mpg.de>](mailto:ishigohoka@evolbio.mpg.de), [Miriam Liedvogel <liedvogel@evolbio.mpg.de>](mailto:liedvogel@evolbio.mpg.de)

Abstract

Genetic variation of the entire genome represents population structure, yet individual loci can show distinct patterns. Such deviations identified through genome scans have often been attributed to effects of selection instead of randomness. This interpretation assumes that long enough genomic intervals average out randomness in underlying genealogies, which represent local genetic ancestries. However, an alternative explanation to distinct patterns has not been fully addressed: too few genealogies to average out the effect of randomness. Specifically, distinct patterns of genetic variation may be due to reduced local recombination rate, which reduces the number of genealogies in a genomic window. Here, we associate distinct patterns of local genetic variation with reduced recombination rates in a songbird, the Eurasian blackcap (*Sylvia atricapilla*), using genome sequences and recombination maps. We find that distinct patterns of local genetic variation reflect haplotype structure at low-recombining regions either shared in most populations or found only in a few populations. At the former species-wide low-recombining regions, genetic variation depicts conspicuous haplotypes segregating in multiple populations. At the latter population-specific low-recombining regions, genetic variation represents variance among cryptic haplotypes within the low-recombining populations. With simulations, we confirm that these distinct patterns of haplotype structure evolve due to reduced recombination rate, on which the effects of selection can be overlaid. Our results highlight that distinct patterns of genetic variation can emerge through evolution of reduced local recombination rate. Recombination landscape as an evolvable trait therefore plays an important role determining the heterogeneous distribution of genetic variation along the genome.

Introduction

Patterns of genetic variation in the genome represent ancestries of sequences and are influenced by population history. While genome-wide genetic variation represents population structure (McVean, 2009; Patterson et al., 2006), randomness in genealogies also contributes to fluctuation of local genetic variation along recombining chromosomes. Specifically, genealogies can differ between loci even under the same population history (Dutheil et al., 2009; Martin & Van Belleghem, 2017; McVean & Cardin, 2005; Pamilo & Nei, 1988; Wakeley, 2008, 2020; Wiuf & Hein, 1999). This is because realisation of a genealogy under a given population history is a probabilistic process: an ancestral haplotype for a set of individuals at one locus is not necessarily a common ancestor of the same set of individuals at another locus (Shipilina et al., 2023). Patterns of local genetic variation along the genome tend to conform with the population structure with random fluctuation (Fig. 1).

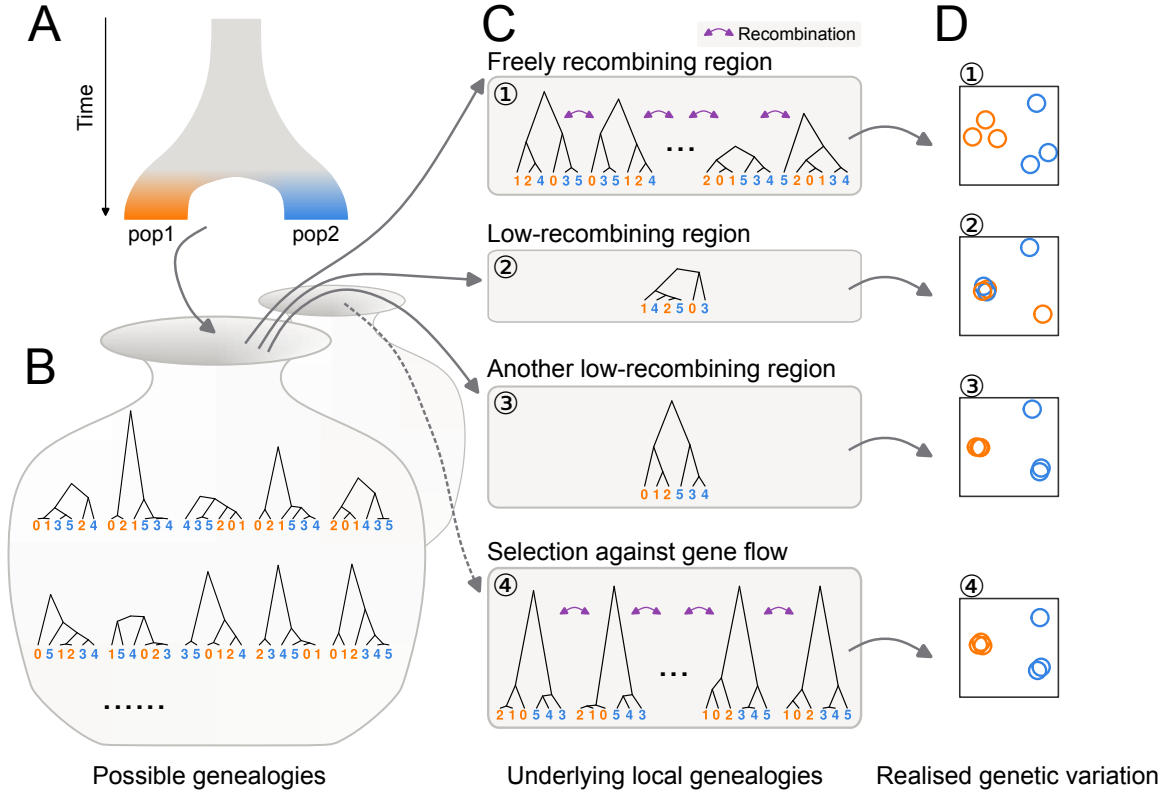


Figure 1: Distinct patterns of genetic variation can be due to reduced recombination rate. Population history (A) affects the distribution of possible genealogies (B) from which local genealogies are drawn (C). The number of genealogies in a genomic interval with a fixed physical length depends on the local recombination rate (C). Mutations occurring on the genealogies (not shown) determine the patterns of realised genetic variation. The realised genetic variation can be summarised and visualised with various methods such as PCA (D). (1) In freely recombining neutral regions, mutations represent many genealogies and hence the pattern of genetic variation converges to the population structure. (2, 3) In low-recombining neutral regions, mutations represent few genealogies covering the region leading to patterns of genetic variation distinct from the population structure. (3) Due to randomness in sampling of genealogies, some of such distinct patterns can be similar to patterns expected at targets of selective factors (c.f. 4). (4) At targets of selection, distribution of possible genealogies is different from that at neutral regions, which is depicted as a different set of possible genealogies in B and the dotted arrow.

Inference of population structure as well as other genome-wide analyses based on genetic variation take advantage of a sufficient number of unlinked variable sites (e.g. single nucleotide polymorphisms (SNPs)) to eliminate the effect of randomness. One of the most common methods to summarise population structure based on this approach is principal component analysis (PCA) applied on a whole-genome genotype table (McVean, 2009; Price et al., 2006). In a whole-genome PCA, variation among individuals based on variable sites of the entire genome are usually projected onto a few major axes (some analyses use many more axes), and

the distances among individuals on these reduced dimensions represent genetic differences. Summarising population structure and other related measures using the entire genome has been proven to be an effective approach to eliminate random fluctuation of genealogies along the genome (Bhatia et al., 2013; Cao et al., 2020; Fedorova et al., 2013; Peter, 2022; Shao et al., 2023).

However, some fundamental biological questions concern selective factors that systematically bias the shape of genealogies at a genomic local scale, shifting the expected patterns of genetic variation from the population structure. For example, patterns of local genetic variation are distinct under selection against gene flow (Fig. 1C4), positive selection and adaptive introgression because they affect coalescence rate, topology, and branch lengths of the underlying genealogies (Hejase et al., 2020; Martin et al., 2015; Setter et al., 2020; Speidel et al., 2019; Wolf & Ellegren, 2017). Empirically, genome scans of population genetic summary statistics have been commonly used to identify regions with distinct patterns of genetic variation (Delmore et al., 2018; Irwin et al., 2018; Kawakami et al., 2017; Roesti et al., 2013; Rougemont et al., 2021). Many of these have identified regions with distinct patterns, such as elevated differentiation and reduced diversity, within low-recombining genomic regions (Geraldes et al., 2011; Kawakami et al., 2017; Renaut et al., 2013; Roesti et al., 2013, 2013; Rougemont et al., 2021). Distinct patterns at low-recombining regions can influence the chromosome-wide (Knief et al., 2016; Neafsey et al., 2010) and even genome-wide population structure (Mérot et al., 2021). These associations between distinct patterns of genetic variation at “outlier regions” or “genomic islands” and reduced recombination rate is often interpreted as linked selection (Burri et al., 2015; Burri, 2017; Delmore et al., 2015, 2018; Irwin et al., 2018; Kawakami et al., 2017; Roesti et al., 2013; Rougemont et al., 2021; Van Doren et al., 2017). However, a non-selective explanation is equally conceivable and yet often overlooked: the focal genomic region may contain too few underlying genealogies for a genome scan to eliminate the effect of random fluctuation simply due to low recombination rate, which is represented as the distinct patterns of genetic variation (Booker et al., 2020; Lotterhos, 2019). Specifically, it has not been well studied what aspects of distinct patterns of genetic variation can be explained by reduced recombination rate, and what other aspects reflect the effect of selection.

We address the effect of reduced recombination rate on local genetic variation using a songbird species, Eurasian blackcap (*Sylvia atricapilla*, hereafter “blackcap”), which is characterised by variability in seasonal migration across its distribution range (Berthold, 1988, 1991; Delmore et al., 2020a; Helbig, 1991). Populations with diverged migratory phenotypes split as recently as ~30,000 years ago, likely corresponding to the last glacial period and now exhibit population structure (Fig. 2A-C, Sup. Fig. 1) (Delmore et al., 2020b). Due to their recent split and relatively large effective population size, genetic differentiation is very low among blackcap populations (Delmore et al., 2020b). The presence of population structure albeit with the low levels of differentiation makes the blackcap a perfect system to investigate local deviations of genetic variation: even the slightest effects of factors that change local genetic variation are likely detectable because such effects are not obscured by population structure. In addition, fine-scale recombination maps for multiple populations are available for this species (Bascón-Cardozo et al., 2022a), facilitating investigation of the relationship between changes in the recombination landscape and locally distinct patterns of genetic variation.

By leveraging a large-scale genomic re-sequencing dataset, we first systematically explore distinct patterns of local genetic variation along the blackcap genome, and compare these with genomic regions exhibiting reduced recombination rate. We further investigate the patterns of genetic variation in outlier regions and associate them with the prevalence of recombination suppression across populations. We also conduct simulations to analyse how reduced local recombination rate in the entire species and in a subpopulation with and without selection affects patterns of genetic variation through time. Finally, we propose a model of local genetic variation representing haplotype structure corresponding to evolutionary changes in local recombination rate.

Results

Chromosome-level reference assembly

To allow population genomic analyses in the blackcap system, we generated a chromosome-level reference genome using the Vertebrate Genomes Project pipeline v1.5 (Rhie et al., 2021). We collected blood of a female blackcap from Tarifa, Spain population. We generated contigs from Pacbio long reads, sorted haplotypes, and scaffolded them with 10X Genomics linked reads, Bionano Genomics optical mapping, and Arima Genomics Hi-C linked reads. Base call errors were polished with both PacBio long reads and Arrow short reads to achieve above Q40 accuracy (no more than 1 error every 10,000 bp). Manual curation identified 33 autosomes and Z and W chromosomes (plus 1 unlocalised W). Autosomes were named in decreasing order of size, and all had counterparts in the commonly used VGP reference zebra finch assembly (Sup. Table 2). The final 1.1 Gb assembly had 99.14% assigned to chromosomes, with a contig N50 of 7.4 Mb, and scaffold N50 of 73 Mb, indicating a high-quality assembly that fulfills the VGP standard metrics. The primary and alternate haplotype assemblies are provided under NCBI BioProject PRJNA558064, accession numbers GCA_009819655.1 and GCA_009819715.1.

Deviation of genetic variation coincides with low-recombining regions

To investigate the genome-wide distribution of genetic variation, we mapped short reads of the whole-genomes of 179 blackcaps including 69 newly sequenced individuals (Sup. Table 1) on a *de novo*-assembled reference genome generated through the Vertebrate Genomes Project (VGP, Rhie et al., 2021), and called SNPs ([Materials and Methods](#)). To characterise genome-wide genetic variation, we performed PCA using SNPs in all autosomes, revealing population structure. While PC1 and PC2 represented differentiation of island populations (Fig. 2B), PC3 represented structure within continental populations with different migratory phenotypes (Fig. 2C). To identify genomic regions with patterns of genetic variation distinct from the population structure, we performed local PCA using **lostruct** (Li & Ralph, 2019). Briefly, **lostruct** performs PCA in sliding genomic windows and dissimilarity of PCA among windows are summarised with multidimensionality scaling (MDS). Distinct patterns of genetic variation of windows relative to the background are represented by extreme values along

the MDS axes. Multiple windows with correlated patterns of genetic variation distinct from the population structure are represented by extreme values along the same MDS axis. This approach allowed systematic and unbiased exploration unaffected by our definition of populations of the blackcaps. We performed `lostruct` on both genotype and phased haplotype data with window size of 1,000 SNPs. We identified outlier windows by applying threshold MDS values (the mode of the distribution ± 0.3). We further identified genomic regions with distinct patterns of genetic variation by finding genomic intervals longer than 100 kb with at least five outlier windows based on the same MDS axis and merging the intervals based on the genotype- and phased haplotype-based approaches. This yielded 32 genomic regions with distinct patterns of variation (hereafter “outlier regions”, Fig. 2D, Sup. Table 3, Sup. Fig. 3). Their size ranged from 0.12 to 8.11 Mb (mean and median of 0.71 and 0.29 Mb), and each region contained 5,000 to 356,000 SNPs. Comparing the genomic distribution of these outlier regions to population-level recombination maps, we found that low-recombining regions (nominally recombination rate lower than the 20 percentile of each chromosome) were significantly enriched in the outlier regions (permutation tests with $n = 1,000$, $p\text{-value} = 0.000$ (Sup. Fig. 10)). Among these 32 outlier regions, 19 coincided with regions in which recombination rate was reduced in most tested populations (“species-wide” low-recombining regions), 11 coincided with regions in which recombination rate was reduced in one or two populations (“population-specific” low-recombining regions), and two did not coincide with low-recombining regions in any population (Fig. 2E, F, Sup. Fig. 9).

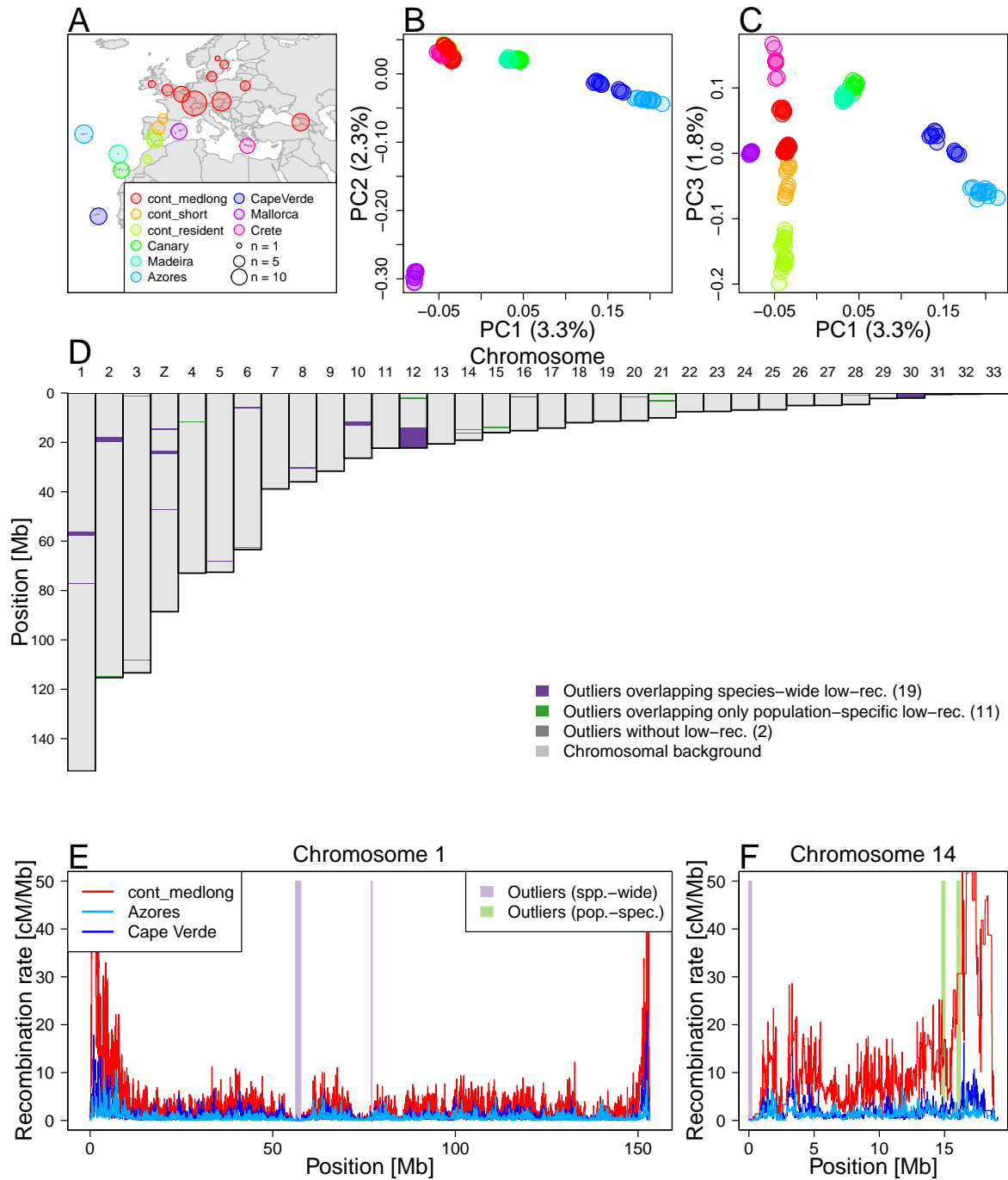


Figure 2: Local PCA outliers coincide with species-wide and population-specific low-recombining regions **A.** Geographic location of blackcap populations included in this study. Each point on the map represents a sampling location where multiple individuals were sampled. Populations were defined based on the geographic location, migratory phenotype, and genomic-wide population structure. **B, C.** Genome-wide PCA illustrating population structure. **D.** Distribution of outlier regions based on local PCA using *lostruct*. **E, F** Inferred recombination rates along two exemplified chromosomes (chromosomes 1 and 14) in three blackcap populations (cont_medlong, Azores, and Cape Verde). In **D-F**, purple and green shades respectively indicate positions of outliers that coincide with species-wide and population-specific low-recombining regions. The two green shades in **F** both overlap with Azores and Cape Verde-specific low-recombining regions. cont_medlong: medium and long distance migrant population breeding on the continent; cont_short: short distance migrant population breeding on the continent; cont_res: resident (non-migrant) population breeding on the continent. All island populations (Canary, Madeira, Azores, Cape Verde, Mallorca and Crete) are resident.

To further investigate the outlier regions, we separately performed PCA using SNPs in each region, revealing diverse patterns of distinct genetic variation (Fig. 3A-C top). First, species-wide low-recombining regions showed different levels of clustering of individuals in PCA (Sup. Fig. 6). Specifically, the PCA projections consisted of either three distinct clusters (Fig. 3A top, Sup. Fig. 6), six loose clusters (Fig. 3B top, Sup. Fig. 6), or mixture of all individuals without apparent clustering (Sup. Fig. 6), suggesting that they represent haplotype structure with different numbers of low-recombining alleles. These clusters did not clearly separate populations, indicating a greater contribution of haplotype structure than the population structure. Four of these (e.g. Fig. 3A top, Sup. Figs. 6, 11) had the clearest clustering patterns with three groups of individuals in PCA, which is expected for a haplotype block with two distinct alleles (Huang et al., 2020; Ma & Amos, 2012; Todesco et al., 2020). Two of these regions showed LD patterns consistent with segregating inversions (Fig. 3A bottom, Sup. Fig. 12), and the other two showed patterns of non-inversion haplotype blocks (Sup. Fig. 12), indicating that recombination suppression with different mechanisms resulted in similar patterns of genetic variation due to presence of two distinct segregating haplotypes.

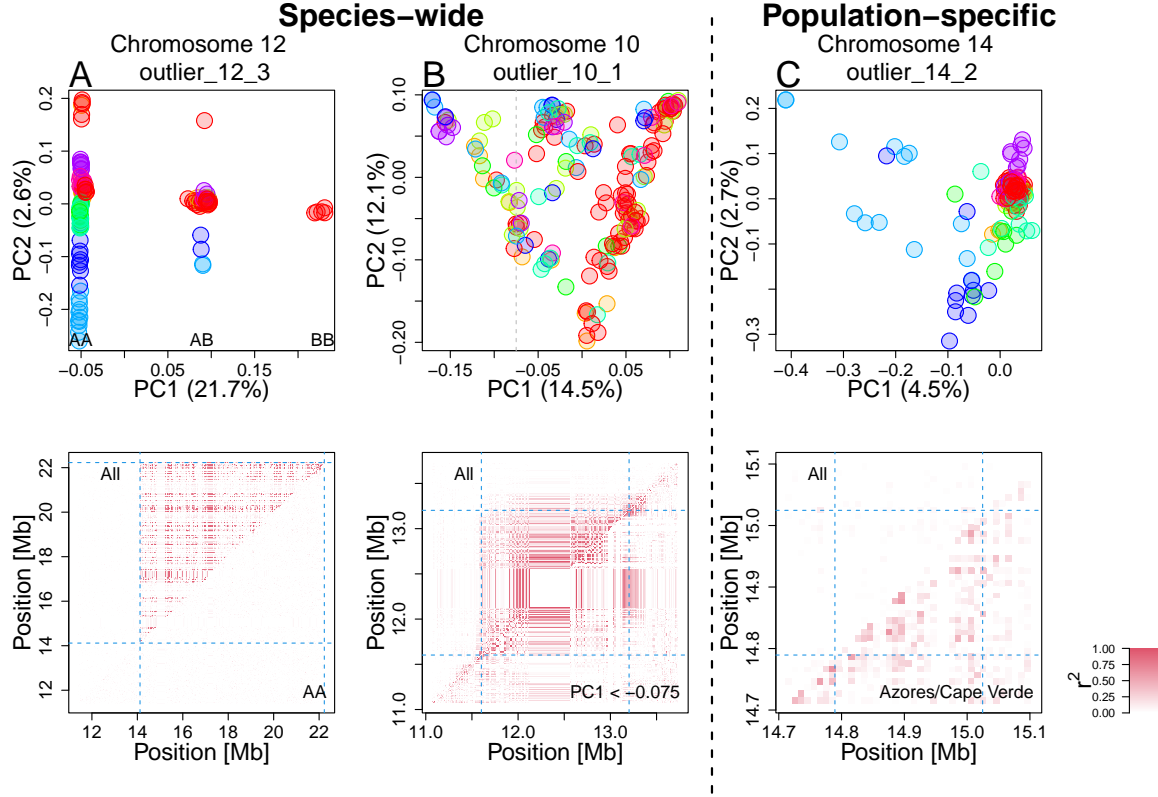


Figure 3: Patterns of genetic variation and linkage disequilibrium at local PCA outliers
Top: PCA at exemplified outlier regions visualising the patterns of local genetic variation. Data points represent blackcap individuals colour-coded by population as depicted in Fig. 2. **Bottom:** LD calculated for all individuals (top-left diagonal) and for subset individuals (bottom-right diagonal). **A.** A putative inversion. Three clusters correspond to combination of two non-recombining alleles possessed by individuals, depicted as AA, AB, and BB. LD calculated using AA individuals is not elevated, in line with heterozygote-specific recombination suppression at an inversion locus (Sup. Fig. 14). **B.** A species-wide low-recombining region with six loose clusters of individuals. LD calculated using subset individuals was elevated, suggesting genotype-non-specific recombination suppression. **C.** A population-specific low-recombining region. The variance in genetic distances between individuals of the low-recombining populations (Azores (blue) and Cape Verde (light blue)) is greater than between other pairs of individuals (top). LD calculated using individuals of the low-recombining populations is elevated (bottom).

Second, population-specific low-recombining regions exhibited distinct patterns of genetic variation consistently across the outlier regions. While individuals from the low-recombining populations were spread in PCA projections, individuals of other populations were more densely clustered (Fig. 3C top, Sup. Fig. 7). This pattern indicates that the variance in genetic distances between a pair of individuals of the low-recombining populations is greater than between individuals of normally recombining populations. LD was elevated only in the low-recombining populations (Fig. 3C bottom), supporting population-specific reduction in

recombination rate.

Reduced recombination rate generates distinct patterns of genetic variation

To discern the effect of reduced recombination rate, demographic history, and unequal sample sizes among population on outlier regions, we performed neutral coalescent simulations using `msprime` (Baumdicker et al., 2022). We prepared 11 scenarios differing in the presence/absence of population subdivision, equal/unequal sizes of populations, presence/absence of gene flow between populations, and recombination rate in the middle of the chromosome relative to the chromosomal background (Sup. Fig. 19, Sup. Table 8). We applied `lostruct` on the simulated data to identify outlier regions. In all 1,000 replicates, reduced local recombination rate resulted in distinct patterns of genetic variation irrespective of the population structure and demographic history (Sup. Fig. 20). We also asked whether population genetic summary statistics are affected. The mean nucleotide diversity (π), Tajima's D, and F_{ST} were not affected, yet the variance of these statistics was greater within the low-recombining region than in the chromosomal background (Sup. Figs. 21, 22, 23).

To address how species-wide and population-specific reduction in recombination rate affect the patterns of genetic variation over time, we performed forward simulations using `SLiM` (Haller & Messer, 2022). First, to investigate the effects of species-wide reduction in local recombination rate, we simulated one ancestral population of 1,000 diploids with a low-recombining genomic region that splits into three subpopulations (pop1, pop2, pop3. Fig. 4A). We sampled individuals over time after the populations split and conducted PCA both in the low-recombining and normally recombining genomic regions. PCA patterns at low-recombining regions (Fig. 4B, C, Sup. Fig. 24) were distinct from normally recombining regions (Fig. 4D). The low-recombining regions exhibited three, six, or more clusters of individuals resembling our empirical results. The clusters of individuals represented genotypes consisting of different combinations of ancestral haplotypes (Sup. Fig. 25). The distinct patterns representing haplotype structure persisted until population structure started to emerge along the PC axes (Fig. 4B, C). Accordingly, the percentages of variation explained by PC1 and PC2 were higher at low-recombining regions than in normally recombining region until this transition (Fig. 4C).

Distinct patterns in the low-recombining regions persisted over longer times than it took for population structure in normally recombining region to emerge (Fig. 4D). These results suggest that distinct patterns of genetic variation in species-wide low-recombining regions represent haplotype structure whose transition to the population structure is slower than in normally recombining regions.

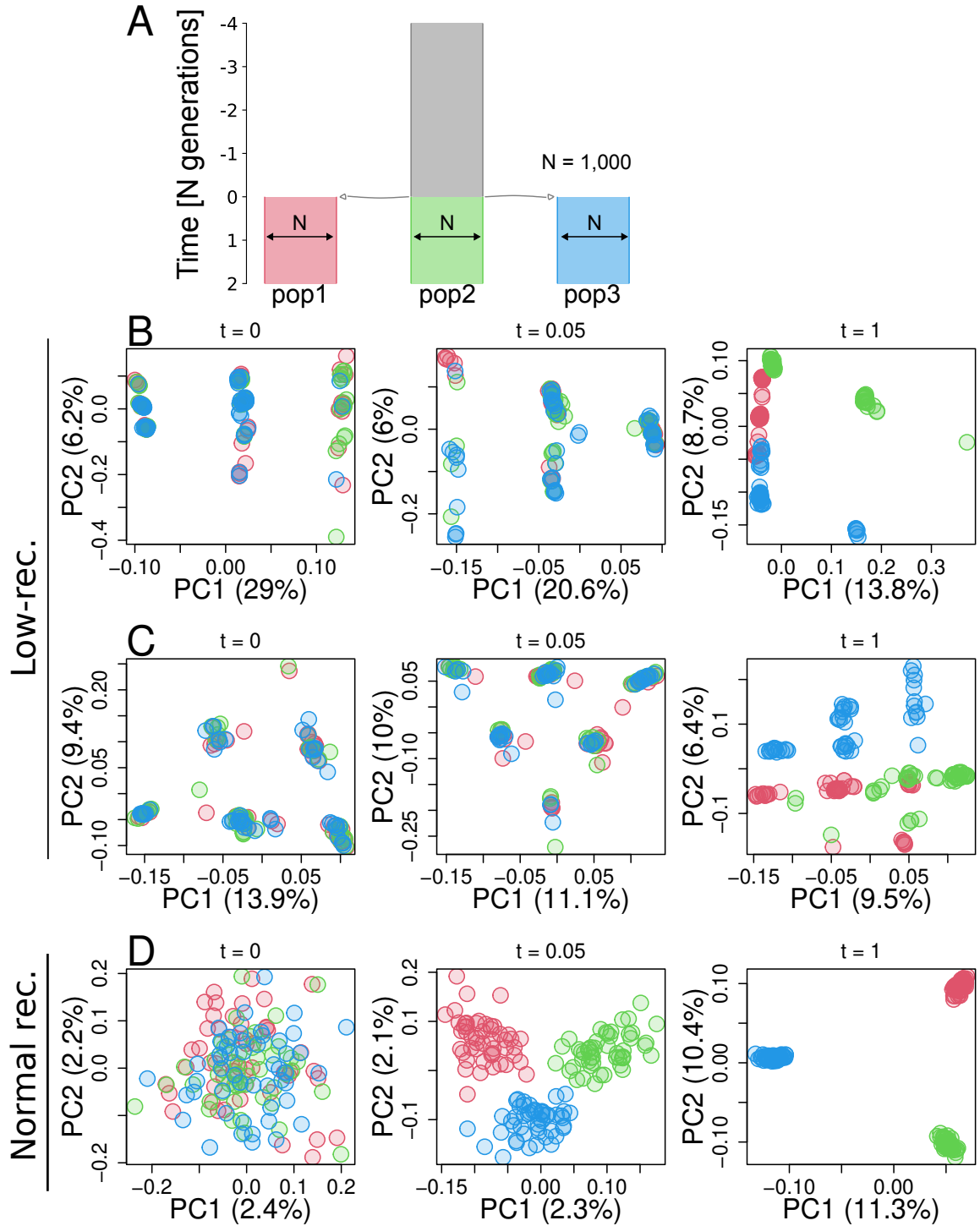


Figure 4: Simulation of a species-wide low-recombining region. **A.** Simulated demography scenario. Our simulated genome contained two chromosomes, one with a low-recombining region and the other without. **B, C.** PCA showing patterns of genetic variation at the species-wide low-recombining region at three time points in three exemplified simulation replicates. **D.** PCA showing patterns of genetic variation at a normally recombining chromosome at three time points in the same replicates as **B.**

Second, to investigate the effects of population-specific reduction in local recombination rate, we performed forward simulations. Three populations (pop1, pop2, and pop3) and their ancestral population had 1,000 diploid individuals, and pop1 evolved a reduced local recombination rate. We considered two cases with respect to when the population-specific reduction in recombination rate is introduced: before or after differentiation of populations. In the first scenario (Sup. Fig. 26), recombination suppression was introduced at the same time as the three populations split, while in the second scenario (Fig. 5A) recombination suppression was introduced 4,000 generations after the split. We conducted PCA in genomic regions with and without population-specific recombination suppression using individuals sampled over time. In both scenarios, the genomic region with population-specific recombination suppression transiently showed distinct patterns of genetic variation (Fig. 5B, Sup. Fig. 26B) resembling the empirical results, while regions without population-specific suppression showed population structure (Fig. 5C). Haplotype structure was not as conspicuous as in species-wide low-recombining regions (Sup. Fig. 27B, F, c.f. Sup. Fig. 25) due to standing genetic variation. Mutations originating in the non-recombining population were enriched in the set of mutations that have the greatest contribution to the distinct pattern of PCA (Sup. Fig. 27C, G. χ^2 tests, p-value = 1.14×10^{-12} for model 1 and p-value = 2.30×10^{-32} for model 2). These mutations were significantly associated with each other in the underlying genealogy sharing common branches compared to other mutations originating in the same population (Sup. Fig. 27D, H. [Materials and Methods](#), Kolmogorov-Smirnov tests, p-value = 7.74×10^{-6} for model 1 and p-value = 0.0012 for model 2), indicating that the distinct pattern of genetic variation represents sets of mutations that occurred in ancestral haplotypes. Associations between these population-specific mutations on ancestral haplotypes would have eventually decayed by recombination events, but in the low-recombining population the association was maintained due to suppressed recombination, resulting in the cryptic haplotype structure.

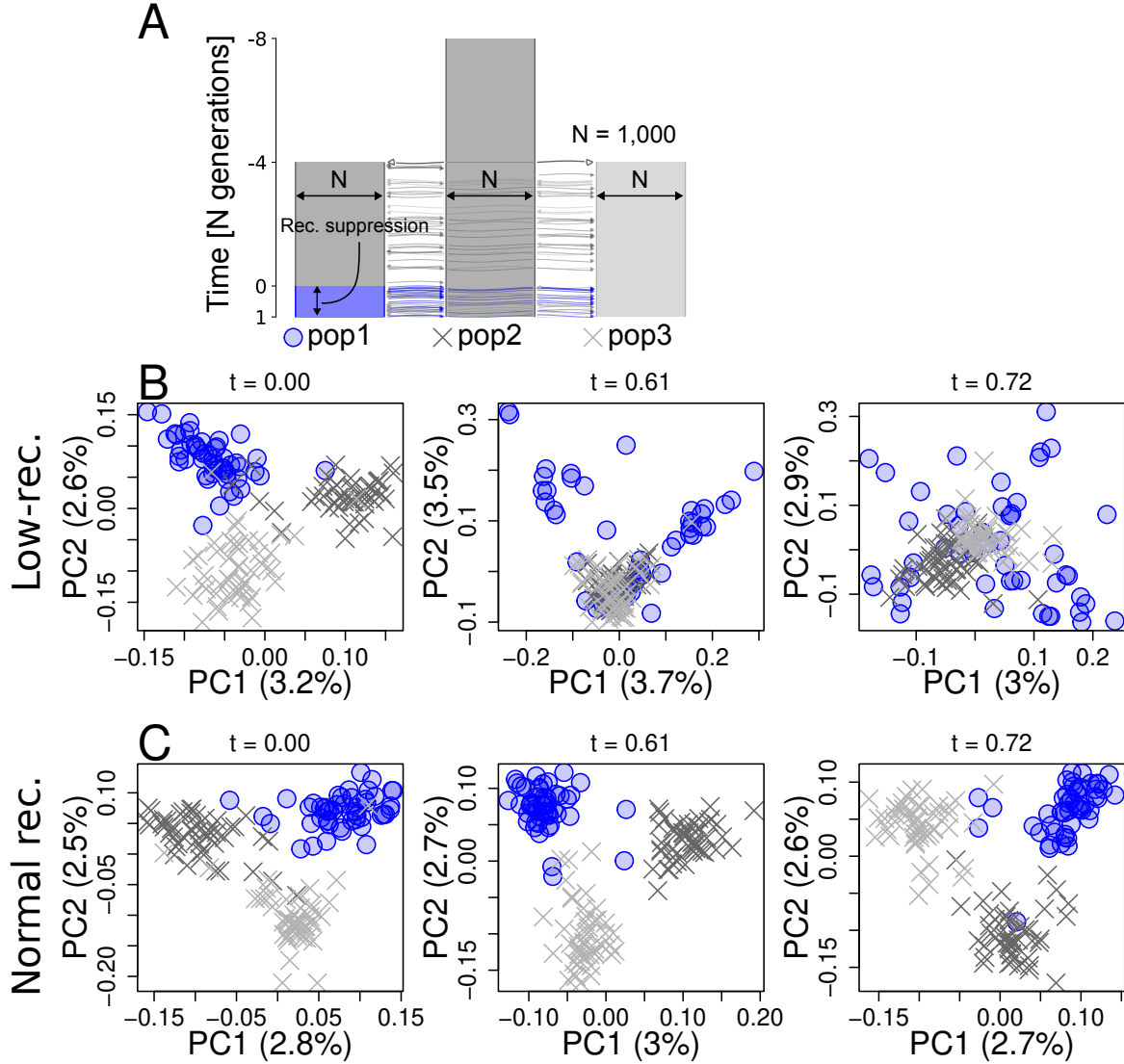


Figure 5: Simulation of a population-specific low-recombining region. **A.** Simulated scenario. Simulated genome contained two chromosomes, one with a population-specific low-recombining region and the other without. **B, C.** PCA showing patterns of genetic variation at the population-specific low-recombining region (**B**) and the normally recombining chromosome (**C**) at three time points in one exemplified simulation replicate.

Effect of selection on patterns of genetic variation

Selection is known to cause distinct patterns of genetic variation (Nielsen, 2005). To test whether the outlier regions based on *lostruct* identified in the blackcap genome are also targets of selection, we measured nucleotide diversity (π) and Tajima's D in each population, as well as ratio between non-synonymous and synonymous substitutions (d_N/d_S) for annotated genes. Many species-wide low-recombining regions showed reduced nucleotide diversity (Sup.

Fig. 28; Sup. Table 9) and Tajima's D (Sup. Fig. 29; Sup. Table 10), suggesting that they are under either positive or purifying selection. Most genes within outlier regions had d_N/d_S below 0 (Sup. Fig. 30) with a few genes with positive d_N/d_S , indicating that most genes are under purifying selection and a few others are under positive selection. Furthermore, sequence analysis indicated that some but not all species-wide low-recombining outlier regions coincide with putative pericentromeric regions with enrichment of long tandem repeats (Sup. Figs. 33, 34). These results indicate that the outlier regions may experience effects of selection in addition to reduced recombination rates.

We asked whether the distinct patterns of local genetic variation at the outlier regions observed in blackcaps represent the effect of selection instead of reduced recombination rates. Specifically, we addressed whether the distinct patterns of genetic variation representing haplotype structure could be caused by (i) purifying or (ii) positive selection alone or if they primarily represent the effect of reduced recombination rate. To this end, we used SLiM to simulate purifying and positive selection with and without reduction in recombination rate, and investigated local genetic variation over time by PCA. First, to investigate the effect of purifying selection, we simulated two chromosomes with and without a species-wide low-recombining region under the same demographic history as the neutral scenario (Fig. 4A) but with different strength of purifying selection by introducing mutations with different ratios between the rates of neutral and deleterious mutations ([Materials and Methods](#)). Distinct patterns of genetic variation representing haplotype structure evolved only in scenarios where recombination rate was reduced irrespective of the distribution of fitness effects (DFE) (Sup. Fig. 31). Stronger purifying selection (DFE with more frequent deleterious mutations in our simulation) decreased the time for distinct patterns of genetic variation at low-recombining regions to be overtaken by population structure (Sup. Fig. 31A, C). Second, to investigate the effect of positive selection, we simulated a chromosome with or without a species-wide low-recombining region under the same demographic history, and introduced a beneficial mutation 100 generations after the population split in one population (Sup. Fig. 32A) or 100 generations before the split in the ancestral population (Sup. Fig. 32D). For simulations in which the beneficial mutation persisted, we recorded the patterns of local genetic variation by

PCA over time. Although positive selection affected patterns of genetic variation compared to the neutral scenario, distinct patterns of genetic variation representing discrete haplotypes were unique to scenarios with reduced recombination rate in both cases (Sup. Fig. 32B-E). These results indicate that distinct patterns of genetic variation represented in local PCA, as in the blackcap outlier regions, primarily reflect haplotype structure due to reduced recombination rate, on which the effect of selection can be overlaid.

Discussion

Distinct patterns of genetic variation at low-recombining regions: Genealogical interpretations

Genealogical noise, genealogical bias, and mutational noise

A number of empirical population genomics studies have identified ecologically and evolutionarily important genomic regions by locating outlier regions with distinct patterns of genetic variation (Jones et al., 2012; Lamichhaney et al., 2016; Lawniczak et al., 2010; Lundberg et al., 2021; Malinsky et al., 2015). Genomic windows in such studies are assumed to be both large enough to eliminate the effect of random fluctuation in local genetic variation and small enough to capture the localised signatures of selection. We showed empirically that genomic regions with distinct patterns of genetic variation identified by a population genomic scan based on principal component analysis (PCA) highly overlap with low-recombining genomic regions (Fig. 2). With simulations, we showed that although selection may affect the amount and pattern of local genetic variation around the target locus, the distinct patterns of genetic variation represented by PCA at low-recombining regions can be primarily explained by haplotype structure due to reduced recombination rate (Figs. 4, 5). We discuss our findings from the perspective of underlying genealogies.

We first define three terms: (1) genealogical noise, (2) genealogical bias, and (3) mutational noise. (1) By “genealogical noise” we refer to the fact that gene genealogies vary along the genome following a null distribution given a population history (Dutheil et al., 2009; Martin & Van Belleghem, 2017; McVean & Cardin, 2005; Wakeley, 2008, 2020; Wiuf & Hein, 1999).

(2) By “genealogical bias” we refer to the fact that selective processes can systematically shift the distribution of local genealogies away from the null distribution. For example, genealogies under positive selection, selection against gene flow, adaptive introgression, and balancing selection are biased due to bursts of coalescence, faster lineage sorting, and introduction and maintenance of long branches (Barton & Etheridge, 2004; Guerrero et al., 2012; Hejase et al., 2020; Martin et al., 2019; Setter et al., 2020; Speidel et al., 2019; Taylor, 2013). On top of these, (3) randomness in the process of mutation causes additional noise in realised genetic variation (Ralph et al., 2020), which we call “mutational noise”. For example, the first and the second halves of a chromosomal interval with a single genealogy can still have slightly different patterns of genetic variation because they represent some finite numbers of different mutations.

Species-wide low-recombining regions

We showed in blackcaps that some distinct patterns of genetic variation are associated with species-wide low-recombining regions (Fig. 2). This is in line with previous studies reporting negative correlation between recombination rate and genetic differentiation (Burri et al., 2015; Burri, 2017; Delmore et al., 2015, 2018; Irwin et al., 2018; Kawakami et al., 2017; Roesti et al., 2013; Rougemont et al., 2021; Van Doren et al., 2017). To investigate what factors affect distinct patterns of genetic variation at low-recombining regions (Fig. 3) in more detail, we performed simulations of low-recombining regions with and without selection, and demonstrated that haplotype structure underlies the distinct patterns which persists only transiently until the effect of the population structure emerges (Figs. 4, 5). This transiency reflects a shift from local genetic variation primarily representing haplotype structure (Lotterhos, 2019; Ma & Amos, 2012) to that representing population structure, which can be interpreted based on the underlying genealogies. Low-recombining regions have few underlying genealogies per interval of a fixed physical length and haplotype structure at such regions tends to reflect their basal branches because basal branches tend to be longer than peripheral branches (Wakeley, 2008). At a time point soon after a population split event, peripheral branches covering more recent times than the population split harbour fewer mutations than basal branches. Therefore, the realised pattern of genetic variation at this stage has the greatest contributions by mutations

on the long basal branches undifferentiated among populations (i.e. consisting standing genetic variation), representing a few ancestral haplotypes that descend the current sample. As time passes after the population split, the proportion of mutations that have occurred after the population split increases while some ancestral haplotypes can be lost by chance (i.e. drift), increasing the contribution of population structure on genetic variation. This type of distinct patterns of genetic variation arises predominantly in low-recombining regions but less so in normally recombining regions. This is because haplotype structure representing a few ancestral lineages would become less prominent with recombination as different segments of a current haplotype can follow distinct ancestries and thus the genealogical noise is effectively averaged out.

Some low-recombining regions may have genealogies with much shorter basal branches than other low-recombining regions because the variance in the basal branch length is greater than peripheral branches (Wakeley, 2008). The over-representation of a few ancestral haplotypes in genetic variation requires long basal branches in the underlying genealogies, and thus low-recombining regions with relatively short basal branches cannot accommodate sufficient mutations to represent distinct ancestral haplotypes. This decreases the relative contribution of genealogical noise compared to mutational noise (Supplementary Notes 1.1). Distinct patterns of genetic variation with varying levels of clustering of individuals in PCA in our empirical results (Sup. Fig. 6) may correspond to different ratios between genealogical and mutational noise due to large variance in the basal branch lengths of underlying genealogies. Specifically, some outlier regions with mixture of individuals from multiple populations without distinct clusters and population subdivision in PCA may have underlying genealogies with short basal branches leading to greater contributions of mutational noise on the realised genetic variation.

Population-specific low-recombining regions

We both empirically and with simulations showed that population-specific low-recombining regions exhibit distinct patterns of genetic variation in which individuals of low-recombining and normally recombining populations have different variance in genetic distances (Fig. 3C, Fig. 5). This unequal variance in low-recombining and normally recombining populations can

be interpreted based on the underlying genealogies (Sup. Fig. 35). We consider the ancestry of current samples of low-recombining and normally recombining populations and split the ancestry at the time T when the population-specific recombination suppression initiated (Sup. Fig. 35A). At time T , there were n_1 and n_2 ancestral haplotypes that descend all current samples in low-recombining and normally recombining populations. At times older than T , the ancestors of the n_1 and n_2 haplotypes may freely recombine within each set, making the genetic distances among ancestral haplotypes within each population close to equidistant (Sup. Fig. 35B). After the initiation of the population-specific reduction in recombination rate, the ancestry of one current sequence of the low-recombining population can be traced back to either one of the n_1 ancestral haplotypes present at the time T (Sup. Fig. 35A). On the contrary, the ancestry of one current sequence of the normally recombining population can be traced back to multiple ancestral haplotypes of the n_2 sequences because of the presence of recombination (Sup. Fig. 35A). From the perspective of mutations, in the low-recombining population, mutations that arose on the same haplotype tend to be linked until the present time because of the suppressed recombination. On the other hand, in the normally recombining population, mutations that arose on the same ancestral haplotype less likely stay linked until the present time because recombination can dissociate them. Because shuffling of haplotypes reduces the variance of genetic distances among sequences, population-specific reduction in recombination rates leads to greater variance in low-recombining population than in normally recombining population as observed in our empirical results and simulations. In short, because of the different recombination rates between the populations, genealogical noise is more efficiently eliminated in the normally recombining population than in the low-recombining population.

The haplotype structure at population-specific low-recombining region is only cryptic and less apparent than in species-wide low-recombining regions because other standing mutations coexist on the same haplotype, which are older than the initiation of the population-specific recombination suppression (Sup. Fig. 27). The elevated PC loadings at linked mutations originating in the low-recombining population could be informative to study evolutionary change in local recombination rate: the ages of such mutations mapped on inferred genealogies might be useful to estimate the timing at which the population-specific recombination suppression

initiated.

In our empirical analyses in blackcaps, we detected the effect of population-specific reduction of recombination rate in Azores and Cape Verde island populations (Fig. 3C, Sup. Fig. 7). It remains unclear why reduced recombination rate in certain populations but not others is reflected as distinct patterns of genetic variation by **lostruct**. The recent split of Azores and Cape Verde populations from other populations, accompanied by reduction in population size and the level of isolation (Delmore et al., 2020b) may have contributed to more efficient spread of reduced recombination rate.

Recombination landscape as a driver of evolution of local genetic variation

Species-wide and population-specific recombination suppression underlying distinct patterns of local genetic variation are probably not independent: reduction in recombination rates that initiates formation of haplotype blocks likely originates from one population and may spread to multiple populations. For example, local recombination rate may be initially reduced in one population in which a segregating inversion originates before it may spread in multiple populations by gene flow (Faria et al., 2019). In line with this view of recombination map as an evolvable trait diverging across populations according to subdivision, recent studies find that divergence in local recombination rate among populations is correlated with genetic divergence (Bascón-Cardozo et al., 2022a; Roesti et al., 2013; Spence & Song, 2019). Future work on the effects of transition from population-specific to species-wide suppression of recombination will fill the gap between the two states.

Besides spread of recombination suppression across populations, there are other paths along which patterns of local genetic variation may change over time. First, change in frequency of one haplotypic variant by drift or gene flow and selection and accumulation of novel mutations may shift the distinct pattern of genetic variation (Rubin et al., 2022). Second, an increase in recombination rate in the region may resolve the distinct pattern of genetic variation and result in emergence of the population structure, because recombination breaks down discrete haplotypes and generates mixed types whereby reducing the variance of genetic variation (Hudson, 1983). These two types of shifts in distinct patterns of genetic

variation are not mutually exclusive. For example, fixation of an inversion results in elevated recombination rate (Smukowski Heil et al., 2015; Stevison et al., 2011) because there are no longer non-recombining heterozygotes in the population. Due to resumed recombination, patterns of local genetic variation in such regions are expected to reflect population structure eventually. The question of how long it takes for an outlier region with distinct patterns of genetic variation to disappear after these events should be focally studied in the future.

In Fig. 6A, we illustrate a model for the evolution of local genetic variation that changes according primarily to the evolution of local recombination rates. Local genetic variation can become distinct from the population structure first by representing emerging haplotype structure associated with population-specific recombination suppression or other types of haplotype blocks (e.g. inversions) in one population. If this recombination suppression spreads throughout all populations, then local genetic variation will start to reflect species-wide haplotype structure. Once the relative contribution of haplotype structure on local genetic variation is reduced by differentiation or disappears by elevated recombination rates, then genetic variation returns to reflect the population structure and consequently the outlier region disappears. The effect of selection on local genetic variation may be overlaid on top (Supplementary Notes 1.2).

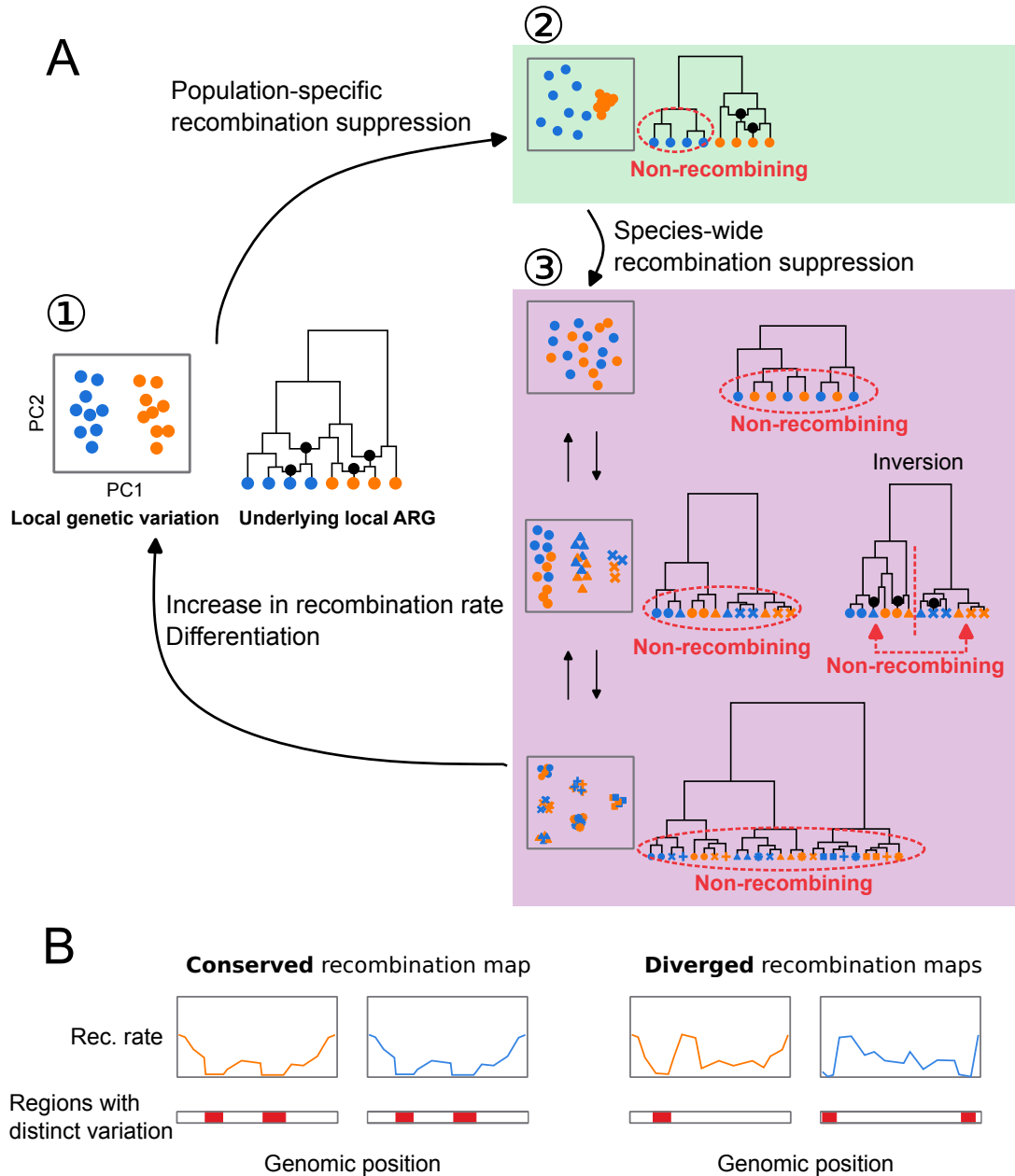


Figure 6: Evolutionary changes in local recombination rate influence evolution of local genetic variation. **A.** Local genetic variation is shown in hypothetical PCA plots. Their underlying genealogies are shown in simplified ancestral recombination graphs (ARGs, (Griffiths & Marjoram, 1997; reviewed in Lewanski et al., 2024)), on which black dots represent ancestral recombination events contributing to the sampled sequences. Points in PCA depict diploid individuals, while those on the ARGs represent haploid sequences. Two colours of these points (blue and orange) indicate two populations. (1) Local genetic variation concordant to population structure. Genetic variation shows separation of individuals from two populations. ARG shows that recombination is suppressed in neither population. (2) Population-specific recombination suppression in the blue population. ARG shows that recombination is suppressed in the blue population. (3) Species-wide recombination suppression. Top: A case in which there are few mutations representing the basal splits of the underlying genealogy at species-wide low-recombining region. Middle: A case in which there are two haplotypic variants at the species-wide low-recombining region. If this is due to presence of an inversion (right ARG), recombination is suppressed between but not within the two clades representing two alleles. Bottom: A case in which there are three haplotypic variants at the species-wide low-recombining region. **B** Evolution of recombination map influences difference in genomic distributions of distinct patterns of genetic variation between species/populations.

Implications

Finally, we discuss technical and biological implications of our study. The technical implication concerns interpretation of genome scans based on local genetic variation. A number of methods based on local genetic variation have been used to detect loci involved in different kinds of selective processes. For example, F_{ST} (differentiation), d_{XY} (divergence), and other population parameters are inferred to detect genomic islands of speciation (Delmore et al., 2018; Hejase et al., 2020; Huang et al., 2020; Malinsky et al., 2015). Reduced diversity (π) is a signature of selection (Delmore et al., 2018; Irwin et al., 2018; Pracana et al., 2017), and by combining it with variation among populations, loci associated with population-specific selection can be also inferred (Yi et al., 2010). Targets of adaptive introgression have been identified by applying statistics based on ABBA-BABA test, which is related to genetic variation (Peter, 2016, 2022), in sliding windows (Kronforst et al., 2013; Martin et al., 2015; Patterson et al., 2012; Reich et al., 2009). However, there are confounding factors that affect inference of these statistics. For example, it has been shown that low diversity can cause elevation in some of these statistics (Cruickshank & Hahn, 2014; Noor & Bennett, 2009). In addition to reduced diversity, this study and others (Booker et al., 2020; Lotterhos, 2019; Renaut et al., 2013) show that reduced recombination rate also causes distinct patterns of genetic variation which can lead to erroneous identification of regions under influence of selective factors. Examining recombination rates at identified regions and comparing them to other regions are necessary to avoid this. For instance, apparent outliers in only few (pairs of) populations at a low-recombining region may reflect high variance, while high variance at low-recombining regions alone cannot explain signals occurring in many (quasi-) independent populations or species at a low-recombining region. Furthermore, corroborating methods based on different aspects of distinct patterns of variation, such as site frequency spectrum (DeGiorgio et al., 2016; Fay & Wu, 2000; Tajima, 1989), LD (Sabeti et al., 2002, 2007; Voight et al., 2006), inferred genealogies (Hejase et al., 2020; Speidel et al., 2019; Stern et al., 2019), local landscape of variation (Setter et al., 2020), and sites of mutations in genes (Nei & Gojobori, 1986), as well as approaches with explicit simulation based on inferred demography (Hager et al., 2022), may be informative.

The biological implication is about evolution of recombination rates and genetic variation

along the genome. Based on our findings of a link between these, we predict that organisms with more conserved recombination landscape along the genome may have more conserved genomic landscapes of distinct patterns of genetic variation (Fig. 6B). In other words, the more conserved recombination maps are, the more correlated genomic distribution of distinct genetic variation may be between species. In vertebrates including placental mammals (with some exceptions), recombination landscape along the genome evolves fast due to continuous turnovers of alleles of PRDM9 (the gene coding a protein that determines recombination hot spots) and its target DNA sequences (Baudat et al., 2010; Myers et al., 2008). For instance, in mammals that possess functional PRDM9, the genomic landscape of recombination rates is distinct between and even within species (Kong et al., 2010; Spence & Song, 2019; Stevison et al., 2016). Importantly, PRDM9 has been pseudogenised (Birtle & Ponting, 2006) or lost (Baker et al., 2017) independently in multiple vertebrate lineages. This shifted the determinants of recombination map from the PRDM9 allele and its target to genomic features such as CpG islands and transcription start sites, stabilising the recombination landscape (Auton et al., 2013; Baker et al., 2017; Singhal et al., 2015). Our results shown in birds, a group lacking PRDM9 (Birtle & Ponting, 2006; Singhal et al., 2015), raises a question whether the evolution of local recombination rates may play an even more important role in shaping local genetic variation in organisms with functional PRDM9. Comparative studies using taxa with and without functional PRDM9 will address this and may link the evolution of genomic landscape of distinct patterns of genetic variation and (in)stability of recombination maps.

Materials and Methods

Empirical analyses

de novo genome assembly

A chromosome-level blackcap reference genome was *de novo* assembled within the Vertebrate Genomes Project (VGP), following pipeline version 1.5 (Rhie et al., 2021). In brief, blood of a female blackcap from the resident Tarifa population in Spain was collected in 100% ethanol on ice and stored at -80 °C (NCBI BioSample accession SAMN12369542). The ethanol

supernatant was removed and the blood pellet was resuspended in Bionano Cell Buffer in a 1:2 dilution. Ultra-long high molecular weight (HMW) DNA was isolated using Bionano agarose plug method (Bionano Frozen Whole Nucleated Blood Stored in Ethanol – DNA Isolation Guidelines (document number 30033)) using the Bionano Prep Blood and Cell Culture DNA Isolation Kit. Four DNA extractions were performed yielding a total of 13.5 μ g HMW DNA. About 6 μ g of DNA was sheared using a 26G blunt end needle (PacBio protocol PN 101-181-000 Version 05) to ~40 kb fragments. A large-insert PacBio library was prepared using the Pacific Biosciences Express Template Prep Kit v1.0 following the manufacturer protocol. The library was then size selected (>15 kb) using the Sage Science BluePippin Size-Selection System. The library was then sequenced on 8 PacBio 1M v3 smrtcells on the Sequel instrument with the sequencing kit 3.0 and 10 hours movie with 2 hours pre-extension time, yielding 77.51 Gb of data (~66.29X coverage) with N50 read length averaging around 22,927 bp. We used the unfragmented HMW DNA to generate a linked-reads library on the 10X Genomics Chromium (Genome Library Kit & Gel Bead Kit v2 , Genome Chip Kit v2 , i7 Multiplex Kit PN-120262). We sequenced this 10X library on an Illumina Novaseq S4 150 bp PE lane to ~60X coverage. Unfragmented HMW DNA was also used for Bionano Genomics optical mapping. Briefly, DNA was labeled using the Bionano Prep Direct Label and Stain (DLS) Protocol (30206E) and run on one Saphyr instrument chip flowcell. 136.31 Gb of data was generated (N50 = 301.9kb with a label density = 16.91 labels/100kb). Optical maps were assembled using Bionano Access (N50 = 27.48 Mb and total length = 1.41 Gb). Hi-C libraries were generated by Arima Genomics and Dovetail Genomics and sequenced on HiSeq X at ~60X coverage following the manufacturer’s protocols. Proximally ligated DNA was produced using the Arima-HiC kit v1 , sheared and size selected (200 – 600 bp) with SRI beads, and fragments containing proximity-ligated DNA were enriched using streptavidin beads. A final Illumina library was prepared using the KAPA Hyper Prep kit following the manufacturer guidelines. FALCON v1.9.0 and FALCON unzip v1.0.6 were used to generate haplotype phased contigs, and purge_haplotigs v1.0.3 was used to further sort out haplotypes (Guan et al., 2020). The phased contigs were first scaffolded with 10X Genomics linked reads using scaff10X 4.1.0 software, followed with Bionano Genomics optical maps using Bionano Solve single enzyme DLS 3.2.1, and Arima Genomics in-vitro cross-linked Hi-C maps using Salsa Hi-C 2.2 software

(Ghurye et al., 2019). Base call errors were polished with both PacBio long reads and Arrow short reads to achieve above Q40 accuracy (no more than 1 error every 10,000 bp). Manual curation was conducted using gEVAL software by the Sanger Institute Curation team (Howe et al., 2021). Curation identified 33 autosomes and Z and W chromosomes (plus 1 unlocalised W). Autosomes were named in decreasing order of size, and autosomes 1 through 30 and sex chromosomes had counterparts in the commonly used VGP reference zebra finch assembly (Sup. Table 2). The total length of the primary haplotype assembly was 1,066,786,587 bp, with 99.14% assigned to chromosomes. The final 1.1 Gb assembly consisted of 601 contigs in 189 scaffolds, with a contig N50 of 7.4 Mb, and scaffold N50 of 73 Mb, indicating a high-quality assembly that fulfills the VGP standard metrics.

Whole-genome resequencing

We resequenced 69 blackcap samples from various populations across the species distribution range (Sup. Table 1) to complement an existing dataset of 110 blackcaps, 5 garden warblers, and 3 African hill babblers that had been sequenced previously (Delmore et al., 2020b). Blood samples from the additional 69 blackcaps were collected from the brachial vein and stored in 100% ethanol. High molecular weight genomic DNA was extracted with a standard salt extraction protocol or through the Nanobind CBB Big DNA Kit Beta following the manufacturer’s instructions. Libraries for short insert fragments between 300 and 500 bp were prepared and were then sequenced for short paired-end reads on either Illumina NextSeq 500, HiSeq 4000 or NovaSeq 5000 (Sup. Table 1).

We performed quality control of the reads with FastQC version 0.11.8 (<https://www.bioinformatics.babraham.ac.uk/projects/fastqc/>). Reads from all samples were mapped against the blackcap reference genome following an adjusted pipeline of `Genome Analysis Toolkit` (GATK version 4.1.7.0, McKenna et al. (2010)) and `Picard` version 2.21.9 (<http://broadinstitute.github.io/picard/>). After resetting the base quality of adapter bases in the sequenced reads to 2 with `Picard MarkIlluminaAdapters`, paired-end reads were mapped to the reference using `BWA mem` (Li, 2013). To ensure that both unmapped mates and secondary/supplementary reads were marked for duplicates, we ran `Picard MarkDuplicates` for sorted reads with the default pixel distance of 100 for reads

from Illumina NextSeq 500 or with a pixel distance of 2,500 for reads from HiSeq 4000 and NovaSeq 5000. Due to low coverage, 10 samples (Sup. Table 1) were sequenced multiple times. Alignment files for these samples (in BAM format) were merged with `Picard MergeSamFiles`. Per-sample quality control of BAM files were performed using `QualiMap` version 2.2.1 (Okonechnikov et al., 2016), `Picard CollectMultipleMetrics`, `CollectRawWgsMetrics` and `CollectWgsMetrics`; and `MultiQC` version 1.8 (Ewels et al., 2016). The minimum and median depth were 7.8X and 20.1X, and the minimum and median coverage were 0.88 and 0.97. We called bases at all positions per sample using `GATK HaplotypeCaller`. We combined gVCF files of 189 individuals into ten evenly sized subsets (to allow parallelisation of the following variant calling step) with `GATK CombineGVCFs`. We genotyped SNPs and INDELs using `GATK GenotypeGVCFs`, and the 10 subsets were concatenated using `Picard GatherVcfs` into one VCF file covering the entire genome. From the VCF file, SNPs were selected (i.e. indels were excluded) using `GATK SelectVariants`, after which we filtered SNPs with the following criteria: $QD < 2.5$; $FS > 45.0$; $SOR > 3.0$; $MG < 40$; $MQRankSum < -12.5$; $ReadPosRankSum < -8.0$. We removed garden warblers and African hill babblers from the multi-species VCF and kept only biallelic sites. We estimated blackcap haplotypes using `SHAPEIT2` (r837) (Delaneau et al., 2013) with the blackcap recombination map (Bascón-Cardozo et al., 2022a), yielding 142,083,056 SNPs.

Genome-wide PCA

To characterise the population structure of blackcaps, we performed principal component analysis (PCA) using `PLINK` (Purcell et al., 2007).

Local PCA

To identify genomic regions with distinct patterns of genetic variation in blackcaps, we performed local PCA in sliding genomic windows of 1,000 SNPs and summarised dissimilarity of windows by multidimensional scaling using `lostrct` (Li & Ralph, 2019) in R version 3.5.3. First, we prepared a genotype and a haplotype table for each chromosome in which rows and columns represented positions and individuals from the phased VCF file using `BCFtools`. Specifically, genotypes were encoded 0, 1, and 2 for the reference allele homozygotes,

heterozygotes, and non-reference allele homozygotes in the genotype table, and 0 and 2 for the reference and the non-reference allele in the haplotype table (encoding 0 and 1 instead of 0 and 2 in haplotype-based analysis gives the same results). Chromosomes shorter than 10 Mb were concatenated to avoid misidentification of short chromosomal background as an outlier region. Distance matrices of windows were computed based on the coordinates (PC1 and PC2) of samples (individuals for genotype-based local PCA, and haplotype for haplotype-based local PCA) within R using **lostruct**. Multidimensional scaling (MDS) was performed to summarise similarities of local genetic variation patterns among windows into 20 axes (MDS1 through MDS20).

Using the **lostruct** output, we identified chromosomal intervals with distinct patterns of genetic variation. In each chromosome, windows with MDS value apart from the mode of the distribution by greater than 0.3 for any one of the 20 axes were defined as outlier windows. This threshold was determined by visualising the distribution of MDS values in each chromosome (Sup. Fig. 2). For each MDS axis, we defined genomic intervals with at least five outlier windows longer than 100 kb as “outlier regions” with distinct patterns of genetic variation. Overlapping intervals across different MDS axes as well as intervals identified based on genotypes and haplotypes were merged using **BEDtools**. To verify that the outliers show pattern of genetic variation distinct from the whole-genome PCA, we performed PCA using all SNPs within each outlier region using **PLINK** ([fig:sup.pcaisland_spp;fig:sup.pcaisland_pop;fig:sup.pcaisland_nosup]). Genomic regions showing similar pattern to the whole genome PCA were identified with visual inspection and discarded from the outliers.

To assess consistency between the pipelines using genotypes and haplotypes, we compared MDS results of genotype- and haplotype-based **lostruct**. We calculated Euclidean distance of windows from the centre of the 20 dimensional space to enable comparison of the same window in genotype- and haplotype-based MDS. We measured this distance instead of comparing the coordinates directly to account for possible rotations of MDS patterns between genotype- and haplotype-based **lostruct**. Because dissimilarity of windows in terms of the pattern of genetic variation was computed per chromosome, we calculated correlation of the above distance between genotype- and haplotype-based methods per chromosome. The comparison

of genotype-based and haplotype-based **lostruct** is in Sup. Fig. 4.

To assess whether **lostruct** can identify outliers irrespective of presence/absence of other outliers on the same chromosome as well as the chromosome length, we ran **lostruct** treating either one part of a blackcap chromosome (“split chromosomes”) or multiple blackcap chromosomes as a single chromosome (“joined chromosome”). If **lostruct** is robust to the chromosomal background, it is expected that the same regions should be detected as outliers with distinct patterns of genetic variation in both split and joined chromosomes compared to per-chromosome results. We prepared four split chromosomes by splitting chromosomes 1 and 2 at the middle, and one joined chromosome by concatenating chromosomes 20, 21, and 28. We performed **lostruct** analysis based both on genotype and haplotype and merged the identified regions. The comparison of **lostruct** between using single chromosomes and split/joined chromosomes is in Sup. Fig. 5.

LD and recombination landscape

To calculate LD around outlier regions, we first extracted SNPs within and 30% length outside each outlier. We then thinned SNPs so that all neighbouring SNP positions were at least 10 kb away from each other. Linkage disequilibrium (LD) between all pairs of thinned SNPs was calculated with **VCFtools** with the `--geno-r2`.

We inferred recombination landscape along blackcap chromosomes using **Pyrho** (Spence & Song, 2019). **Pyrho** infers demography-aware recombination rates with a composite-likelihood approach from SNPs data of unrelated samples making use of likelihood lookup tables generated by simulations based on demography and sample size of each population. In all inferences, we used demography of focal populations inferred in Delmore et al. (2020b). Before the recombination inference, focal samples were filtered and singletons were removed. We ran **Pyrho** with mutation rate of 4.6×10^{-9} per site per generation (Smeds et al., 2016), block penalty of 20, and window size of 50 kb to infer population-level recombination landscape in Azores, Cape Verde, continental resident, and medium-long distance migrants (represented by medium distance south-west migrants). We computed mean recombination rate in 10 kb sliding windows for each population.

We defined low-recombining regions and evaluated overlaps between outlier regions and low-recombining regions in the following four steps. 1. define low-recombining regions for each population recombination map, 2. test for association between all outlier regions and the low-recombining regions for each population, 3. define species-wide and population-specific low-recombining regions, and 4. label outlier regions with species-wide or population-specific low-recombining regions or no overlap with any low-recombining region.

1. For the recombination map of each of the four populations (`med_sw`, `cont_res`, Azores, Cape Verde), we defined low-recombining regions as the set of 10 kb windows with recombination rate lower than 20 percentile for each chromosome. This mild threshold was set to account for large variation in the recombination landscapes among chromosomes and to capture population-specific reduction in recombination rate which could be with weaker reduction in recombination rate than at species-wide low-recombining regions.
2. For the set of low-recombining regions of each population, we performed a permutation test by shuffling observed outlier regions within the chromosome and counted the total length of overlap with (any) low-recombining regions (in bp) using `BEDTools`. We repeated this 1,000 times, and compared the empirical null distribution of the overlap length (in bp) with observed overlaps.
3. To define species-wide and population-specific low-recombining regions, at all positions along the genome we counted the number of population recombination maps sharing low-recombining regions. If a region was labelled low-recombining in three or four populations at step 1, we defined it to be species-wide low-recombining region. If a region was labelled low-recombining in one or two populations, we defined it to be a population-specific low-recombining region, recording which populations were low-recombining.
4. We first labelled outlier regions overlapping species-wide low-recombining regions. We intersected the species-wide low-recombining regions defined in step 3 and outlier regions. We labelled an outlier region with species-wide low-recombining if it had a coverage of species-wide low-recombining regions greater than 0.5. Two exceptions were `outlier_12_3` and `outlier_30_1`, which are putative inversions. They had coverage of species-wide low-recombining regions of 0.30 and 0.23 but this is largely due to heterokaryotype-

specific recombination suppression and inclusion of homokaryotypes in recombination rate inference. Because these putative inversions were segregated in most populations, we defined them to be species-wide low-recombining regions. We next labelled outlier regions overlapping population-specific low-recombining regions. We intersected the population-specific low-recombining region defined in step 3 with outlier regions excluding those overlapping with species-wide low-recombining regions. We labelled an outlier region overlapping with population-specific low-recombining regions if it had a coverage greater than 0.01 for any (pair of) population(s). Finally, the remaining outlier regions were labelled no reduction in recombination rate.

To characterise genotype-specific LD and recombination landscape at the five outlier regions with three clusters of individuals in PCA, we applied `vcftools --geno-r2` and `Pyrho` (Spence & Song, 2019) to our empirical data using each genotype (AA, AB, and BB in Sup. Fig. 11) separately. Validation of this procedure is described in “Simulation: Validation of LD-based inference of recombination landscape using non-randomly chosen samples”.

Inversion breakpoints

Three clusters of individuals observed in PCA with genotype-specific LD at two outlier regions on chromosomes 12 and 30 were indicative of polymorphic inversion (Ma & Amos, 2012; Ruiz-Arenas et al., 2019). To further characterise whether they represent polymorphic inversions, we intended to locate breakpoints by two independent approaches.

Soft-clip reads We attempted to identify positions where presence of soft-clipping of mapped reads is associated with PCA-based genotype of the putative inversions. First, we extracted focal regions around boundaries of the outliers (Sup. Table 4) from read mapping file of all individuals using `SAMtools` (Danecek et al., 2021). Next, we identified soft clip reads in each extracted region using `samextractclip` (Lindenbaum, 2015), and obtained reference position corresponding to the position of soft clipping in mapped reads using a custom script. At all extracted soft-clip positions, we counted the number of reads that switch to soft-clip (“soft-clip depth”), as well as the depth of mapped reads, using `SAMtools`. At each of all positions with at least one read supporting soft-clip switch, we calculated proportion of reads

with soft-clip switch relative to all mapped reads (depth of the position) for each individual (“soft-clip proportion”). This resulted in “position-by-individual” matrix whose entry depicts the proportion of soft-clip in all reads mapped at the focal position for the focal individual. Using this matrix, we fit a linear model (soft-clip proportion \sim PCA – based genotype) in R at each position treating genotypes AA, AB, and BB as 0, 1, and 2. Based on the significance of genotype and R^2 of the linear models, we generated a list of 14 positions at which soft-clip proportion was significantly associated with genotype of the putative inversions. We visualised the distribution of the soft-clip proportion at these positions (Sup. Fig. 15) and selected six positions for which the soft-clip proportion of BB was high enough and that of AB was around a half of BB based on the assumption that soft clip reads covering an inversion breakpoint should originate from haplotype B and non-soft clip reads should originate from haplotype A (Sup. Table 5). To investigate whether some of these six positions represent inversion breakpoints, we asked whether the soft-clipped segments of the reads have homologous sequences at the other end of the outlier regions. We extracted soft-clipped segments of reads mapped at the focal six positions in AB and BB individuals using a custom script, and re-mapped these segments (instead of the entire reads) to the blackcap reference using **BWA mem**. We computed the depth of mapped segments in each position using **SAMtools** (Sup. Table 5).

10x linked read We used an independent set of blackcap individuals (hereafter “10x individuals”) whose genomes were sequenced with the 10x linked-read technology (Delmore et al., 2023, NCBI BioProject PRJEB65115). We genotyped the 10x individuals at the two putative inversion loci (i.e. AA, AB, or BB) based on genotypes at diagnostic SNP positions. We started by determining diagnostic SNP positions using our Illumina short read-based resequence data. Because usable diagnostic SNP positions should have genotypes perfectly associated with PCA-based genotype, we focused on positions at which F_{ST} was 1 between AA and BB, and all AB were heterozygous, using **VCFtools** and **BCFtools**. We also recorded mapping between an allele at the diagnostic positions and a genotype of the putative inversion (“A- and B-diagnostic alleles”, e.g. G for haplotype A, T for haplotype B).

We then counted the number of sites with A- and B-diagnostic allele in each of 10x samples. To convert coordinates of 10x assemblies to the reference coordinate, we mapped

the 10x pseudo-haplotyped assemblies to the blackcap reference using `minimap2` (Li, 2018). To determine the putative inversion genotype in the 10x individuals, we counted the number of positions with A-diagnostic and B-diagnostic alleles for each 10x pseudo-haplotype, and calculated the proportion of sites with A-diagnostic and B-diagnostic sites. In principle, an AA and a BB individual respectively are expected to have proportion of 100% and 0% of A-diagnostic sites in both of two pseudo-haplotypes, while an AB individual is expected to have 100% of A-diagnostic sites in one pseudo-haplotype and 0% for the other. For genotyping, we set the following three thresholds.

1. Missingness at the diagnostic positions is less than 10%, after removing positions with non-unique `minimap2` mapping (i.e. at least 90% of all diagnostic positions should have depth of 1x).
2. More than 90% of all diagnostic sites should agree per pseudo-haplotype.
3. The second criterion should be fulfilled for both pseudo-haplotypes of an individual.

We identified two BB individuals for each of the putative inversions on chromosomes 12 and 30. There were no AB individuals passing the above threshold, indicating 10x pseudo-haplotyping is not accurate in separating two diverged non-recombining alleles at a long range in an individual that has both. To identify breakpoints, we aligned the pseudo-haplotype assemblies of these BB individuals as well as one AA individual for each putative inversion to the blackcap reference using `Nucmer4` (Marçais et al., 2018), and generated dot plots (Sup. Fig. 16).

Sequence analysis at breakpoint of putative inversion on chromosome 12 10x contigs of pseudo-haplotype B aligned next to the putative breakpoint position of blackcap reference chromosome 12 had an un-aligned flanking sequence. To characterise the DNA sequence of these flanking segments, we extracted the flanking sequences using `SAMtools`, aligned the sequences to themselves using `minimap2`, and generated self-dot plots (Sup. Fig. 17), revealing presence of tandem repeats. To identify unit of tandem repeats within the flanking sequences, we ran `TandemRepeatsFinder` against these extracted sequences, resulting in four consensus unit sequences of 144 bp based on two contigs from two individuals. To

confirm that the four consensus sequences represent the same tandem repeat (because the unit of identical tandem repeat can have different phases), we ran **BLASTn** (version 2.10.1, Altschul et al., 1990) with each consensus as query against dimers of the consensus. To investigate whether the tandem repeat found at the putative breakpoint of chromosome 12 in haplotype B is present in chromosome 12 and other chromosomes of the reference and corresponding position of haplotype A, we ran **BLASTn** with the 144 bp consensus of the tandem repeat unit as the query against blackcap reference and a contig of an AA individual that spans the breakpoint position, and counted how many copies were found in each reference chromosome/scaffold and the 10x contig (Sup. Fig. 18).

Selection in blackcaps

To test for selection in different outlier regions and to compare them with the genome-wide base line, we computed nucleotide diversity (π) and Tajima's D in 10 kb sliding windows per population using **PopGenome** (Pfeifer et al., 2014) and **VCFtools** (Danecek et al., 2011) respectively. The effects of the outlier regions on these statistics were tested using a linear mixed effects model (**nlme::lme** (Pinheiro et al., 2021)) and a generalised linear mixed effects model with a Gamma distribution (**lme4::glmer** (Bates et al., 2015)). To test for selection in genes d_N/d_S were computed following the counting method by Nei & Gojobori (1986). Gene annotation of the blackcap was obtained from Bascón-Cardozo et al. (2022b).

Tandem repeats within and outside outlier regions

To characterise correlation between outlier regions with distinct patterns of genetic variation and tandem repeats, we identified tandem repeats in the reference genome and compared the distribution of the tandem repeats with genomic regions with distinct patterns of genetic variation. First, **TandemRepeatsFinder** (Benson, 1999) was run on the blackcap reference genome with the parameter set recommended on the documentation (**trf </path/to/fast> 2 7 7 80 10 50 500 -f -d -m -h**). The output was formatted and summarised for visualisation using custom scripts. Briefly, distribution of tandem repeats with a different unit size along the genome was summarised in 100 kb sliding windows in blocks of repeat unit sizes of 10 bp step (Sup. Fig. 33). Tandem repeats with the six longest repeat unit size were extracted per

chromosome, and copy number for each tandem repeat was counted (Sup. Fig. 34).

Next, we tested whether the number of tandem repeats with long repeat unit were enriched in outlier regions at species-wide and population-specific low-recombining regions. We extracted tandem repeats with repeat unit size greater than or equal to 150 bp, and counted the number of tandem repeats (instead of total copy number) within and outside outlier regions. We performed Fisher’s exact tests to test independence between the number of long tandem repeats and the mode of recombination suppression (species-wide/population-specific) (Sup. Table 7) using `fisher.test` function in R.

Simulation

Validation of LD-based inference of recombination landscape using non-randomly chosen samples

We asked whether LD-based recombination map inference using individuals chosen based on the karyotype instead of at random is informative of the underlying mode of recombination suppression. To this end, we simulated two 5 Mb-long chromosomes with neutral mutation rate of 4.6×10^{-8} in a population of 1,000 individuals in SLiM. The purpose of these simulations was to investigate the effect of an inversion and additional recombination suppression on recombination rate inference and LD in general, rather than investigating the effects specific to blackcap demography. As such, we kept the population size smaller than the blackcap effective population size and the mutation rate greater than assumed in order to minimise the time and computational resource for simulations. We introduced a mutation (inversion marker) on one chromosome at 1 Mb position at the 50th generation. We simulated an inversion on the chromosome by suppressing recombination in an interval from 1 Mb to 4 Mb position if the inversion marker site was heterozygous. We defined additional suppression according to different scenarios (models 1-6 in Sup. Table 6). We applied negative frequency-dependent selection (fitness of inversion is $1 - (p_{inv} - 0.2)$ where p_{inv} is the frequency of the inversion allele). 1,000 generations after the inversion event, we recorded the mutations in all samples, making a VCF file including all samples. Although 1,000 generations is relatively short given the population size of 1,000, the haplotype structure at the inversion locus was stable in test

runs of model-1 (inversion frequency of 0.2 without additional recombination suppression). Based on the genotype at 1 Mb position, we randomly chose 10 samples for each inversion genotype. *Pyrho* was run to estimate recombination rates using the chosen 10 samples, with the block penalty 50 and window size 50. The inferred recombination maps are in Sup. Fig. 13.

Effects of recombination suppression model on recombination rate inference at an inversion

Three clusters of individuals observed in PCA at five outlier regions indicate presence of distinct haplotypes. Polymorphic inversions are known to show this pattern due to suppression of recombination between the normal and inverted alleles (Wellenreuther & Bernatchez, 2018). To test whether some of the five outlier regions represent polymorphic inversions, we intended to infer recombination rates using AA, AB, and BB individuals separately based on linkage disequilibrium (LD) patterns. Before addressing this in blackcaps empirically, we assessed how different types of recombination suppression at a haplotype block affect inference of recombination landscape using a set of individuals with a certain combination of haplotypes. To investigate the effect of a genotype-specific suppression of recombination on LD-based inference of recombination rate, we simulated different modes of recombination suppression using *SLiM* version 3.5 (Haller & Messer, 2019) under six scenarios listed in Sup. Table 6. Specifically, we performed 1,000 replicates of forward-time simulations of two 500 kb-long chromosomes with neutral mutation rate of 1×10^{-7} [per site per generation] and recombination rate of 1×10^{-6} [per site per generation] in a population of 1,000 diploid individuals under the Wright-Fisher model (We downscaled the population size and upscaled mutation rate to minimise the time and computational resource for simulation). We introduced a mutation (inversion marker) on one chromosome at 100 kb position at the 50th generation. We modelled an inversion by suppressing recombination in an interval from 100 kb to 400 kb position if the inversion marker site was heterozygous. We defined additional suppression according to different scenarios (models 1-6). To allow for the inversion to remain in the population, we applied negative frequency-dependent selection (fitness of inversion is $1 - (p_{inv} - 0.2)$ for models 1-3 and $1 - (p_{inv} - 0.8)$ for models 4-6 where p_{inv} is the frequency of the inversion

allele). 1,000 generations after the inversion event, we recorded the mutations in all samples, making a VCF file including all individuals. Although 1,000 generations is relatively short given the population size of 1,000, the haplotype structure at the inversion locus was stable in test runs of model-1 (inversion frequency of 0.2 without additional recombination suppression). Based on the genotype at the marker, we randomly sampled 10 individuals for each inversion genotype. *Pyrho* was run to estimate recombination rates using the sampled 10 individuals, with the block penalty 50 and window size 50. The inferred recombination landscape is in Sup. Fig. 13.

Coalescent simulation of species-wide reduction of recombination rate

To discern the effect of reduced recombination rate, demographic history, and unequal sample sizes among population on outlier regions identified by *lostruct*, we performed neutral coalescent simulations using *msprime* version 1.2.0 (Baumdicker et al., 2022). We simulated a 1-Mb long recombining chromosome with a mutation rate of 4.6×10^{-9} [per site per generation]. We implemented 11 models differing in the recombination maps, population subdivision, and demographic history (Sup. Fig. 19). In models 1-3, the recombination rate was set to 4.6×10^{-9} [per site per generation] throughout the entire chromosome, and they differ in population subdivision (model 1: panmictic, model 2, subdivision of five equal populations without gene flow, model 3: subdivision of equally-sized populations with gene flow between two pairs of populations (symmetric migration rate of 0.025 [per generation])). In models with five populations, we distributed the sample of 100 individuals unequally, as in our blackcap dataset (50, 20, 10, 10, 10 individuals for five populations). In models 4-7, we introduced reduced recombination rate in the middle of the chromosome (0.4 to 0.6 Mb) with the same demographic histories as models 2 and 3. In addition to the uniform recombination map, we prepared two recombination maps with reduced recombination rate: “low-rec” with one-hundredth the background recombination rate, and “no-rec” with recombination rate of 0. In models 8-11, we used the same two recombination maps with reduced recombination rate in the middle, with different demography: 10 times increase in effective population size in one population, and 10 times decrease in effective population size in three populations, which roughly reflects inferred demography of blackcap populations (Delmore et al., 2020b). For each model, we ran

1,000 replicates of simulations and recorded SNPs in VCF format.

To identify outlier regions, we ran **lostruct** the same way as in the empirical analysis. To evaluate how reduced recombination rate affects the mean and variance of population genetic summary statistics, we computed nucleotide diversity (π), Tajima's D, and F_{ST} , using **VCFTools**. The outliers detected by **lostruct** are in Sup. Fig. 20. The summary statistics are in Sup. Figs. 21, 22, 23.

Forward simulation of species-wide reduction of recombination rate

To investigate how species-wide low-recombining regions affect patterns of local genetic variation depicted in local PCA, we performed forward simulation with **SLiM** version 4.0.1 (Haller & Messer, 2022). We simulated 100 replicates of two 500 kb-long chromosomes with neutral mutation rate of 1×10^{-7} [per site per generation] and recombination rate of 1×10^{-6} [per site per generation] except for an interval from 100 to 400 [kb] of the first chromosome where recombination rate was set to 1×10^{-9} , which is 1/1000 of the normally recombining chromosome. First, we ran a burn-in of 4,000 generations for an ancestral population of 1,000 diploids. After the burn-in, we made three populations of 1,000 diploids (pop1, pop2, and pop3) split from the ancestral population. We sampled 50 individuals per population every 20 generations over 1,000 generations after the population split and recorded SNPs in VCF. For each time point of each of 100 simulation replicates, we performed PCA with **PLINK**, using SNPs either within 100 to 400 [kb] of the first chromosome (pop1-specific suppression) or the normally recombining chromosome.

We investigated how reduced recombination rate affects representation of population subdivision in local PCA. To evaluate whether the individuals from different populations were distributed differently in local PCA at the low-recombining region, we performed Fasano-Franceschini test (Fasano & Franceschini, 1987), which is a multi-dimensional extension of Kolmogorov-Smirnov test, in three pairs of populations (pop1-pop2, pop1-pop3, pop2-pop3). We counted the number of significant pairs of populations (0, 1, 2, or 3) for each time point of each replicate. We compared between the low-recombining and normally recombining regions the number of pairs of populations with distinct distribution in PCA (Sup. Fig. 31).

Forward simulation of population-specific reduction of recombination rate

To investigate how evolution of low-recombining regions in population(s) affect patterns of local genetic variation depicted in local PCA, we performed forward simulation with SLiM version 4.0.1. We simulated two 500kb-long chromosomes with neutral mutation rate and recombination rate of 1×10^{-7} [per site per generation] and 1×10^{-6} [per site per generation]. First, we ran a burn-in of 4,000 generations for an ancestral population of 1,000 diploids. After the burn-in, we made three populations of 1,000 diploids (pop1, pop2, and pop3) split from the ancestral population, after which gene flow between all pairs of populations were set to 0.0025. We introduced recombination suppression in pop1 from 100 to 400 [kb] of the first chromosome in two scenarios. In the first scenario, recombination suppression was introduced at the same time of the split. In the second scenario, recombination suppression was introduced 4,000 generations after the population split event, allowing the three populations to differentiate before population-specific recombination suppression was introduced in pop1. We sampled 50 individuals per population every 20 generations over 1,000 generations after the introduction of the population-specific suppression of recombination and recorded SNPs in VCF. For each time point of each of 1,000 simulation replicates, we performed PCA with PLINK, using SNPs either within 100 to 400 [kb] of the first chromosome (pop1-specific suppression) or the normally recombining chromosome.

To characterise factors represented in the primary axes of distinct local PCA at population-specific low-recombining regions, we performed one replicate of SLiM simulation with the same scenarios of models 1 and 2 recording the full ancestry and mutations in tree sequence, with an increased duration of burn-in (40,000 generations) to make sure that all lineages at sampling time coalesce. We loaded the tree sequence with mutations in `tskit` (Kelleher et al., 2018) and sampled 50 diploids per population, and saved SNPs in VCF. Using the VCF files for each time point for each model, we performed PCA using PLINK at the population-specific low-recombining region, and determined one time point per model showing typical spread of individuals from the low-recombining population in PCA (Sup. Fig. 27A, E). For these PCAs we identified 5% SNPs with the highest loadings to the first two PC axes. We analysed these mutations on the underlying genealogies using `tskit`. Specifically, we investigated

whether mutations originating from the low-recombining population were enriched in the high-loading mutations (Sup. Fig. 27C, G) with a χ^2 test. We also assessed whether multiple mutations originating in the low-recombining population occurring on the same genealogical branches (i.e. mutations on the same ancestral haplotypes) were enriched in the high-loading mutations (Sup. Fig. 27D, H). For this, we compared the number of mutations sharing the same genealogical branches among the high-loading mutations originating from the low-recombining population and the same number of randomly-selected mutations originating from the low-recombining population by a Kolmogorov-Smirnov test.

Effects of linked selection on local PCA

Background selection To investigate the linked effect of purifying selection at low-recombining regions (background selection) on patterns of local genetic variation represented in local PCA, we performed forward simulation with SLiM version 4.0.1. We simulated a species-wide low-recombining region in three populations as described above, except we changed the distribution of fitness effect of mutations with three different ratios between neutral (“n”, $s = 0$) and deleterious (“d”, $s = -0.05$ and $h = 0.5$) mutations of $n/(n + d) = 0, 0.25, 0.5, 0.75$. To evaluate whether individuals from different populations were distributed differently in the local PCA at the low-recombining region, we performed Fasano-Franceschini test between three pairs of populations (pop1-pop2, pop1-pop3, pop2-pop3). We counted the number of significant pairs of populations (0, 1, 2, or 3) for each sampled time point of each replicate (out of 100) for each DFE (Sup. Fig. 31).

Positive selection To investigate the linked effect of positive selection at low-recombining regions on patterns of local genetic variation represented in local PCA, we performed forward simulation with SLiM version 4.0.1 under four scenarios: population-specific sweep and sweep before populations split, with and without reduced local recombination rate. We simulated 10 replicates of one 500 kb-long chromosome with neutral mutation rate of 1×10^{-7} [per site per generation] and recombination rate of 1×10^{-6} [per site per generation]. In scenarios with reduced recombination rate, we introduced a reduced recombination rate within an interval from 100 to 400 [kb] of the chromosome where recombination rate was set to 1×10^{-9} ,

which is 1/1000 of the normally recombining regions. For all scenarios, we ran a burn-in of 4,000 generations for an ancestral population of 1,000 diploids. In the scenarios with population-specific sweep, we made three populations of 1,000 diploids (pop1, pop2, and pop3) split from the ancestral population at the 4000-th generation. We introduced a strongly beneficial mutation ($s = 1$ and $h = 0.5$) in the middle of a chromosome of one randomly selected sample of the first population at the 100-th generation after the populations split. In the scenarios with sweep before split, we introduced a strongly beneficial mutation ($s = 1$ and $h = 0.5$) in the middle of the chromosome of one randomly selected sample of the ancestral population, and made the three populations of 1,000 diploids split at the 100-th generation after the introduction of the beneficial mutation. We sampled 100 diploid individuals per population every 20 generations since the introduction of the beneficial mutation (scenarios of population-specific sweep) or the split (scenarios of ancestral sweep) and recorded the SNPs in VCF format. We performed PCA using PLINK.

Acknowledgment

This work was supported by the Max Planck Society (Max Planck Research Group grant MFFALIMN0001 to ML), the DFG (project Z02 and Nav05 within SFB 1372 – Magnetoreception and Navigation in Vertebrates to ML), and DFG Research Infrastructure NGS_CC (project 407495230) as part of the Next Generation Sequencing Competence Network (project 423957469). AR was supported by the Intramural Research Program of the NHGRI, NIH (1ZIAHG200398). JCI was funded by two research grants from the Spanish Ministry of Science, Innovation and Universities, and the European Regional Development Fund (PGC2018-097575-B-I00; PID2022-140091NB-I00). We thank Britta Meyer, Tianhao Zhao, Hanna Koch, Conny Burghardt, and Sven Künzel for DNA extraction, library preparation, and/or sequencing. We are grateful to Julien Dutheil, Diethard Tautz, Linda Odenthal-Hesse, Tobias Kaiser, Carolina Peralta, and Matthias Weissensteiner for constructive discussion. We are grateful to Thord Fransson, Christos Barboutis, Zura Javakhishvili, Martim Melo, Álvaro Ramírez, and Helena Batalha for providing us with samples. Permits were provided to JCI for samples collected on Cape Verde (Ministerio do Ambiente - Habitacao e Ordenamento

do Territorio, 18/CITES/DNA, 17 Dec 2015), Canary Islands (Ref.: 2012/0710), Madeira (Ref.: 02/2016), and the Azores (Instituto da Conservacao da Natureza e da Biodiversidade, 171/2008, 31 Mar 2009); to JP-T for samples collected on Mallorca (CAP 64/2009); to Thord Fransson for samples collected on Crete (6Υ0Ξ4653Π8-ΥΓ5 issued by the Hellenic Ministry of Environment and Energy), and to Zura Javakhishvili for samples collected in Georgia (889-0-2-202303291450 by the Ministry of Environment and Agriculture of Georgia). A preprint version of this article has been peer-reviewed and recommended by PCIEvolBiol (<https://doi.org/10.24072/pci.evolbiol.100711>).

Data availability

The primary and alternate haplotype assemblies of the blackcap reference genome can be found under NCBI BioProject PRJNA558064 (accession GCA_009819655.1) and PRJNA558065 (accession GCA_009819715.1). Raw Illumina reads for the resequencing data can be accessed under NCBI BioProject PRJEB66075 (SRA accession ERP151147). Processed data and scripts for analysis and simulation are found in Zenodo (<https://doi.org/10.5281/zenodo.10623362>).

Conflict of interest

The authors declare no conflict of interest.

Author contributions

JI and ML designed the study. Reference genome was generated by JF, AR, JM, BH, WC, JC, KH, MU, OF, and EDJ. JP-T and JCI collected samples for resequencing. AB performed read mapping, variant calling, and data filtration. KB-C inferred recombination maps. JI conducted haplotype inference, population genomics analyses, simulations, sequence analyses, statistical modelling, and data visualisation. JI and ML wrote the manuscript with inputs from other authors.

References

- Altschul, S. F., Gish, W., Miller, W., Myers, E. W., & Lipman, D. J. (1990). Basic local alignment search tool. *Journal of Molecular Biology*, 215(3), 403–410. [https://doi.org/10.1016/S0022-2836\(05\)80360-2](https://doi.org/10.1016/S0022-2836(05)80360-2)
- Auton, A., Li, Y. R., Kidd, J., Oliveira, K., Nadel, J., Holloway, J. K., Hayward, J. J., Cohen, P. E., Grealis, J. M., Wang, J., Bustamante, C. D., & Boyko, A. R. (2013). Genetic Recombination Is Targeted towards Gene Promoter Regions in Dogs. *PLOS Genetics*, 9(12), e1003984. <https://doi.org/10.1371/journal.pgen.1003984>
- Baker, Z., Schumer, M., Haba, Y., Bashkirova, L., Holland, C., Rosenthal, G. G., & Przeworski, M. (2017). Repeated losses of PRDM9-directed recombination despite the conservation of PRDM9 across vertebrates. *eLife*, 6, e24133. <https://doi.org/10.7554/eLife.24133>
- Barton, N. H., & Etheridge, A. M. (2004). The Effect of Selection on Genealogies. *Genetics*, 166(2), 1115–1131. <https://doi.org/10.1093/genetics/166.2.1115>
- Bascón-Cardozo, K., Bours, A., Ishigohoka, J., Odenthal-Hesse, L., & Liedvogel, M. (2022a). *Historical recombination maps diverge between Eurasian blackcap populations with distinct migratory strategies* [Preprint]. Authorea. <https://doi.org/10.22541/au.166790167.72861799/v1>
- Bascón-Cardozo, K., Bours, A., Manthey, G., Pruisscher, P., Durieux, G., Dutheil, J., Odenthal-Hesse, L., & Liedvogel, M. (2022b). *Fine-scale map reveals highly variable recombination rates associated with genomic features in the European blackcap* [Preprint]. Authorea. <https://doi.org/10.22541/au.165423614.49331155/v1>
- Bates, D., Mächler, M., Bolker, B., & Walker, S. (2015). Fitting Linear Mixed-Effects Models Using lme4. *Journal of Statistical Software*, 67(1), 1–48. <https://doi.org/10.18637/jss.v067.i01>
- Baudat, F., Buard, J., Grey, C., Fledel-Alon, A., Ober, C., Przeworski, M., Coop, G., & Massy, B. de. (2010). PRDM9 Is a Major Determinant of Meiotic Recombination Hotspots in Humans and Mice. *Science*, 327(5967), 836–840. <https://doi.org/10.1126/science.1183439>
- Baumdicker, F., Bisschop, G., Goldstein, D., Gower, G., Ragsdale, A. P., Tsambos, G., Zhu, S., Eldon, B., Ellerman, E. C., Galloway, J. G., Gladstein, A. L., Gorjanc, G., Guo, B., Jeffery, B., Kretschmar, W. W., Lohse, K., Matschiner, M., Nelson, D., Pope, N. S., et al. (2022). Efficient ancestry and mutation simulation with msprime 1.0. *Genetics*, 220(3), iyab229. <https://doi.org/10.1093/genetics/iyab229>
- Benson, G. (1999). Tandem repeats finder: A program to analyze DNA sequences. *Nucleic Acids Research*, 27(2), 573–580. <https://doi.org/10.1093/nar/27.2.573>
- Berthold, P. (1988). Evolutionary aspects of migratory behavior in European warblers. *Journal of Evolutionary Biology*, 1(3), 195–209. <https://doi.org/https://doi.org/10.1046/j.1420-9101.1998.1030195.x>

- Berthold, P. (1991). Genetic control of migratory behaviour in birds. *Trends in Ecology and Evolution*, 6(8), 254–257. [https://doi.org/10.1016/0169-5347\(91\)90072-6](https://doi.org/10.1016/0169-5347(91)90072-6)
- Bhatia, G., Patterson, N., Sankararaman, S., & Price, A. L. (2013). Estimating and interpreting FST: The impact of rare variants. *Genome Research*, 23(9), 1514–1521. <https://doi.org/10.1101/gr.154831.113>
- Birtle, Z., & Ponting, C. P. (2006). Meisetz and the birth of the KRAB motif. *Bioinformatics*, 22(23), 2841–2845. <https://doi.org/10.1093/bioinformatics/btl498>
- Booker, T. R., Yeaman, S., & Whitlock, M. C. (2020). Variation in recombination rate affects detection of outliers in genome scans under neutrality. *Molecular Ecology*, 29(22), 4274–4279. <https://doi.org/https://doi.org/10.1111/mec.15501>
- Burri, R. (2017). Interpreting differentiation landscapes in the light of long-term linked selection. *Evolution Letters*, 1(3), 118–131. <https://doi.org/https://doi.org/10.1002/evl3.14>
- Burri, R., Nater, A., Kawakami, T., Mugal, C. F., Olason, P. I., Smeds, L., Suh, A., Dutoit, L., Bureš, S., Garamszegi, L. Z., Hogner, S., Moreno, J., Qvarnström, A., Ružić, M., Sæther, S.-A., Sætre, G.-P., Török, J., & Ellegren, H. (2015). Linked selection and recombination rate variation drive the evolution of the genomic landscape of differentiation across the speciation continuum of Ficedula flycatchers. *Genome Research*, 25(11), 1656–1665. <https://doi.org/10.1101/gr.196485.115>
- Cao, Y., Li, L., Xu, M., Feng, Z., Sun, X., Lu, J., Xu, Y., Du, P., Wang, T., Hu, R., Ye, Z., Shi, L., Tang, X., Yan, L., Gao, Z., Chen, G., Zhang, Y., Chen, L., Ning, G., et al. (2020). The ChinaMAP analytics of deep whole genome sequences in 10,588 individuals. *Cell Research*, 30(9), 717–731. <https://doi.org/10.1038/s41422-020-0322-9>
- Cruickshank, T. E., & Hahn, M. W. (2014). Reanalysis suggests that genomic islands of speciation are due to reduced diversity, not reduced gene flow. *Molecular Ecology*, 23(13), 3133–3157. <https://doi.org/https://doi.org/10.1111/mec.12796>
- Danecek, P., Auton, A., Abecasis, G., Albers, C. A., Banks, E., DePristo, M. A., Handsaker, R. E., Lunter, G., Marth, G. T., Sherry, S. T., McVean, G., Durbin, R., & 1000 Genomes Project Analysis Group. (2011). The variant call format and VCFtools. *Bioinformatics*, 27(15), 2156–2158. <https://doi.org/10.1093/bioinformatics/btr330>
- Danecek, P., Bonfield, J. K., Liddle, J., Marshall, J., Ohan, V., Pollard, M. O., Whitwham, A., Keane, T., McCarthy, S. A., Davies, R. M., & Li, H. (2021). Twelve years of SAMtools and BCFtools. *GigaScience*, 10(giab008). <https://doi.org/10.1093/gigascience/giab008>
- DeGiorgio, M., Huber, C. D., Hubisz, M. J., Hellmann, I., & Nielsen, R. (2016). SweepFinder2: Increased sensitivity, robustness and flexibility. *Bioinformatics*, 32(12), 1895–1897. <https://doi.org/10.1093/bioinformatics/btw051>
- Delaneau, O., Zagury, J.-F., & Marchini, J. (2013). Improved whole-chromosome phasing for disease and population genetic studies. *Nature Methods*, 10(1), 5–6. <https://doi.org/10.1038/nmeth.2307>
- Delmore, K., Doren, B. M. V., Ullrich, K., Curk, T., Jeugd, H. P. van der, & Liedvogel, M. (2023). *Structural genomic variation and migratory behavior in wild songbirds* [Preprint].

- Delmore, K. E., Hübner, S., Kane, N. C., Schuster, R., Andrew, R. L., Câmara, F., Guigó, R., & Irwin, D. E. (2015). Genomic analysis of a migratory divide reveals candidate genes for migration and implicates selective sweeps in generating islands of differentiation. *Molecular Ecology*, 24(8), 1873–1888. <https://doi.org/https://doi.org/10.1111/mec.13150>
- Delmore, K. E., Lugo Ramos, J. S., Van Doren, B. M., Lundberg, M., Bensch, S., Irwin, D. E., & Liedvogel, M. (2018). Comparative analysis examining patterns of genomic differentiation across multiple episodes of population divergence in birds. *Evolution Letters*, 2(2), 76–87. <https://doi.org/10.1002/evl3.46>
- Delmore, K. E., Van Doren, B. M., Conway, G. J., Curk, T., Garrido-Garduño, T., Germain, R. R., Hasselmann, T., Hiemer, D., Jeugd, H. P. van der, Justen, H., Lugo Ramos, J. S., Maggini, I., Meyer, B. S., Phillips, R. J., Remisiewicz, M., Roberts, G. C. M., Sheldon, B. C., Vogl, W., & Liedvogel, M. (2020a). Individual variability and versatility in an eco-evolutionary model of avian migration. *Proceedings of the Royal Society B: Biological Sciences*, 287(1938), 20201339. <https://doi.org/10.1098/rspb.2020.1339>
- Delmore, K., Illera, J. C., Pérez-Tris, J., Segelbacher, G., Ramos, J. S., Durieux, G., Ishigohoka, J., & Liedvogel, M. (2020b). The evolutionary history and genomics of european blackcap migration. *eLife*, 9, e54462. <https://doi.org/10.7554/eLife.54462>
- Dutheil, J. Y., Ganapathy, G., Hobolth, A., Mailund, T., Uyenoyama, M. K., & Schierup, M. H. (2009). Ancestral Population Genomics: The Coalescent Hidden Markov Model Approach. *Genetics*, 183(1), 259–274. <https://doi.org/10.1534/genetics.109.103010>
- Ewels, P., Magnusson, M., Lundin, S., & Käller, M. (2016). MultiQC: Summarize analysis results for multiple tools and samples in a single report. *Bioinformatics*, 32(19), 3047–3048. <https://doi.org/10.1093/bioinformatics/btw354>
- Faria, R., Johannesson, K., Butlin, R. K., & Westram, A. M. (2019). Evolving Inversions. *Trends in Ecology & Evolution*, 34(3), 239–248. <https://doi.org/10.1016/j.tree.2018.12.005>
- Fasano, G., & Franceschini, A. (1987). A multidimensional version of the Kolmogorov–Smirnov test. *Monthly Notices of the Royal Astronomical Society*, 225(1), 155–170. <https://doi.org/10.1093/mnras/225.1.155>
- Fay, J. C., & Wu, C.-I. (2000). Hitchhiking Under Positive Darwinian Selection. *Genetics*, 155(3), 1405–1413. <https://doi.org/10.1093/genetics/155.3.1405>
- Fedorova, S. A., Reidla, M., Metspalu, E., Metspalu, M., Rootsi, S., Tambets, K., Trofimova, N., Zhadanov, S. I., Kashani, B. H., Olivieri, A., Voevoda, M. I., Osipova, L. P., Platonov, F. A., Tomsy, M. I., Khusnutdinova, E. K., Torroni, A., & Vilems, R. (2013). Autosomal and uniparental portraits of the native populations of Sakha (Yakutia): Implications for the peopling of Northeast Eurasia. *BMC Evolutionary Biology*, 13(1), 127. <https://doi.org/10.1186/1471-2148-13-127>
- Geraldes, A., Basset, P., Smith, K. L., & Nachman, M. W. (2011). Higher differentiation among subspecies of the house mouse (*Mus musculus*) in genomic regions with low

- recombination. *Molecular Ecology*, 20(22), 4722–4736. <https://doi.org/10.1111/j.1365-294X.2011.05285.x>
- Ghurye, J., Rhie, A., Walenz, B. P., Schmitt, A., Selvaraj, S., Pop, M., Phillippy, A. M., & Koren, S. (2019). Integrating Hi-C links with assembly graphs for chromosome-scale assembly. *PLOS Computational Biology*, 15(8), e1007273. <https://doi.org/10.1371/journal.pcbi.1007273>
- Griffiths, R. C., & Marjoram, P. (1997). An ancestral recombination graph. In P. Donnelly & S. Tavaré (Eds.), *Progress in Population Genetics and Human Evolution* (Vol. 87, pp. 257–270). Springer. <http://lamastex.org/recomb/ima.pdf>
- Guan, D., McCarthy, S. A., Wood, J., Howe, K., Wang, Y., & Durbin, R. (2020). Identifying and removing haplotypic duplication in primary genome assemblies. *Bioinformatics*, 36(9), 2896–2898. <https://doi.org/10.1093/bioinformatics/btaa025>
- Guerrero, R. F., Rousset, F., & Kirkpatrick, M. (2012). Coalescent patterns for chromosomal inversions in divergent populations. *Philosophical Transactions of the Royal Society B: Biological Sciences*, 367(1587), 430–438. <https://doi.org/10.1098/rstb.2011.0246>
- Hager, E. R., Harringmeyer, O. S., Wooldridge, T. B., Theingi, S., Gable, J. T., McFadden, S., Neugeboren, B., Turner, K. M., Jensen, J. D., & Hoekstra, H. E. (2022). A chromosomal inversion contributes to divergence in multiple traits between deer mouse ecotypes. *Science*, 377(6604), 399–405. <https://doi.org/10.1126/science.abg0718>
- Haller, B. C., & Messer, P. W. (2019). SLiM 3: Forward Genetic Simulations Beyond the Wright–Fisher Model. *Molecular Biology and Evolution*, 36(3), 632–637. <https://doi.org/10.1093/molbev/msy228>
- Haller, B. C., & Messer, P. W. (2022). SLiM 4: Multispecies Eco-Evolutionary Modeling. *The American Naturalist*, E000–E000. <https://doi.org/10.1086/723601>
- Hejase, H. A., Salman-Minkov, A., Campagna, L., Hubisz, M. J., Lovette, I. J., Gronau, I., & Siepel, A. (2020). Genomic islands of differentiation in a rapid avian radiation have been driven by recent selective sweeps. *Proceedings of the National Academy of Sciences*, 117(48), 30554–30565. <https://doi.org/10.1073/pnas.2015987117>
- Helbig, A. J. (1991). Inheritance of migratory direction in a bird species: A cross-breeding experiment with SE- and SW-migrating blackcaps (*Sylvia atricapilla*). *Behavioral Ecology and Sociobiology*, 28(1), 9–12. <https://doi.org/10.1007/BF00172133>
- Howe, K., Chow, W., Collins, J., Pelan, S., Pointon, D.-L., Sims, Y., Torrance, J., Tracey, A., & Wood, J. (2021). Significantly improving the quality of genome assemblies through curation. *GigaScience*, 10(1), giaa153. <https://doi.org/10.1093/gigascience/giaa153>
- Huang, K., Andrew, R. L., Owens, G. L., Ostevik, K. L., & Rieseberg, L. H. (2020). Multiple chromosomal inversions contribute to adaptive divergence of a dune sunflower ecotype. *Molecular Ecology*, 29(14), 2535–2549. <https://doi.org/10.1111/mec.15428>
- Hudson, R. R. (1983). Properties of a neutral allele model with intragenic recombination. *Theoretical Population Biology*, 23(2), 183–201. [https://doi.org/10.1016/0040-5809\(83\)90013-8](https://doi.org/10.1016/0040-5809(83)90013-8)

- Irwin, D. E., Milá, B., Toews, D. P. L., Brelsford, A., Kenyon, H. L., Porter, A. N., Grossen, C., Delmore, K. E., Alcaide, M., & Irwin, J. H. (2018). A comparison of genomic islands of differentiation across three young avian species pairs. *Molecular Ecology*, *27*(23), 4839–4855. <https://doi.org/https://doi.org/10.1111/mec.14858>
- Jones, F. C., Grabherr, M. G., Chan, Y. F., Russell, P., Mauceli, E., Johnson, J., Swofford, R., Pirun, M., Zody, M. C., White, S., Birney, E., Searle, S., Schmutz, J., Grimwood, J., Dickson, M. C., Myers, R. M., Miller, C. T., Summers, B. R., Knecht, A. K., et al. (2012). The genomic basis of adaptive evolution in threespine sticklebacks. *Nature*, *484*(7392), 55–61. <https://doi.org/10.1038/nature10944>
- Kawakami, T., Mugal, C. F., Suh, A., Nater, A., Burri, R., Smeds, L., & Ellegren, H. (2017). Whole-genome patterns of linkage disequilibrium across flycatcher populations clarify the causes and consequences of fine-scale recombination rate variation in birds. *Molecular Ecology*, *26*(16), 4158–4172. <https://doi.org/10.1111/mec.14197>
- Kelleher, J., Thornton, K. R., Ashander, J., & Ralph, P. L. (2018). Efficient pedigree recording for fast population genetics simulation. *PLOS Computational Biology*, *14*(11), e1006581. <https://doi.org/10.1371/journal.pcbi.1006581>
- Knief, U., Hemmrich-Stanisak, G., Wittig, M., Franke, A., Griffith, S. C., Kempnaers, B., & Forstmeier, W. (2016). Fitness consequences of polymorphic inversions in the zebra finch genome. *Genome Biology*, *17*(1), 199. <https://doi.org/10.1186/s13059-016-1056-3>
- Kong, A., Thorleifsson, G., Gudbjartsson, D. F., Masson, G., Sigurdsson, A., Jonasdottir, A., Walters, G. B., Jonasdottir, A., Gylfason, A., Kristinsson, K. T., Gudjonsson, S. A., Frigge, M. L., Helgason, A., Thorsteinsdottir, U., & Stefansson, K. (2010). Fine-scale recombination rate differences between sexes, populations and individuals. *Nature*, *467*(7319), 1099–1103. <https://doi.org/10.1038/nature09525>
- Kronforst, M. R., Hansen, M. E. B., Crawford, N. G., Gallant, J. R., Zhang, W., Kulathinal, R. J., Kapan, D. D., & Mullen, S. P. (2013). Hybridization Reveals the Evolving Genomic Architecture of Speciation. *Cell Reports*, *5*(3), 666–677. <https://doi.org/10.1016/j.celrep.2013.09.042>
- Lamichhaney, S., Han, F., Berglund, J., Wang, C., Almén, M. S., Webster, M. T., Grant, B. R., Grant, P. R., & Andersson, L. (2016). A beak size locus in Darwin's finches facilitated character displacement during a drought. *Science*, *352*(6284), 470–474. <https://doi.org/10.1126/science.aad8786>
- Lawniczak, M. K. N., Emrich, S. J., Holloway, A. K., Regier, A. P., Olson, M., White, B., Redmond, S., Fulton, L., Appelbaum, E., Godfrey, J., Farmer, C., Chinwalla, A., Yang, S.-P., Minx, P., Nelson, J., Kyung, K., Walenz, B. P., Garcia-Hernandez, E., Aguiar, M., et al. (2010). Widespread Divergence Between Incipient *Anopheles gambiae* Species Revealed by Whole Genome Sequences. *Science*, *330*(6003), 512–514. <https://doi.org/10.1126/science.1195755>
- Lewanski, A. L., Grundle, M. C., & Bradburd, G. S. (2024). The era of the ARG: An introduction to ancestral recombination graphs and their significance in empirical evolutionary genomics. *PLOS Genetics*, *20*(1), e1011110. <https://doi.org/10.1371/journal.pgen.1011110>

- Li, H. (2013). *Aligning sequence reads, clone sequences and assembly contigs with BWA-MEM* [Preprint]. arXiv. <https://doi.org/https://doi.org/10.48550/arXiv.1303.3997>
- Li, H. (2018). Minimap2: Pairwise alignment for nucleotide sequences. *Bioinformatics*, *34*(18), 3094–3100. <https://doi.org/10.1093/bioinformatics/bty191>
- Li, H., & Ralph, P. (2019). Local PCA Shows How the Effect of Population Structure Differs Along the Genome. *Genetics*, *211*(1), 289–304. <https://doi.org/10.1534/genetics.118.301747>
- Lindenbaum, P. (2015). *JVarkit: Java-based utilities for Bioinformatics*. <https://doi.org/10.6084/m9.figshare.1425030.v1>
- Lotterhos, K. E. (2019). The Effect of Neutral Recombination Variation on Genome Scans for Selection. *G3 GenesGenomesGenetics*, *9*(6), 1851–1867. <https://doi.org/10.1534/g3.119.400088>
- Lundberg, M., Mackintosh, A., Petri, A., & Bensch, S. (2021). *Inversions maintain differences between migratory phenotypes of a songbird*. bioRxiv. <https://doi.org/10.1101/2021.04.05.438456>
- Ma, J., & Amos, C. I. (2012). Investigation of Inversion Polymorphisms in the Human Genome Using Principal Components Analysis. *PLOS ONE*, *7*(7), e40224. <https://doi.org/10.1371/journal.pone.0040224>
- Malinsky, M., Challis, R. J., Tyers, A. M., Schiffels, S., Terai, Y., Ngatunga, B. P., Miska, E. A., Durbin, R., Genner, M. J., & Turner, G. F. (2015). Genomic islands of speciation separate cichlid ecomorphs in an East African crater lake. *Science*, *350*(6267), 1493–1498. <https://doi.org/10.1126/science.aac9927>
- Marçais, G., Delcher, A. L., Phillippy, A. M., Coston, R., Salzberg, S. L., & Zimin, A. (2018). MUMmer4: A fast and versatile genome alignment system. *PLOS Computational Biology*, *14*(1), e1005944. <https://doi.org/10.1371/journal.pcbi.1005944>
- Martin, S. H., Davey, J. W., & Jiggins, C. D. (2015). Evaluating the Use of ABBA–BABA Statistics to Locate Introgressed Loci. *Molecular Biology and Evolution*, *32*(1), 244–257. <https://doi.org/10.1093/molbev/msu269>
- Martin, S. H., Davey, J. W., Salazar, C., & Jiggins, C. D. (2019). Recombination rate variation shapes barriers to introgression across butterfly genomes. *PLoS Biology*, *17*(2), 1–28. <https://doi.org/10.1371/journal.pbio.2006288>
- Martin, S. H., & Van Belleghem, S. M. (2017). Exploring Evolutionary Relationships Across the Genome Using Topology Weighting. *Genetics*, *206*(1), 429–438. <https://doi.org/10.1534/genetics.116.194720>
- McKenna, A., Hanna, M., Banks, E., Sivachenko, A., Cibulskis, K., Kernytzky, A., Garimella, K., Altshuler, D., Gabriel, S., Daly, M., & DePristo, M. A. (2010). The Genome Analysis Toolkit: A MapReduce framework for analyzing next-generation DNA sequencing data. *Genome Research*, *20*(9), 1297–1303. <https://doi.org/10.1101/gr.107524.110>
- McVean, G. (2009). A Genealogical Interpretation of Principal Components Analysis. *PLOS Genetics*, *5*(10), e1000686. <https://doi.org/10.1371/journal.pgen.1000686>

- McVean, G. A. T., & Cardin, N. J. (2005). Approximating the coalescent with recombination. *Philosophical Transactions of the Royal Society B: Biological Sciences*, 360(1459), 1387–1393. <https://doi.org/10.1098/rstb.2005.1673>
- Mérot, C., Berdan, E. L., Cayuela, H., Djambazian, H., Ferchaud, A.-L., Laporte, M., Normandeau, E., Ragoussis, J., Wellenreuther, M., & Bernatchez, L. (2021). Locally Adaptive Inversions Modulate Genetic Variation at Different Geographic Scales in a Seaweed Fly. *Molecular Biology and Evolution*, 38(9), 3953–3971. <https://doi.org/10.1093/molbev/msab143>
- Myers, S., Freeman, C., Auton, A., Donnelly, P., & McVean, G. (2008). A common sequence motif associated with recombination hot spots and genome instability in humans. *Nature Genetics*, 40(9), 1124–1129. <https://doi.org/10.1038/ng.213>
- Neafsey, D. E., Lawniczak, M. K. N., Park, D. J., Redmond, S. N., Coulibaly, M. B., Traoré, S. F., Sagnon, N., Costantini, C., Johnson, C., Wiegand, R. C., Collins, F. H., Lander, E. S., Wirth, D. F., Kafatos, F. C., Besansky, N. J., Christophides, G. K., & Muskavitch, M. A. T. (2010). SNP Genotyping Defines Complex Gene-Flow Boundaries Among African Malaria Vector Mosquitoes. *Science*, 330(6003), 514–517. <https://doi.org/10.1126/science.1193036>
- Nei, M., & Gojobori, T. (1986). Simple methods for estimating the numbers of synonymous and nonsynonymous nucleotide substitutions. *Molecular Biology and Evolution*, 3(5), 418–426. <https://doi.org/10.1093/oxfordjournals.molbev.a040410>
- Nielsen, R. (2005). Molecular Signatures of Natural Selection. *Annual Review of Genetics*, 39(1), 197–218. <https://doi.org/10.1146/annurev.genet.39.073003.112420>
- Noor, M., & Bennett, S. (2009). Islands of speciation or mirages in the desert? Examining the role of restricted recombination in maintaining species. *Heredity*, 103, 439–444.
- Okonechnikov, K., Conesa, A., & García-Alcalde, F. (2016). Qualimap 2: Advanced multi-sample quality control for high-throughput sequencing data. *Bioinformatics*, 32(2), 292–294. <https://doi.org/10.1093/bioinformatics/btv566>
- Pamilo, P., & Nei, M. (1988). Relationships between gene trees and species trees. *Molecular Biology and Evolution*, 5(5), 568–583. <https://doi.org/10.1093/oxfordjournals.molbev.a040517>
- Patterson, N., Moorjani, P., Luo, Y., Mallick, S., Rohland, N., Zhan, Y., Genschoreck, T., Webster, T., & Reich, D. (2012). Ancient Admixture in Human History. *Genetics*, 192(3), 1065–1093. <https://doi.org/10.1534/genetics.112.145037>
- Patterson, N., Price, A. L., & Reich, D. (2006). Population Structure and Eigenanalysis. *PLOS Genetics*, 2(12), e190. <https://doi.org/10.1371/journal.pgen.0020190>
- Peter, B. M. (2016). Admixture, Population Structure, and F-Statistics. *Genetics*, 202(4), 1485–1501. <https://doi.org/10.1534/genetics.115.183913>
- Peter, B. M. (2022). A geometric relationship of F2, F3 and F4-statistics with principal component analysis. *Philosophical Transactions of the Royal Society B: Biological Sciences*, 377(1852), 20200413. <https://doi.org/10.1098/rstb.2020.0413>

- Pfeifer, B., Wittelsbuerger, U., Ramos-Onsins, S. E., & Lercher, M. J. (2014). PopGenome: An Efficient Swiss Army Knife for Population Genomic Analyses in R. *Molecular Biology and Evolution*, *31*, 1929–1936. <https://doi.org/10.1093/molbev/msu136>
- Pinheiro, J., Bates, D., DebRoy, S., Sarkar, D., & R Core Team. (2021). *Nlme: Linear and Nonlinear Mixed Effects Models*. <https://CRAN.R-project.org/package=nlme>
- Pracana, R., Priyam, A., Leventis, I., Nichols, R. A., & Wurm, Y. (2017). The fire ant social chromosome supergene variant Sb shows low diversity but high divergence from SB. *Molecular Ecology*, *26*(11), 2864–2879. <https://doi.org/10.1111/mec.14054>
- Price, A. L., Patterson, N. J., Plenge, R. M., Weinblatt, M. E., Shadick, N. A., & Reich, D. (2006). Principal components analysis corrects for stratification in genome-wide association studies. *Nature Genetics*, *38*(8), 904–909. <https://doi.org/10.1038/ng1847>
- Purcell, S., Neale, B., Todd-Brown, K., Thomas, L., Ferreira, M. A. R., Bender, D., Maller, J., Sklar, P., Bakker, P. I. W. de, Daly, M. J., & Sham, P. C. (2007). PLINK: A Tool Set for Whole-Genome Association and Population-Based Linkage Analyses. *The American Journal of Human Genetics*, *81*(3), 559–575. <https://doi.org/10.1086/519795>
- Ralph, P., Thornton, K., & Kelleher, J. (2020). Efficiently Summarizing Relationships in Large Samples: A General Duality Between Statistics of Genealogies and Genomes. *Genetics*, *215*(3), 779–797. <https://doi.org/10.1534/genetics.120.303253>
- Reich, D., Thangaraj, K., Patterson, N., Price, A. L., & Singh, L. (2009). Reconstructing Indian population history. *Nature*, *461*(7263), 489–494. <https://doi.org/10.1038/nature08365>
- Renaut, S., Grassa, C. J., Yeaman, S., Moyers, B. T., Lai, Z., Kane, N. C., Bowers, J. E., Burke, J. M., & Rieseberg, L. H. (2013). Genomic islands of divergence are not affected by geography of speciation in sunflowers. *Nature Communications*, *4*(1), 1827. <https://doi.org/10.1038/ncomms2833>
- Rhie, A., McCarthy, S. A., Fedrigo, O., Damas, J., Formenti, G., Koren, S., Uliano-Silva, M., Chow, W., Fungtammasan, A., Kim, J., Lee, C., Ko, B. J., Chaisson, M., Gedman, G. L., Cantin, L. J., Thibaud-Nissen, F., Haggerty, L., Bista, I., Smith, M., et al. (2021). Towards complete and error-free genome assemblies of all vertebrate species. *Nature*, *592*(7856), 737–746. <https://doi.org/10.1038/s41586-021-03451-0>
- Roesti, M., Moser, D., & Berner, D. (2013). Recombination in the threespine stickleback genome—patterns and consequences. *Molecular Ecology*, *22*(11), 3014–3027. <https://doi.org/10.1111/mec.12322>
- Rougemont, Q., Xuereb, A., Dallaire, X., Moore, J.-S., Normandeau, E., Rondeau, E. B., Withler, R. E., Van Doornik, D. M., Crane, P. A., Naish, K. A., Garza, J. C., Beacham, T. D., Koop, B. F., & Bernatchez, L. (2021). Long-distance migration is a major factor driving local adaptation at continental scale in Coho salmon. *Molecular Ecology*, n/a(n/a). <https://doi.org/10.1111/mec.16339>
- Rubin, C.-J., Enbody, E. D., Dobrev, M. P., Abzhanov, A., Davis, B. W., Lamichhaney, S., Pettersson, M., Sendell-Price, A. T., Sprehn, C. G., Valle, C. A., Vasco, K., Wallerman, O., Grant, B. R., Grant, P. R., & Andersson, L. (2022). Rapid adaptive radiation

- of Darwin's finches depends on ancestral genetic modules. *Science Advances*, 8(27), eabm5982. <https://doi.org/10.1126/sciadv.abm5982>
- Ruiz-Arenas, C., Cáceres, A., López-Sánchez, M., Tolosana, I., Pérez-Jurado, L., & González, J. R. (2019). scoreInvHap: Inversion genotyping for genome-wide association studies. *PLOS Genetics*, 15(7), e1008203. <https://doi.org/10.1371/journal.pgen.1008203>
- Sabeti, P. C., Reich, D. E., Higgins, J. M., Levine, H. Z. P., Richter, D. J., Schaffner, S. F., Gabriel, S. B., Platko, J. V., Patterson, N. J., McDonald, G. J., Ackerman, H. C., Campbell, S. J., Altshuler, D., Cooper, R., Kwiatkowski, D., Ward, R., & Lander, E. S. (2002). Detecting recent positive selection in the human genome from haplotype structure. *Nature*, 419(6909), 832–837. <https://doi.org/10.1038/nature01140>
- Sabeti, P. C., Varilly, P., Fry, B., Lohmueller, J., Hostetter, E., Cotsapas, C., Xie, X., Byrne, E. H., McCarroll, S. A., Gaudet, R., Schaffner, S. F., Lander, E. S., Frazer, K. A., Ballinger, D. G., Cox, D. R., Hinds, D. A., Stuve, L. L., Gibbs, R. A., Belmont, J. W., et al. (2007). Genome-wide detection and characterization of positive selection in human populations. *Nature*, 449(7164), 913–918. <https://doi.org/10.1038/nature06250>
- Setter, D., Mousset, S., Cheng, X., Nielsen, R., DeGiorgio, M., & Hermisson, J. (2020). VolcanoFinder: Genomic scans for adaptive introgression. *PLOS Genetics*, 16(6), e1008867. <https://doi.org/10.1371/journal.pgen.1008867>
- Shao, C., Sun, S., Liu, K., Wang, J., Li, S., Liu, Q., Deagle, B. E., Seim, I., Biscontin, A., Wang, Q., Liu, X., Kawaguchi, S., Liu, Y., Jarman, S., Wang, Y., Wang, H.-Y., Huang, G., Hu, J., Feng, B., et al. (2023). The enormous repetitive Antarctic krill genome reveals environmental adaptations and population insights. *Cell*, 186(6), 1279–1294.e19. <https://doi.org/10.1016/j.cell.2023.02.005>
- Shipilina, D., Pal, A., Stankowski, S., Chan, Y. F., & Barton, N. H. (2023). On the origin and structure of haplotype blocks. *Molecular Ecology*, 32(6), 1441–1457. <https://doi.org/10.1111/mec.16793>
- Singhal, S., Leffler, E. M., Sannareddy, K., Turner, I., Venn, O., Hooper, D. M., Strand, A. I., Li, Q., Raney, B., Balakrishnan, C. N., Griffith, S. C., McVean, G., & Przeworski, M. (2015). Stable recombination hotspots in birds. *Science*, 350(6263), 928–932. <https://doi.org/10.1126/science.aad0843>
- Smeds, L., Qvarnström, A., & Ellegren, H. (2016). Direct estimate of the rate of germline mutation in a bird. *Genome Research*, 26(9), 1211–1218. <https://doi.org/10.1101/gr.204669.116>
- Smukowski Heil, C. S., Ellison, C., Dubin, M., & Noor, M. A. F. (2015). Recombining without Hotspots: A Comprehensive Evolutionary Portrait of Recombination in Two Closely Related Species of *Drosophila*. *Genome Biology and Evolution*, 7(10), 2829–2842. <https://doi.org/10.1093/gbe/evv182>
- Speidel, L., Forest, M., Shi, S., & Myers, S. R. (2019). A method for genome-wide genealogy estimation for thousands of samples. *Nature Genetics*, 51(9), 1321–1329. <https://doi.org/10.1038/s41588-019-0484-x>

- Spence, J. P., & Song, Y. S. (2019). Inference and analysis of population-specific fine-scale recombination maps across 26 diverse human populations. *Science Advances*, 5(10), eaaw9206. <https://doi.org/10.1126/sciadv.aaw9206>
- Stern, A. J., Wilton, P. R., & Nielsen, R. (2019). An approximate full-likelihood method for inferring selection and allele frequency trajectories from DNA sequence data. *PLoS Genetics*, 15(9), 1–32. <https://doi.org/10.1371/journal.pgen.1008384>
- Stevison, L. S., Hoehn, K. B., & Noor, M. A. F. (2011). Effects of Inversions on Within- and Between-Species Recombination and Divergence. *Genome Biology and Evolution*, 3, 830–841. <https://doi.org/10.1093/gbe/evr081>
- Stevison, L. S., Woerner, A. E., Kidd, J. M., Kelley, J. L., Veeramah, K. R., McManus, K. F., Great Ape Genome Project, Bustamante, C. D., Hammer, M. F., & Wall, J. D. (2016). The Time Scale of Recombination Rate Evolution in Great Apes. *Molecular Biology and Evolution*, 33(4), 928–945. <https://doi.org/10.1093/molbev/msv331>
- Tajima, F. (1989). Statistical method for testing the neutral mutation hypothesis by DNA polymorphism. *Genetics*, 123(3), 585–595. <https://doi.org/PMC1203831>
- Taylor, J. E. (2013). The effect of fluctuating selection on the genealogy at a linked site. *Theoretical Population Biology*, 87, 34–50. <https://doi.org/10.1016/j.tpb.2013.03.004>
- Todesco, M., Owens, G. L., Bercovich, N., Légaré, J.-S., Soudi, S., Burge, D. O., Huang, K., Ostevik, K. L., Drummond, E. B. M., Imerovski, I., Lande, K., Pascual-Robles, M. A., Nanavati, M., Jahani, M., Cheung, W., Staton, S. E., Muños, S., Nielsen, R., Donovan, L. A., et al. (2020). Massive haplotypes underlie ecotypic differentiation in sunflowers. *Nature*, 584(7822), 602–607. <https://doi.org/10.1038/s41586-020-2467-6>
- Van Doren, B. M., Campagna, L., Helm, B., Illera, J. C., Lovette, I. J., & Liedvogel, M. (2017). Correlated patterns of genetic diversity and differentiation across an avian family. *Molecular Ecology*, 26(15), 3982–3997. <https://doi.org/10.1111/mec.14083>
- Voight, B. F., Kudaravalli, S., Wen, X., & Pritchard, J. K. (2006). A Map of Recent Positive Selection in the Human Genome. *PLOS Biology*, 4(3), e72. <https://doi.org/10.1371/journal.pbio.0040072>
- Wakeley, J. (2008). *Coalescent Theory: An Introduction* (1st ed.). W. H. Freeman.
- Wakeley, J. (2020). Developments in coalescent theory from single loci to chromosomes. *Theoretical Population Biology*, 133, 56–64. <https://doi.org/10.1016/j.tpb.2020.02.002>
- Wellenreuther, M., & Bernatchez, L. (2018). Eco-Evolutionary Genomics of Chromosomal Inversions. *Trends in Ecology & Evolution*, 33(6), 427–440. <https://doi.org/10.1016/j.tree.2018.04.002>
- Wiuf, C., & Hein, J. (1999). Recombination as a Point Process along Sequences. *Theoretical Population Biology*, 55(3), 248–259. <https://doi.org/10.1006/tpbi.1998.1403>
- Wolf, J. B. W., & Ellegren, H. (2017). Making sense of genomic islands of differentiation in light of speciation. *Nature Reviews Genetics*, 18(2), 87–100. <https://doi.org/10.1038/nrg.2016.133>

Yi, X., Liang, Y., Huerta-Sanchez, E., Jin, X., Cuo, Z. X. P., Pool, J. E., Xu, X., Jiang, H., Vinckenbosch, N., Korneliussen, T. S., Zheng, H., Liu, T., He, W., Li, K., Luo, R., Nie, X., Wu, H., Zhao, M., Cao, H., et al. (2010). Sequencing of 50 Human Exomes Reveals Adaptation to High Altitude. *Science*, 329(5987), 75–78. <https://doi.org/10.1126/science.1190371>

Supplementary Information

Distinct patterns of genetic variation at low-recombining genomic regions represent haplotype structure

Jun Ishigohoka^{1,*} Karen Bascón-Cardozo¹ Andrea Bours¹ Janina Fuß²
Arang Rhie³ Jacquelyn Mountcastle⁴ Bettina Haase⁴ William Chow⁵
Joanna Collins⁵ Kerstin Howe⁵ Marcela Uliano-Silva⁵ Olivier Fedrigo⁴
Erich D. Jarvis^{4,6,7} Javier Pérez-Tris⁸ Juan Carlos Illera⁹
Miriam Liedvogel^{1,10,*}

¹Max Planck Institute for Evolutionary Biology, Plön, Germany

²Institute of Clinical Molecular Biology (IKMB), Kiel University, Kiel, Germany

³Genome Informatics Section, Computational and Statistical Genomics Branch, National Human Genome Research Institute, National Institutes of Health, Bethesda, MD, USA

⁴The Vertebrate Genome Lab, Rockefeller University, New York, NY, USA

⁵Wellcome Sanger Institute, Cambridge, UK

⁶Laboratory of Neurogenetics of Language, Rockefeller University, New York, NY, USA

⁷The Howards Hughes Medical Institute, Chevy Chase, MD, USA

⁸Department of Biodiversity, Ecology and Evolution, Complutense University of Madrid, Madrid, Spain

⁹Research Unit of Biodiversity (UO-CSIC-PA), Oviedo University, Mieres, Spain

¹⁰Institute of Avian Research, Wilhelmshaven, Germany

* Correspondence: [Jun Ishigohoka <ishigohoka@evolbio.mpg.de>](mailto:ishigohoka@evolbio.mpg.de), [Miriam Liedvogel <liedvogel@evolbio.mpg.de>](mailto:liedvogel@evolbio.mpg.de)

Contents

1 Supplementary Notes

- 1.1 Discussion: Contribution of genealogical and mutational noise on local genetic variation
- 1.2 Discussion: Effects of selection on distinct genetic variation
- 1.3 Results and discussion: Spread of individuals of low-recombining populations in local PCA

2 Supplementary Tables

3 Supplementary Figures

- 3.1 Whole-genome PCA
- 3.2 Local PCA and recombination map
- 3.3 Putative inversions
 - 3.3.1 PCA
 - 3.3.2 LD and genotype-specific recombination map
 - 3.3.3 Breakpoint analysis
- 3.4 Effect of reduced recombination rate on pattern of local genetic variation
 - 3.4.1 Effect of demography and local recombination rate (coalescent simulation)
 - 3.4.2 Species-wide reduction of local recombination rate (forward simulation)
 - 3.4.3 Population-specific reduction of local recombination rate (forward simulation)
- 3.5 Effect of selection
 - 3.5.1 Effects of selection in blackcap genome
 - 3.5.2 Effects of selection at low-recombining regions (forward simulation)
- 3.6 Pericentromeric regions in outlier regions
- 3.7 Genealogical interpretation

4 References

1 Supplementary Notes

1.1 Discussion: Contribution of genealogical and mutational noise on local genetic variation

The amount of genealogical and mutational noise on realised genetic variation is influenced by the number of genealogies, the length of the genomic interval, and the length of branches. First, the effect of genealogical noise on realised genetic variation reduces as the number of genealogies increases (i.e. as the local recombination rate increases). If a genomic interval contains only one genealogy with enough mutations, then the realised genetic variation tends to reflect this particular tree (i.e. without removal of the genealogical noise) instead of a set of trees with different probabilities expected under the population history. On the contrary, if a genomic interval contains many genealogies each with enough mutations (i.e. with removal of genealogical noise), then the realised genetic variation tends to reflect the expectation under the population history. Second, the effect of mutational noise on realised genetic variation reduces as the product of branch length and the genomic interval increases. This is because the product represents total amount of substrate for mutations to occur in one ancestral haplotype (Shipilina et al., 2023). When this product is small, length of genealogical branches may be disproportionately represented by the number of mutations, increasing the relative effect of mutational noise.

1.2 Discussion: Effects of selection on distinct genetic variation

Using neutral simulations and comparing them with simulations with selection, we showed that primary axes of PCA represent effect of genealogical noise at low-recombining regions, instead of effect of selection (distorted genealogies). The prominent effect of reduced recombination rate over selection may be partly due to the scenarios tested in our simulations. For example, we tested the effects of positive selection under the hard sweep model, in which selection acted on a novel mutation in a single copy, resulting in fixation of a single haplotype. Other scenarios of selection causing multiple haplotypes, such as selection on standing genetic variation (Stephan, 2019), may result in greater contribution by selection on haplotype structure than by reduced recombination rate.

1.3 Results and discussion: Spread of individuals of low-recombining populations in local PCA

We note that the observed patterns of genetic variation at the population-specific low-recombining regions in the blackcap are also qualitatively similar to transient effect of population-specific selection (spread of individuals of population without selection (Sup. Fig. 32B)). However, the selection scenario cannot explain the empirical observations of moderate levels of nucleotide diversity (Sup. Fig. 28) and Tajima's D values around the genome-wide average (Sup. Fig. 29), and is hence unlikely.

2 Supplementary Tables

Supplementary Table 1: Samples used in this study. The spreadsheet can be downloaded from bioRxiv.

Supplementary Table 2: Zebra finch chromosomes (GCA_003957565.4) and corresponding blackcap chromosomes in our *de novo*-assembled genome. Note that Sylvioidea, to which the blackcap belongs, has neo-sex chromosome segments (in Z and W) originating from a part of chromosome 4A (zebra finch, homologous to blackcap chromosome 21) (Leroy et al., 2021; Pala et al., 2012; Sigeman et al., 2020, 2021).

Chr. (Zebra finch)	Length [bp]	Chr. (Blackcap)	Length [bp]
1	114,020,016	2	115,287,908
1A	71,569,005	5	72,605,035
2	151,653,088	1	153,194,430
3	112,598,992	3	113,359,798
4	70,982,421	4	72,978,054
4A	19,491,698	21	10,058,197
5	61,663,524	6	63,423,007
6	35,592,820	8	35,969,369
7	37,979,234	7	38,862,568
8	31,251,066	9	31,650,914
9	25,529,500	10	26,389,481
10	20,543,327	13	20,608,123
11	21,108,237	12	22,249,080
12	20,384,687	11	22,342,531
13	18,052,104	14	19,084,229
14	16,340,488	15	16,052,774
15	13,771,869	17	14,194,216
16	1,095,113	17	14,194,216
17	11,257,394	19	11,408,529
18	11,152,170	18	11,994,622
19	8,335,140	20	11,247,436
20	14,749,488	16	15,230,834
21	7,924,511	22	7,560,935
22	4,608,043	28	4,652,909
23	6,804,446	24	6,883,216
24	7,620,594	23	7,468,107
25	2,880,192	30	2,016,562
26	6,804,938	25	6,775,589
27	5,378,928	27	5,004,062
28	5,866,305	26	5,062,550
29	2,636,872	29	2,201,499
W	20,846,394	W	21,688,951
Z	75,396,176	Z	88,576,696

Supplementary Table 3: Genomic regions with distinct pattern of genetic variation (“outliers” based on local PCA using *lostruct*).

Outlier ID	Chromosome	From [bp]	To [bp]	Length [bp]	Red. rec.
outlier_1_1	1	56,264,814	57,679,298	1,414,485	Spp-wide
outlier_1_2	1	76,931,639	77,195,852	264,214	Spp-wide
outlier_2_1	2	17,876,150	18,183,386	307,237	Spp-wide
outlier_2_2	2	18,301,736	19,824,380	1,522,645	Spp-wide
outlier_2_3	2	114,618,118	114,874,768	256,651	CapeVerde
outlier_3_1	3	1,317,747	1,464,754	147,008	No reduction
outlier_3_2	3	108,194,892	108,406,259	211,368	Azores
outlier_4_1	4	11,647,463	11,966,907	319,445	med_sw
outlier_5_1	5	68,065,279	68,294,444	229,166	Spp-wide
outlier_6_1	6	5,687,267	6,323,968	636,702	Spp-wide
outlier_6_2	6	62,340,071	62,456,329	116,259	No reduction
outlier_8_1	8	30,282,659	30,636,429	353,771	Spp-wide
outlier_10_1	10	11,602,450	13,202,422	1,599,973	Spp-wide
outlier_12_1	12	61	208,254	208,194	Spp-wide
outlier_12_2	12	1,850,450	2,310,703	460,254	CapeVerde
outlier_12_3	12	14,118,030	22,229,395	8,111,366	Spp-wide
outlier_14_1	14	43	207,189	207,147	Spp-wide
outlier_14_2	14	14,789,430	15,024,671	235,242	Azores;CapeVerde
outlier_14_3	14	15,956,522	16,206,154	249,633	Azores;CapeVerde
outlier_15_1	15	13,458,327	14,146,280	687,954	Azores;CapeVerde
outlier_15_2	15	15,846,846	16,049,116	202,271	Spp-wide
outlier_16_1	16	1,510,566	1,842,318	331,753	Spp-wide
outlier_17_1	17	13,936,617	14,179,092	242,476	Spp-wide
outlier_20_1	20	25,274	338,180	312,907	Spp-wide
outlier_20_2	20	1,499,745	1,627,522	127,778	Azores;CapeVerde
outlier_21_1	21	611,083	757,333	146,251	Azores
outlier_21_2	21	3,003,124	3,440,115	436,992	Azores;CapeVerde
outlier_28_1	28	939,876	1,143,638	203,763	Azores;CapeVerde
outlier_30_1	30	72	1,471,845	1,471,774	Spp-wide
outlier_Z_1	Z	14,585,807	14,978,909	393,103	Spp-wide
outlier_Z_2	Z	23,428,533	24,628,650	1,200,118	Spp-wide
outlier_Z_3	Z	47,230,133	47,412,498	182,366	Spp-wide

Supplementary Table 4: Genomic regions within which soft-clipped reads were analysed to identify breakpoints of putative inversions at outlier_12_3 and outlier_30_1.

Chromosome	From	To
12	14,080,000	14,250,000
12	20,500,000	22,249,080
30	0	160,000
30	1,340,000	1,475,000

Supplementary Table 5: Soft-clipped segments remapped to the blackcap reference. The first two columns are filtered positions (detailed in Materials and Methods and Sup. Fig. 15) of putative breakpoints based on soft clip reads associated with PCA-based genotype at putative inversions at outlier_12_3 and outlier_30_1. The third through the sixth columns show summary of remapped soft-clipped segments. The absence of mapping to the other end of the outlier region indicates that our analysis based on soft-clip proportion of Illumina short reads failed to locate breakpoints of the putative inversions.

Chromosome	Position [bp]	Chromosome	From [bp]	To [bp]	Mean depth
12	14,174,953	13	20,601,341	20,601,412	66.96
12	14,174,953	3	113,350,210	113,350,264	96.27
12	14,174,961	5	68,337,734	68,337,769	30.61
12	14,174,961	5	68,337,771	68,337,824	79.78
12	21,703,198	12	21,703,358	21,703,473	108.40
12	21,800,952	scaffold_096	14,484	14,525	17.31
12	21,800,952	scaffold_096	21,919	21,967	26.78
12	21,800,952	scaffold_133	19,291	19,372	111.66
12	22,046,831	1	141,582,638	141,582,679	29.71
12	22,046,831	2	85,518,469	85,518,525	22.98
12	22,046,831	W	3,399,537	3,399,588	58.15
12	22,046,831	W	3,765,336	3,765,394	22.64
12	22,046,831	W	19,239,977	19,240,059	50.27
30	142,877	30	143,588	143,705	217.43

Supplementary Table 6: Six models of recombination suppression at a haplotype block simulated with SLiM. We investigated whether inference of genotype-specific recombination maps can capture heterozygote-specific suppression of recombination at polymorphic inversions by performing simulation under the six models of recombination suppression. N: normal (non-inversion) allele; I: inversion allele. The results are shown in Sup. Fig. 13.

	Model 1	Model 2	Model 3	Model 4	Model 5	Model 6
Derived haplotype frequency	0.2	0.2	0.2	0.8	0.8	0.8
Recombination suppression N-I	Yes	Yes	Yes	Yes	Yes	Yes
Recombination suppression I-I	No	Yes	Yes	No	Yes	Yes
Recombination suppression N-N	No	No	Yes	No	No	Yes

Supplementary Table 7: Result of Fisher's exact tests for the number of tandem repeats with unit sizes longer than or equal to 150 bp within and outside of outlier regions. Genomic distribution of tandem repeats is visualised in Sup. Fig. 33.

class	n. long TRs in	n. long TRs out	total length [bp]	95% CI of odds ratio	p-value
spp-wide	10	62	19,191,668	3.9-16.8	<0.001
pop-specific	0	72	3,335,331	0.0-16.3	1.000

Supplementary Table 8: 11 models of demography and recombination maps simulated with msprime.

Scenario	Relative rec. rate	Pop. subdivision	Unequal pop. size	Gene flow
1	1.00	No	-	-
2	1.00	Yes	No	No
3	1.00	Yes	No	Yes
4	0.01	Yes	No	No
5	0.00	Yes	No	No
6	0.01	Yes	No	Yes
7	0.00	Yes	No	Yes
8	0.01	Yes	Yes	No
9	0.01	Yes	Yes	Yes
10	0.00	Yes	Yes	No
11	0.00	Yes	Yes	Yes

Supplementary Table 9: Generalised linear mixed-effects model (GLMM) with Gamma distribution with log-link function testing the fixed effects of outlier regions on π , treating chromosome, population, and species-wide/population-specific low-recombining region as random effects variables.

	Estimate	SE	t-value	p-value
Intercept	-5.683314	0.054636	-104.022	<2e-16
outlier_1_1	-1.356542	0.014813	-91.576	<2e-16
outlier_1_2	-0.815256	0.032498	-25.087	<2e-16
outlier_2_1	-1.149724	0.029935	-38.408	<2e-16
outlier_2_2	-1.973864	0.015217	-129.712	<2e-16
outlier_2_3	0.314815	0.031690	9.934	<2e-16
outlier_3_1	-1.068258	0.046546	-22.951	<2e-16
outlier_3_2	0.440471	0.035297	12.479	<2e-16
outlier_4_1	-0.615527	0.030914	-19.911	<2e-16
outlier_5_1	-1.426243	0.032550	-43.817	<2e-16
outlier_6_1	-2.233589	0.021155	-105.584	<2e-16
outlier_6_2	0.156340	0.046986	3.327	0.000877
outlier_8_1	-2.110366	0.027630	-76.380	<2e-16
outlier_10_1	-1.681078	0.016472	-102.056	<2e-16
outlier_12_1	-1.059585	0.035687	-29.691	<2e-16
outlier_12_2	-2.917098	0.027999	-104.185	<2e-16
outlier_13_3	-0.006737	0.008072	-0.835	0.403969
outlier_14_1	-0.973331	0.034501	-28.212	<2e-16
outlier_14_2	0.186851	0.033156	5.636	1.75e-08
outlier_14_3	-2.485696	0.038057	-65.315	<2e-16
outlier_15_1	0.377986	0.020905	18.081	<2e-16
outlier_15_2	-1.212848	0.034497	-35.158	<2e-16
outlier_16_1	-1.482747	0.028237	-52.510	<2e-16
outlier_17_1	-0.800511	0.032404	-24.704	<2e-16
outlier_20_1	-2.039013	0.029654	-68.761	<2e-16
outlier_20_2	-0.268680	0.042148	-6.375	1.83e-10
outlier_21_1	0.002279	0.040307	0.057	0.954921
outlier_21_2	0.211965	0.025634	8.269	<2e-16

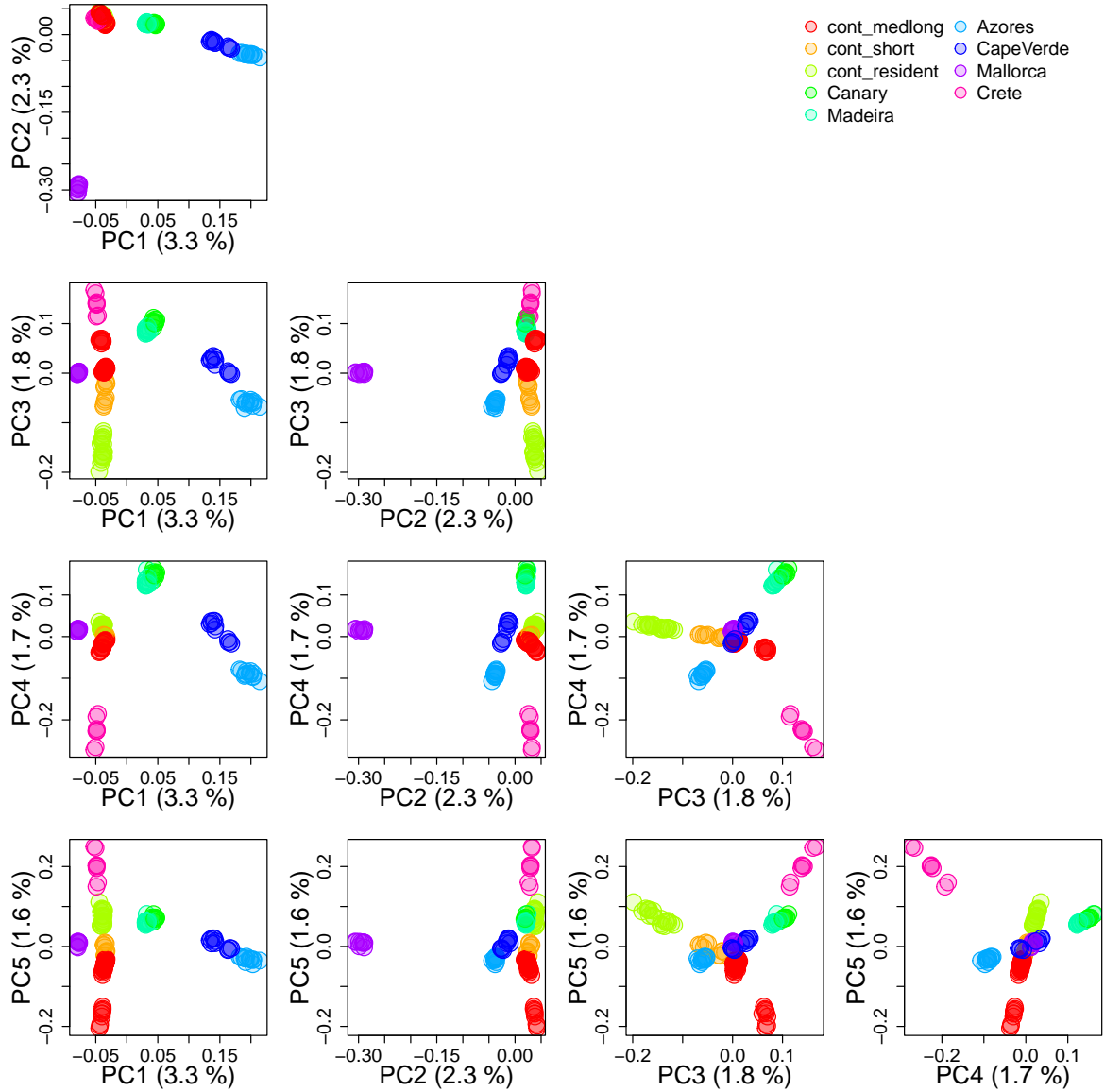
	Estimate	SE	t-value	p-value
outlier_28_1	-0.661910	0.035531	-18.629	<2e-16
outlier_30_1	0.487019	0.025900	18.804	<2e-16
outlier_Z_1	0.809887	0.039414	20.548	<2e-16
outlier_Z_2	-0.886677	0.015829	-56.017	<2e-16
outlier_Z_3	-0.666644	0.036808	-18.111	<2e-16

Supplementary Table 10: Linear mixed-effects model testing the fixed effects of outlier regions on Tajima's D, treating chromosome, population, and species-wide/population-specific low-recombining region as random effects variables.

	Estimate	SE	t-value	p-value
Intercept	-0.2196099	0.12894037	-1.70319	0.0885
outlier_1_1	-0.7610205	0.01809935	-42.04684	0.0000
outlier_1_2	-0.2288175	0.03922094	-5.83406	0.0000
outlier_2_1	-0.0892122	0.03723778	-2.39574	0.0166
outlier_2_2	-0.7153382	0.01943918	-36.79879	0.0000
outlier_2_3	0.3177984	0.01801459	17.64116	0.0000
outlier_3_1	0.2517975	0.02484491	10.13477	0.0000
outlier_3_2	-0.0288526	0.02100110	-1.37386	0.1695
outlier_4_1	-0.3321943	0.01922048	-17.28335	0.0000
outlier_5_1	-0.6917180	0.04515554	-15.31856	0.0000
outlier_6_1	-1.2596634	0.02867480	-43.92929	0.0000
outlier_6_2	0.3531770	0.02928475	12.06010	0.0000
outlier_8_1	-1.4311088	0.03868169	-36.99706	0.0000
outlier_10_1	-0.1856898	0.01995984	-9.30317	0.0000
outlier_12_1	0.0202982	0.04782549	0.42442	0.6713
outlier_12_2	0.3645219	0.01734986	21.01008	0.0000
outlier_12_3	0.1153698	0.00717804	16.07261	0.0000
outlier_14_1	0.0395049	0.04697090	0.84105	0.4003
outlier_14_2	0.0401297	0.01945566	2.06263	0.0391
outlier_14_3	0.2814038	0.02327442	12.09069	0.0000
outlier_15_1	0.2511851	0.01110711	22.61479	0.0000
outlier_15_2	-0.5317589	0.04838627	-10.98987	0.0000
outlier_16_1	-0.3228744	0.03712518	-8.69691	0.0000
outlier_17_1	0.1660338	0.04238137	3.91761	0.0001
outlier_20_1	-1.2035238	0.04124938	-29.17678	0.0000
outlier_20_2	-0.0907998	0.02876938	-3.15613	0.0016
outlier_21_1	0.1726014	0.02510559	6.87502	0.0000
outlier_21_2	0.1919318	0.01356198	14.15220	0.0000
outlier_28_1	-0.0454387	0.02369477	-1.91767	0.0552
outlier_30_1	0.1352691	0.01609042	8.40681	0.0000
outlier_Z_1	0.6877002	0.05775299	11.90761	0.0000
outlier_Z_2	-0.6255465	0.02026285	-30.87160	0.0000
outlier_Z_3	-0.5121660	0.05049917	-10.14207	0.0000

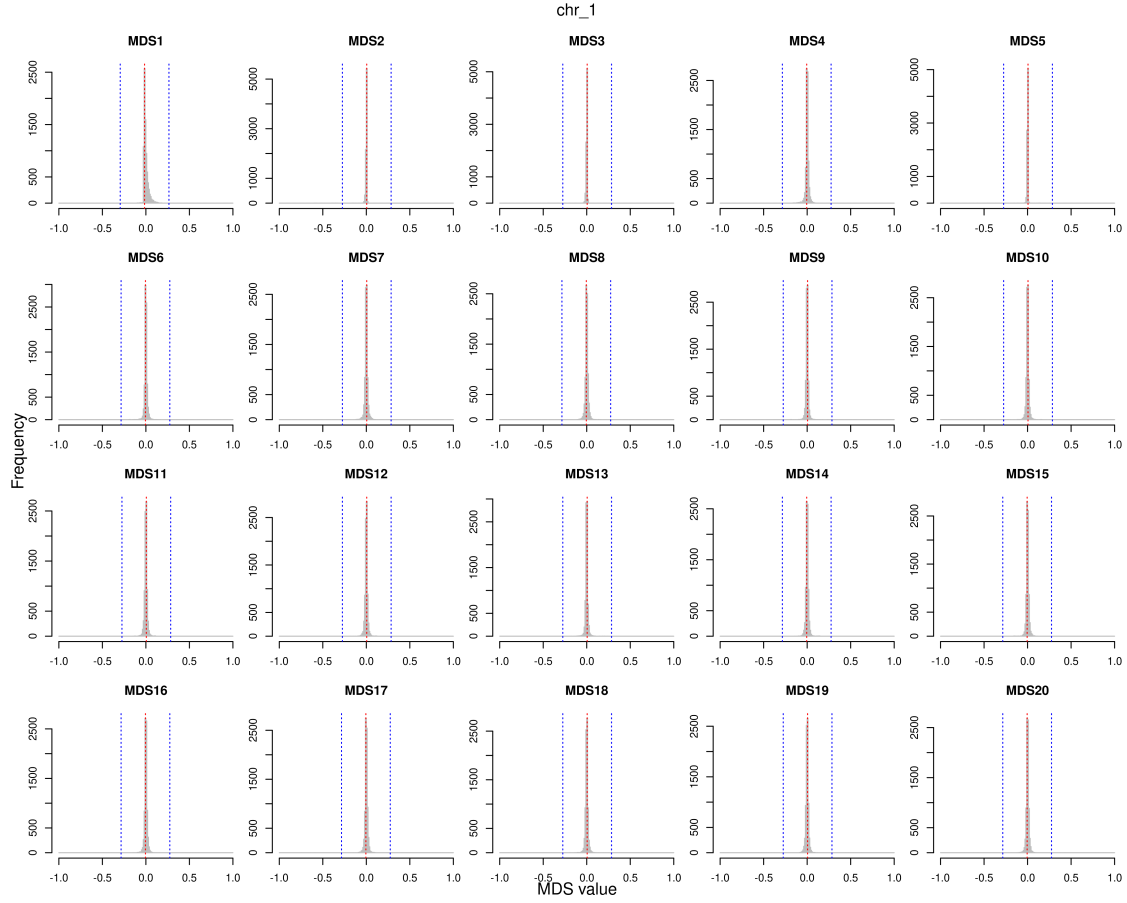
3 Supplementary Figures

3.1 Whole-genome PCA

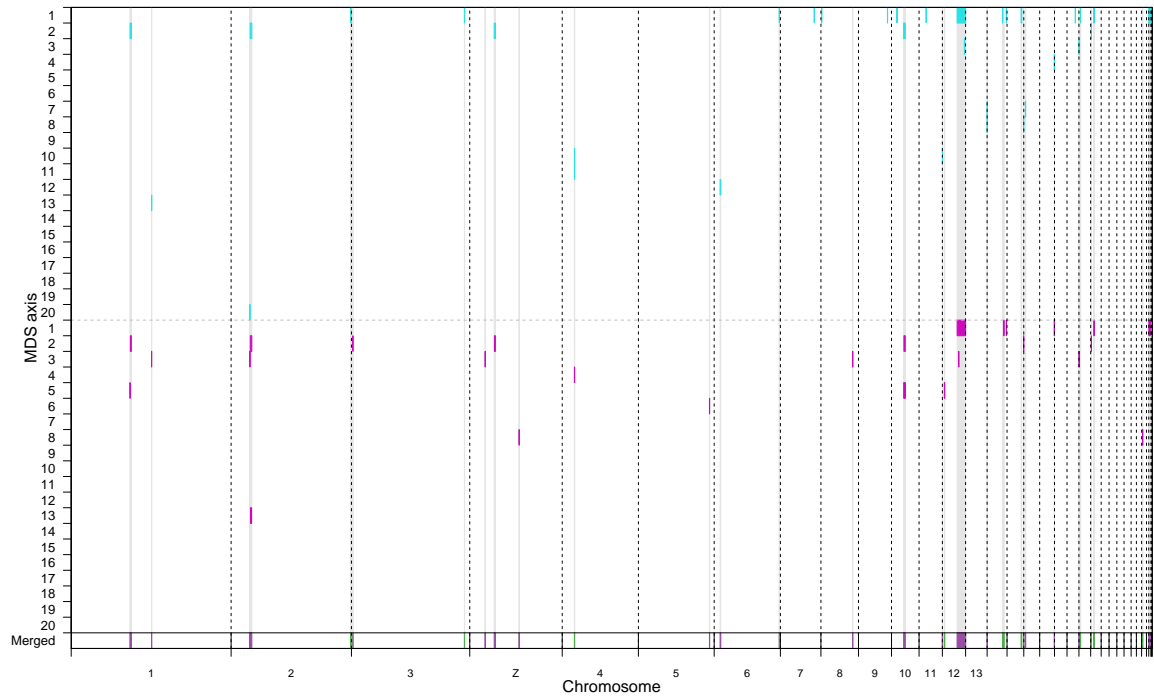


Supplementary Figure 1: Population structure analysed with whole-genome PCA. Supplementary data related to Fig. 2B, C. The first five PCs are shown.

3.2 Local PCA and recombination map



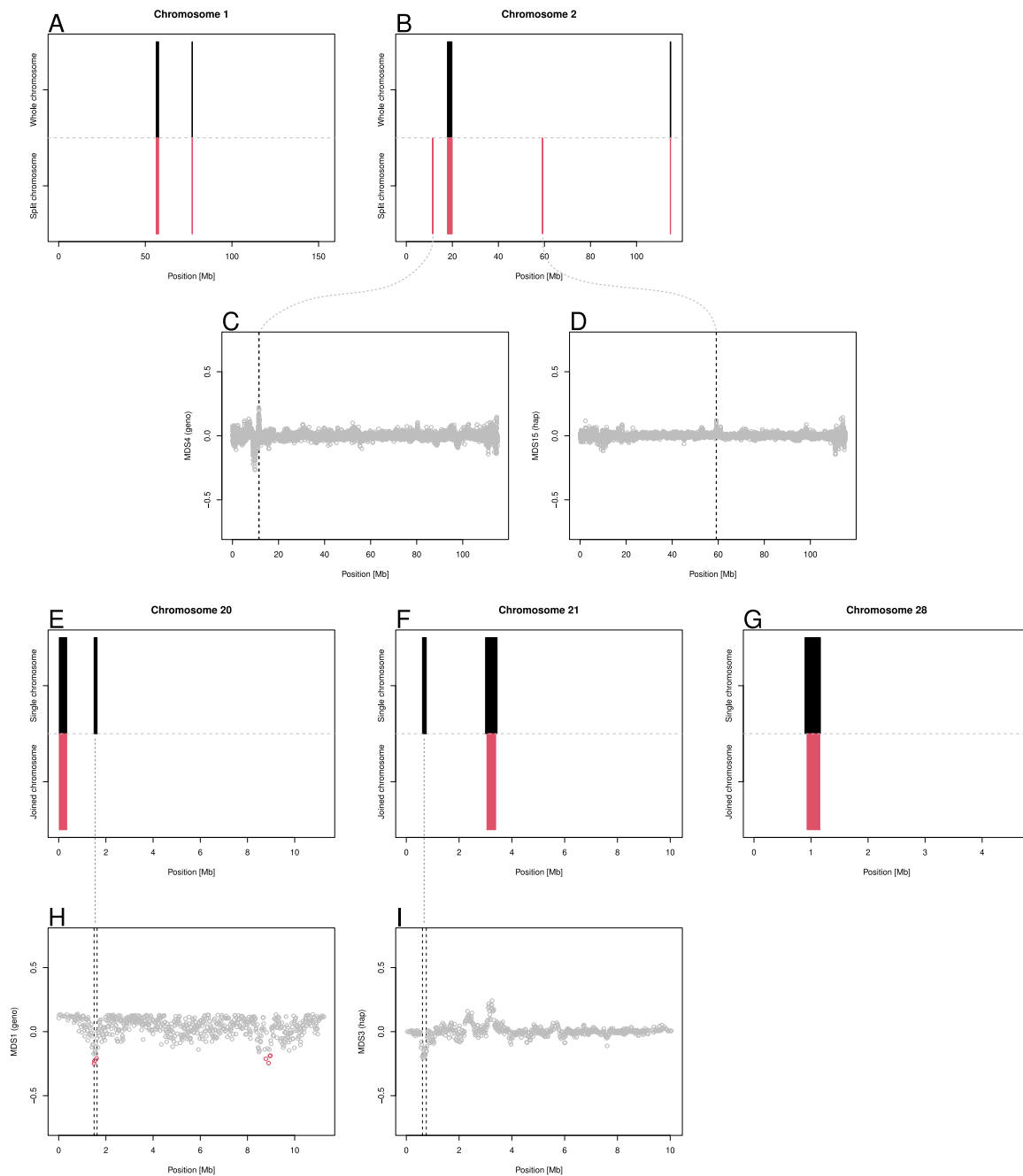
Supplementary Figure 2: Distribution of MDS values of windows of a chromosome in `lostruct`. Each panel shows the distribution of MDS values of windows in an exemplified chromosome (chromosome 1) in local PCA using `lostruct` based on genotypes. Red lines show median of MDS values. Genomic regions with at least 10 windows with MDS values away from the median by 0.3 (blue lines) were defined as “outliers” (see Materials and Methods).



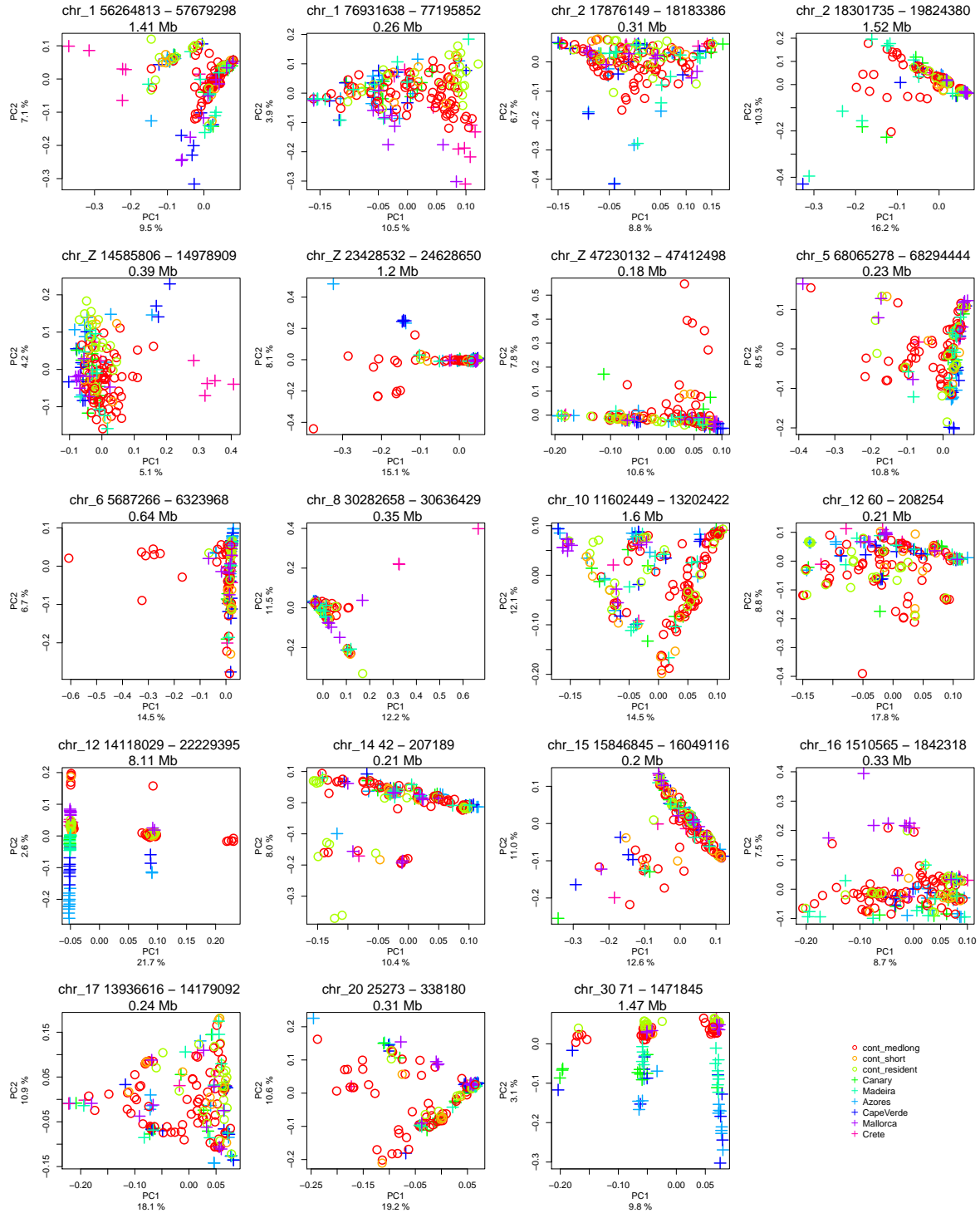
Supplementary Figure 3: Genomic regions with distinct patterns of genetic variation identified with *lostruct*. Supplementary content related to Fig. 2D. The y-axis shows the MDS axes along which projected component of genetic variation is deviated in genotype-based (top half, cyan) and haplotype-based (bottom half, purple) analysis of *lostruct*. The x-axis shows the genomic position. The bottom row (colours correspond to species-wide, population-specific, and no low-recombining in Fig. 2D) shows coordinates of outlier intervals which we determined as final outliers by merging results of the genotype- and haplotype-based analyses.



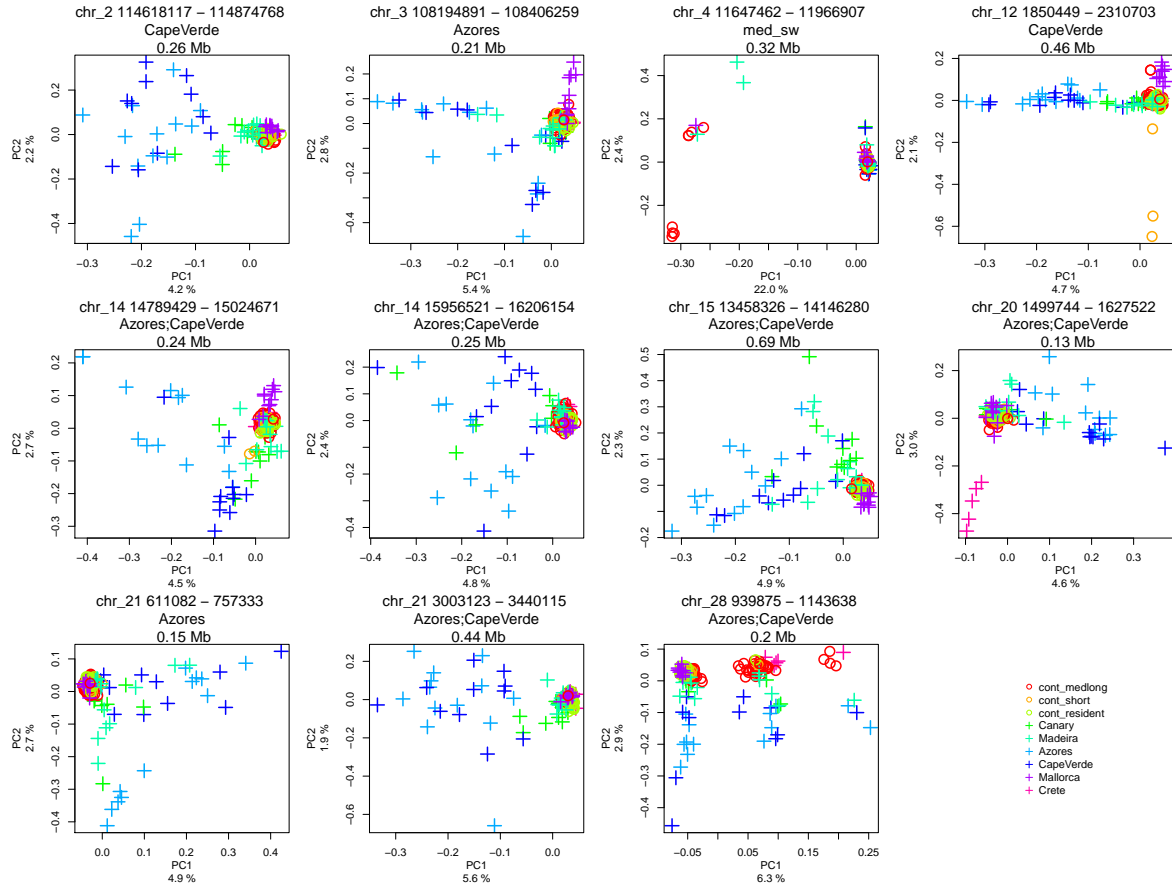
Supplementary Figure 4: Consistency of genotype- and haplotype-based *lostruct*. To answer whether genotype- and haplotype-based local PCA using *lostruct* were consistent, Euclidean distance of windows in the 20 dimensional space was compared between these approaches. Red points depict windows with deviated MDS value along a MDS axis in at least one of genotype- or haplotype-based analyses.



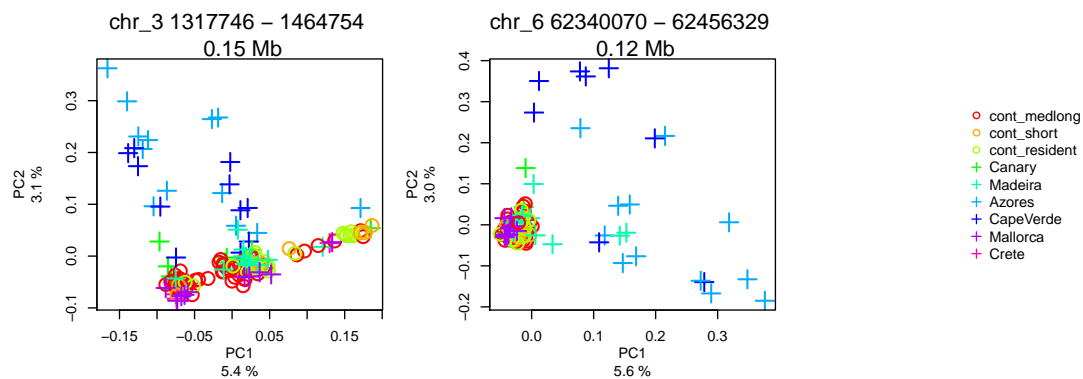
Supplementary Figure 5: Robustness of lostruct. To address whether lostruct is robust to the chromosomal background and the length of the chromosome, we performed lostruct using artificially synthesised chromosomes. Blackcap chromosomes 1 and 2 were split into halves in the middle, and chromosomes 20, 21, 28 were joined into a single chromosome. lostruct was performed for these split/joined chromosomes and results were compared with single chromosome analysis. **A, B, E-G.** Summary of lostruct analysis based on a single chromosome (black) and split/joined chromosome (red). **C, D, H, I.** MDS of single chromosome (**C, D**) and joined chromosome (**H, I**) lostruct. Red points depict windows with MDS value beyond the threshold. Per-chromosome analysis was mostly consistent with split/joined chromosome analysis. In regions with inconsistent results, MDS values still show sub-threshold deviation.



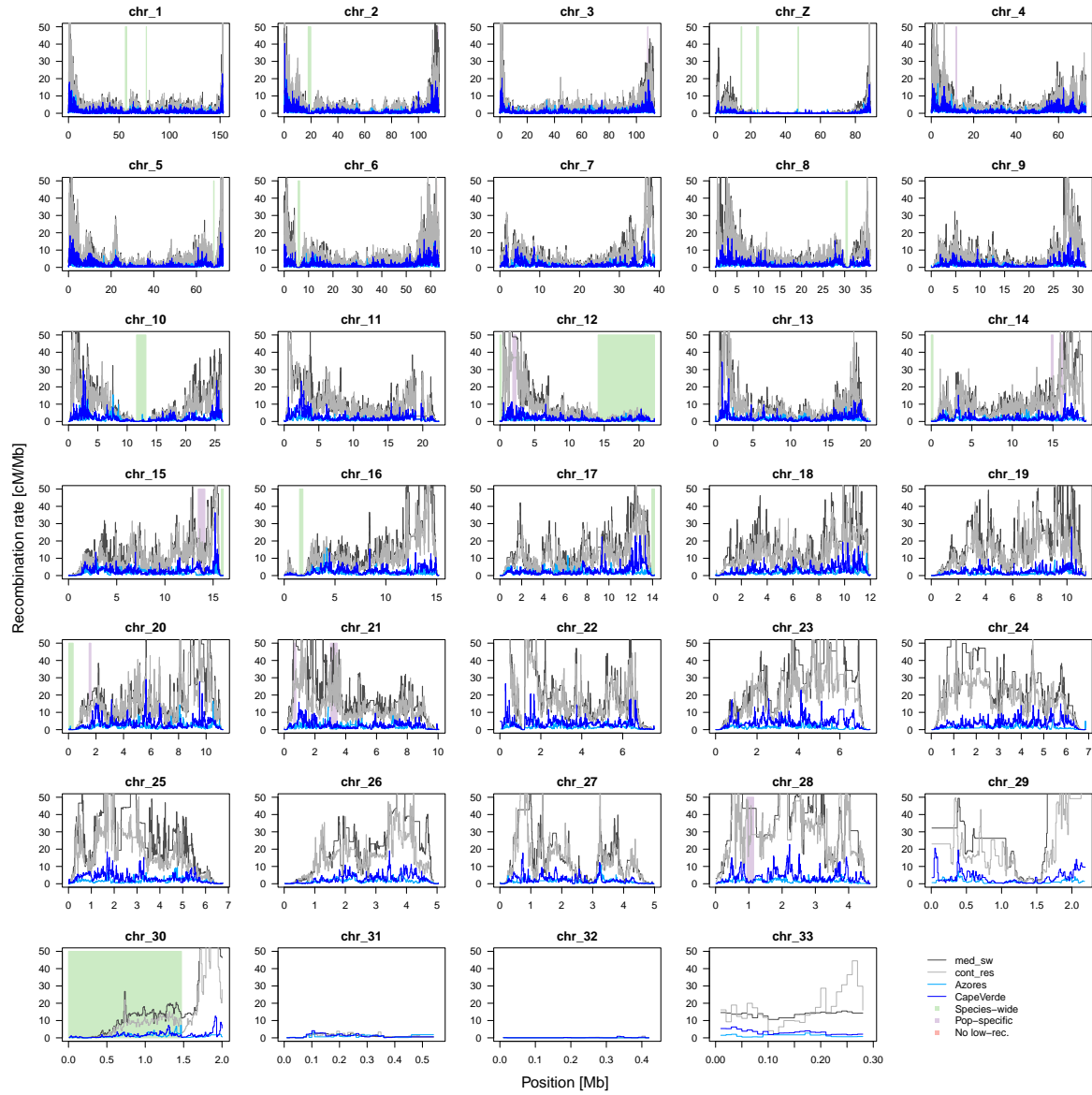
Supplementary Figure 6: PCA for outliers overlapping species-wide low-recombining regions. Supplementary data related to Fig. 3. PCA plots represent patterns of genetic variation at 19 outlier regions in the blackcap genome overlapping species-wide low-recombining regions (data points represent blackcap individuals and colours depict populations). The patterns were distinct from population structure (Fig. 2B, C).



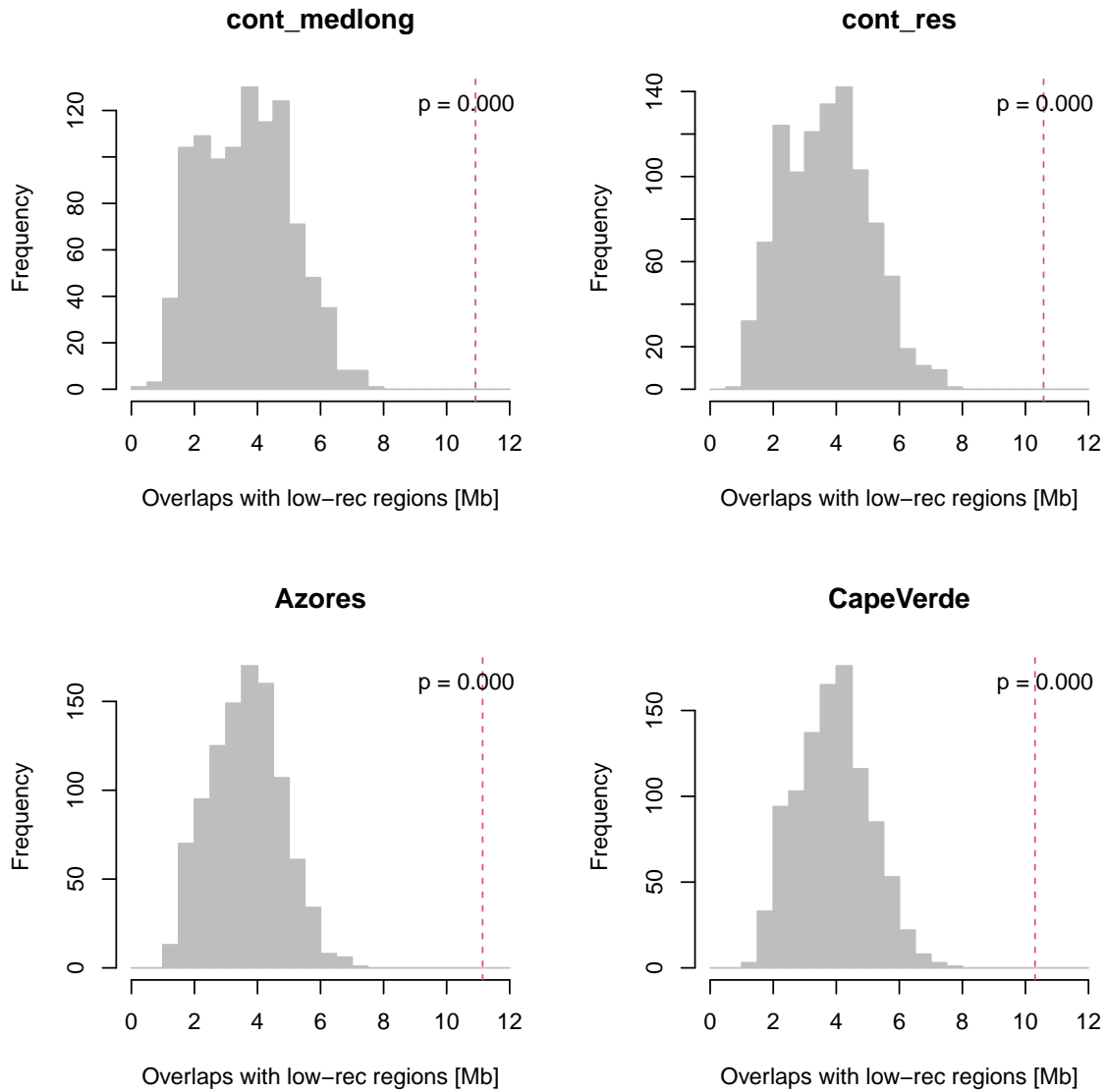
Supplementary Figure 7: PCA for outliers overlapping only with population-specific low-recombining regions. Supplementary data related to Fig. 3. PCA plots represent patterns of genetic variation at 11 outlier regions in the blackcap genome overlapping only with population-specific low-recombining regions (data points represent blackcap individuals and colours depict populations). The patterns were distinct from population structure (Fig. 2B, C). Population labels on top of each panel depict the population(s) in which low-recombining regions are found within the outlier.



Supplementary Figure 8: PCA for outlier regions without overlaps with low-recombining regions. Supplementary data related to Fig. 3. PCA plots represent patterns of genetic variation at two outlier regions in the blackcap genome (data points represent blackcap individuals and colours depict populations).



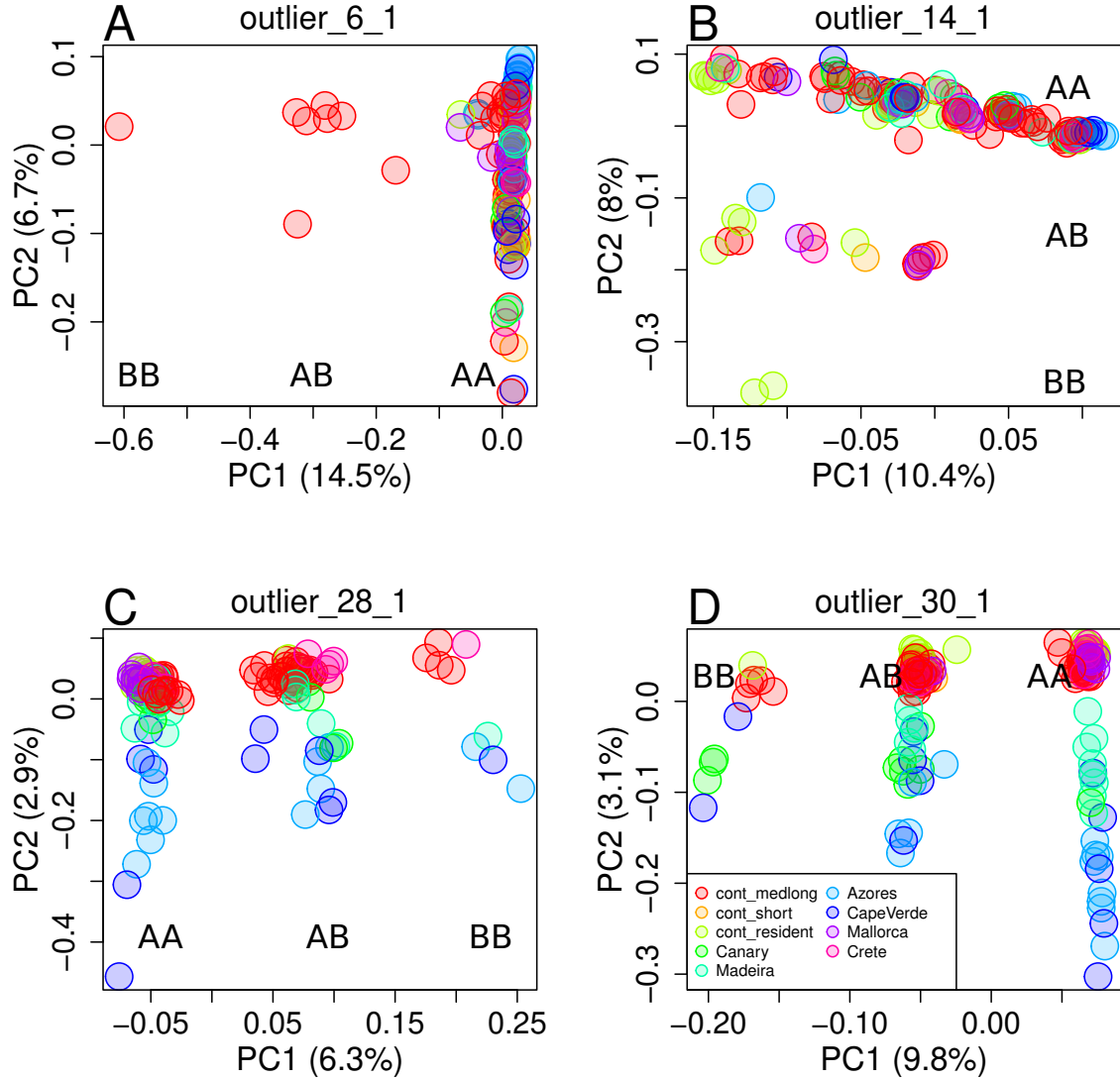
Supplementary Figure 9: Recombination landscape and lostruct outliers. Supplementary data related to Fig. 2E, F. Four lines depict recombination maps inferred for four blackcap populations. Background shades depict positions of outliers identified by local PCA using lostruct.



Supplementary Figure 10: Permutation tests for the number of overlaps between local PCA outliers and low-recombining regions. To test whether the 32 outlier regions in the blackcap genome based on local PCA significantly overlap with low-recombining regions, permutation tests were performed ($n = 1,000$). In each permutation, intervals of observed outlier regions were shuffled in each chromosome, and the total length of overlaps with low-recombining regions (below 20 percentile per chromosome) was recorded (see Materials and Methods). Red lines represent observed length of overlaps.

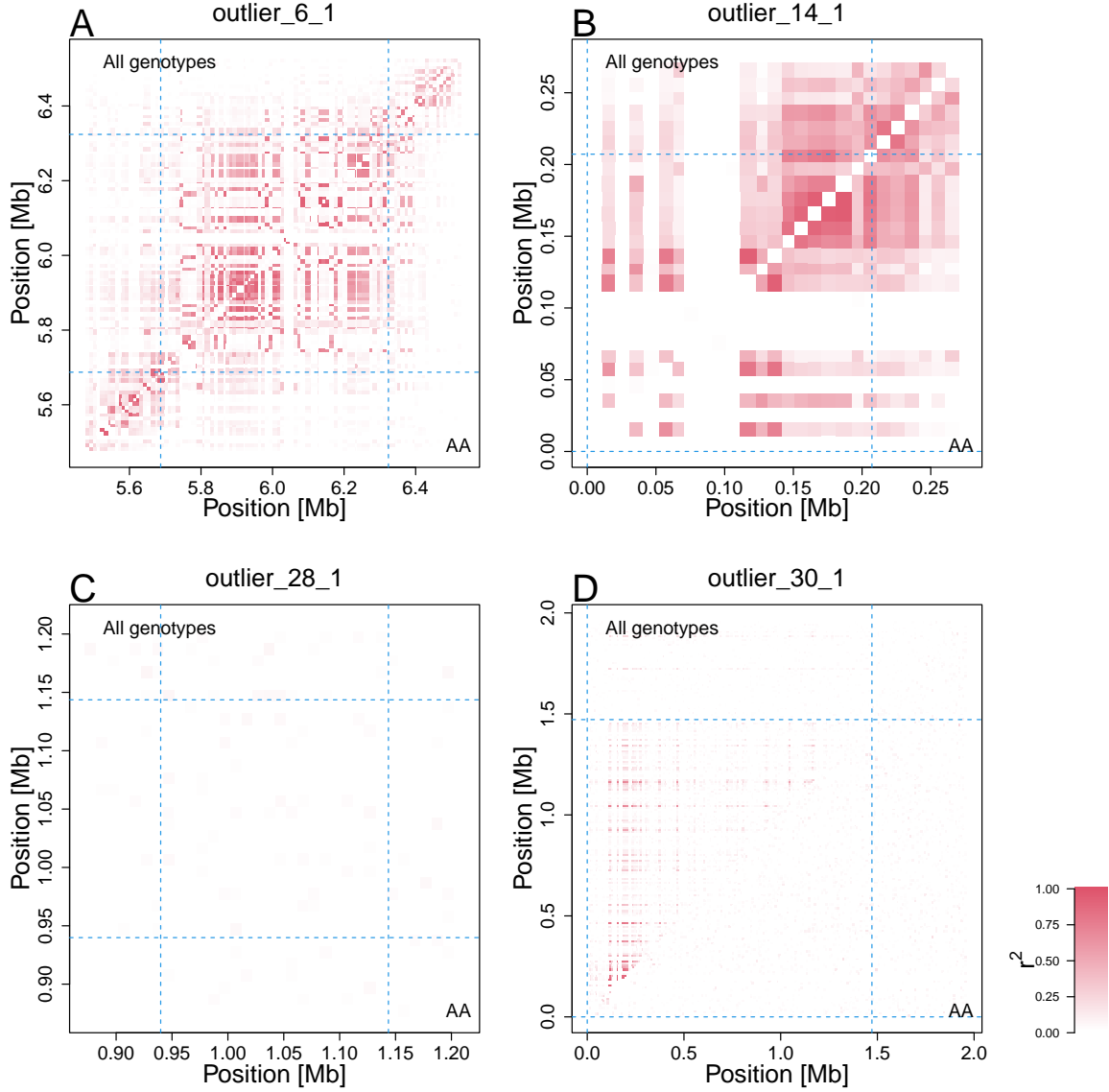
3.3 Putative inversions

3.3.1 PCA

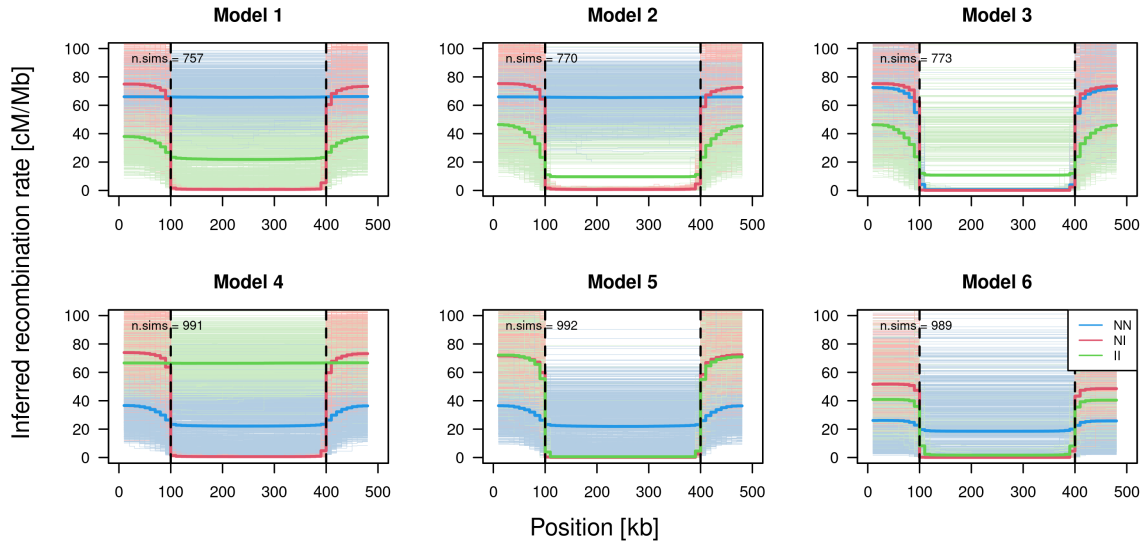


Supplementary Figure 11: PCA at outliers with three clusters of individuals. Supplementary data related to Fig. 3A (top). Five outlier regions found in the blackcap genome show patterns of genetic variation in PCA with three clusters of individuals, some of which may represent polymorphic inversions (Huang et al., 2020; Ma & Amos, 2012; Todesco et al., 2020). We investigated this possibility in Sup. Figs. 12, 13, 14. In each region, we named the major and minor alleles A and B, and the three genotypes AA, AB, and BB.

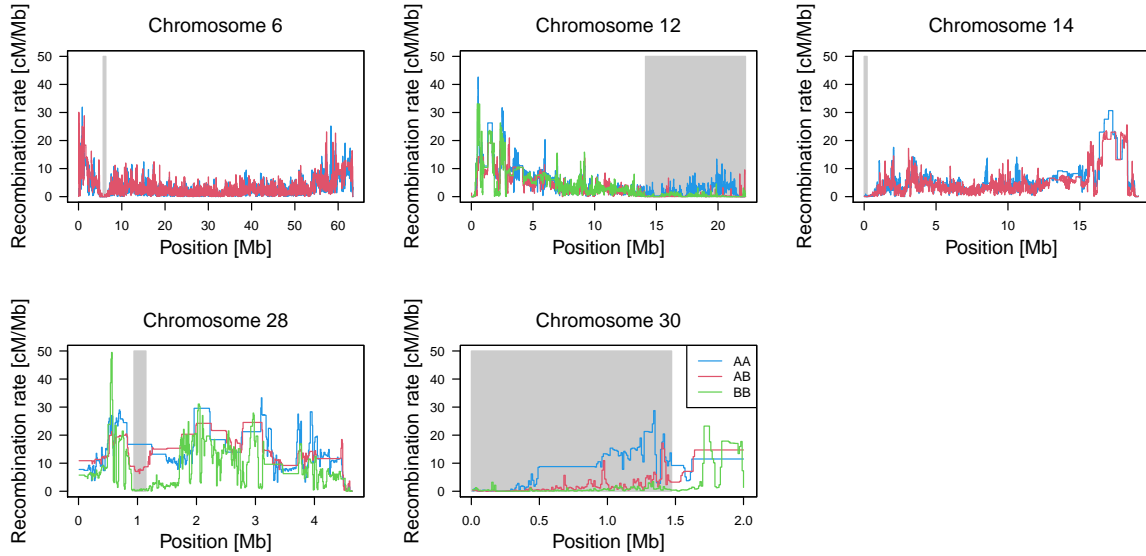
3.3.2 LD and genotype-specific recombination map



Supplementary Figure 12: Linkage disequilibrium (LD) at outliers with three clusters in PCA. Supplementary data related to Fig. 3A (bottom). We investigated whether the five outliers in Sup. Fig. 11 represent five inversions. An inversion locus is expected to show high LD in all individuals but not in homozygous individuals while a non-inversion haplotype block is expected to show high LD irrespective of the genotype. In two outlier regions (outlier_12_3 (Fig. 3A) and outlier_30_1 (D)), LD was elevated when all individuals were used, but not when only AA individuals were used, indicating that these two outliers represent putative inversions. The other three did not show this pattern and thus represent non-inversion low-recombining regions. The top-left diagonal shows LD calculated using all blackcap samples. The bottom right diagonal shows LD calculated using AA individuals.



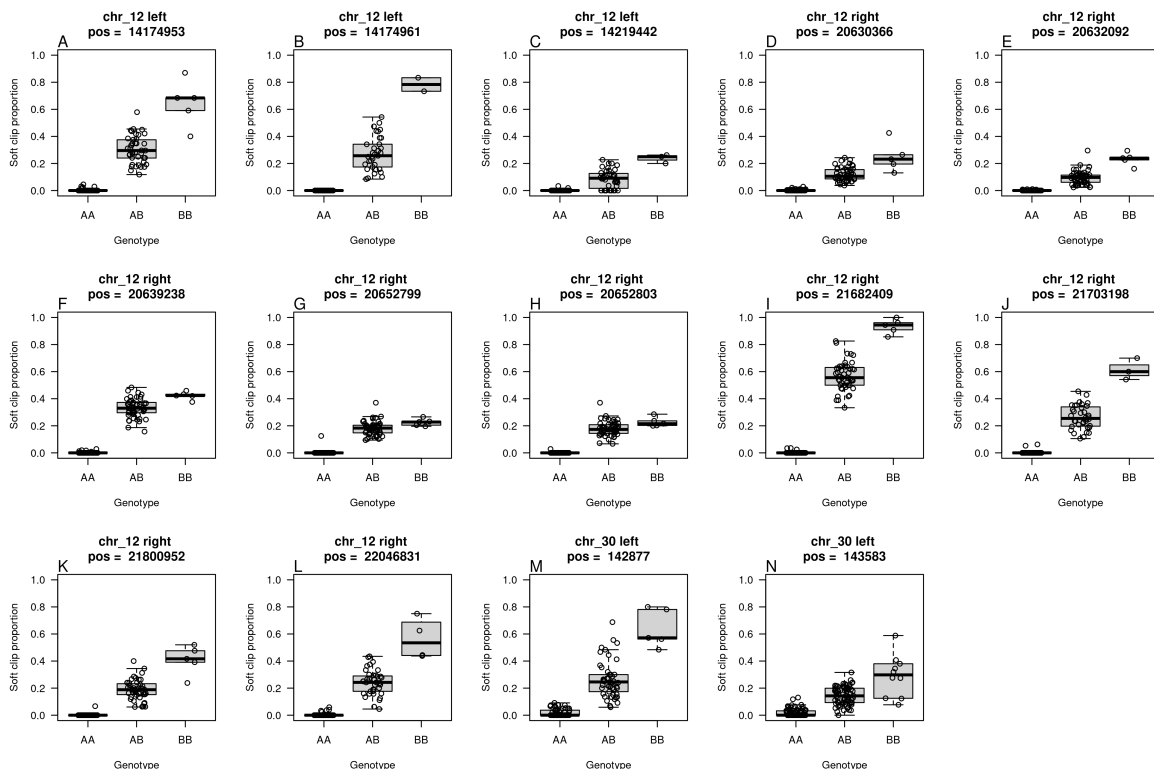
Supplementary Figure 13: Recombination rate inference by Pyrro performed on a chromosome simulated by SLiM with different models of recombination suppression. Supplementary data related to Sup. Fig. 14. We investigated whether inference of genotype-specific recombination maps can capture heterozygote-specific suppression of recombination at polymorphic inversions using simulation before applying this approach to the blackcap data. Six different models of genotype-specific recombination suppression was simulated with SLiM (see Materials and Methods and Sup. Table. 6), and recombination map was inferred for each genotype (heterozygotes in red, homozygotes in blue (normal-normal) and green (inversion-inversion)). Thin lines depict inferences for individual simulation replicates, and thick lines depict average of all replicates. The vertical black dotted lines depict the boundary positions of the haplotype block defined by recombination suppression. The result shows that heterozygote-specific suppression can be captured (red lines in models 1 and 4) but normal recombination rates in minor allele homozygotes (green in model 1 and blue in model 4) are not well reflected in inferred maps. Recombination suppression irrespective of genotypes (models 3 and 6) is reflected in all inferred genotype-specific recombination maps.



Supplementary Figure 14: Recombination maps inferred with AA, AB, and BB samples in outlier regions with three clusters of individuals in PCA. Supplementary data related to Fig. 3A (bottom) and Sup. Fig. 12. Gray shades depict positions of the outlier regions with three clusters of individuals in PCA (Sup. Fig. 11). In line with Sup. Figs. 12, 13, reduced recombination rate in AB with moderate levels of recombination rate in AA was observed at outlier_12_3 and outlier_30_1, indicating these two represent polymorphic inversions. The other three showed reduced recombination rate both in AA and AB, indicating they represent low-recombining regions without inversions.

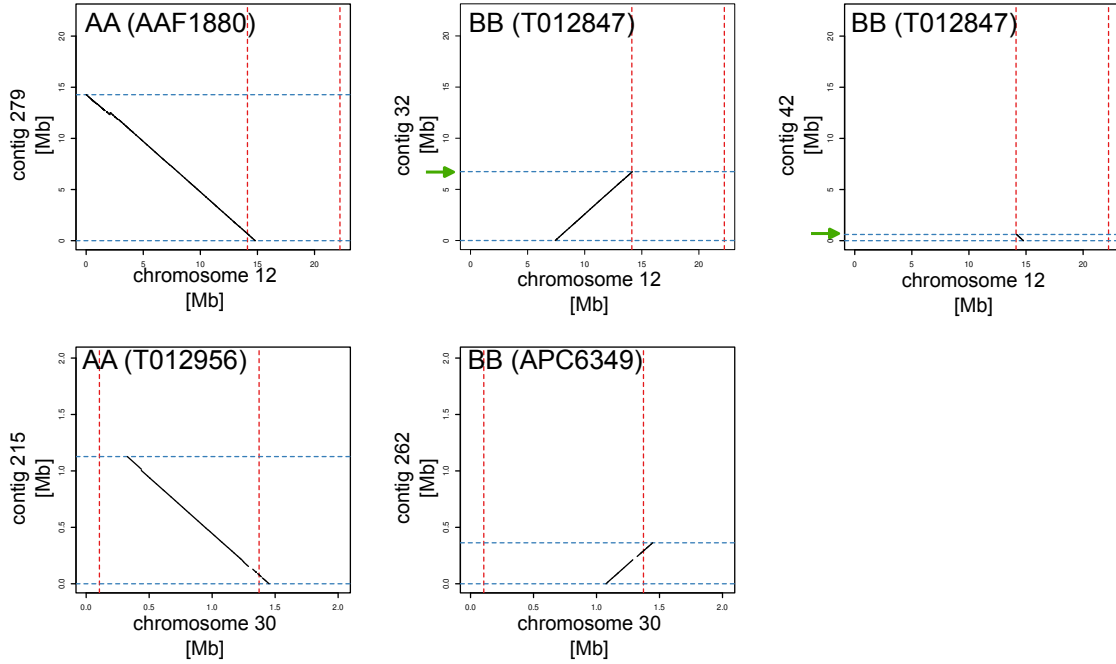
3.3.3 Breakpoint analysis

3.3.3.1 Illumina short reads with soft clip

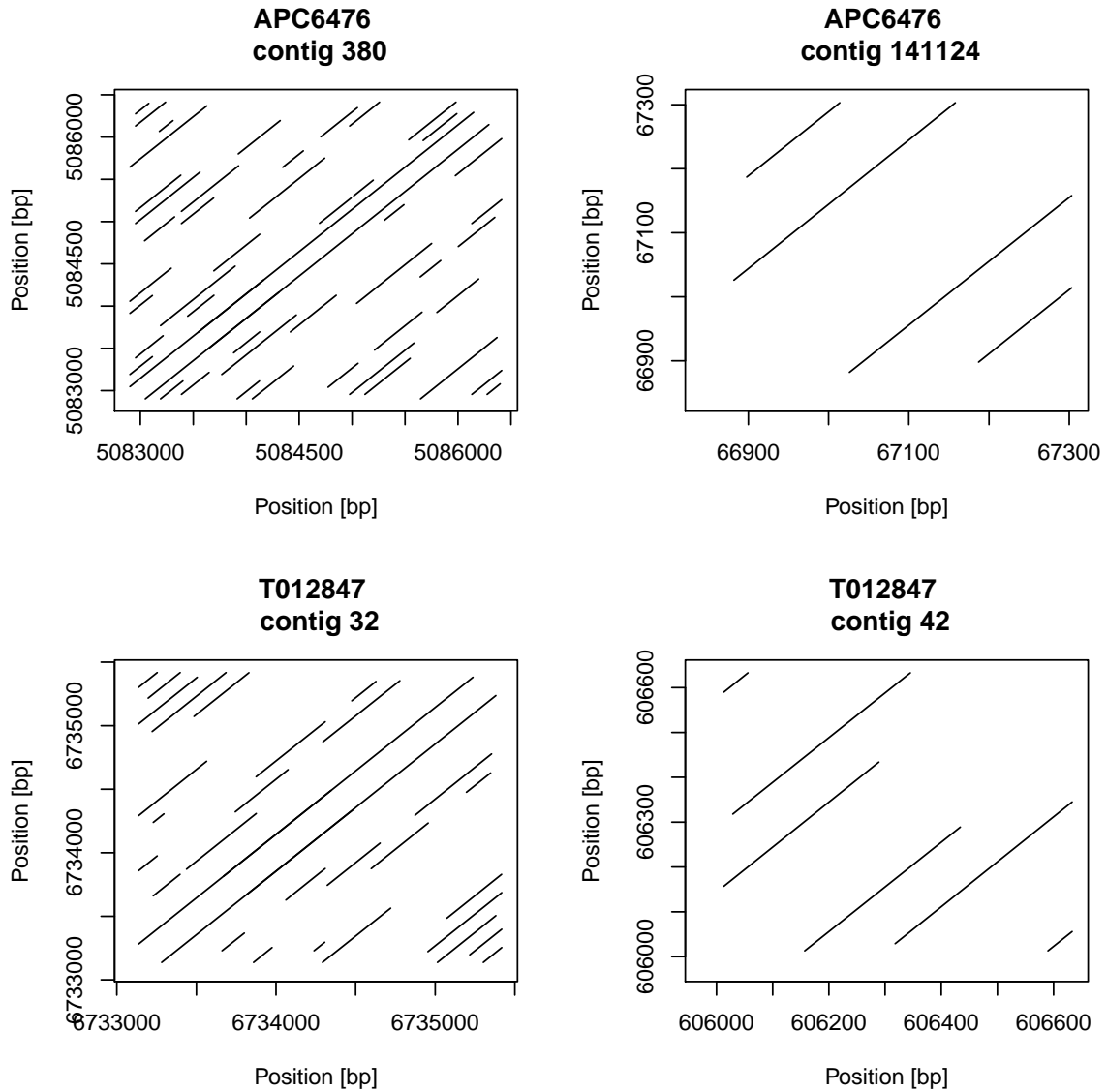


Supplementary Figure 15: Soft-clip proportion at 14 candidate positions where soft-clip proportion and genotype of putative inversions are associated. Supplementary data related to Sup. Table. 5. We analysed alignment of Illumina short reads to identify breakpoints of putative inversions at outlier_12_3 and outlier_30_1 (detailed in Materials and Methods). At 14 positions, the proportion of soft-clipped reads was correlated with the genotypes (AA, AB, BB. Detailed in Materials and Methods). The plots show soft-clip proportion of all individuals with three putative inversion genotypes at these 14 positions. Based on these plots, we excluded positions in **C-H** from further analysis in Sup. Table. 5 because the soft-clip proportion of BB was not high or that of AB was not around a half that of BB.

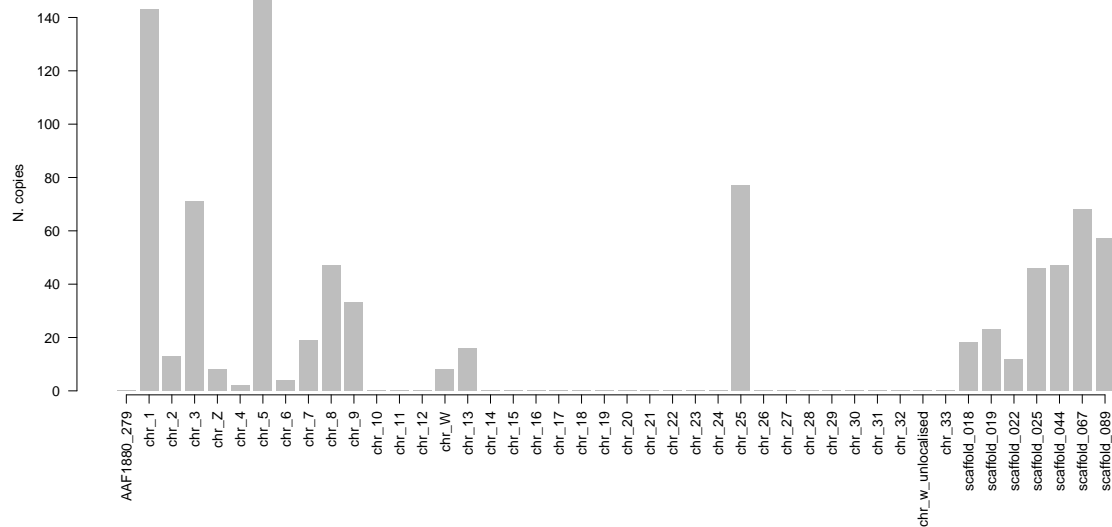
3.3.3.2 10x linked-read sequencing



Supplementary Figure 16: Dot plots between blackcap reference chromosomes 12 or 30 and 10X pseudo-haplotyped contigs of AA and BB individuals. To identify breakpoints of the putative inversions, we aligned pseudo-haplotyped contigs (based on 10x linked-read sequencing) of AA and BB individuals for outlier_12_3 (top) and outlier_30_1 (bottom) to the blackcap reference genome (Detailed in Materials and Methods). The x-axis shows the coordinate of the blackcap reference chromosomes, and the y-axis shows the coordinate of the 10x pseudo-haplotyped contigs. The red dotted lines depict local PCA-based breakpoint positions in the reference coordinate. The blue dotted lines depict two ends of 10x contigs. In AA individuals (AAF1880 for outlier_12_3 and T012956 for outlier_30_1), one contig was aligned across the putative breakpoint based on local PCA (red dotted lines), supporting the absence of large structural variation. In BB individuals (T012847 for outlier_12_3 and APC6349 for outlier_30_1), no contigs were aligned across the ends of local PCA-based outlier regions, but instead alignment of two 10x contigs terminated (blue dotted lines) at either side of the putative breakpoint, indicating the presence of structural variation in B allele for both outlier_12_3 and outlier_30_1. Presence of large inversions is inconclusive because the ends of these pseudo-haplotyped contigs were not aligned to the other ends of the outlier regions. We investigated why the sequences of B allele is not contiguous across the putative breakpoints in Sup. Fig. 17. Green arrows depict regions in which repeat analyses were performed in Sup. Figs. 17, 18.



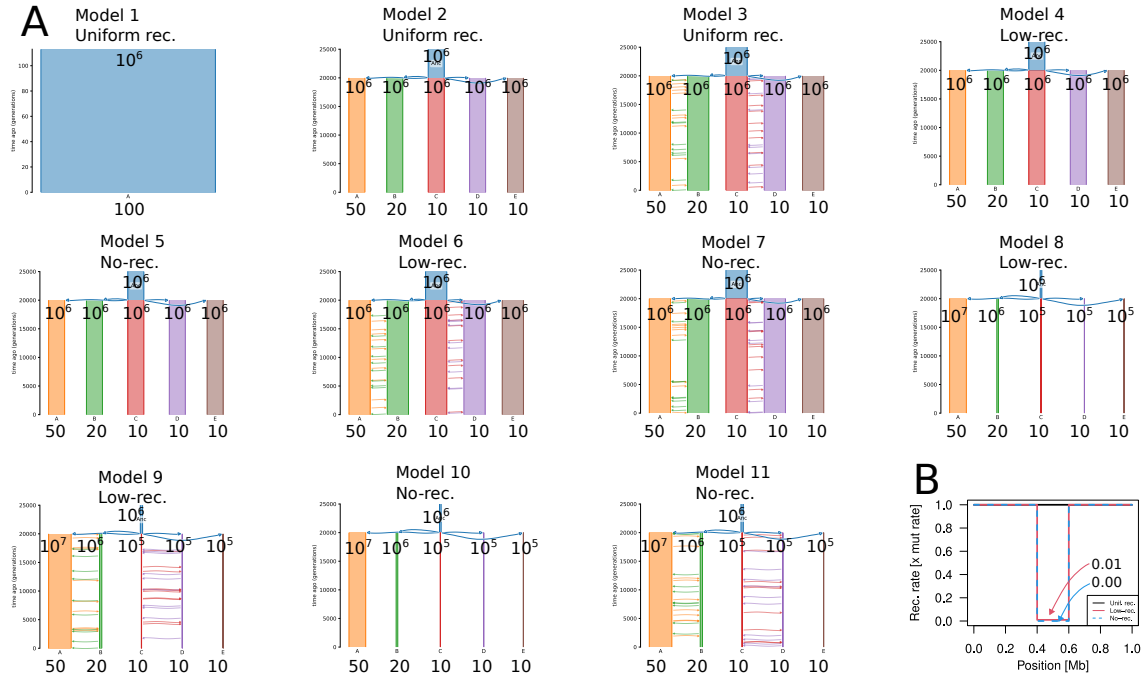
Supplementary Figure 17: Self dot plots of flanking sequences of 10x linked-read contigs around putative breakpoint of chromosome 12. Supplementary data related to Sup. Fig. 16. To investigate why 10x contigs of individuals with B allele (presumably inversion) break at the putative breakpoints, we aligned the flanking sequence of the 10x contigs that was aligned next to the putative breakpoint of outlier_12_3 to itself. The plots show the presence of repeats in the sequence flanking the putative breakpoint.



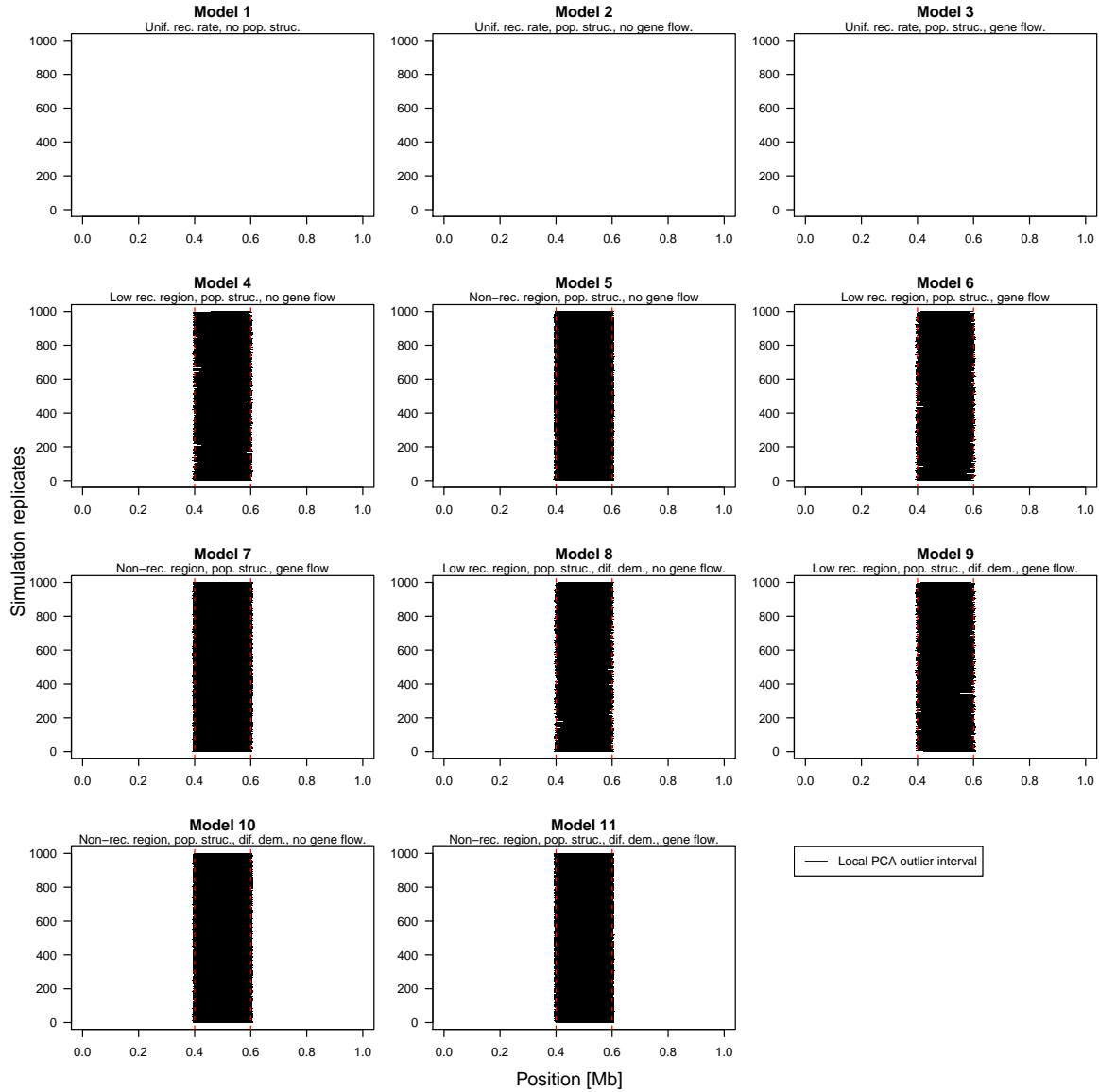
Supplementary Figure 18: Tandem repeats found at putative inversion breakpoint of chromosome 12 are absent in ancestral allele but present in other chromosomes. Supplementary data related to Sup. Fig. 17. A 144 bp-long tandem repeat was identified in flanking sequence of the 10x contigs aligned next to the putative inversion breakpoint of outlier_12_3 (Detailed in Materials and Methods). To investigate whether this repeat is present elsewhere in the pseudohaplotype of A allele and the reference, **BLASTn** was performed with the consensus sequence of the tandem repeat unit as the query and contig 279 of AAF1880 (A haplotype contig of 10x) and the blackcap reference as target. The bar plot depicts the number of hits in each chromosome/contig. The result shows the tandem repeat is present in other chromosomes but not on the A allele of chromosome 12.

3.4 Effect of reduced recombination rate on pattern of local genetic variation

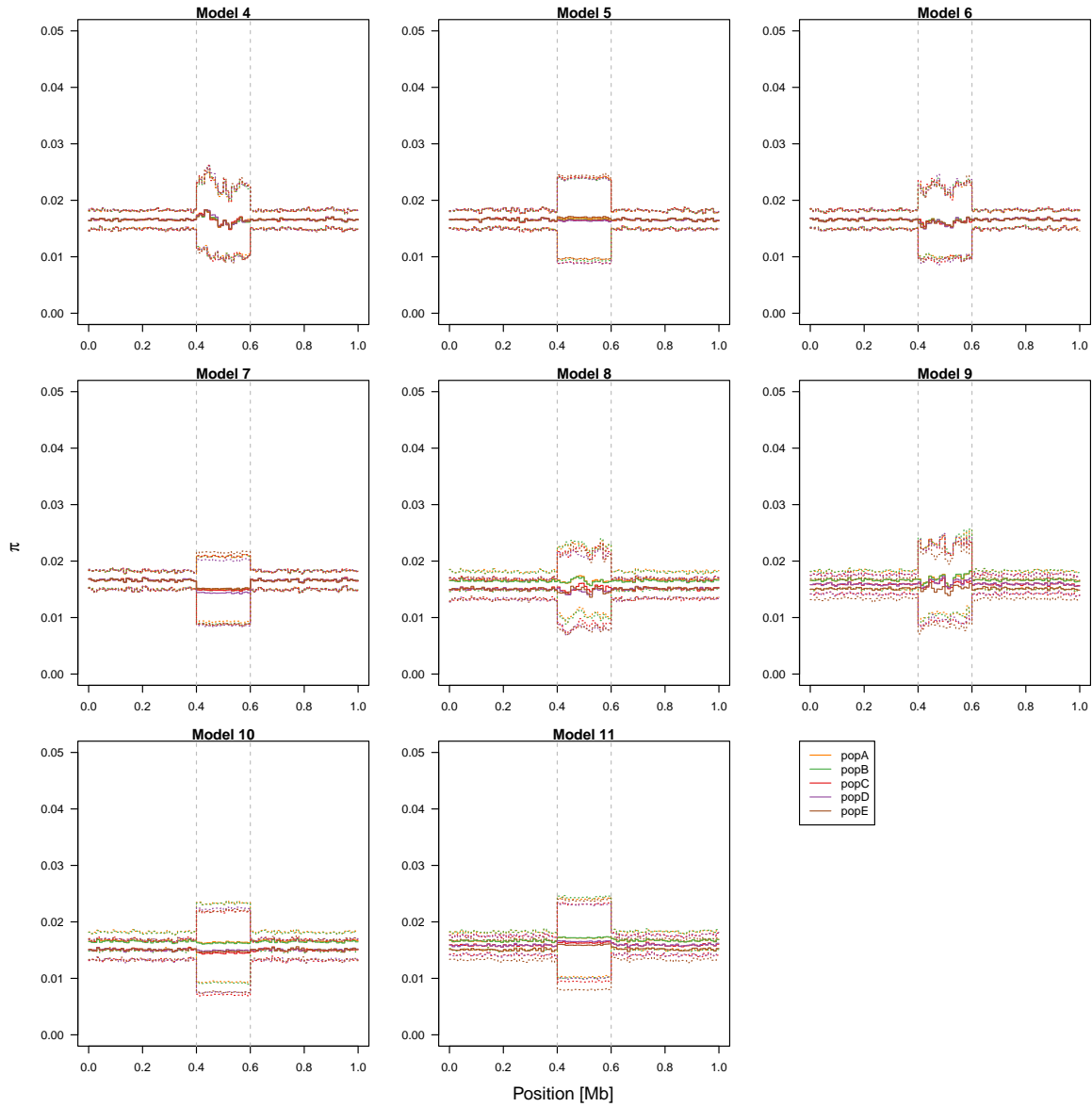
3.4.1 Effect of demography and local recombination rate (coalescent simulation)



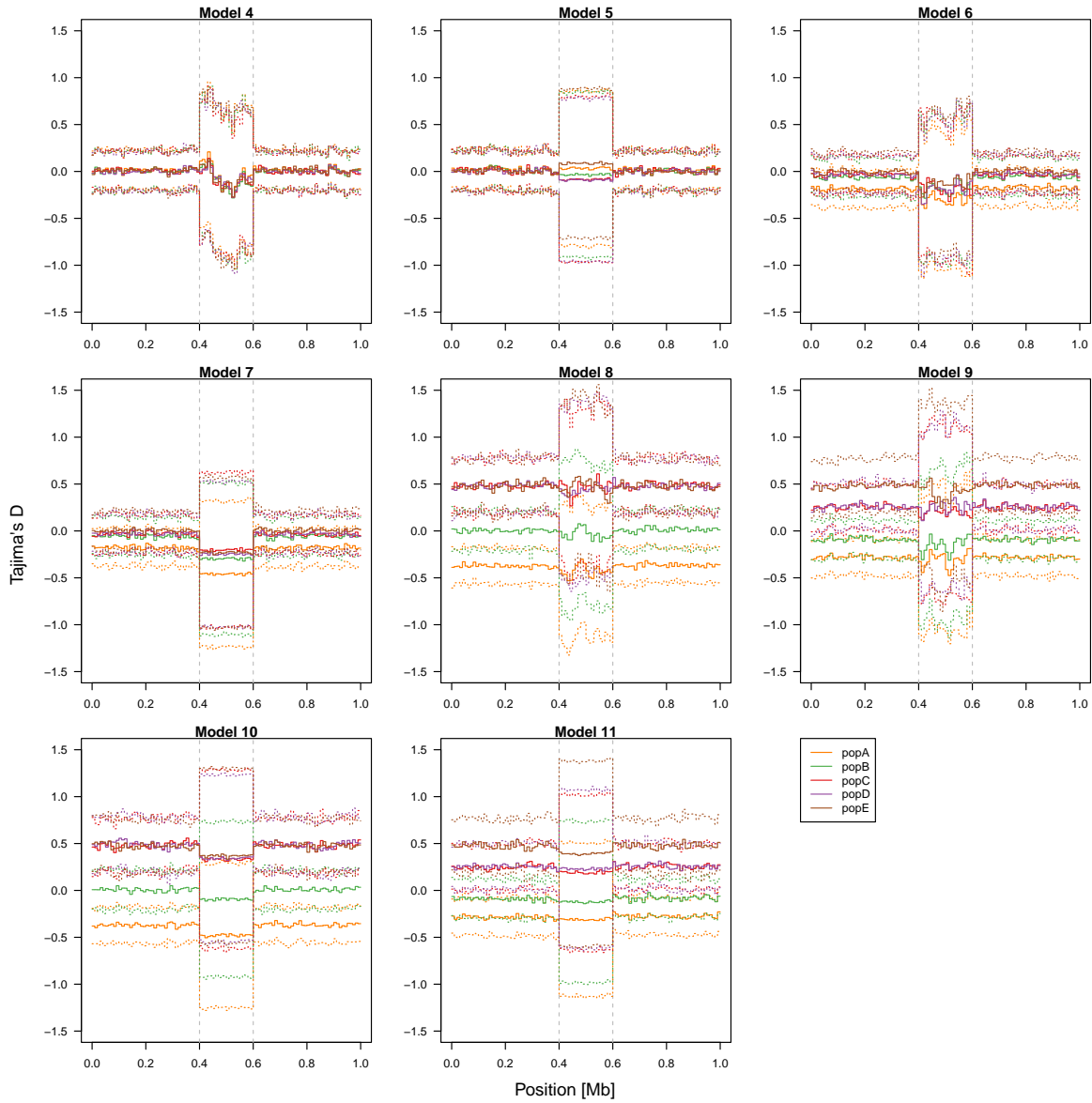
Supplementary Figure 19: Demography models and recombination maps for neutral coalescent simulations. Supplementary data related to Sup. Table. 8. To investigate the effects of local recombination rate and demography on genetic variation, we implemented 11 scenarios of demographic history and recombination landscapes ([tab:sup.msp_models]) and simulated SNPs under coalescent with recombination with `msprime` 1,000 times. **A.** 11 models of demographic history. The numbers shown on the populations depict the effective population size, and the numbers below the populations depict the numbers of sampled diploid individuals. Note that demographies for models 2, 4 and 5, models 3, 6 and 7, models 8 and 9, and models 10 and 11 are respectively the same, differing by the recombination map (**B**). **B.** Three recombination maps differing by the recombination rate in the middle of the chromosome. Within the middle interval (0.4 to 0.6 Mb), recombination rate is reduced to 1/100 of the background region in the “low-recombining” scenarios, while in the “no-recombining” scenarios recombination rate is reduced to 0.



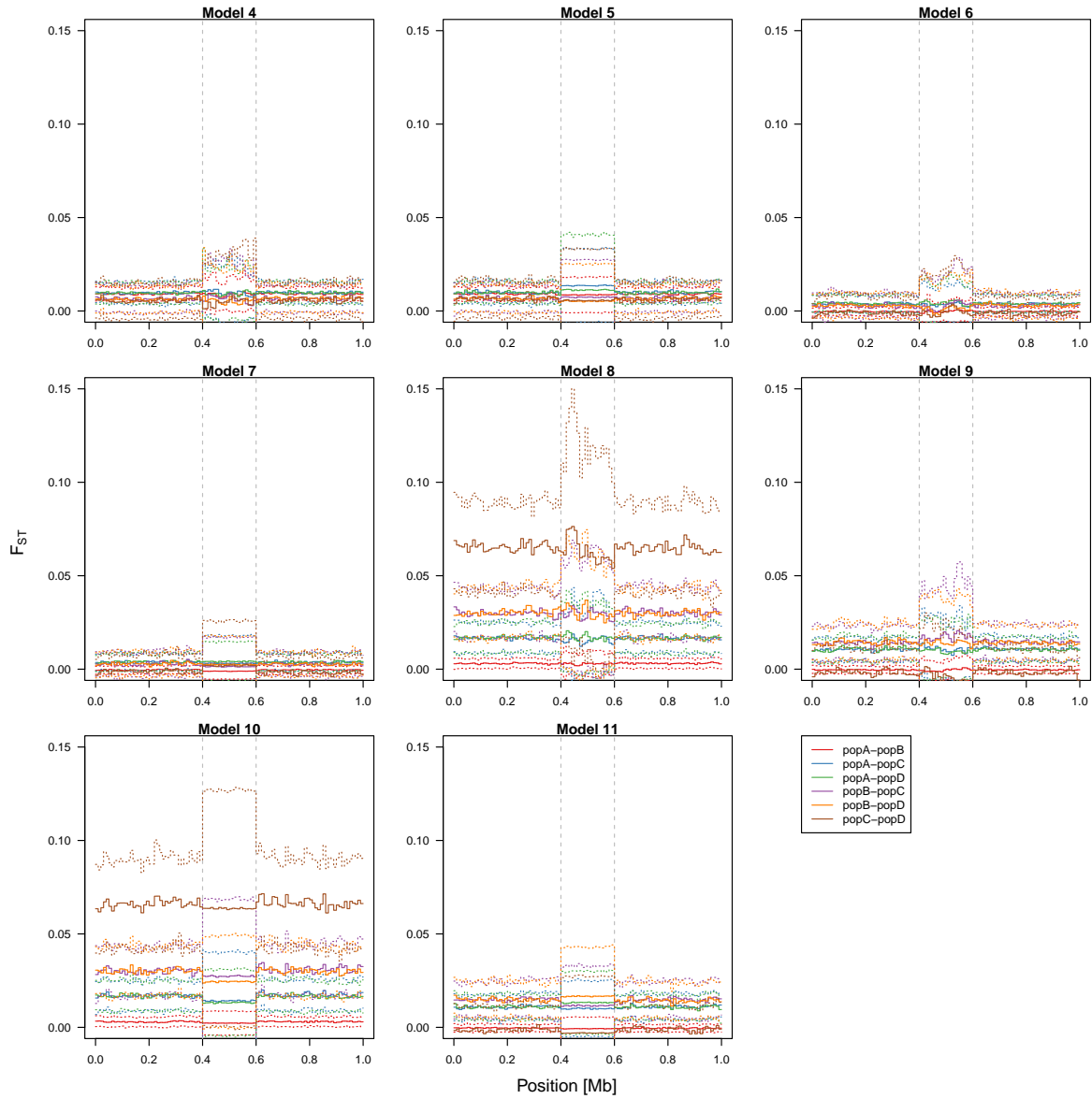
Supplementary Figure 20: Reduced recombination rate, but not demography, causes distinct patterns of genetic variation. Supplementary data related to Sup. Fig. 19 and Sup. Table. 8. To identify outlier regions, `lostruct` was performed for each of 1,000 replicates of the 11 scenarios in Sup. Fig. 19. The results show that no outlier regions were detected without reduced recombination rate (models 1-3), and outliers were always detected with reduced recombination rates (models 4-11). This is irrespective of the presence of population structure, unequal demographic history, and unbalanced sample size among populations. These results indicate that reduced recombination rate, but not demography, causes distinct patterns of genetic variation.



Supplementary Figure 21: Reduced recombination rate increases variance of summary statistics. Supplementary data related to Sup. Fig. 19 and Sup. Table. 8. Using the same data as Sup. Fig. 19, we asked how reduced recombination rates affect mean and variance of nucleotide diversity. Solid lines show the mean of the first 100 replicates (out of 1,000 simulated) and dotted lines show the standard deviation.

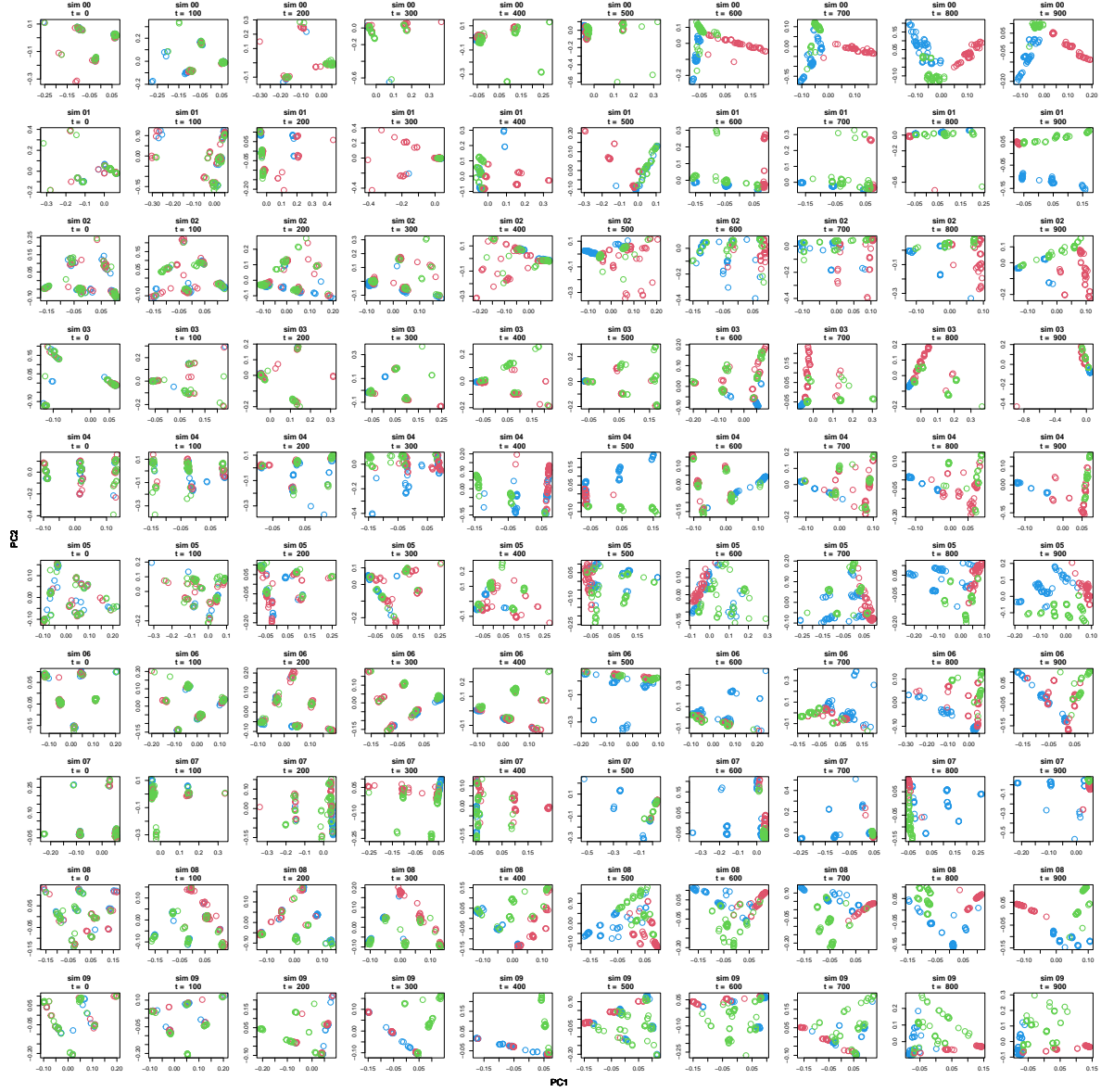


Supplementary Figure 22: Reduced recombination rate increases variance of summary statistics. Supplementary data related to Sup. Fig. 19 and Sup. Table. 8. Using the same data as Sup. Fig. 19, we asked how reduced recombination rates affect mean and variance of Tajima's D. Solid lines show the mean of the first 100 replicates (out of 1,000 simulated) and dotted lines show the standard deviation.

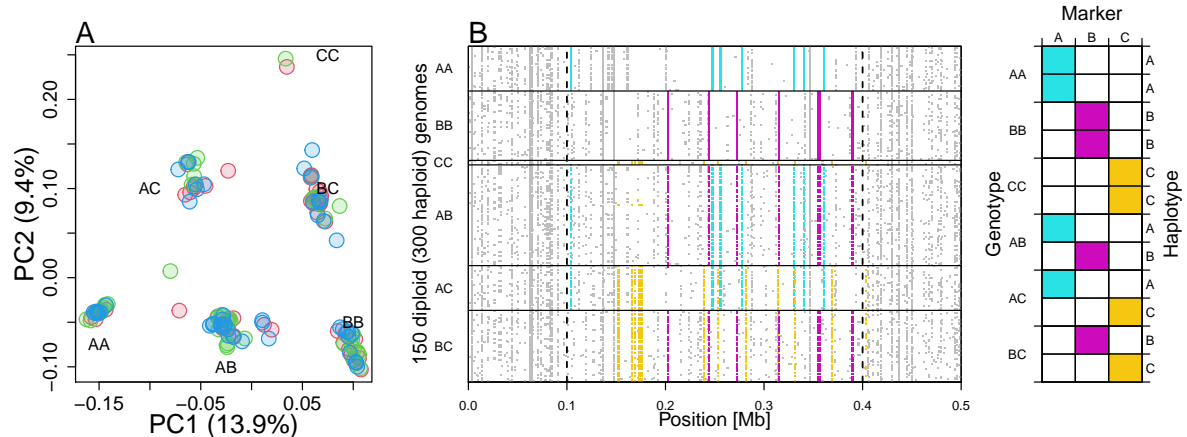


Supplementary Figure 23: Reduced recombination rate increases variance of summary statistics. Supplementary data related to Sup. Fig. 19 and Sup. Table. 8. Using the same data as Sup. Fig. 19, we asked how reduced recombination rates affect mean and variance of F_{ST} between five population pairs (of all 10 pairs). Solid lines show the mean of the first 100 replicates (out of 1,000 simulated) and dotted lines show the standard deviation.

3.4.2 Species-wide reduction of local recombination rate (forward simulation)

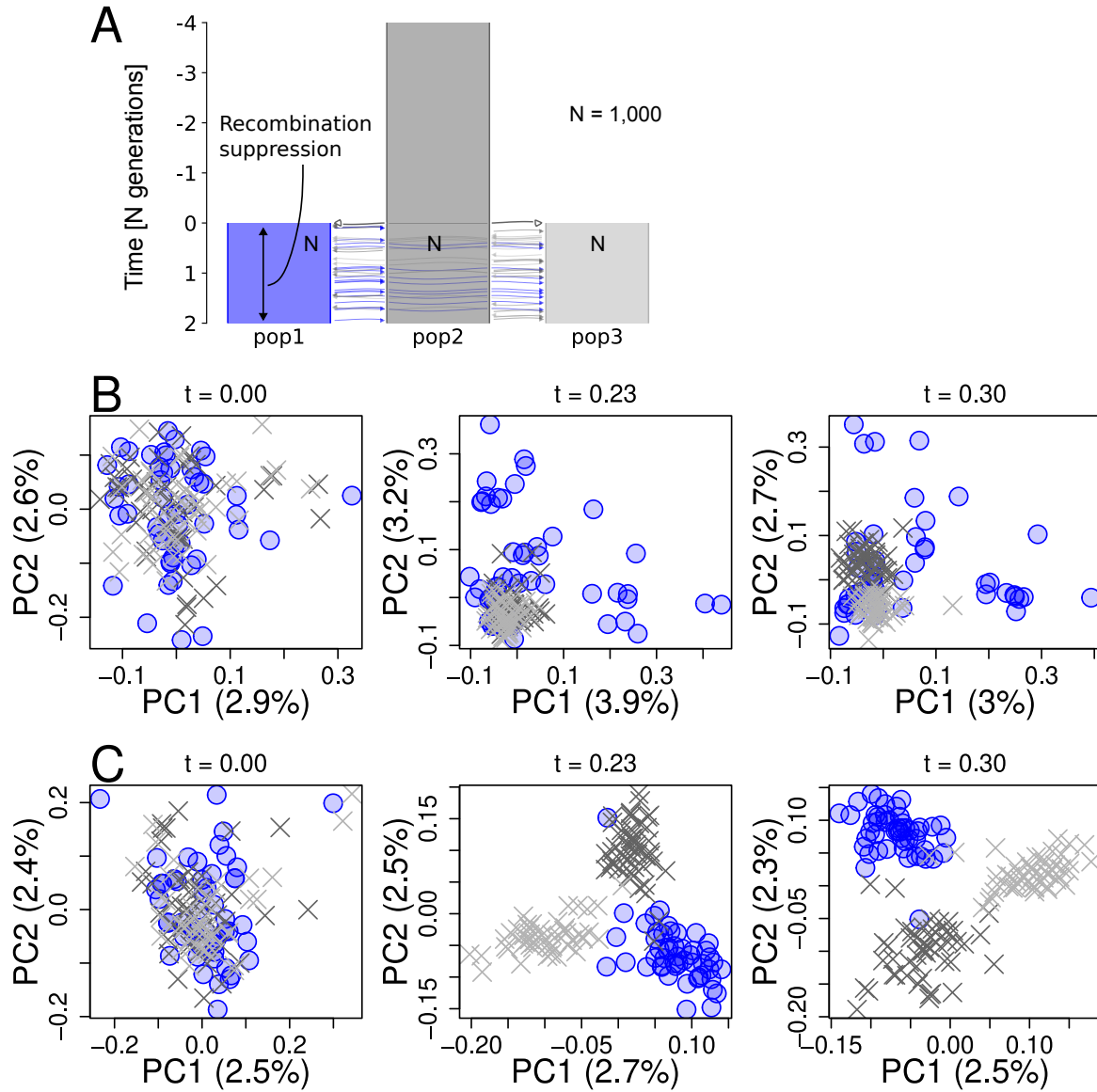


Supplementary Figure 24: PCA at a species-wide low-recombining region at ten time points of ten exemplified simulation replicates. Supplementary data related to Fig. 4. To investigate the effects of species-wide reduction in local recombination rate, we simulated one ancestral population of 1,000 diploids with a low-recombining genomic region that splits into three subpopulations (pop1, pop2, pop3. Fig. 4A). All mutations were neutral. We sampled individuals over time after the population split and conducted PCA in the low-recombining genomic region. 10 rows represent 10 simulation replicates (out of 100, see Materials and Methods). 10 columns represent 10 time points. Data points with three different clours depict individuals from three different populations. In addition to Fig. 4B and C, these exemplified results show high variability in realised genetic variation at low-recombining regions across replicates with three to six clusters with different degrees of mixture of individuals in PCA and transitioning from haplotype structure to population structure over time.

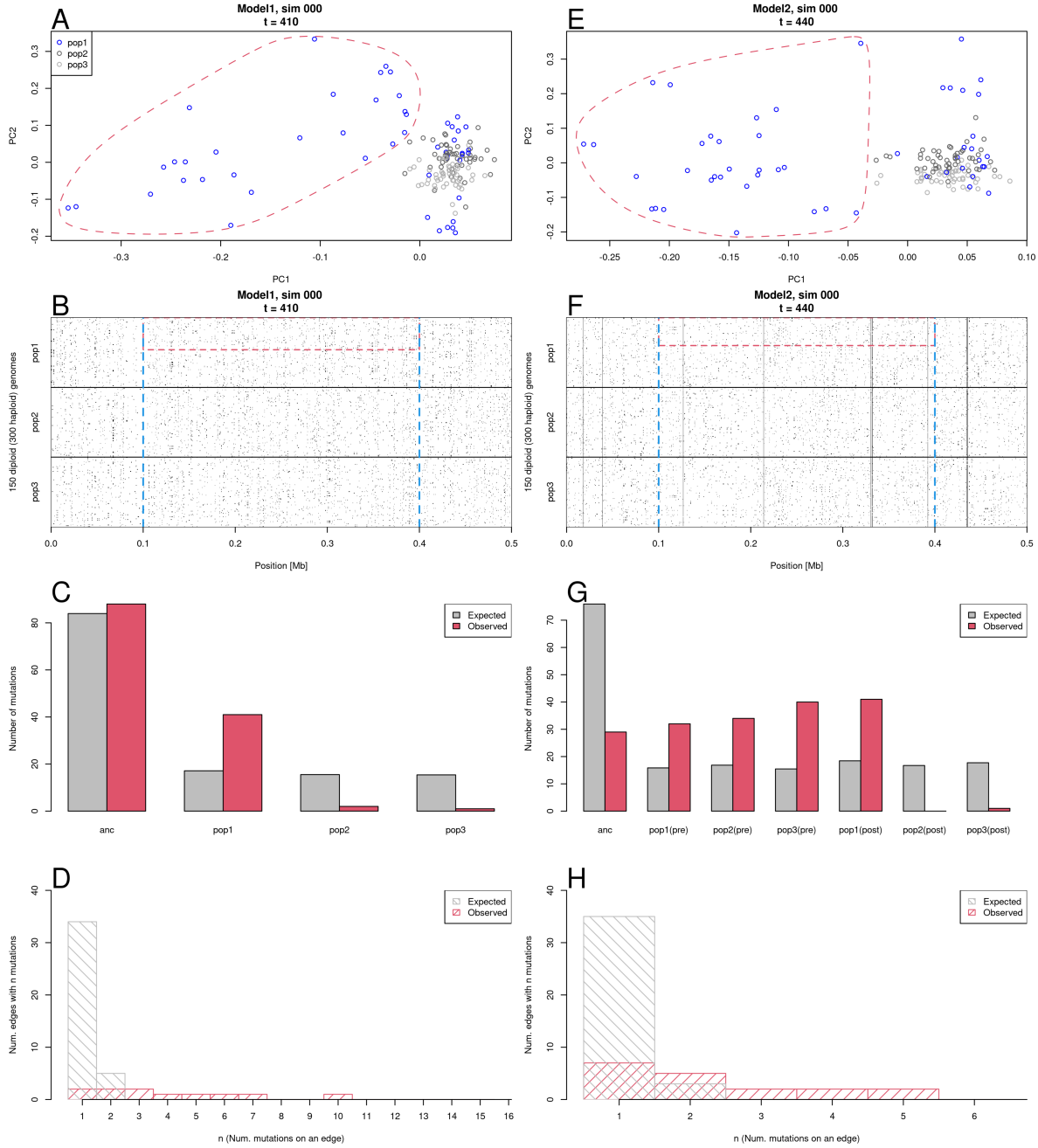


Supplementary Figure 25: Clusters of individuals in local PCA represent haplotype structure. Supplementary data related to Figs. 3, 4. **A.** Local PCA of a species-wide low-recombining region simulated showing six clusters of individuals (the same as Fig. 4C, $t=0$). **B.** Genotypes at thinned mutation sites. Cyan, magenta, and yellow correspond to A-, B-, and C-specific mutations. The distribution of these mutations in homozygous (AA, BB, CC) and heterozygous (AB, AC, BC) individuals suggests that the clusters of individuals in PCA represent combination of haplotypes possessed by diploid individuals.

3.4.3 Population-specific reduction of local recombination rate (forward simulation)



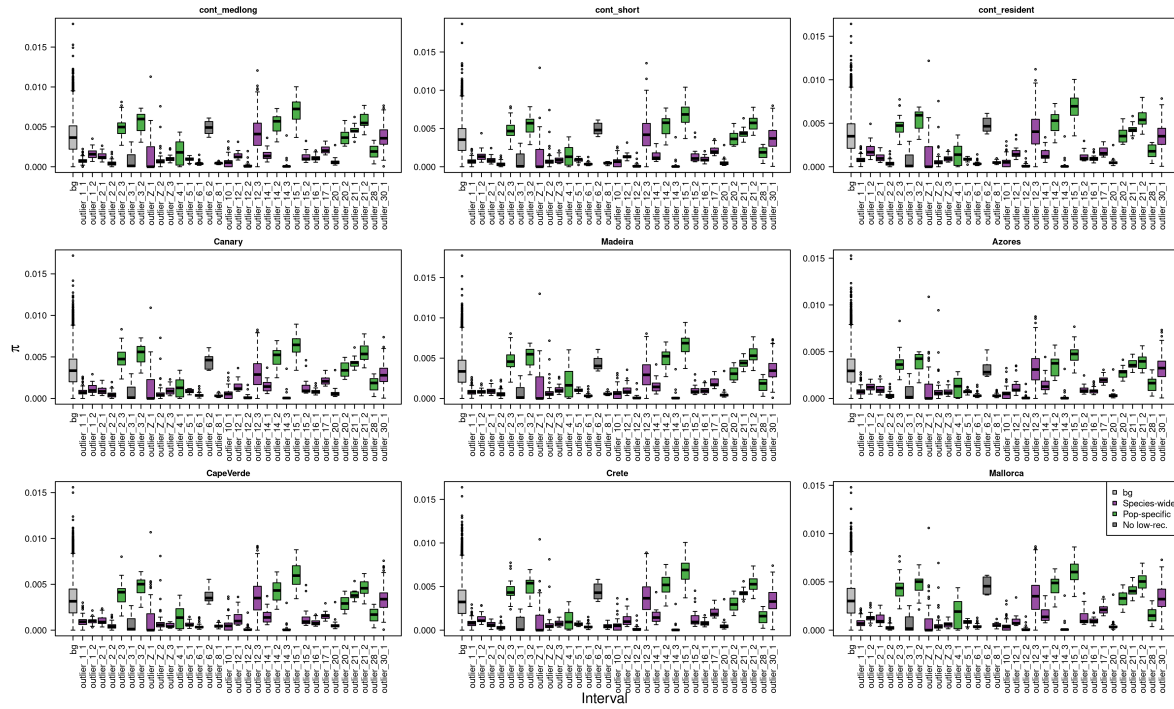
Supplementary Figure 26: Summary of model 1 of population-specific recombination suppression. Supplementary data related to Fig. 5. **A.** Simulated scenario. Simulated genome contained two chromosomes, one with a population-specific low-recombining region and the other without. **B, C.** PCA showing patterns of genetic variation at the population-specific low-recombining region (**B**) and the normally recombining chromosome (**C**) at three time points in one exemplified simulation replicate.



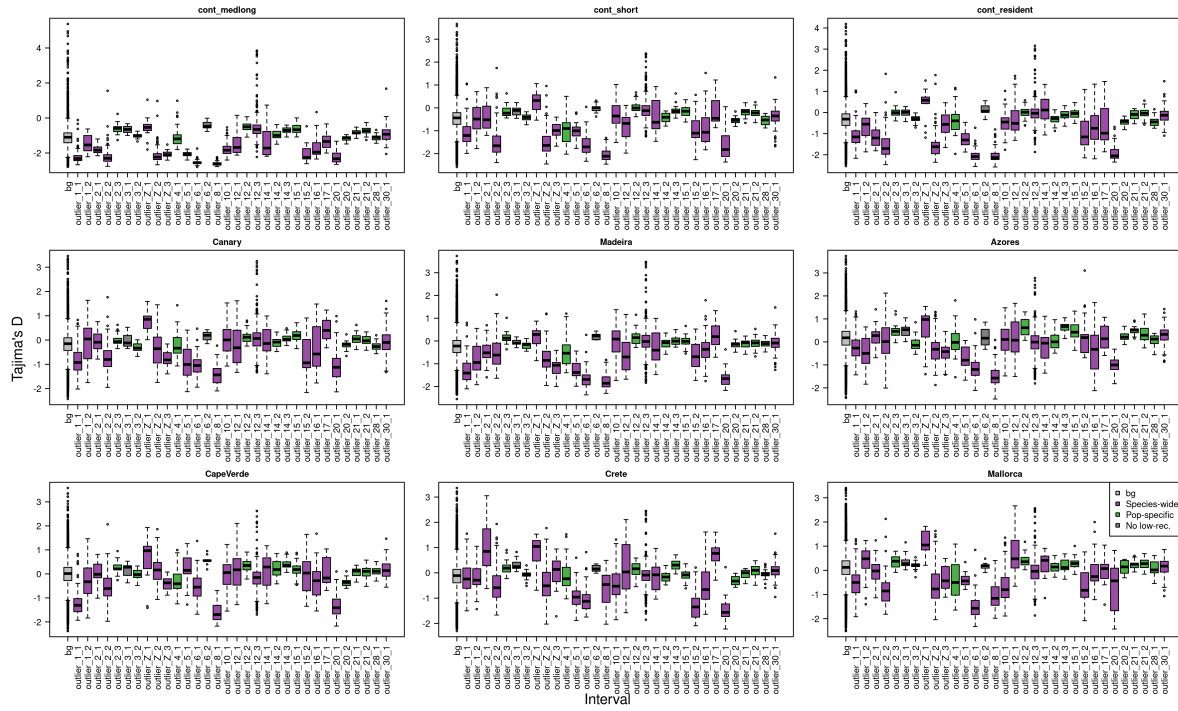
Supplementary Figure 27: Distinct local PCAs at population-specific low-recombining region represent cryptic haplotype structure. To characterise factors represented in the primary axes of distinct local PCA at population-specific low-recombining regions, we performed one replicate of SLiM simulation with the scenarios of models 1 (**A-D**) and model 2 (**E-H**) recording the full ancestry and mutations in tree sequence in addition to VCF files (Detailed in Materials and Methods). We performed PCA, and identified mutations with the highest contributions to the PC1 and PC2. We analysed the tree sequence to address whether mutations that occurred in certain population (e.g. ancestral population, low-recombining population) were enriched in the set of mutations contributing to the PC1 and PC2. **A, E.** Local PCA at population-specific low-recombining region. **B, F.** No visible haplotype structure were found at population-specific low-recombining region. **C, G.** Mutations originating from the low-recombining population after the population-specific recombination suppression were enriched in mutations with high loading to the distinct pattern of local PCA. **D, H.** Mutations originating from the low-recombining population with high PCA loading share common genealogical edges. Due to recombination suppression, the mutations on the same edge are on the same haplotype in the current sample.

3.5 Effect of selection

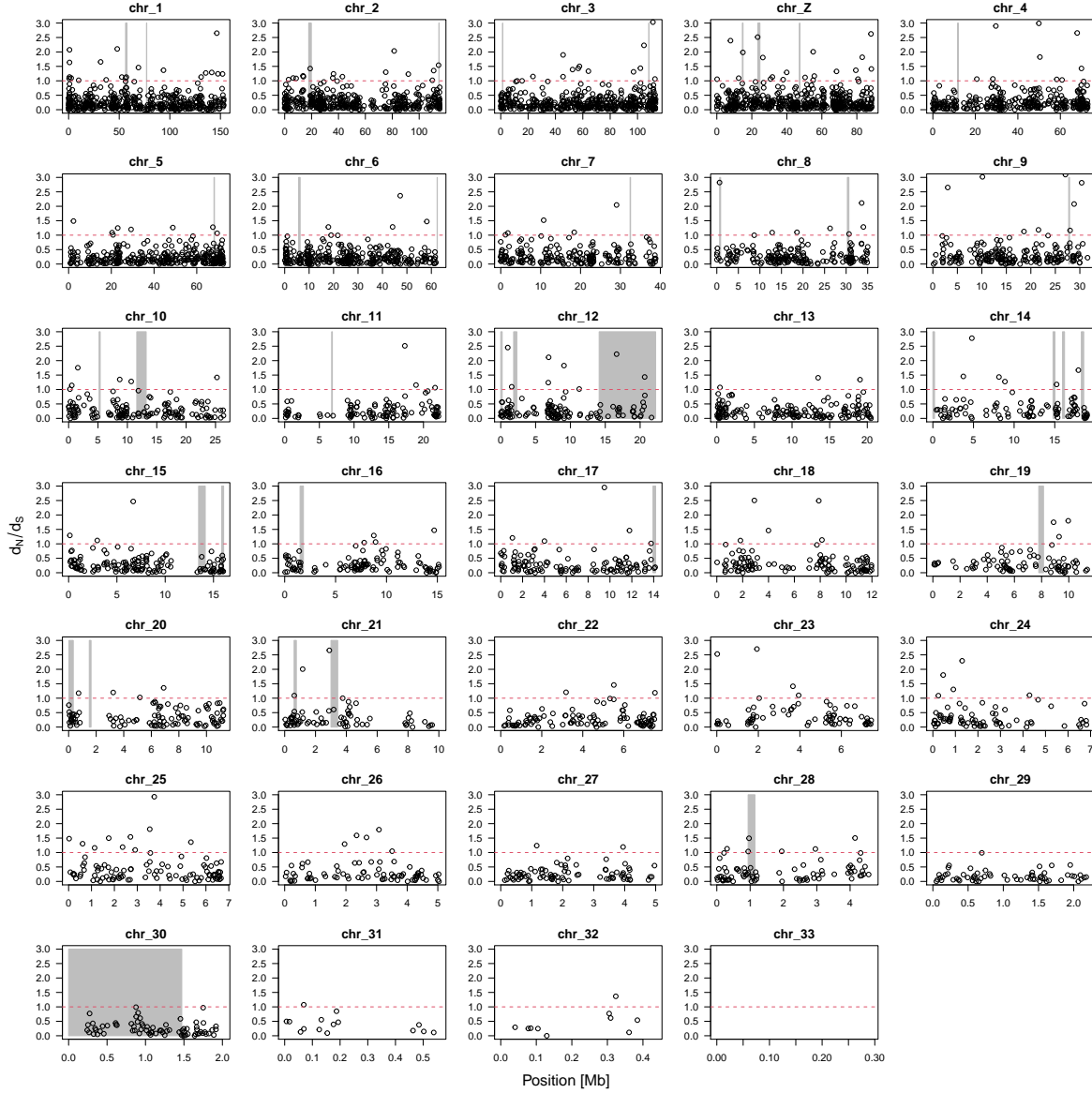
3.5.1 Effects of selection in blackcap genome



Supplementary Figure 28: Nucleotide diversity (π) in genomic regions with distinct pattern of genetic variation. Supplementary data related to *Results: Effect of selection on patterns of genetic variation* and Sup. Table. 9. “bg” depicts distribution of π in non-outlier regions of local PCA.



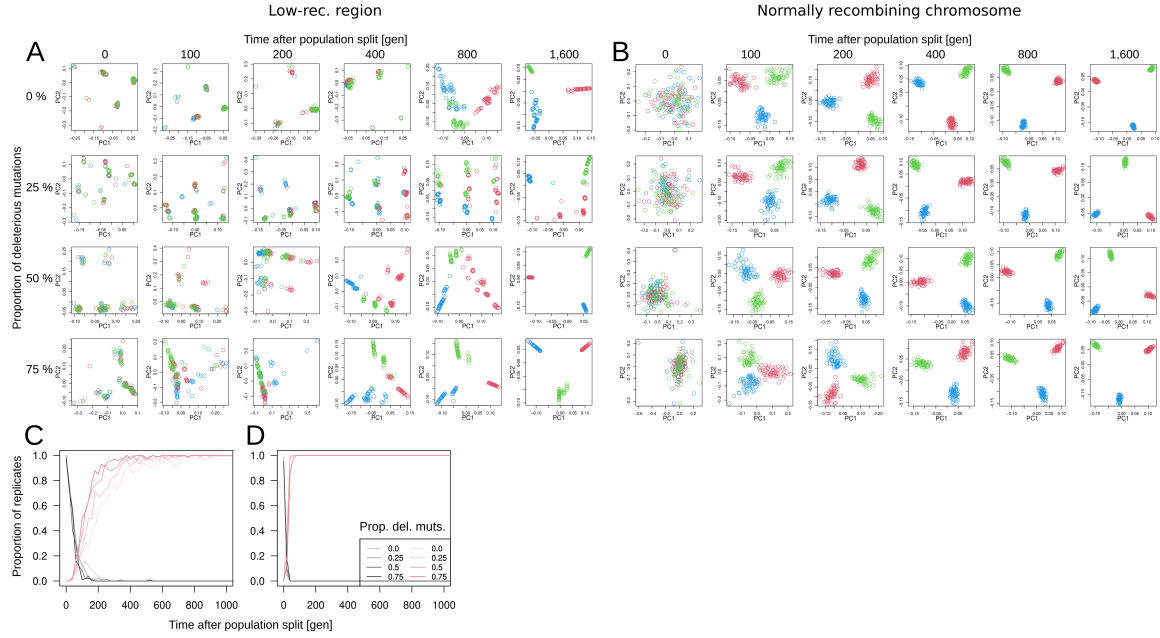
Supplementary Figure 29: Tajima's D in genomic regions with distinct pattern of genetic variation. Supplementary data related to *Results: Effect of selection on patterns of genetic variation* and Sup. Table. 10. Box plots depict the distribution of Tajima's D in windows within 32 outlier regions and in non-outlier regions ("bg").



Supplementary Figure 30: d_N/d_S of blackcap genes. Supplementary data related to *Results: Effect of selection on patterns of genetic variation*. Gray shades depict positions of 32 outlier regions.

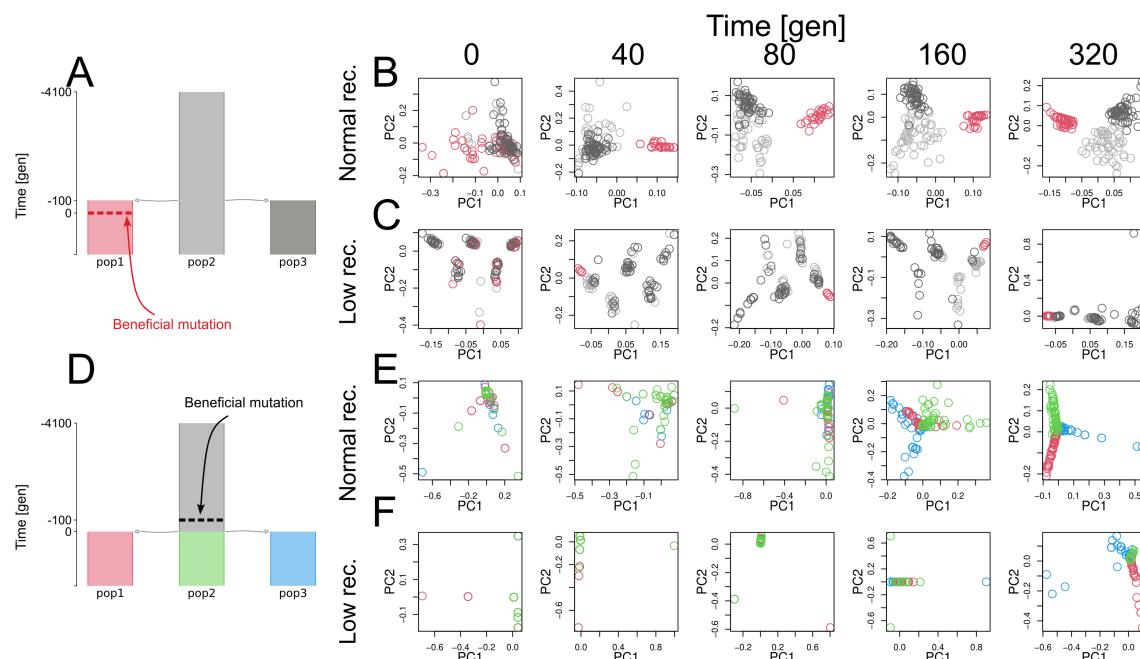
3.5.2 Effects of selection at low-recombining regions (forward simulation)

3.5.2.1 Purifying selection



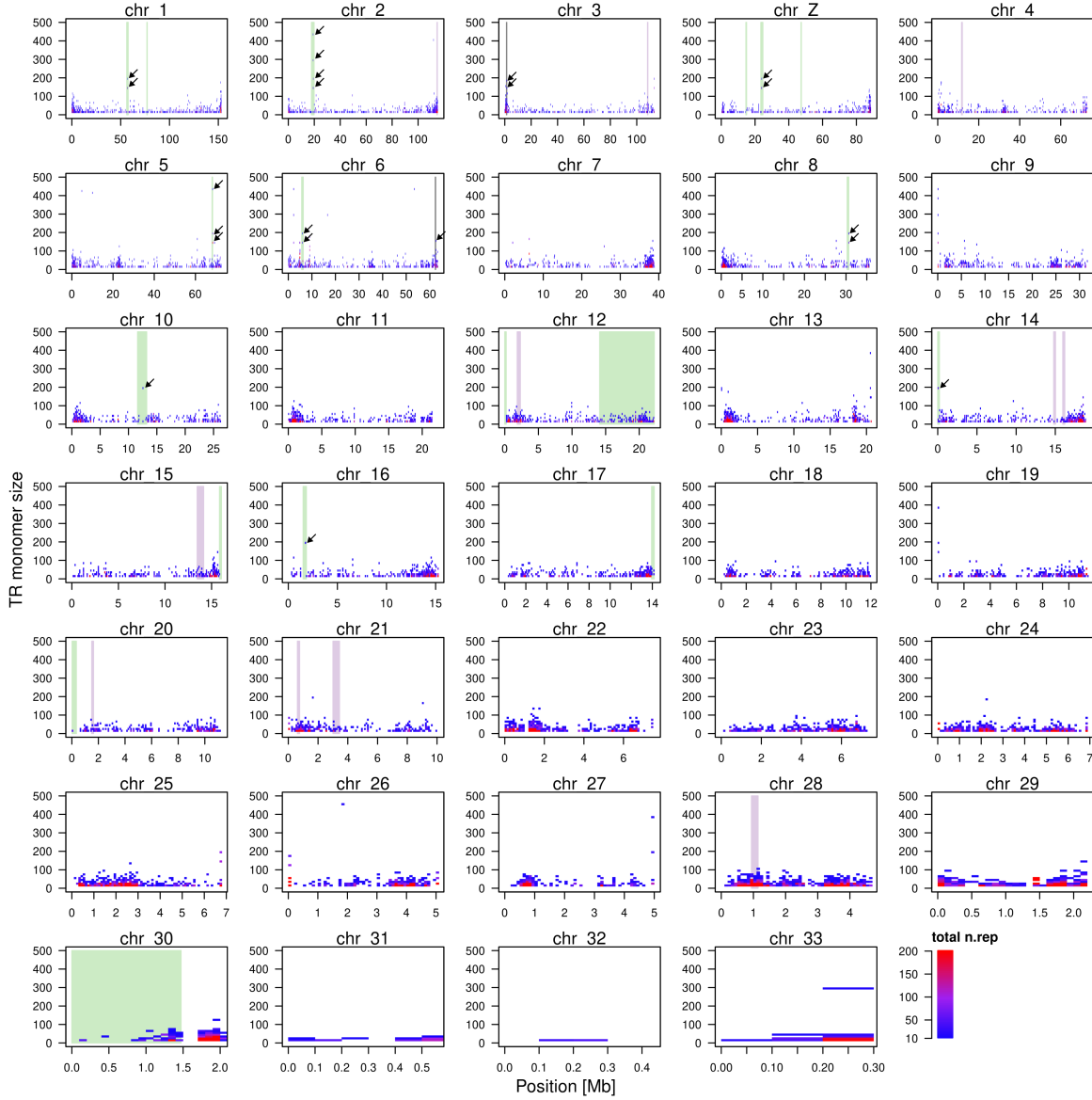
Supplementary Figure 31: Species-wide reduction in recombination rate and purifying selection affect rate at which local genetic variation changes. To investigate the effect of purifying selection on patterns of genetic variation at low-recombining regions, we simulated three populations with a species-wide low-recombining region, varying the distribution of fitness effect (DFE) of mutations by specifying three different ratios between neutral and deleterious mutations (Detailed in Materials and Methods). We performed PCA within and outside the low-recombining region over time, and tested whether the distribution of individuals in PCA is distinct between populations by applying Fasano-Franceschini tests. **A.** PCA at low-recombining region over time in one exemplified replicate under the four scenarios of DFE. Points with three different colours depict individuals of three different populations. **B.** PCA with the normally recombining chromosome over time in the same replicate in **A** under the four scenarios of DFE. Clusters of individuals representing haplotype structure is present at all scenarios, but population structure emerges at different rates across DFEs. **C, D.** Summary of Fasano-Franceschini tests in low-recombining (**B**) and normally recombining (**C**) regions. Red lines show the proportion of simulation replicates in which Fasano-Franceschini tests were significant in all three pairs of populations. Black/gray lines show the proportion of simulation replicates in which none of the three pairs of populations were significant in Fasano-Franceschini test. These results show that (1) species-wide recombination reduction slows down change in pattern of local genetic variation (differentiation at a genomic local scale) after a population split event, and (2) purifying selection accelerates the slowed change in pattern of local genetic variation in a chromosomal region with species-wide recombination reduction.

3.5.2.2 Positive selection

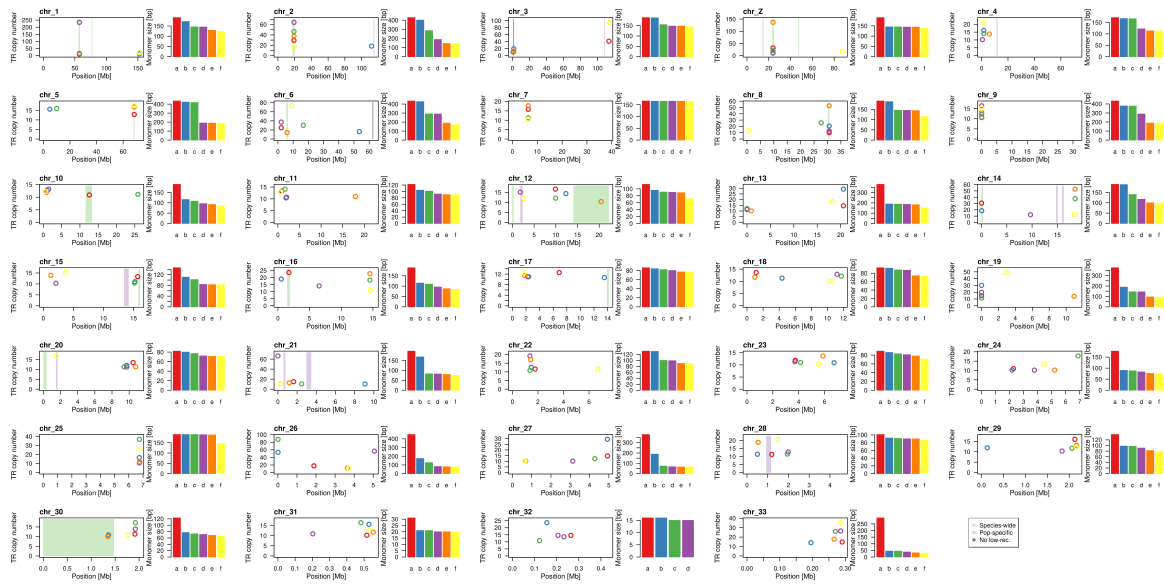


Supplementary Figure 32: Positive selection at species-wide low-recombining region. To investigate how positive selection affects patterns of genetic variation at low-recombining regions, we simulated three populations with or without a species-wide low-recombining region and introduced a beneficial mutation before or after population split. We performed PCA over time. **A.** Scenario of population-specific positive selection. A beneficial mutation was introduced in pop1 100 generations after the population split. **B.** PCA around the position of beneficial mutation in the scenario of **A** without a low-recombining region. **C.** PCA around the position of beneficial mutation within a low-recombining region in the scenario of **A**. **D.** Scenario of positive selection in an ancestral population. A beneficial mutation was introduced in the ancestral population 100 generations before the population split. **E.** PCA around the position of beneficial mutation in the scenario of **D** without a low-recombining region. **F.** PCA around the position of beneficial mutation within a low-recombining region in the scenario of **D**. These results show that positive selection affects local genetic variation which is overlaid on the effect of haplotype structure by reduced recombination rate. Only five time points of one simulation replicate are shown in this figure.

3.6 Pericentromeric regions in outlier regions

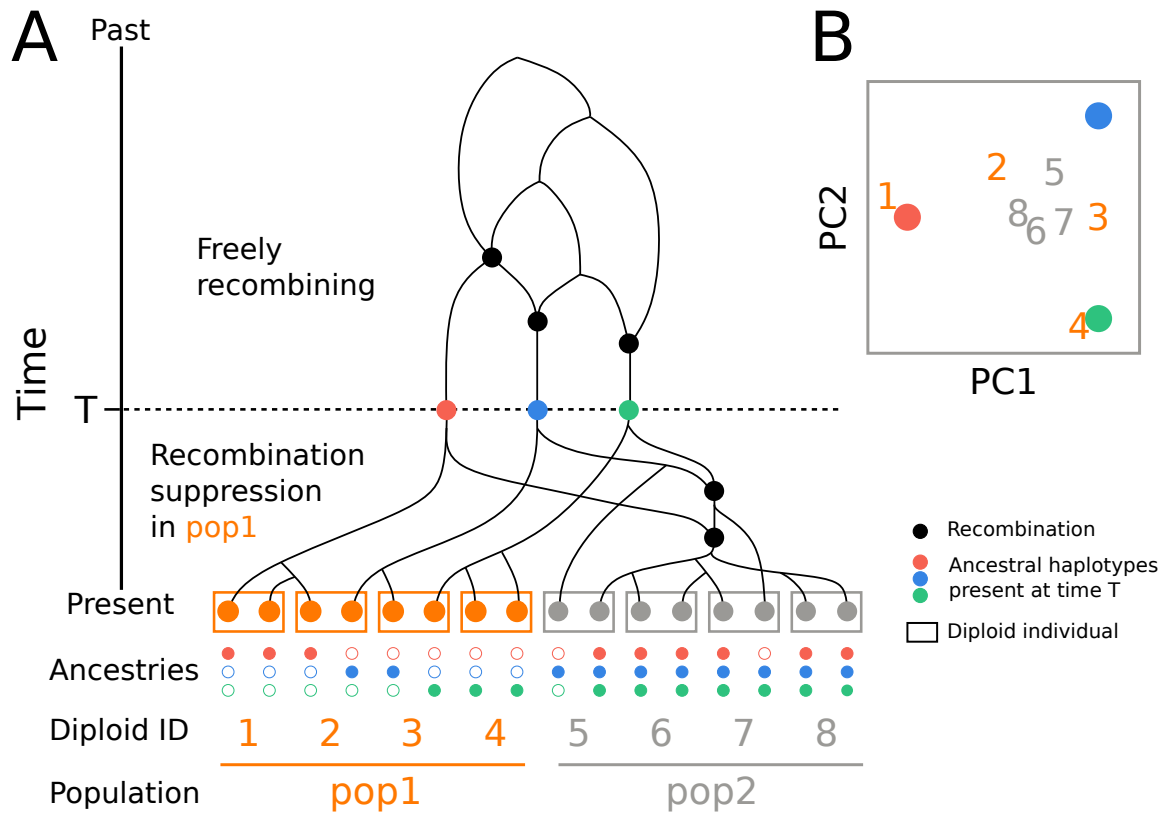


Supplementary Figure 33: Genomic distribution of tandem repeats. Shades indicate outlier regions based on *lostruct*. Each cell in the heatmap shows the number of copies of tandem repeats (colour-coded) with unit size of the focal range (y-axis) found in the focal genomic window of 100 kb (x-axis). Black arrows point long tandem repeats coinciding with *lostruct* outlier regions.



Supplementary Figure 34: Genomic distribution of tandem repeats with long repeat unit. In each chromosome, six tandem repeats with the longest repeat units are shown. Shades indicate genomic regions with distinct patterns of genetic variation.

3.7 Genealogical interpretation



Supplementary Figure 35: Genealogical interpretation of the effect of population-specific recombination suppression on local genetic variation. **A.** An ancestral recombination graph (ARG) representing ancestries of 16 hypothetical haploid sequences of 8 diploid sampled individuals from two populations. Their ancestries can be traced back to $n_1 = n_2 = 3$ ancestral haplotypes (the same set for simplicity) present at time T when population-specific recombination suppression initiated in pop1. The ancestries of these n_1 and n_2 ancestral haplotypes freely recombine at times older than T . At the bottom, the ancestries of each current haplotype are shown. Closed and open circles represent presence and absence of contribution from the respective ancestral haplotype. **B.** A hypothetical PCA representing the pattern of genetic variation of the focal region. Individuals from the low-recombining population (pop1) are spread in the hypothetical PCA because each diploid has a combination of discrete ancestries. The individuals of normally recombining populations (pop2) are clustered around the centre because they have mixed haplotypes due to continued recombination after T .

4 References

- Huang, K., Andrew, R. L., Owens, G. L., Ostevik, K. L., & Rieseberg, L. H. (2020). Multiple chromosomal inversions contribute to adaptive divergence of a dune sunflower ecotype. *Molecular Ecology*, 29(14), 2535–2549. <https://doi.org/10.1111/mec.15428>
- Leroy, T., Anselmetti, Y., Tilak, M.-K., Bérard, S., Csukonyi, L., Gabrielli, M., Scornavacca, C., Milá, B., Thébaud, C., & Nabholz, B. (2021). A bird’s white-eye view on avian sex chromosome evolution. *Peer Community Journal*, 1. <https://doi.org/10.24072/pcjournal.70>
- Ma, J., & Amos, C. I. (2012). Investigation of Inversion Polymorphisms in the Human Genome Using Principal Components Analysis. *PLOS ONE*, 7(7), e40224. <https://doi.org/10.1371/journal.pone.0040224>
- Pala, I., Naurin, S., Stervander, M., Hasselquist, D., Bensch, S., & Hansson, B. (2012). Evidence of a neo-sex chromosome in birds. *Heredity*, 108(3), 264–272. <https://doi.org/10.1038/hdy.2011.70>
- Shipilina, D., Pal, A., Stankowski, S., Chan, Y. F., & Barton, N. H. (2023). On the origin and structure of haplotype blocks. *Molecular Ecology*, 32(6), 1441–1457. <https://doi.org/10.1111/mec.16793>
- Sigeman, H., Ponnikas, S., & Hansson, B. (2020). Whole-genome analysis across 10 songbird families within Sylvioidea reveals a novel autosome–sex chromosome fusion. *Biology Letters*, 16(4), 20200082. <https://doi.org/10.1098/rsbl.2020.0082>
- Sigeman, H., Strandh, M., Proux-Wéra, E., Kutschera, V. E., Ponnikas, S., Zhang, H., Lundberg, M., Soler, L., Bunikis, I., Tarka, M., Hasselquist, D., Nystedt, B., Westerdahl, H., & Hansson, B. (2021). Avian Neo-Sex Chromosomes Reveal Dynamics of Recombination Suppression and W Degeneration. *Molecular Biology and Evolution*, 38(12), 5275–5291. <https://doi.org/10.1093/molbev/msab277>
- Stephan, W. (2019). Selective Sweeps. *Genetics*, 211(1), 5–13. <https://doi.org/10.1534/genetics.118.301319>
- Todesco, M., Owens, G. L., Bercovich, N., Légaré, J.-S., Soudi, S., Burge, D. O., Huang, K., Ostevik, K. L., Drummond, E. B. M., Imerovski, I., Lande, K., Pascual-Robles, M. A., Nanavati, M., Jahani, M., Cheung, W., Staton, S. E., Muños, S., Nielsen, R., Donovan, L. A., et al. (2020). Massive haplotypes underlie ecotypic differentiation in sunflowers. *Nature*, 584(7822), 602–607. <https://doi.org/10.1038/s41586-020-2467-6>

3

High-Recombining Genomic Regions Affect Demography Inference

“It’s—it’s a variable.” Kaplan was shaking, white-lipped and pale. “Something from which no inference can be made. The man from the past. The machines can’t deal with him. The variable man!”

– Philip K. Dick, *The Variable Man* (1953)

High-recombining genomic regions affect demography inference

Jun Ishigohoka^{1,*}

Miriam Liedvogel^{1,2,3,*}

¹MPRG Behavioural Genomics, Max Planck Institute for Evolutionary Biology, 24306 Plön, Germany

²Institute of Avian Research, An der Vogelwarte 21, 26386 Wilhelmshaven, Germany

³Department of Biology and Environmental Sciences, Carl von Ossietzky Universität Oldenburg, Ammerländer Heerstraße 114-118, 26129 Oldenburg, Germany

* Correspondence: [Jun Ishigohoka <ishigohoka@evolbio.mpg.de>](mailto:ishigohoka@evolbio.mpg.de), [Miriam Liedvogel <liedvogel@evolbio.mpg.de>](mailto:liedvogel@evolbio.mpg.de)

Keywords: demography inference, ancestral recombination graph, recombination rate, population genomics, non-model species, *Sylvia atricapilla*.

Running title: Recombination rate and demography inference.

Abstract

Inference of population history of non-model species is important in evolutionary and conservation biology. Multiple methods of population genomics, including those to infer population history, are based on the ancestral recombination graph (ARG). These methods use observed mutations to model local genealogies changing along chromosomes. Breakpoints at which genealogies change effectively represent the positions of historical recombination events. However, inference of underlying genealogies is difficult in regions with high recombination rate relative to mutation rate. This is because genealogies cover genomic intervals that are too short to accommodate sufficiently many mutations informative of the structure of the underlying genealogies. Despite the prevalence of high-recombining genomic regions in some non-model organisms, such as birds, its effect on ARG-based demography inference has not been well studied. Here, we use population genomics simulations to investigate the impact of high-recombining regions on ARG-based demography inference. We demonstrate that inference of effective population size and the time of population split events is systematically affected when high-recombining regions cover wide breadths of the chromosomes. We also show that excluding high-recombining genomic regions can practically mitigate this effect. Finally, we confirm the relevance of our findings in empirical analysis by contrasting demography inferences applied for a bird species, the Eurasian blackcap (*Sylvia atricapilla*), using different parts of the genome with high and low recombination rates. Our results suggest that demography inference using ARG-based methods should be carried out with caution when applied in species whose reference genomes contain long stretches of high-recombining regions.

Introduction

Population history affects the patterns of genetic variation, and conversely observed genetic variation in genomes allows inference of historical demographic parameters. The increasing availability of genome data of various species at a population level has facilitated development and application of a number of population genomics methods for demography inference (Excoffier et al., 2013; Gutenkunst et al., 2009; Harris & Nielsen, 2013; Li & Durbin, 2011; Liu & Fu, 2020; Schiffels & Durbin, 2014; Terhorst et al., 2017). These approaches are typically first applied to human data to understand the population history of our own species and for validation of the new methods (Excoffier et al., 2013; Gutenkunst et al., 2009; Harris & Nielsen, 2013; Li & Durbin, 2011; Liu & Fu, 2020; Schiffels & Durbin, 2014; Terhorst et al., 2017), but thereafter adopted to other species including domesticated and wild organisms to answer evolutionary questions (Alonso-Blanco et al., 2016; Groenen et al., 2012; Lanier et al., 2015; Liu et al., 2014; Nadachowska-Brzyska et al., 2016) and to assist conservation efforts (Dussex et al., 2021; Hohenlohe et al., 2021; Li et al., 2014; Pacheco et al., 2022). Despite the wide application of demography inference methods in non-model organisms, their performance outside the parameter space of humans has not been well evaluated.

Some methods for demography inference are based on the ancestral recombination graph (ARG) (Li & Durbin, 2011; Schiffels & Durbin, 2014; Speidel et al., 2019; Terhorst et al., 2017). The ARG is a structure that describes the full ancestries of sampled genomes along recombining chromosomes (Griffiths & Marjoram, 1997). It essentially consists of a series of marginal genealogical trees changing in the topology and branch lengths along the chromosome, and their breakpoints effectively represent historical recombinations contributing to the sampled genomes (Fig. 1). The full ARG provides rich information on the population history (i.e. all coalescence and recombination events through time and mutations mapped on branches), making ARG-based methods a powerful population genomics approach to study evolutionary processes (Hubisz et al., 2020; Schaefer et al., 2021; Speidel et al., 2019; Stern et al., 2019; Wohns et al., 2022). In practice, however, ARG-based methods depend on inference of the ARG (Ignatieva et al., 2021; Kelleher et al., 2019; Mirzaei & Wu, 2017; Rasmussen et al., 2014; Speidel et al., 2019; Wohns et al., 2022), or representations of underlying genealogies (Li &

Durbin, 2011; Schiffels & Durbin, 2014; Terhorst et al., 2017), which in turn relies on observed mutations. Importantly, the presence of mutations representing an ARG branch depends on recombination and mutation rates. If an ancestral haplotype breaks by a recombination before accommodating mutations, the corresponding branch on the ARG is not represented by any mutations (Fig. 1B) (Hayman et al., 2023; Shipilina et al., 2023). Therefore, high recombination rates (relative to the mutation rate) makes it difficult to accurately infer the underlying ARG, limiting the performance of the ARG-based approach (Sellinger et al., 2020, 2021; Terhorst et al., 2017).

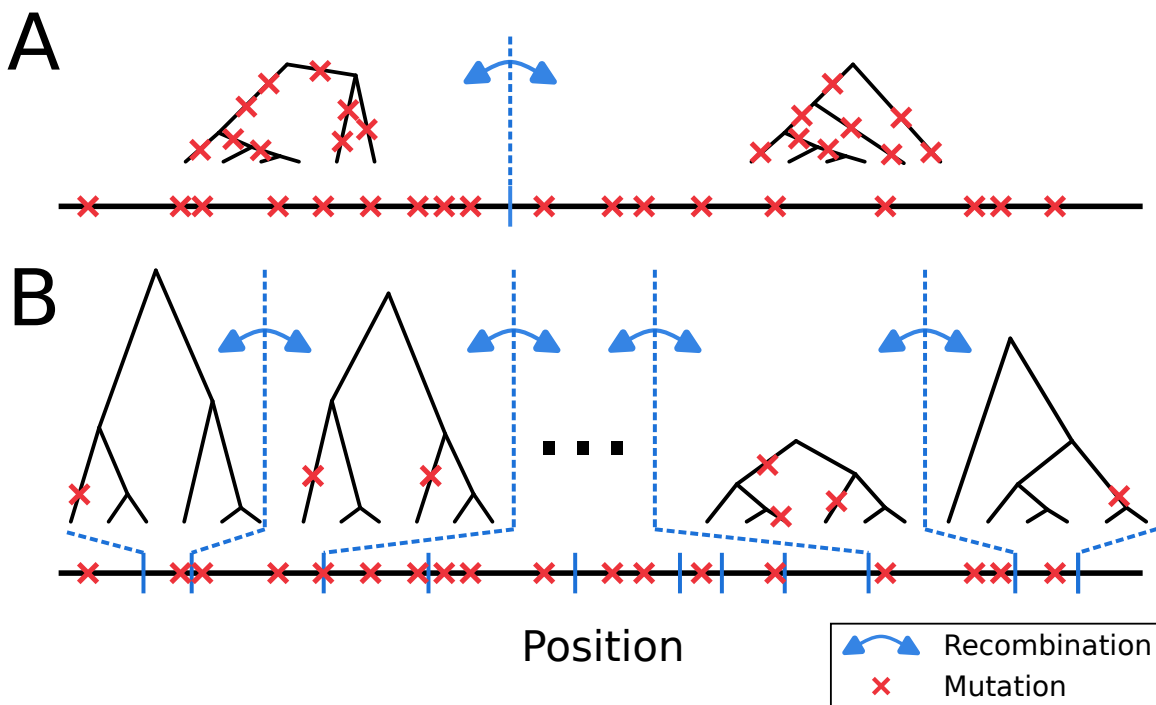


Figure 1: The presence of mutations representing ARG branches depends on recombination rate. **A.** When recombination rate is moderately low, branches of ARG are represented by mutations. This allows inference of the underlying ARG based on observed mutations. **B.** When recombination rate is high, many branches of ARG are not represented by any mutations. We ask whether this affects ARG-based demography inference.

The impact of high recombination rate on ARG-based demography inference is presumably negligible in humans (Li & Durbin, 2011; Terhorst et al., 2017) where recombination rate is low except for narrow recombination hotspots (Myers et al., 2010; Stevenson et al., 2016). However, this type of recombination landscape is not universal to all organisms (Auton et al., 2013; Baker et al., 2017; Lam & Keeney, 2015; Singhal et al., 2015), including species with ecological and

evolutionary relevance or of conservation concern. The difference in recombination landscapes can be partially attributed to the presence and absence of PRDM9, a transcription factor that determines the genomic position of recombination hotspots. PRDM9 introduces histone modifications to recruit the molecular machinery initiating DNA double-strand breaks (DSBs), which is required for meiotic recombination (Baker et al., 2015; Baudat et al., 2010; Paigen & Petkov, 2018). PRDM9 has been lost independently at least thirteen times in vertebrates (Cavassim et al., 2022), which shifted the recombination hotspots from rapidly evolving PRDM9 motifs (Baker et al., 2015; Myers et al., 2010; Oliver et al., 2009) to genome features such as transcription start sites and CpG-islands (Auton et al., 2013; Baker et al., 2017; Kawakami et al., 2017; Paigen & Petkov, 2018; Singhal et al., 2015). Hotspots of PRDM9-independent recombination in birds (Bascón-Cardozo et al., 2024; Kawakami et al., 2017; Singhal et al., 2015), dogs (Auton et al., 2013) and percomorph fish (Baker et al., 2017) appear to be wider than PRDM9-dependent hotspots in primates (Durbin et al., 2010; Myers et al., 2010; Stevison et al., 2016). On top of the recombination landscape, the average recombination rate is highly variable between chromosomes and species (Stapley et al., 2017). These differences in meiotic recombination could potentially impact modelling of the local ARGs in non-human species.

In this study, we ask how recombination landscapes affect ARG-based demography inference. To this end, we simulate genome data under a simple demographic history with various recombination maps, and evaluate the accuracy of demography inference by different ARG-based methods. Specifically, we focus on two ARG-based methods, **MSMC2** (Malaspinas et al., 2016; Wang et al., 2020) and **Relate** (Speidel et al., 2019), differing in the way the ARG is modelled. While **Relate** infers a series of marginal genealogies along the genome with their topology and branch lengths collectively representing the full ARG of the sample, **MSMC2** models the distribution of the coalescence times between pairs of sampled sequences along the genome based on the sequentially Markovian coalescent (SMC, McVean & Cardin (2005)). To demonstrate the relevance of our findings based on simulations, we translate our findings to empirical data of a non-model organism with wide high-recombining genomic regions. To this end, we use whole-genome resequencing (WGR) data and fine-scale recombination maps of a songbird species, the Eurasian blackcap (*Sylvia atricapilla*), and contrast ARG-based

demography inferences using genomic regions differing in recombination rates.

Results

Simulations of different recombination maps

To investigate the effect of the recombination landscape on ARG-based demography inference, we used **msprime** (Kelleher et al., 2018) to simulate a simple demographic history (Fig. 2A) with five different recombination maps (Fig. 2B). In all simulations, three subpopulations (pop1, pop2, and pop3) split from a constant-sized ancestral population of 1 million diploids 10,000 generations before the present, after which they followed different trajectories of effective population size (constant (pop1), exponential increase (pop2), and exponential decrease (pop3)). Under this demography model, we simulated 16 Mb-long chromosomes (Fig. 2B) with a constant mutation rate and heterogeneous recombination rate along the chromosome (color-coded from orange (no high-recombining regions) to dark red (extreme high-recombining regions)). Specifically, the 10 Mb stretch in the middle of the chromosome (“middle”) had a recombination rate one-tenth the mutation rate in all five scenarios, while the recombination rate increased in a stepwise manner at the 3 Mb ends of the chromosome. To test whether masking high-recombining regions improves ARG-based demography inference, we applied masks accounting for the length of chromosomes in two ways: masking a total of 6 Mb within the central part of the chromosome without elevated recombination rate (“control”, Fig. 2C top) or masking the 3 Mb ends of the chromosome covering the entire high-recombining regions (Fig. 2C bottom). Mean recombination-mutation ratios of the five scenarios for the control condition (after applying the masks) were 0.1, 0.25, 1, 4, and 10 (Fig. 2B, C)). We inferred the demography with two ARG-based methods, **MSMC2** and **Relate**. We also inferred demography using **Stairway plot 2**, an SFS-based method expected to be unaffected by elevated local recombination rate. In summary, we tested the performance of demography inference in grids of five scenarios (differing in recombination maps), three demography inference methods (two ARG-based and one SFS-based), and two conditions of masking (masking high-recombining and background regions).

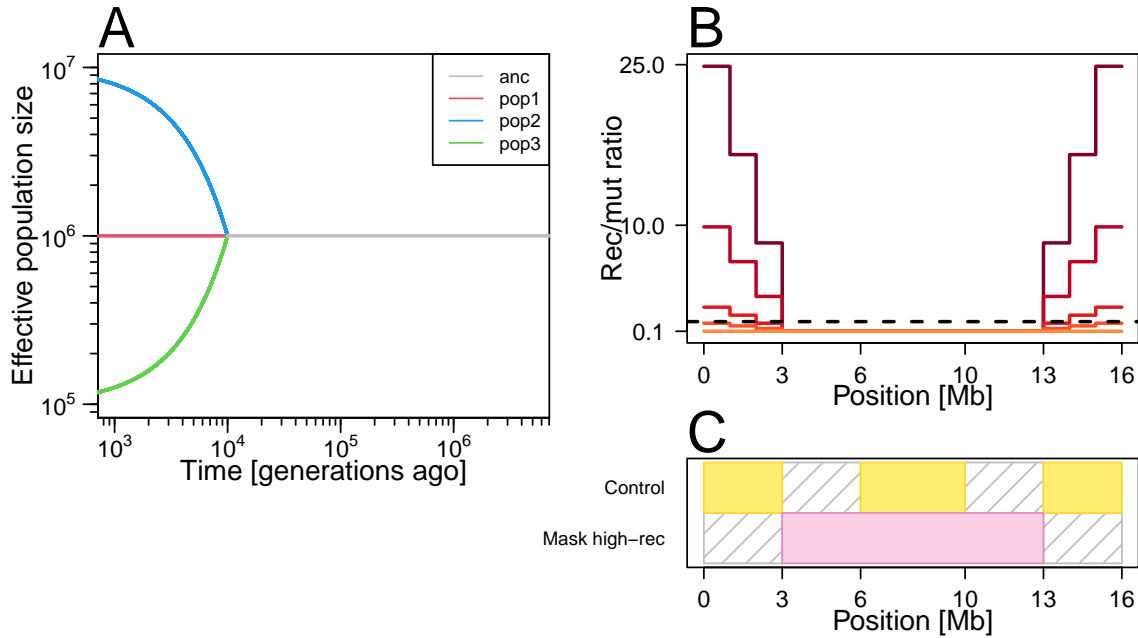


Figure 2: Design of our simulation study. **A.** Simulated demographic history. We simulated three populations (pop1, pop2, pop3) that split from one ancestral population simultaneously 10,000 generations before the present. After the population split, these three populations follow distinct trajectories of effective population size. **B.** Recombination maps used in our simulations for a hypothetical chromosome. We considered five scenarios with different recombination maps that are depicted by five solid color-coded lines. In all scenarios, recombination rate (Y axis) is 1/10 of the mutation rate in the middle of the chromosome. Recombination rate increases in a stepwise manner (scenarios with different levels of increase are color-coded from orange to dark red) towards the ends of the chromosome. The horizontal black dotted line indicates the recombination-to-mutation ratio of 1. **C.** Two settings of demography inference masking different parts of the chromosomes (yellow blocks depict genomic regions used for demography inference. Gray shades depict regions masked from demography inference). We asked whether the presence of high-recombining regions (i.e. towards the chromosome ends in the simulated scenario illustrated in C) in the genome affects demography inference and whether masking them improves demography inference. We applied methods of demography inference on the simulated data using different parts of the chromosome: either including the high-recombining regions (“control”, top) or masking the 6 Mb of high-recombining regions (bottom). To control for the total sequence length used in the inferences, we applied a total of 6 Mb masks outside the high-recombining regions in the first setting (top).

Effect of wide high-recombining regions on inference of effective population size

We first investigated the effect of high-recombining regions on the inference of historical effective population size under the control condition, in which high-recombining regions were not masked (Fig. 3A-C). Inference by MSMC2 was too noisy in the recent past to inspect the timing of the split event based on inferred effective population size especially in scenarios

with mild or no elevation of recombination rates at the chromosomal ends (Fig. 3, left column. Results of all five recombination landscapes are in Sup. Fig. 1). This noisiness in **MSMC2** inference is unlikely to be the effect of recombination rate, as the inference was noisy even for the scenario without a high-recombining region (Fig. 3A, left column), but rather results from insufficient data (eight haploids of ten chromosomes of 16 Mb) and the simulated split time being too recent compared to the effective population size. When the mean recombination rate was lower than or equal to the mutation rate, **MSMC2** inferred effective population size accurately in the deep past (Fig. 3A, B, left column). However, when the mean recombination rate was greater than the mutation rate, the inference of effective population size by **MSMC2** was systematically deviated in the deep past with a characteristic wave-shaped pattern in the skyline plot (Fig. 3C, left column). Inference by **Relate**, which exploited a total of 300 haploids from the three subpopulations, was less noisy compared to **MSMC2** even in the recent past (Fig. 3, middle column. Results of all five recombination landscapes are in Sup. Fig. 1). In the case without high-recombining regions (Fig. 3B, middle column), the apparent split time as well as the post-split trajectories of the effective population sizes were accurately inferred, albeit slightly smaller effective population size before the split event was estimated. However, effective population sizes of pop1 (red, constant size) and pop2 (blue, exponential growth) were systematically underestimated after the population split as the mean recombination rate increased. In contrast to the two ARG-based methods, demography inference by SFS-based **Stairway plot 2** was robust to the presence of high-recombining regions (Fig. 3, right column).

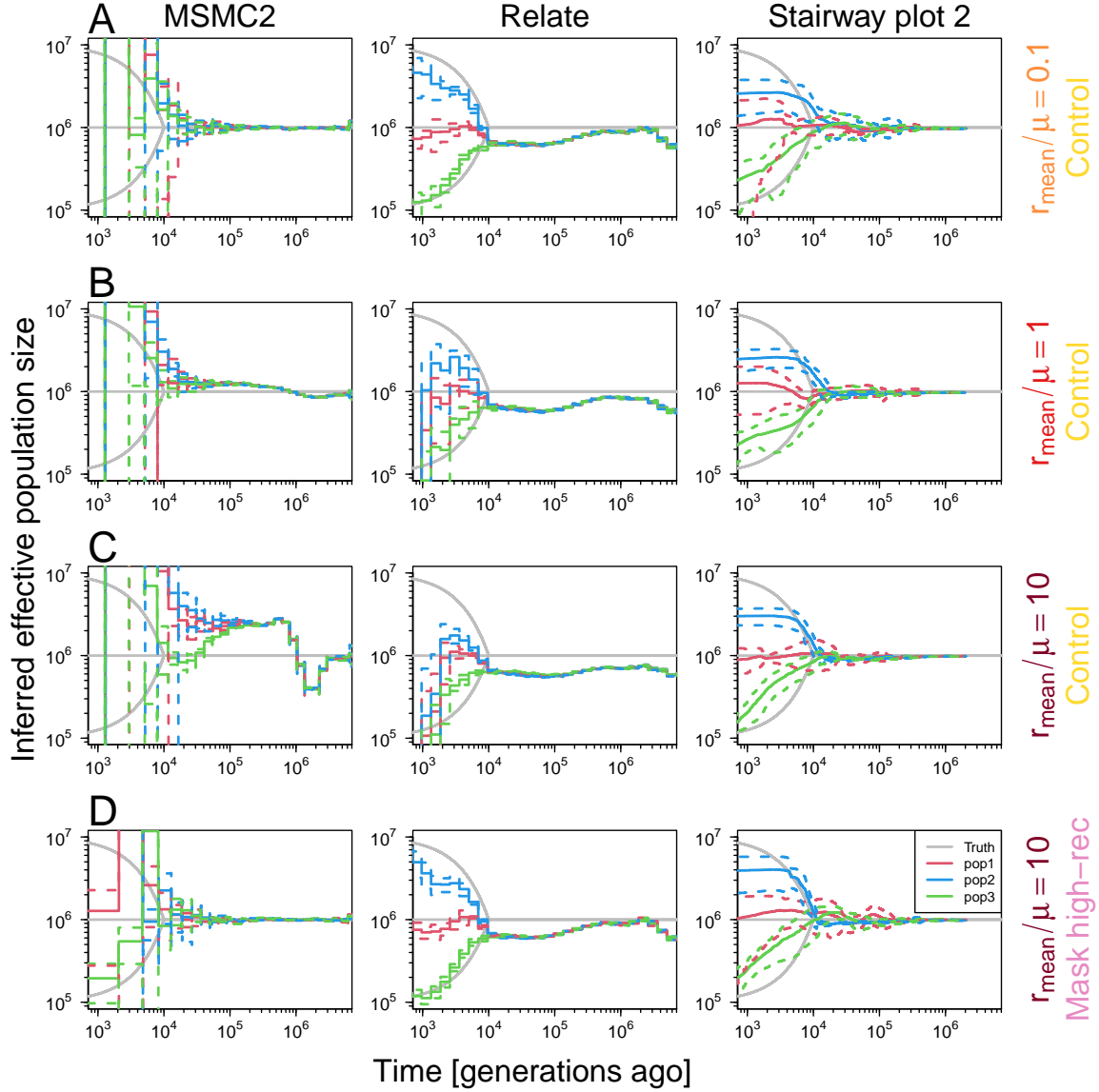


Figure 3: Inference of historical effective population size. The inferences by MSMC2 (left) and Relate (middle) without masking high-recombining regions (A–C) show that ARG-based methods are biased in the presence of high-recombining regions. Removing the high-recombining regions eliminated the bias (D). The results for Stairwayplot 2 (right) confirm the expectation that the SFS-based method is less affected by the presence of high-recombining regions. In each panel, gray lines depict the simulated truths (as in Fig. 2A), solid and dashed colored lines depict the mean and mean \pm SD of the inferences (see Materials and Methods for details on how replicates were treated).

To investigate whether the deviations in the demography inferences by ARG-based methods are due to errors in inferred local ARGs within the high-recombining regions or global errors throughout the entire chromosome, we compared coalescence time metrics in inferred (representation of) ARGs with the simulated truth. For MSMC2, we compared discretized

time to the most recent common ancestor (TMRCA) between a pair of haplotypes along chromosomes with the true coalescence times. For **Relate**, we compared TMRCA of the entire ARG of 300 sequences along chromosomes between the inference and the truth. In both ARG-based methods, correlation between the inference and the truth was reduced specifically in the high-recombining regions (Sup. Figs. 3, 4). Furthermore, masking high-recombining regions improved demography inference in both methods (Fig. 3D). Our findings indicate that ARG-based demography inference is affected by localized errors within the high-recombining regions.

Effect of wide high-recombining regions on the inference of population splits

Next, we investigated the effect of high-recombining regions on ARG-based inference of population split events under the control condition (without masking high-recombining regions) between pairs of populations by inferring historical relative cross-coalescence rate (rCCR) by **MSMC2** and **Relate** (Fig. 4A-C. Results of all five recombination landscapes are illustrated in Sup. Fig. 2). rCCR is a metric informative of split events and gene flow between a pair of populations: it increases from 0 to 1 backwards in time (i.e. it drops from 1 to 0 forward in time) at the population split event, and the rate of this change in respect to time essentially depicts how fast the split occurred (Schiffels & Durbin, 2014).

Inferred rCCR based on **MSMC2** started to drop (forward in time) earlier than the true split time (Fig. 4). This was especially true for subpopulation pairs involving pop3 (exponential reduction in effective population size) as the mean recombination rate increased. This pattern is consistent with the older apparent split based on effective population size inferred by **MSMC2** with high-recombining regions (Fig. 3C, left column). In inference by **Relate**, rCCR decreased (forward in time) at the true split time, but increased again towards the present time in scenarios with high-recombining regions (Fig. 4). Importantly, we were able to mitigate these effects by masking the high-recombining regions (Fig. 4D). To summarize, our simulation study illustrates that the presence of high-recombining regions affects ARG-based inference of both historical effective population size and population split time. We could show that these effects can be mitigated by masking high-recombining regions of the genome in the analysis.

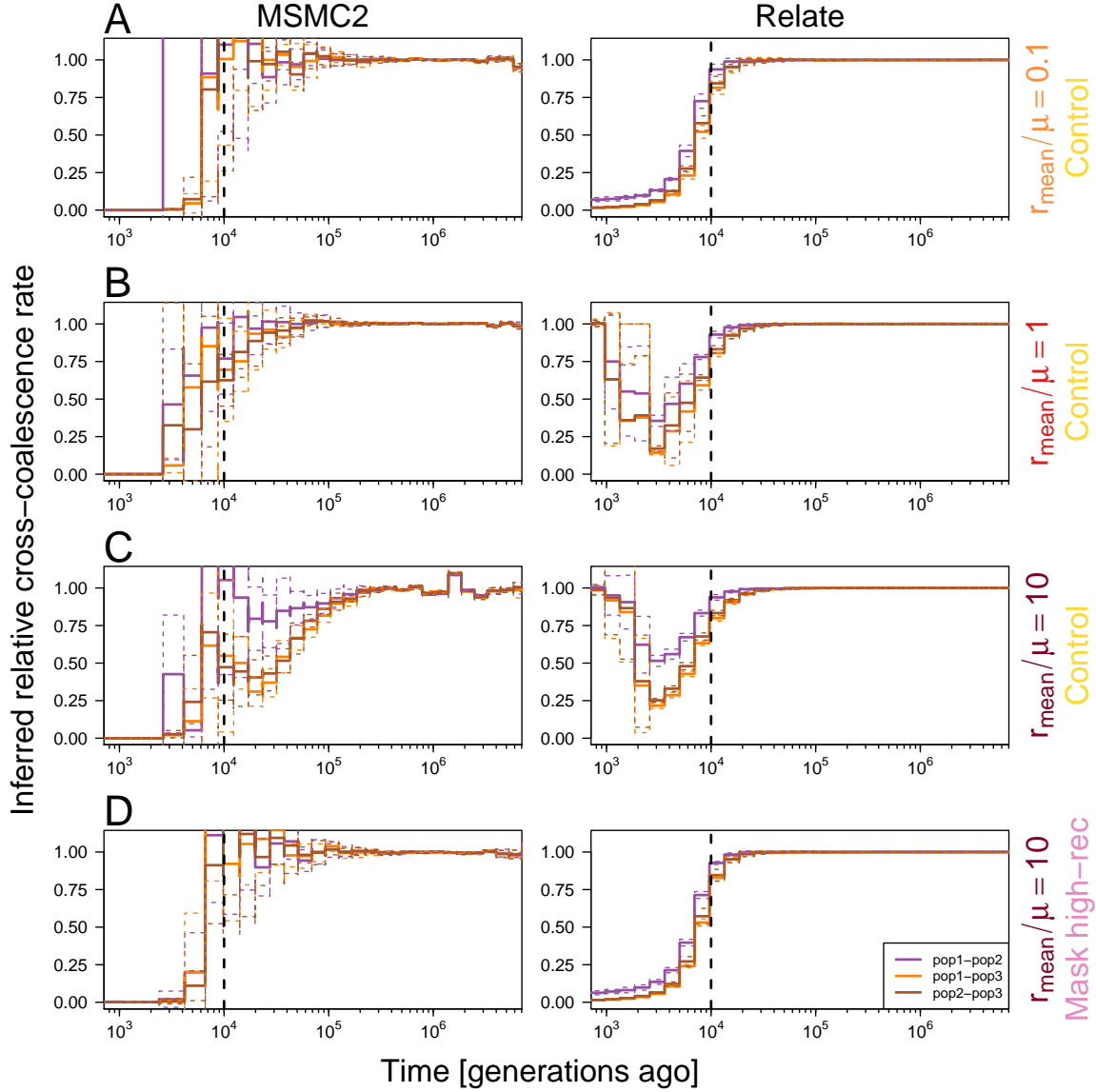


Figure 4: Inference of population split events. Vertical dotted lines depict the true split time. Colored lines depict inferred rCCR for pairs of populations. Three colors indicate three pairs of populations. **MSMC2** (left column). Solid lines depict mean of inferences of the ten down-samples, and dotted lines depict mean \pm SD. The results show that the presence of high-recombining regions biases the inference of population splits, and removing the high-recombining regions reduces this bias. **Relate** (right column). Solid lines depict mean of inferences of the ten replicates, and dotted lines depict mean \pm SD. The results show that the presence of high-recombining regions biases the inference of population splits, and removing the high-recombining regions reduces this bias.

Effect of a narrow high-recombining region on demography inference

To further explore how different levels of heterogeneity in the local recombination rate along chromosomes might affect ARG-based demography inference, we simulated the same demo-

graphic history with two additional sets of recombination maps. Both sets consisted of five recombination maps (Sup. Fig. 5): the first set with uniform recombination rates along the chromosome (“Uniform”. 0.1, 0.25, 1, 4 and 10 times the mutation rate); and the second with a single narrow region of high recombination rate Fig. 2B (“Narrow high-rec.”. Ratios between mean recombination rate and mutation rate of 0.1, 0.25, 1, 4, and 10 as in Fig. 2 but with a narrower region of high recombination rate). For the uniform scenario, inference by both MSMC2 and Relate were affected by recombination rate similarly to the stepwise recombination maps as the recombination rate increased (Sup. Fig. 6). For the narrow high-rec. scenario, inference by MSMC2 was slightly affected when the mean recombination rate was greater than the mutation rate (Sup. Fig. 7). In contrast, inference by Relate was robust to the presence of the narrow high-recombining region. These results indicate that the ARG-based methods are affected by a wide coverage of regions with recombination rate greater than mutation rate. Additionally, the ARG-based methods differ in their robustness to the presence of high-recombining regions. This may represent an inherent difference of the robustness between MSMC2 and Relate, but it also could reflect the different sample sizes used as the input owing to different scalability between the two methods: in our study we used 150 diploids (300 haploid genomes) for inference by Relate, while only eight haploid genomes per population were used for MSMC2.

Application to empirical data

Birds lack PRDM9 and their recombination is characterized by higher rates and wider hotspots compared to PRDM9-dependent recombination in primates (see [Introduction](#)). Additionally, per-generation mutation rate is lower in many birds than in humans (Bergeron et al., 2023). These factors are manifested as wider breadth of genomic regions with high recombination-mutation ratio, which could bias ARG-based methods for demography inference as shown in our simulation study. To address the relevance of our findings to empirical applications, we revisited genome data of the Eurasian blackcap (*Sylvia atricapilla*, “blackcap” here after) as a representative of birds. The data consist of whole-genome resequencing of 179 individuals of ten populations across the species’ distribution range (Delmore et al., 2020; Ishigohoka et al., 2023), covering variation in population-typical phenotypes of seasonal migration. To

investigate the effect of recombination rate on ARG-based methods of demography inference with the blackcap dataset, we split the blackcap genome into low- and high- recombining halves, based on local recombination rates characterized in a previous study (Bascón-Cardozo et al., 2024) (see [Materials and Methods](#) for details). We performed demography inference (effective population size and rCCR) with **MSMC2** and **Relate** for each half separately.

Inference by **MSMC2** showed apparent effects of high-recombining regions consistent with our simulation. Historical effective population size inferred using the high-recombining half had characteristic wave-shaped trajectory in the deep past of the skyline plot (Fig. 5B) compared to that using the low-recombining half (Fig. 5A). The apparent split time between populations based on effective population size was older using the high-recombining half (Fig. 5B) than using the low-recombining half (Fig. 5A). In line with this, direct comparison of inferred rCCR for pairs of blackcap populations between the high- and low-recombining halves revealed inference of systematically older split time using the high-recombining half than the low-recombining half (Fig. 5C, D). These differences are consistent with our simulation study (Figs. 3, 4), indicating that the effect of high-recombining regions on inference by **MSMC2** is relevant for empirical analysis. In contrast, **Relate** was robust to the difference in recombination rate between the two conditions (Sup. Fig. 8). This difference between **MSMC2** and **Relate** suggests different levels of robustness of ARG-based methods to the presence of high-recombining regions, which is in line with our simulation study.

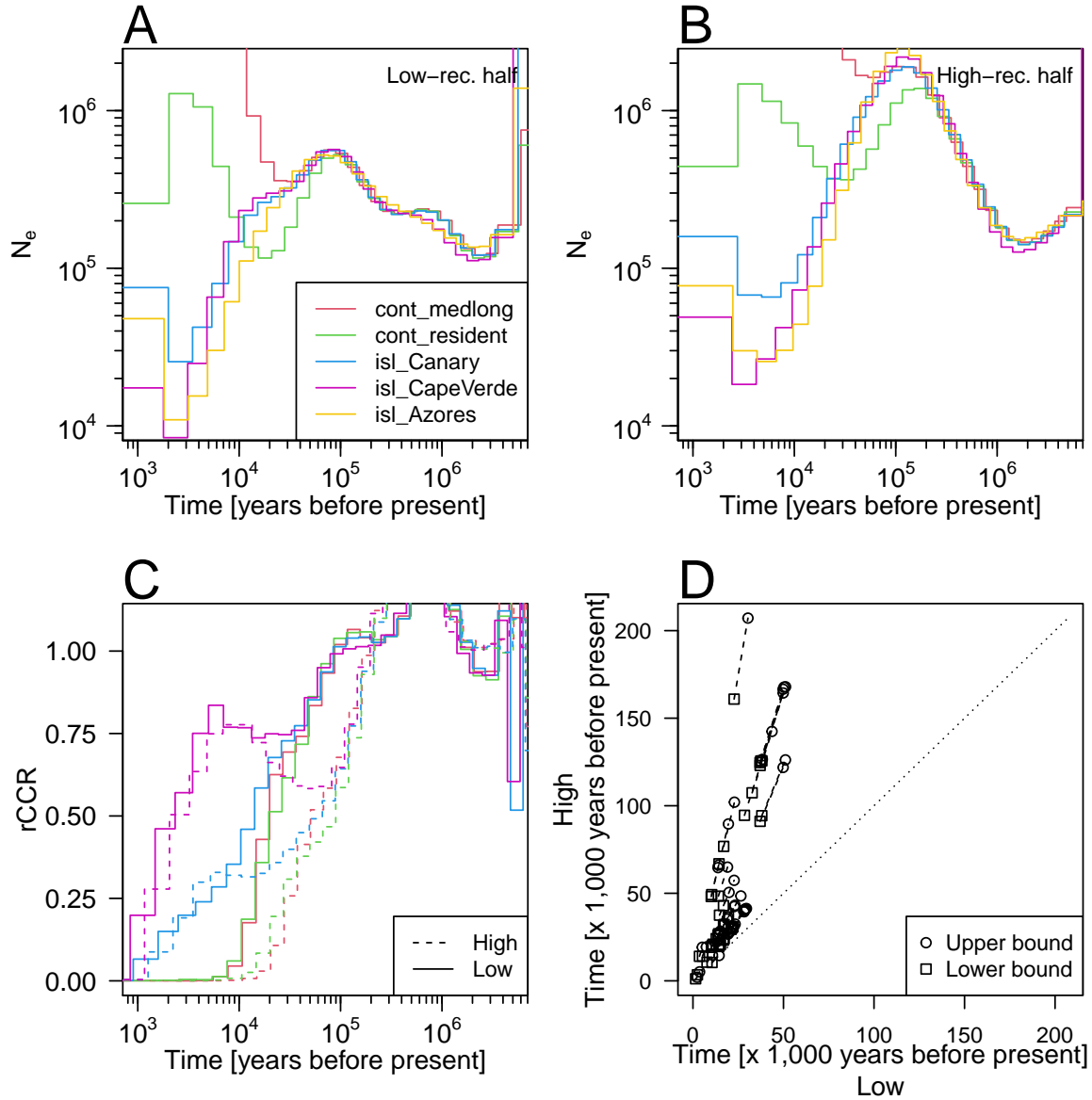


Figure 5: High-recombining regions can affect demography inference in empirical analysis. **A, B.** Inference of historical effective population size by MSMC2. Results for five exemplified blackcap populations are shown using the lower (**A**) or the higher (**B**) half of the genome based on local recombination rates. **C.** Inference of relative cross-coalescence rate (rCCR) with MSMC2 between Azores population and each of all other four populations in **A** and **B** using the lower (solid lines) and the higher (dotted lines) half of the genome based on local recombination rates. **D.** Comparison of split times inferred by MSMC2 using the lower higher halves of the genome based on recombination rates. Segments represent inference between 45 pairs of 10 populations. Two ends of a segment represent the lower and upper boundaries of two consecutive discretized epochs between which rCCR crosses the threshold of 0.5.

Discussion

Our results suggest that demography inference using ARG-based methods should be carried out with caution in organisms that are likely to harbor recombination landscapes distinct from humans, for which these methods were initially developed. In many animals with functional PRDM9, including humans, recombination events are concentrated in narrow recombination hotspots (Myers et al., 2010; Stevison et al., 2016). Thus, we expect that ARG-based methods will be robust. Other species have high-recombining regions more widely distributed around genomic features along the genome (Baker et al., 2017; Kawakami et al., 2017; Singhal et al., 2015) and thus ARG-based methods can be more susceptible to the effect of high-recombining regions. Using simulations we demonstrated that masking high-recombining regions improves the ARG-based demography inference in such cases. In practice, however, this raises another question of how to define regions to mask, which can be challenging due to multiple factors. First, defining a threshold value of the recombination rate using inferred recombination maps may be problematic. This is because methods for inference of fine-scale recombination maps can be inaccurate, especially when the recombination rate is higher than the mutation rate (Raynaud et al., 2023; Spence & Song, 2019). Second, long-enough contiguous chromosomal segments are essential in ARG-based methods (Sellinger et al., 2021), hence masking every high-recombining region can be problematic as it might split the genome into pieces too small for ARG-based methods to be applied. An additional factor to take into account is variation among chromosomes. For example, in multiple taxa, the chromosome lengths can substantially vary, and the recombination rate is negatively correlated with the chromosome length (Bascón-Cardozo et al., 2024; Kawakami et al., 2014; Martin et al., 2019; Singhal et al., 2015), potentially leading to different applicability of ARG-based methods among chromosomes. Finally, additional masks may be necessary for demography inference if large blocks that do not represent neutral evolution exist in the genome. For example, large polymorphic inversions under long-term balancing selection (Giraldo-Deck et al., 2022; Hager et al., 2022; Harringmeyer & Hoekstra, 2022; Kim et al., 2017; Knief et al., 2016, 2017; Küpper et al., 2015; Lamichhaney et al., 2015; Mérot et al., 2021) may be excluded, which may leave little data for inference in species with small genomes. We suggest to run simulations tailored to the species

under study to assess whether ARG-based methods can be used with some confidence. This is especially necessary in species without functional PRDM9, with broad high-recombining regions, high genome-wide mean recombination rates, small genomes, highly heterogeneous chromosomes, and large structural variations.

An SFS-based method for demography inference, **Stairway plot 2**, performed well without high-recombining regions and even better without high-recombining regions in our simulation study. We propose that this accuracy under the presence of high-recombining regions can represent a general characteristic of SFS-based methods that they benefit from high-recombining regions, from which ARG-based methods suffer. The problem of high-recombining regions for ARG-based methods is the fact that branches of genealogies are not represented by mutations (Hayman et al., 2023). In other words from the perspective of mutations, ARG-based methods suffer from independence of mutations in a local genomic window. This independence of mutations, however, is the assumption to compute SFS (Gutenkunst et al., 2009), allowing SFS-based methods to perform accurately with high-recombining regions. Localized errors in the inference of (representation of) genealogies within high-recombining regions in our study indicate that the issue of high-recombining regions in ARG-based methods is not specific to demography inference but can be critical in other applications, including inference of selection (Hejase et al., 2020; Speidel et al., 2019; Stern et al., 2019). In regions with high recombination rates, inferred genealogies may be too inaccurate to perform ARG-based selection tests, while SFS-based methods may be used on the local variation data (Fay & Wu, 2000; Tajima, 1989). Combining ARG- and SFS-based approaches, giving them complementary weights according to the local recombination rate, may make the most of the variation data in demography inference.

In this study, we demonstrated that the recombination landscape can influence ARG-based approaches of population genomics. Although the true ARGs should have rich information on the population history and evolutionary processes, the effects of errors in inferred local ARGs within regions of elevated recombination rate are, in some cases, not negligible. Our findings are likely relevant not only to birds but likely in a wide range of species, because PRDM9 has been lost at least thirteen times independently in vertebrates (five clades of

ray-finned fish, four clades of amphibians, a clade of lizards, the entire clade of birds and crocodiles, and two clades of mammals (dogs and platypus) (Cavassim et al., 2022)). In addition to the recombination rate, other factors, such as the genomic landscape and spectra of mutation (Jiang et al., 2021; Monroe et al., 2022; Sasani et al., 2022; Wu et al., 2020), local effective population size (reflecting selection: Nielsen, 2005; Burri, 2017; Ellegren & Galtier, 2016), and effective migration rate (reflecting barriers to gene flow: Westram et al., 2022) are distributed non-uniformly along the genome, and they may similarly affect population genomics summary statistics and inferences. Novel approaches jointly modelling heterogeneity of some of these factors are emerging (Barroso & Dutheil, 2023; Korfmann et al., 2023; Laetsch et al., 2023). Nonetheless, we highlight that evaluating the performance and limitation of population genomics methods under non-canonical parameter space relevant in individual cases is necessary to draw meaningful interpretations.

Materials and Methods

Simulation study

Simulation

To investigate the effect of high-recombining regions on demography inference, we simulated ARGs and mutations with `msprime` version 1.2.0 (Baumdicker et al., 2022) under the standard neutral coalescent with recombination (Hudson, 1983). The demography model consisted of an ancestral population of 1,000,000 diploids splitting into three populations (pop1, pop2, and pop3) at 10,000 generations before the present time. The population size of pop1 was constant at 10,000, and exponential increase and decrease of 10 folds over 10,000 generations were introduced in pop2 and pop3 after the split event. The mutation rate was set to 4.6×10^{-9} per generation per site.

We prepared three sets of recombination maps, each of which consists of five scenarios. The first set (“stepwise”) was 16 Mb long, and the recombination rate was set to one tenth the mutation rate (4.6×10^{-10}) at the central 10 Mb, with a step-wise increase in recombination rate at 3 Mb ends of the chromosome (Fig. 2B), such that the mean recombination rate (after

masking 6 Mb of the middle) were 0.1, 0.25, 1, 4, and 10 times the mutation rate. The second set (“narrow high-rec.”) was 11 Mb long, and the recombination rate was set to 4.6×10^{-10} throughout the chromosome, except a 1 Mb segment in the middle, where recombination rate was elevated such that the mean recombination rate were 0.1, 0.25, 1, 4, and 10 times the mutation rate Sup. Fig. 5A. The third set (“uniform”) consisted of five uniform recombination maps of 10 Mb with recombination rate of 0.1, 0.25, 1, 4, and 10 times the mutation rate Sup. Fig. 5B. For the first set, we simulated 10 replicates of 150 diploid individuals (50 individuals per population). For the second and third sets, we simulated one replicate. We recorded the true ARGs in TreeSeq format, and also recorded haplotype data in VCF format using `tskit` version 0.4.1 (Kelleher et al., 2018).

Demography inference

MSMC2 For the narrow high-rec. and uniform scenarios, we used four diploid individuals from each population for demography inference with **MSMC2** (Malaspinas et al., 2016; Wang et al., 2020). For the stepwise scenario, we treated ten simulations as ten independent chromosomes, and downsampled four diploid individuals (eight haploid sequences) per population without replacement ten times as ten “replicates” (Note that they are not true independent replicates because they were sampled from a common ARG for each chromosome). Input multihetsep files were generated from the VCF file and masks for each chromosome of each downsample of each replicate using `genrate_multihetsep.py` of **msmc-tools** (Schiffels & Wang, 2020). We ran **MSMC2** for each population or population pair to infer historical coalescence rates. The estimates of historical effective population size were obtained as the inverse of the inferred coalescence rate for each population, scaled with the true mutation rate of 4.6×10^{-9} . The rCCR was obtained by dividing the between-populations coalescence rate with the average within-population coalescence rate. For visualization in Figs. 3, 4, we computed mean and standard deviation of the inferred effective population size and rCCR with a custom script.

Relate For the stepwise scenario, we treated ten simulations as ten independent replicates. We applied filtering of variable sites based on the position according to masking conditions using **BCFTools** version 1.9 (Danecek et al., 2021). We inferred ARGs from the masked

VCF using **Relate** version 1.1.6 (Speidel et al., 2019) specifying the true mutation rate, true recombination maps, and haploid population size of 2,000,000, and inferred demography with two iterations. The estimates of historical effective population size were obtained as the inverse of the inferred coalescence rate for each population, scaled with the true mutation rate of 4.6×10^{-9} . The rCCR was obtained by dividing the coalescence rate between populations with the average within-population coalescence rate. For visualization in Figs. 3, 4, we computed mean and standard deviation of the inferred effective population size and rCCR with a custom script.

Stairway plot 2 We ran **Stairway plot 2** version 2.1 (Liu & Fu, 2020) for the stepwise scenario. We treated ten simulations as ten independent replicates. We split the VCF by population applying masks with **VCFTools** version 0.1.16 (Danecek et al., 2011). We computed the unfolded SFS and prepared blueprint configuration files using custom scripts, and ran **Stairway plot 2** with default parameter values. For visualization in Fig. 3, we computed mean and standard deviation of the inferred effective population size with a custom script.

Coalescence time analysis

MSMC2 We focused on two haploids of the first chromosome (simulation run) of the first downsample in pop1, and compared true TMRCA recorded in the true ARG (in TreeSeq format) and inference by **MSMC2**. We extracted the true TMRCA of the focal pair of haploid genomes in TreeSeq with **tskit**. To obtain inference by **MSMC2**, we ran the **decode** program of **MSMC2** with **decode -m 0.0092 -r 0.00736 -I 0,1 -t 32 -s 1000**. Based on the output of **decode**, we recorded the index of epoch with the highest probability for each window. We aligned true and inferred TMRCA treating an intersected range as a unit, and computed Spearman’s correlation coefficient in R version 4.3.1 (R Core Team, 2023).

Relate We focused on TMRCA of the entire genealogy of 300 haploid genomes of the first simulation replicate. We extracted TMRCA along the chromosome from the true ARG in TreeSeq using **tskit**. To obtain TMRCA along the chromosome of the ARG inferred by **Relate**, we converted the genealogies (in mut and anc format) to TreeSeq using **RelateFileFormats**

program in `Relate`, and extracted TMRCA along the chromosome using `tskit`. We aligned true and inferred TMRCA treating an intersected range as a unit, and computed Spearman’s correlation coefficient in `R`.

Empirical study

Data

We used phased whole-genome resequencing (WGR) data of 179 blackcaps (Ishigohoka et al., 2023), and unphased five garden warblers and three African hill babblers (Delmore et al., 2020). We computed mean recombination rate in 10-kb sliding windows along the blackcap genome based on (Bascón-Cardozo et al., 2024).

Demography inference

MSMC2 We first applied callability masks to the blackcap genome and defined high- and low-recombining halves of the genome for each population or population pair. Specifically, we chose for each population at most four individuals with mean read depth of at least 15x, excluding pairs of related individuals based on kinship coefficient (Manichaikul et al., 2010) computed using `relatedness2` option in `VCFTools`. We created a mask file per individual using `bamCaller.py` of `msmc-tools` (Schiffels & Wang, 2020) and merged them for each population or population pair using `bedtools merge` (Quinlan & Hall, 2010). The mask for each population or population pair was applied on the blackcap recombination map (Bascón-Cardozo et al., 2024), and we ordered genomic intervals within the unmasked regions according to the recombination rate. Regions in the first and the second halves were defined as the lower- and higher-recombining halves.

After defining the regions to be used for inference, input `multihetsep` files were generated from the phased VCF and the mask file using `generate_multihetsep.py` of `msmc-tools` (Schiffels & Wang, 2020). We ran **MSMC2** for each population or population pair to infer historical coalescence rates. The estimates of historical effective population size were obtained as the inverse of the inferred coalescence rate for each population, scaled with a mutation rate of 4.6×10^{-9} estimated in the collared flycatcher (Smeds et al., 2016). The `rCCR` was obtained

by dividing the between-population coalescence rate with the average within-population coalescence rate.

Relate **Relate** requires haplotype data with polarized mutations. We polarized biallelic SNPs in blackcaps using allele frequencies in two outgroup species, garden warblers (n=5) and African hill babblers (n=3). Specifically, after removing SNPs with more than two alleles including the three species, we split blackcap SNPs into the following five categories.

1. Sites at which all garden warblers had missing genotype.
2. Sites fixed in garden warblers
3. Sites segregated among garden warblers and missing in all African hill babblers
4. Sites segregated among both garden warblers and African hill babblers
5. Sites segregated among garden warblers and fixed in African hill babblers

For each category we applied the following heuristics to polarize mutations. For sites of the first type, we defined the minor allele among blackcaps to be the derived state (i.e. the major allele is the ancestral state). For sites of the second type, we defined the allele possessed by garden warbler to be the ancestral state. For sites of the third or fourth type, we defined the minor allele among blackcaps to be the derived state (i.e. the major allele is the ancestral state). For sites of the fifth type, we defined the allele possessed by African hill babbler to be the ancestral state.

We defined low- and high-recombining halves of the genome in BED format based on the blackcap recombination map (Bascón-Cardozo et al., 2024). Based on these BED files to mask high/low-recombining half and repeats retrieved from UCSC Genome Browser tracks (Raney et al., 2023) for the blackcap assembly (GenBank: GCA_009819655.1), we made a mask file in FASTA format for each condition using `BEDTools maskfasta`. Using the phased and polarized VCF, recombination map, and the mask, we ran **Relate** to infer genealogies with mutation rate of 4.6×10^{-9} and effective population size of 500,000. We inferred demography from the genealogies using **RelateCoalescenceRate** program of **Relate** with mutation rate of 4.6×10^{-9} and five times of iterations. The estimates of historical effective population size were obtained as the inverse of the inferred coalescence rate for each population with rescaling of

time by generation time of 2 years (Delmore et al., 2020). The rCCR was obtained by dividing the between-population coalescence rate with the average within-population coalescence rate.

Acknowledgments

This work was supported by the Max Planck Society (Max Planck Research Group grant MFFALIMN0001 to ML), and the DFG (project Nav05 within SFB 1372 – Magnetoreception and Navigation in Vertebrates (395940726) to ML). We thank Julien Dutheil, Linda Odenthal-Hesse, and Diethard Tautz for feedback.

Data availability

Scripts used for the simulations and input data, processed output data and scripts for the empirical analyses are found in Zenodo (<https://doi.org/10.5281/zenodo.10613446>).

Conflict of interest

The authors declare no conflict of interest.

References

- Alonso-Blanco, C., Andrade, J., Becker, C., Bemm, F., Bergelson, J., Borgwardt, K. M., Cao, J., Chae, E., Dezwaan, T. M., Ding, W., Ecker, J. R., Exposito-Alonso, M., Farlow, A., Fitz, J., Gan, X., Grimm, D. G., Hancock, A. M., Henz, S. R., Holm, S., ... Zhou, X. (2016). 1,135 Genomes Reveal the Global Pattern of Polymorphism in *Arabidopsis thaliana*. *Cell*, 166(2), 481–491. <https://doi.org/10.1016/j.cell.2016.05.063>
- Auton, A., Li, Y. R., Kidd, J., Oliveira, K., Nadel, J., Holloway, J. K., Hayward, J. J., Cohen, P. E., Grealis, J. M., Wang, J., Bustamante, C. D., & Boyko, A. R. (2013). Genetic Recombination Is Targeted towards Gene Promoter Regions in Dogs. *PLOS Genetics*, 9(12), e1003984. <https://doi.org/10.1371/journal.pgen.1003984>
- Baker, C. L., Kajita, S., Walker, M., Saxl, R. L., Raghupathy, N., Choi, K., Petkov, P. M., & Paigen, K. (2015). PRDM9 Drives Evolutionary Erosion of Hotspots in *Mus musculus* through Haplotype-Specific Initiation of Meiotic Recombination. *PLOS Genetics*, 11(1), e1004916. <https://doi.org/10.1371/journal.pgen.1004916>
- Baker, Z., Schumer, M., Haba, Y., Bashkirova, L., Holland, C., Rosenthal, G. G., & Przeworski, M. (2017). Repeated losses of PRDM9-directed recombination despite the conservation of PRDM9 across vertebrates. *eLife*, 6, e24133. <https://doi.org/10.7554/eLife.24133>
- Barroso, G. V., & Dutheil, J. Y. (2023). The landscape of nucleotide diversity in *Drosophila melanogaster* is shaped by mutation rate variation. *Peer Community Journal*, 3. <https://doi.org/10.24072/pcjournal.267>
- Bascón-Cardozo, K., Bours, A., Manthey, G., Durieux, G., Dutheil, J. Y., Pruisscher, P., Odenthal-Hesse, L., & Liedvogel, M. (2024). Fine-Scale Map Reveals Highly Variable Recombination Rates Associated with Genomic Features in the Eurasian Blackcap. *Genome Biology and Evolution*, 16(1), evad233. <https://doi.org/10.1093/gbe/evad233>
- Baudat, F., Buard, J., Grey, C., Fledel-Alon, A., Ober, C., Przeworski, M., Coop, G., & Massy, B. de. (2010). PRDM9 Is a Major Determinant of Meiotic Recombination Hotspots in Humans and Mice. *Science*, 327(5967), 836–840. <https://doi.org/10.1126/science.1183439>
- Baumdicker, F., Bisschop, G., Goldstein, D., Gower, G., Ragsdale, A. P., Tsambos, G., Zhu, S., Eldon, B., Ellerman, E. C., Galloway, J. G., Gladstein, A. L., Gorjanc, G., Guo, B., Jeffery, B., Kretschmar, W. W., Lohse, K., Matschiner, M., Nelson, D., Pope, N. S., ... Kelleher, J. (2022). Efficient ancestry and mutation simulation with msprime 1.0. *Genetics*, 220(3), iyab229. <https://doi.org/10.1093/genetics/iyab229>
- Bergeron, L. A., Besenbacher, S., Zheng, J., Li, P., Bertelsen, M. F., Quintard, B., Hoffman, J. I., Li, Z., St. Leger, J., Shao, C., Stiller, J., Gilbert, M. T. P., Schierup, M. H., & Zhang, G. (2023). Evolution of the germline mutation rate across vertebrates. *Nature*, 615(7951), 285–291. <https://doi.org/10.1038/s41586-023-05752-y>
- Burri, R. (2017). Interpreting differentiation landscapes in the light of long-term linked selection. *Evolution Letters*, 1(3), 118–131. <https://doi.org/https://doi.org/10.1002/ev>

- Cavassim, M. I. A., Baker, Z., Hoge, C., Schierup, M. H., Schumer, M., & Przeworski, M. (2022). PRDM9 losses in vertebrates are coupled to those of paralogs ZCWPW1 and ZCWPW2. *Proceedings of the National Academy of Sciences*, 119(9), e2114401119. <https://doi.org/10.1073/pnas.2114401119>
- Danecek, P., Auton, A., Abecasis, G., Albers, C. A., Banks, E., DePristo, M. A., Handsaker, R. E., Lunter, G., Marth, G. T., Sherry, S. T., McVean, G., & Durbin, R. (2011). The variant call format and VCFtools. *Bioinformatics*. <https://doi.org/10.1093/bioinformatics/btr330>
- Danecek, P., Bonfield, J. K., Liddle, J., Marshall, J., Ohan, V., Pollard, M. O., Whitwham, A., Keane, T., McCarthy, S. A., Davies, R. M., & Li, H. (2021). Twelve years of SAMtools and BCFtools. *GigaScience*, 10(giab008). <https://doi.org/10.1093/gigascience/giab008>
- Delmore, K., Illera, J. C., Pérez-Tris, J., Segelbacher, G., Lugo Ramos, J. S., Durieux, G., Ishigohoka, J., & Liedvogel, M. (2020). The evolutionary history and genomics of European blackcap migration. *eLife*, 9, e54462. <https://doi.org/10.7554/eLife.54462>
- Durbin, R. M., Altshuler, D., Durbin, R. M., Abecasis, G. R., Bentley, D. R., Chakravarti, A., Clark, A. G., Collins, F. S., De La Vega, F. M., Donnelly, P., Egholm, M., Flicek, P., Gabriel, S. B., Gibbs, R. A., Knoppers, B. M., Lander, E. S., Lehrach, H., Mardis, E. R., McVean, G. A., ... The Translational Genomics Research Institute. (2010). A map of human genome variation from population-scale sequencing. *Nature*, 467(7319), 1061–1073. <https://doi.org/10.1038/nature09534>
- Dussex, N., Valk, T. van der, Morales, H. E., Wheat, C. W., Díez-del-Molino, D., Seth, J. von, Foster, Y., Kutschera, V. E., Guschanski, K., Rhie, A., Phillippy, A. M., Korlach, J., Howe, K., Chow, W., Pelan, S., Mendes Damas, J. D., Lewin, H. A., Hastie, A. R., Formenti, G., ... Dalén, L. (2021). Population genomics of the critically endangered kākāpō. *Cell Genomics*, 1(1), 100002. <https://doi.org/10.1016/j.xgen.2021.100002>
- Ellegren, H., & Galtier, N. (2016). Determinants of genetic diversity. *Nature Reviews Genetics*, 17(7), 422–433. <https://doi.org/10.1038/nrg.2016.58>
- Excoffier, L., Dupanloup, I., Huerta-Sánchez, E., Sousa, V. C., & Foll, M. (2013). Robust Demographic Inference from Genomic and SNP Data. *PLOS Genetics*, 9(10), e1003905. <https://doi.org/10.1371/journal.pgen.1003905>
- Fay, J. C., & Wu, C.-I. (2000). Hitchhiking Under Positive Darwinian Selection. *Genetics*, 155(3), 1405–1413. <https://doi.org/10.1093/genetics/155.3.1405>
- Giraldo-Deck, L. M., Loveland, J. L., Goymann, W., Tschirren, B., Burke, T., Kempnaers, B., Lank, D. B., & Küpper, C. (2022). Intralocus conflicts associated with a supergene. *Nature Communications*, 13(1), 1384. <https://doi.org/10.1038/s41467-022-29033-w>
- Griffiths, R. C., & Marjoram, P. (1997). An ancestral recombination graph. In P. Donnelly & S. Tavaré (Eds.), *Progress in Population Genetics and Human Evolution* (Vol. 87, pp. 257–270). Springer. <http://lamastex.org/recomb/ima.pdf>
- Groenen, M. A. M., Archibald, A. L., Uenishi, H., Tuggle, C. K., Takeuchi, Y., Rothschild, M. F., Rogel-Gaillard, C., Park, C., Milan, D., Megens, H.-J., Li, S., Larkin, D. M., Kim,

- H., Frantz, L. A. F., Caccamo, M., Ahn, H., Aken, B. L., Anselmo, A., Anthon, C., ... Schook, L. B. (2012). Analyses of pig genomes provide insight into porcine demography and evolution. *Nature*, 491(7424), 393–398. <https://doi.org/10.1038/nature11622>
- Gutenkunst, R. N., Hernandez, R. D., Williamson, S. H., & Bustamante, C. D. (2009). Inferring the Joint Demographic History of Multiple Populations from Multidimensional SNP Frequency Data. *PLOS Genetics*, 5(10), e1000695. <https://doi.org/10.1371/journal.pgen.1000695>
- Hager, E. R., Harringmeyer, O. S., Wooldridge, T. B., Theingi, S., Gable, J. T., McFadden, S., Neugeboren, B., Turner, K. M., Jensen, J. D., & Hoekstra, H. E. (2022). A chromosomal inversion contributes to divergence in multiple traits between deer mouse ecotypes. *Science*, 377(6604), 399–405. <https://doi.org/10.1126/science.abg0718>
- Harringmeyer, O. S., & Hoekstra, H. E. (2022). Chromosomal inversion polymorphisms shape the genomic landscape of deer mice. *Nature Ecology & Evolution*, 1–15. <https://doi.org/10.1038/s41559-022-01890-0>
- Harris, K., & Nielsen, R. (2013). Inferring Demographic History from a Spectrum of Shared Haplotype Lengths. *PLOS Genetics*, 9(6), e1003521. <https://doi.org/10.1371/journal.pgen.1003521>
- Hayman, E., Ignatieva, A., & Hein, J. (2023). Recoverability of ancestral recombination graph topologies. *Theoretical Population Biology*, 154, 27–39. <https://doi.org/10.1016/j.tpb.2023.07.004>
- Hejase, H. A., Salman-Minkov, A., Campagna, L., Hubisz, M. J., Lovette, I. J., Gronau, I., & Siepel, A. (2020). Genomic islands of differentiation in a rapid avian radiation have been driven by recent selective sweeps. *Proceedings of the National Academy of Sciences*, 117(48), 30554–30565. <https://doi.org/10.1073/pnas.2015987117>
- Hohenlohe, P. A., Funk, W. C., & Rajora, O. P. (2021). Population genomics for wildlife conservation and management. *Molecular Ecology*, 30(1), 62–82. <https://doi.org/10.1111/mec.15720>
- Hubisz, M. J., Williams, A. L., & Siepel, A. (2020). Mapping gene flow between ancient hominins through demography-aware inference of the ancestral recombination graph. *PLOS Genetics*, 16(8), e1008895. <https://doi.org/10.1371/journal.pgen.1008895>
- Hudson, R. R. (1983). Properties of a neutral allele model with intragenic recombination. *Theoretical Population Biology*, 23(2), 183–201. [https://doi.org/10.1016/0040-5809\(83\)90013-8](https://doi.org/10.1016/0040-5809(83)90013-8)
- Ignatieva, A., Lyngsø, R. B., Jenkins, P. A., & Hein, J. (2021). KwARG: Parsimonious reconstruction of ancestral recombination graphs with recurrent mutation. *Bioinformatics*, 37(19), 3277–3284. <https://doi.org/10.1093/bioinformatics/btab351>
- Ishigohoka, J., Bascón-Cardozo, K., Bours, A., Fuß, J., Rhie, A., Mountcastle, J., Haase, B., Chow, W., Collins, J., Howe, K., Uliano-Silva, M., Fedrigo, O., Jarvis, E. D., Pérez-Tris, J., Illera, J. C., & Liedvogel, M. (2023). *Distinct patterns of genetic variation at low-recombining genomic regions represent haplotype structure*. bioRxiv. <https://doi.org/10.1101/2021.12.22.473882>

- Jiang, P., Ollodart, A. R., Sudhesh, V., Herr, A. J., Dunham, M. J., & Harris, K. (2021). A modified fluctuation assay reveals a natural mutator phenotype that drives mutation spectrum variation within *Saccharomyces cerevisiae*. *eLife*, *10*, e68285. <https://doi.org/10.7554/eLife.68285>
- Kawakami, T., Mugal, C. F., Suh, A., Nater, A., Burri, R., Smeds, L., & Ellegren, H. (2017). Whole-genome patterns of linkage disequilibrium across flycatcher populations clarify the causes and consequences of fine-scale recombination rate variation in birds. *Molecular Ecology*, *26*(16), 4158–4172. <https://doi.org/10.1111/mec.14197>
- Kawakami, T., Smeds, L., Backström, N., Husby, A., Qvarnström, A., Mugal, C. F., Olason, P., & Ellegren, H. (2014). A high-density linkage map enables a second-generation collared flycatcher genome assembly and reveals the patterns of avian recombination rate variation and chromosomal evolution. *Molecular Ecology*, *23*(16), 4035–4058. <https://doi.org/10.1111/mec.12810>
- Kelleher, J., Thornton, K. R., Ashander, J., & Ralph, P. L. (2018). Efficient pedigree recording for fast population genetics simulation. *PLOS Computational Biology*, *14*(11), e1006581. <https://doi.org/10.1371/journal.pcbi.1006581>
- Kelleher, J., Wong, Y., Wohns, A. W., Fadil, C., Albers, P. K., & McVean, G. (2019). Inferring whole-genome histories in large population datasets. *Nature Genetics*, *51*(9), 1330–1338. <https://doi.org/10.1038/s41588-019-0483-y>
- Kim, K.-W., Bennison, C., Hemmings, N., Brookes, L., Hurley, L. L., Griffith, S. C., Burke, T., Birkhead, T. R., & Slate, J. (2017). A sex-linked supergene controls sperm morphology and swimming speed in a songbird. *Nature Ecology & Evolution*, *1*(8), 1168–1176. <https://doi.org/10.1038/s41559-017-0235-2>
- Knief, U., Forstmeier, W., Pei, Y., Ihle, M., Wang, D., Martin, K., Opatová, P., Albrechtová, J., Wittig, M., Franke, A., Albrecht, T., & Kempnaers, B. (2017). A sex-chromosome inversion causes strong overdominance for sperm traits that affect siring success. *Nature Ecology & Evolution*, *1*(8), 1177–1184. <https://doi.org/10.1038/s41559-017-0236-1>
- Knief, U., Hemmrich-Stanisak, G., Wittig, M., Franke, A., Griffith, S. C., Kempnaers, B., & Forstmeier, W. (2016). Fitness consequences of polymorphic inversions in the zebra finch genome. *Genome Biology*, *17*(1), 199. <https://doi.org/10.1186/s13059-016-1056-3>
- Korfmann, K., Sellinger, T., Freund, F., Fumagalli, M., & Tellier, A. (2023). *Simultaneous Inference of Past Demography and Selection from the Ancestral Recombination Graph under the Beta Coalescent*. bioRxiv. <https://doi.org/10.1101/2022.09.28.508873>
- Küpper, C., Stocks, M., Risse, J. E., Dos Remedios, N., Farrell, L. L., McRae, S. B., Morgan, T. C., Karlionova, N., Pinchuk, P., Verkuil, Y. I., Kitaysky, A. S., Wingfield, J. C., Piersma, T., Zeng, K., Slate, J., Blaxter, M., Lank, D. B., & Burke, T. (2015). A supergene determines highly divergent male reproductive morphs in the ruff. *Nature Genetics*, *48*(1), 79–83. <https://doi.org/10.1038/ng.3443>
- Laetsch, D. R., Bisschop, G., Martin, S. H., Aeschbacher, S., Setter, D., & Lohse, K. (2023). Demographically explicit scans for barriers to gene flow using gIMble. *PLOS Genetics*, *19*(10), e1010999. <https://doi.org/10.1371/journal.pgen.1010999>

- Lam, I., & Keeney, S. (2015). Nonparadoxical evolutionary stability of the recombination initiation landscape in yeast. *Science*, *350*(6263), 932–937. <https://doi.org/10.1126/science.aad0814>
- Lamichhaney, S., Fan, G., Widemo, F., Gunnarsson, U., Thalmann, D. S., Hoepfner, M. P., Kerje, S., Gustafson, U., Shi, C., Zhang, H., Chen, W., Liang, X., Huang, L., Wang, J., Liang, E., Wu, Q., Lee, S. M. Y., Xu, X., Höglund, J., ... Andersson, L. (2015). Structural genomic changes underlie alternative reproductive strategies in the ruff (*Philomachus pugnax*). *Nature Genetics*, *48*(1), 84–88. <https://doi.org/10.1038/ng.3430>
- Lanier, H. C., Massatti, R., He, Q., Olson, L. E., & Knowles, L. L. (2015). Colonization from divergent ancestors: Glaciation signatures on contemporary patterns of genomic variation in Collared Pikas (*Ochotona collaris*). *Molecular Ecology*, *24*(14), 3688–3705. <https://doi.org/10.1111/mec.13270>
- Li, H., & Durbin, R. (2011). Inference of human population history from individual whole-genome sequences. *Nature*, *475*(7357), 493–496. <https://doi.org/10.1038/nature10231>
- Li, S., Li, B., Cheng, C., Xiong, Z., Liu, Q., Lai, J., Carey, H. V., Zhang, Q., Zheng, H., Wei, S., Zhang, H., Chang, L., Liu, S., Zhang, S., Yu, B., Zeng, X., Hou, Y., Nie, W., Guo, Y., ... Yan, J. (2014). Genomic signatures of near-extinction and rebirth of the crested ibis and other endangered bird species. *Genome Biology*, *15*(12), 557. <https://doi.org/10.1186/s13059-014-0557-1>
- Liu, S., Lorenzen, E. D., Fumagalli, M., Li, B., Harris, K., Xiong, Z., Zhou, L., Korneliussen, T. S., Somel, M., Babbitt, C., Wray, G., Li, J., He, W., Wang, Z., Fu, W., Xiang, X., Morgan, C. C., Doherty, A., O’Connell, M. J., ... Wang, J. (2014). Population Genomics Reveal Recent Speciation and Rapid Evolutionary Adaptation in Polar Bears. *Cell*, *157*(4), 785–794. <https://doi.org/10.1016/j.cell.2014.03.054>
- Liu, X., & Fu, Y.-X. (2020). Stairway Plot 2: Demographic history inference with folded SNP frequency spectra. *Genome Biology*, *21*(1), 280. <https://doi.org/10.1186/s13059-020-02196-9>
- Malaspinas, A.-S., Westaway, M. C., Muller, C., Sousa, V. C., Lao, O., Alves, I., Bergström, A., Athanasiadis, G., Cheng, J. Y., Crawford, J. E., Heupink, T. H., Macholdt, E., Peischl, S., Rasmussen, S., Schiffels, S., Subramanian, S., Wright, J. L., Albrechtsen, A., Barbieri, C., ... Willerslev, E. (2016). A genomic history of Aboriginal Australia. *Nature*, *538*(7624), 207–214. <https://doi.org/10.1038/nature18299>
- Manichaikul, A., Mychaleckyj, J. C., Rich, S. S., Daly, K., Sale, M., & Chen, W.-M. (2010). Robust relationship inference in genome-wide association studies. *Bioinformatics*, *26*(22), 2867–2873. <https://doi.org/10.1093/bioinformatics/btq559>
- Martin, S. H., Davey, J. W., Salazar, C., & Jiggins, C. D. (2019). Recombination rate variation shapes barriers to introgression across butterfly genomes. *PLOS Biology*, *17*(2), e2006288. <https://doi.org/10.1371/journal.pbio.2006288>
- McVean, G. A. T., & Cardin, N. J. (2005). Approximating the coalescent with recombination. *Philosophical Transactions of the Royal Society B: Biological Sciences*, *360*(1459), 1387–1393. <https://doi.org/10.1098/rstb.2005.1673>

- Mérot, C., Berdan, E. L., Cayuela, H., Djambazian, H., Ferchaud, A.-L., Laporte, M., Normandeau, E., Ragoussis, J., Wellenreuther, M., & Bernatchez, L. (2021). Locally Adaptive Inversions Modulate Genetic Variation at Different Geographic Scales in a Seaweed Fly. *Molecular Biology and Evolution*, 38(9), 3953–3971. <https://doi.org/10.1093/molbev/msab143>
- Mirzaei, S., & Wu, Y. (2017). RENT+: An improved method for inferring local genealogical trees from haplotypes with recombination. *Bioinformatics*, 33(7), 1021–1030. <https://doi.org/10.1093/bioinformatics/btw735>
- Monroe, J. G., Srikant, T., Carbonell-Bejerano, P., Becker, C., Lensink, M., Exposito-Alonso, M., Klein, M., Hildebrandt, J., Neumann, M., Kliebenstein, D., Weng, M.-L., Imbert, E., Ågren, J., Rutter, M. T., Fenster, C. B., & Weigel, D. (2022). Mutation bias reflects natural selection in *Arabidopsis thaliana*. *Nature*, 1–5. <https://doi.org/10.1038/s41586-021-04269-6>
- Myers, S., Bowden, R., Tumian, A., Bontrop, R. E., Freeman, C., MacFie, T. S., McVean, G., & Donnelly, P. (2010). Drive Against Hotspot Motifs in Primates Implicates the PRDM9 Gene in Meiotic Recombination. *Science*, 327(5967), 876–879. <https://doi.org/10.1126/science.1182363>
- Nadachowska-Brzyska, K., Burri, R., Smeds, L., & Ellegren, H. (2016). PSMC analysis of effective population sizes in molecular ecology and its application to black-and-white *Ficedula* flycatchers. *Molecular Ecology*, 25(5), 1058–1072. <https://doi.org/10.1111/mec.13540>
- Nielsen, R. (2005). Molecular Signatures of Natural Selection. *Annual Review of Genetics*, 39(1), 197–218. <https://doi.org/10.1146/annurev.genet.39.073003.112420>
- Oliver, P. L., Goodstadt, L., Bayes, J. J., Birtle, Z., Roach, K. C., Phadnis, N., Beatson, S. A., Lunter, G., Malik, H. S., & Ponting, C. P. (2009). Accelerated Evolution of the Prdm9 Speciation Gene across Diverse Metazoan Taxa. *PLOS Genetics*, 5(12), e1000753. <https://doi.org/10.1371/journal.pgen.1000753>
- Pacheco, C., Stronen, A. V., Jędrzejewska, B., Plis, K., Okhlopkov, I. M., Mamaev, N. V., Drovetski, S. V., & Godinho, R. (2022). Demography and evolutionary history of grey wolf populations around the Bering Strait. *Molecular Ecology*, 31(18), 4851–4865. <https://doi.org/10.1111/mec.16613>
- Paigen, K., & Petkov, P. M. (2018). PRDM9 and its role in genetic recombination. *Trends in Genetics : TIG*, 34(4), 291–300. <https://doi.org/10.1016/j.tig.2017.12.017>
- Quinlan, A. R., & Hall, I. M. (2010). BEDTools: A flexible suite of utilities for comparing genomic features. *Bioinformatics*, 26(6), 841–842. <https://doi.org/10.1093/bioinformatics/btq033>
- Raney, B. J., Barber, G. P., Benet-Pagès, A., Casper, J., Clawson, H., Cline, M. S., Diekhans, M., Fischer, C., Navarro Gonzalez, J., Hickey, G., Hinrichs, A. S., Kuhn, R. M., Lee, B. T., Lee, C. M., Le Mercier, P., Miga, K. H., Nassar, L. R., Nejad, P., Paten, B., ... Haeussler, M. (2023). The UCSC Genome Browser database: 2024 update. *Nucleic Acids Research*, gkad987. <https://doi.org/10.1093/nar/gkad987>

- Rasmussen, M. D., Hubisz, M. J., Gronau, I., & Siepel, A. (2014). Genome-Wide Inference of Ancestral Recombination Graphs. *PLoS Genetics*, 10(5). <https://doi.org/10.1371/journal.pgen.1004342>
- Raynaud, M., Gagnaire, P.-A., & Galtier, N. (2023). Performance and limitations of linkage-disequilibrium-based methods for inferring the genomic landscape of recombination and detecting hotspots: A simulation study. *Peer Community Journal*, 3. <https://doi.org/10.24072/pcjournal.254>
- R Core Team. (2023). *R: A Language and Environment for Statistical Computing*. R Foundation for Statistical Computing. <https://www.R-project.org/>
- Sasani, T. A., Ashbrook, D. G., Beichman, A. C., Lu, L., Palmer, A. A., Williams, R. W., Pritchard, J. K., & Harris, K. (2022). A natural mutator allele shapes mutation spectrum variation in mice. *Nature*, 605(7910), 497–502. <https://doi.org/10.1038/s41586-022-04701-5>
- Schaefer, N. K., Shapiro, B., & Green, R. E. (2021). An ancestral recombination graph of human, Neanderthal, and Denisovan genomes. *Science Advances*, 7(29), eabc0776. <https://doi.org/10.1126/sciadv.abc0776>
- Schiffels, S., & Durbin, R. (2014). Inferring human population size and separation history from multiple genome sequences. *Nature Genetics*, 46(8), 919–925. <https://doi.org/10.1038/ng.3015>
- Schiffels, S., & Wang, K. (2020). MSMC and MSMC2: The Multiple Sequentially Markovian Coalescent. In J. Y. Dutheil (Ed.), *Statistical Population Genomics* (pp. 147–166). Springer US. https://doi.org/10.1007/978-1-0716-0199-0_7
- Sellinger, T. P. P., Abu-Awad, D., & Tellier, A. (2021). Limits and convergence properties of the sequentially Markovian coalescent. *Molecular Ecology Resources*, 21(7), 2231–2248. <https://doi.org/10.1111/1755-0998.13416>
- Sellinger, T. P. P., Awad, D. A., Moest, M., & Tellier, A. (2020). Inference of past demography, dormancy and self-fertilization rates from whole genome sequence data. *PLOS Genetics*, 16(4), e1008698. <https://doi.org/10.1371/journal.pgen.1008698>
- Shipilina, D., Pal, A., Stankowski, S., Chan, Y. F., & Barton, N. H. (2023). On the origin and structure of haplotype blocks. *Molecular Ecology*, 32(6), 1441–1457. <https://doi.org/10.1111/mec.16793>
- Singhal, S., Leffler, E. M., Sannareddy, K., Turner, I., Venn, O., Hooper, D. M., Strand, A. I., Li, Q., Raney, B., Balakrishnan, C. N., Griffith, S. C., McVean, G., & Przeworski, M. (2015). Stable recombination hotspots in birds. *Science*, 350(6263), 928–932. <https://doi.org/10.1126/science.aad0843>
- Smeds, L., Qvarnström, A., & Ellegren, H. (2016). Direct estimate of the rate of germline mutation in a bird. *Genome Research*, 26(9), 1211–1218. <https://doi.org/10.1101/gr.204669.116>
- Speidel, L., Forest, M., Shi, S., & Myers, S. R. (2019). A method for genome-wide genealogy estimation for thousands of samples. *Nature Genetics*, 51(9), 1321–1329. <https://doi.org/10.1038/s41588-019-0484-x>

- Spence, J. P., & Song, Y. S. (2019). Inference and analysis of population-specific fine-scale recombination maps across 26 diverse human populations. *Science Advances*, 5(10), eaaw9206. <https://doi.org/10.1126/sciadv.aaw9206>
- Stapley, J., Feulner, P. G. D., Johnston, S. E., Santure, A. W., & Smadja, C. M. (2017). Variation in recombination frequency and distribution across eukaryotes: Patterns and processes. *Philosophical Transactions of the Royal Society B: Biological Sciences*, 372(1736), 20160455. <https://doi.org/10.1098/rstb.2016.0455>
- Stern, A. J., Wilton, P. R., & Nielsen, R. (2019). An approximate full-likelihood method for inferring selection and allele frequency trajectories from DNA sequence data. *PLoS Genetics*, 15(9), 1–32. <https://doi.org/10.1371/journal.pgen.1008384>
- Stevison, L. S., Woerner, A. E., Kidd, J. M., Kelley, J. L., Veeramah, K. R., McManus, K. F., Great Ape Genome Project, Bustamante, C. D., Hammer, M. F., & Wall, J. D. (2016). The Time Scale of Recombination Rate Evolution in Great Apes. *Molecular Biology and Evolution*, 33(4), 928–945. <https://doi.org/10.1093/molbev/msv331>
- Tajima, F. (1989). Statistical method for testing the neutral mutation hypothesis by DNA polymorphism. *Genetics*, 123(3), 585–595. <https://doi.org/PMC1203831>
- Terhorst, J., Kamm, J. A., & Song, Y. S. (2017). Robust and scalable inference of population history from hundreds of unphased whole genomes. *Nature Genetics*, 49(2), 303–309. <https://doi.org/10.1038/ng.3748>
- Wang, K., Mathieson, I., O’Connell, J., & Schiffels, S. (2020). Tracking human population structure through time from whole genome sequences. *PLOS Genetics*, 16(3), e1008552. <https://doi.org/10.1371/journal.pgen.1008552>
- Westram, A. M., Stankowski, S., Surendranadh, P., & Barton, N. (2022). What is reproductive isolation? *Journal of Evolutionary Biology*, 35(9), 1143–1164. <https://doi.org/10.1111/jeb.14005>
- Wohns, A. W., Wong, Y., Jeffery, B., Akbari, A., Mallick, S., Pinhasi, R., Patterson, N., Reich, D., Kelleher, J., & McVean, G. (2022). A unified genealogy of modern and ancient genomes. *Science*, 375(6583), eabi8264. <https://doi.org/10.1126/science.abi8264>
- Wu, F. L., Strand, A. I., Cox, L. A., Ober, C., Wall, J. D., Moorjani, P., & Przeworski, M. (2020). A comparison of humans and baboons suggests germline mutation rates do not track cell divisions. *PLOS Biology*, 18(8), e3000838. <https://doi.org/10.1371/journal.pbio.3000838>

Supplementary Information

High-recombining genomic regions affect demography inference

Jun Ishigohoka^{1,*}

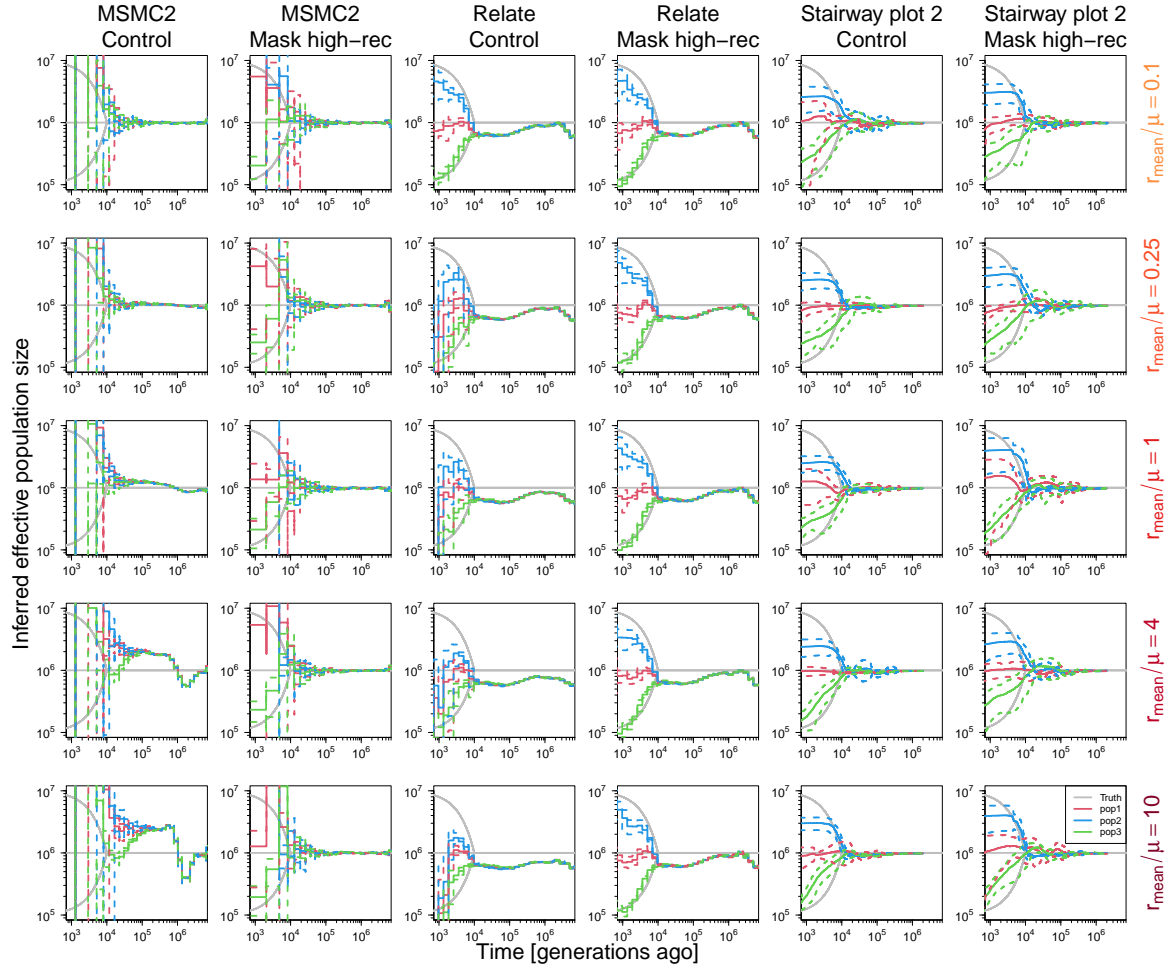
Miriam Liedvogel^{1,2,3,*}

¹MPRG Behavioural Genomics, Max Planck Institute for Evolutionary Biology, Plön, Germany

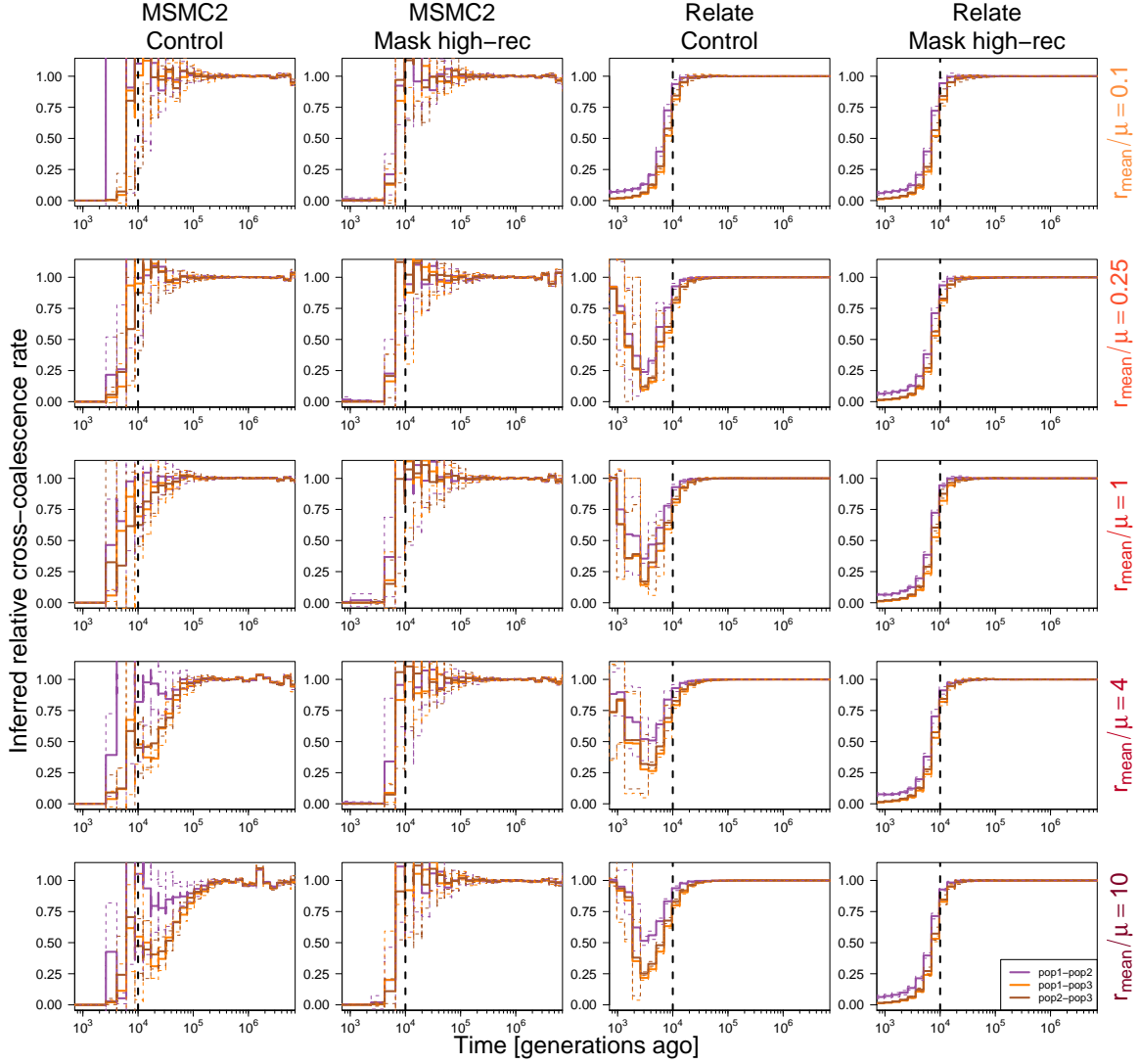
²Institute of Avian Research, Wilhelmshaven, Germany

³Department of Biology and Environmental Sciences, Carl von Ossietzky Universität Oldenburg, Oldenburg, Germany

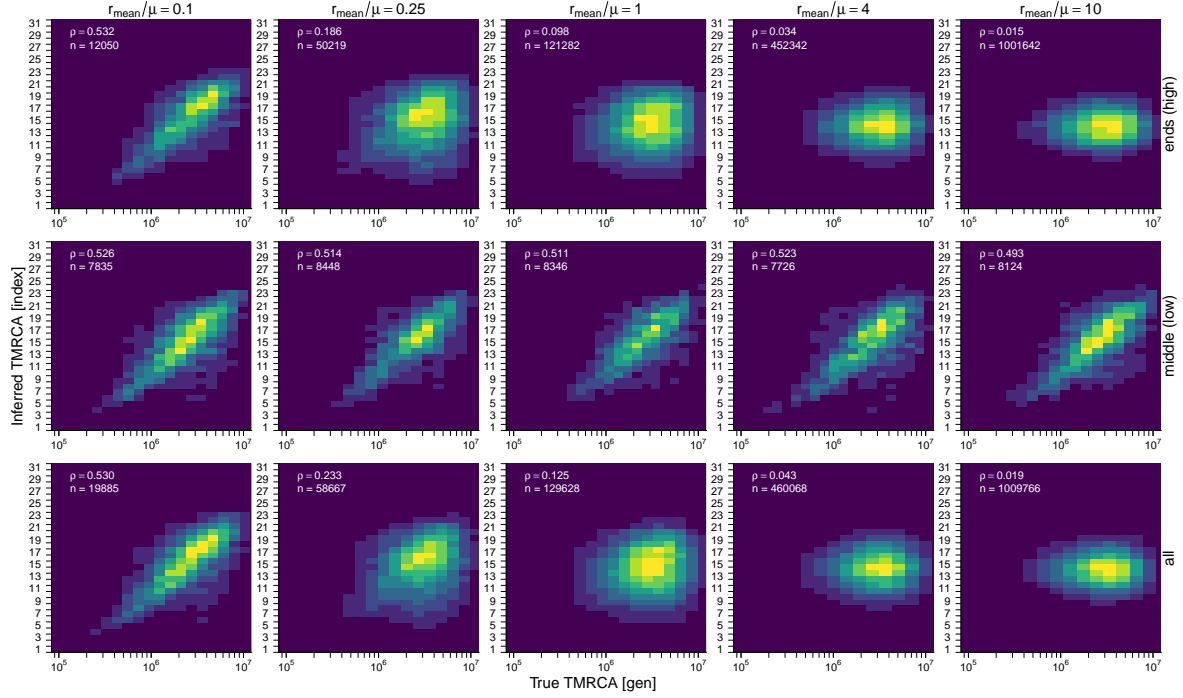
* Correspondence: [Jun Ishigohoka <ishigohoka@evolbio.mpg.de>](mailto:ishigohoka@evolbio.mpg.de), [Miriam Liedvogel <liedvogel@evolbio.mpg.de>](mailto:liedvogel@evolbio.mpg.de)



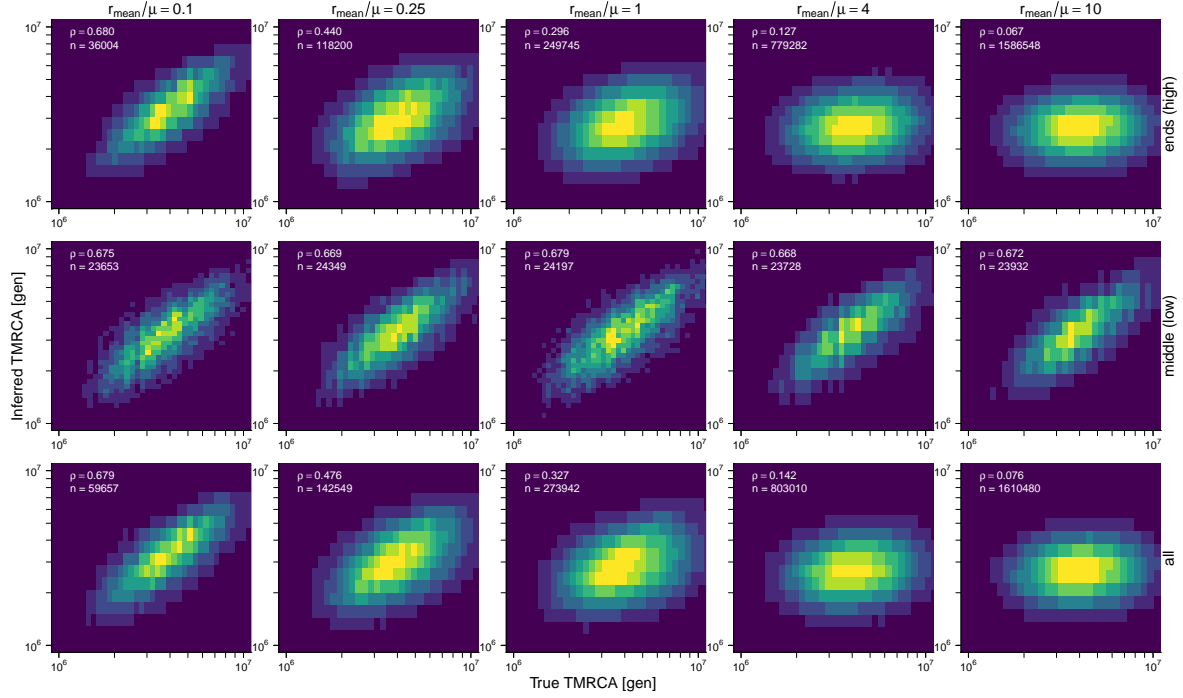
Supplementary Figure 1: Inference of historical effective population size with stepwise recombination landscapes. The inferences by MSMC2, Relate without masking high-recombining regions show that presence of high-recombining regions deviated ARG-based methods. Masking the high-recombining regions eliminated the deviation. Stairwayplot 2 is not affected by the presence of high-recombining regions. In each panel, gray lines depict the simulated truths (as in Fig. 2A), solid and dashed coloured lines depict the mean and mean \pm SD of the inferences (see Materials and Methods for details on how replicates were treated).



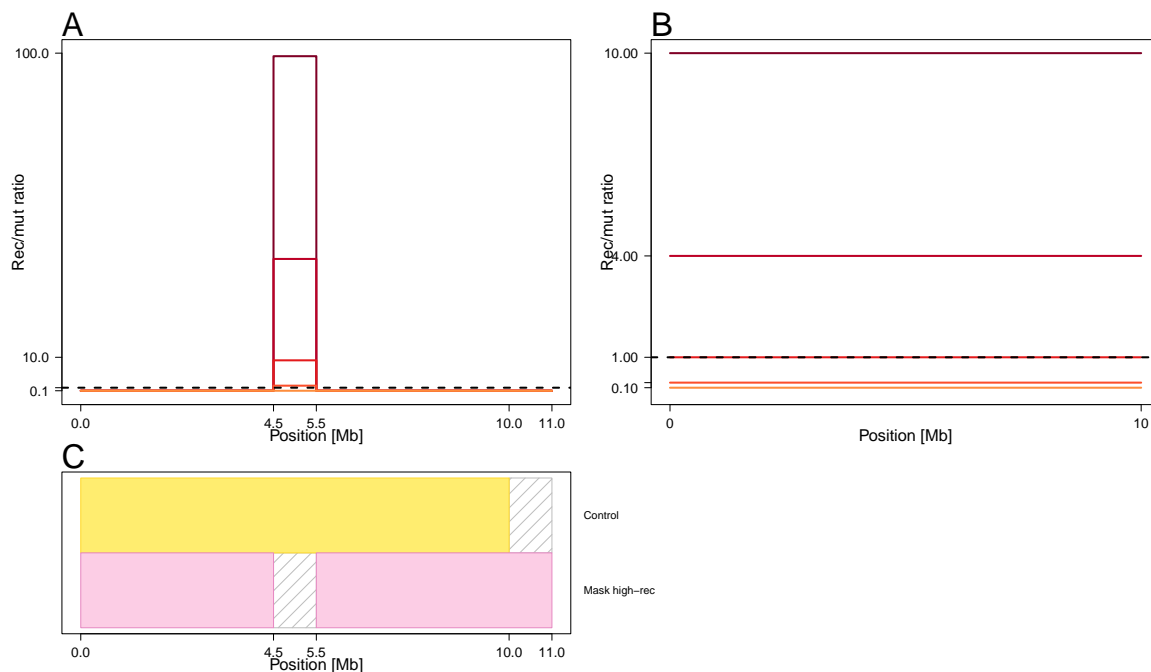
Supplementary Figure 2: Inference of relative cross-coalescence rate with stepwise recombination landscapes. Vertical dotted lines depict the true split time. Coloured lines depict inferred rCCR for pairs of populations. Three colours indicate three pairs of populations. **MSMC2** (left two columns). Solid lines depict mean of inferences of the ten down-samples, and dotted lines depict mean \pm SD. The results show that presence of high-recombining regions affects inference of population splits, and removing the high-recombining regions improves it. **Relate** (right two columns). Solid lines depict mean of inferences of the ten replicates, and dotted lines depict mean \pm SD. The results show that presence of high-recombining regions affects inference of population splits, and removing the high-recombining regions improves it.



Supplementary Figure 3: Inference of representation of genealogies by MSMC2 is affected specifically within high-recombining regions. Coalescence time between two sequences (haplotypes 0 and 1 (pop1)) were compared between the simulated truth (x axis) and inference by MSMC2 (the discretised epoch with the highest likelihood, y axis). Top row: two 3-Mb intervals in both ends of the simulated chromosome with elevated recombination rates. Middle row: a 6-Mb intervals in the centre of the chromosome with recombination rate 1/10 of mutation rate. Bottom row: both two 3-Mb ends and 6-Mb middle intervals. Five columns correspond to different recombination maps shown in Fig. 2. n is the number of genomic intervals whose boundaries are defined by either a true genealogy or an HMM window in MSMC2. ρ is the Spearman's coefficient of correlation.

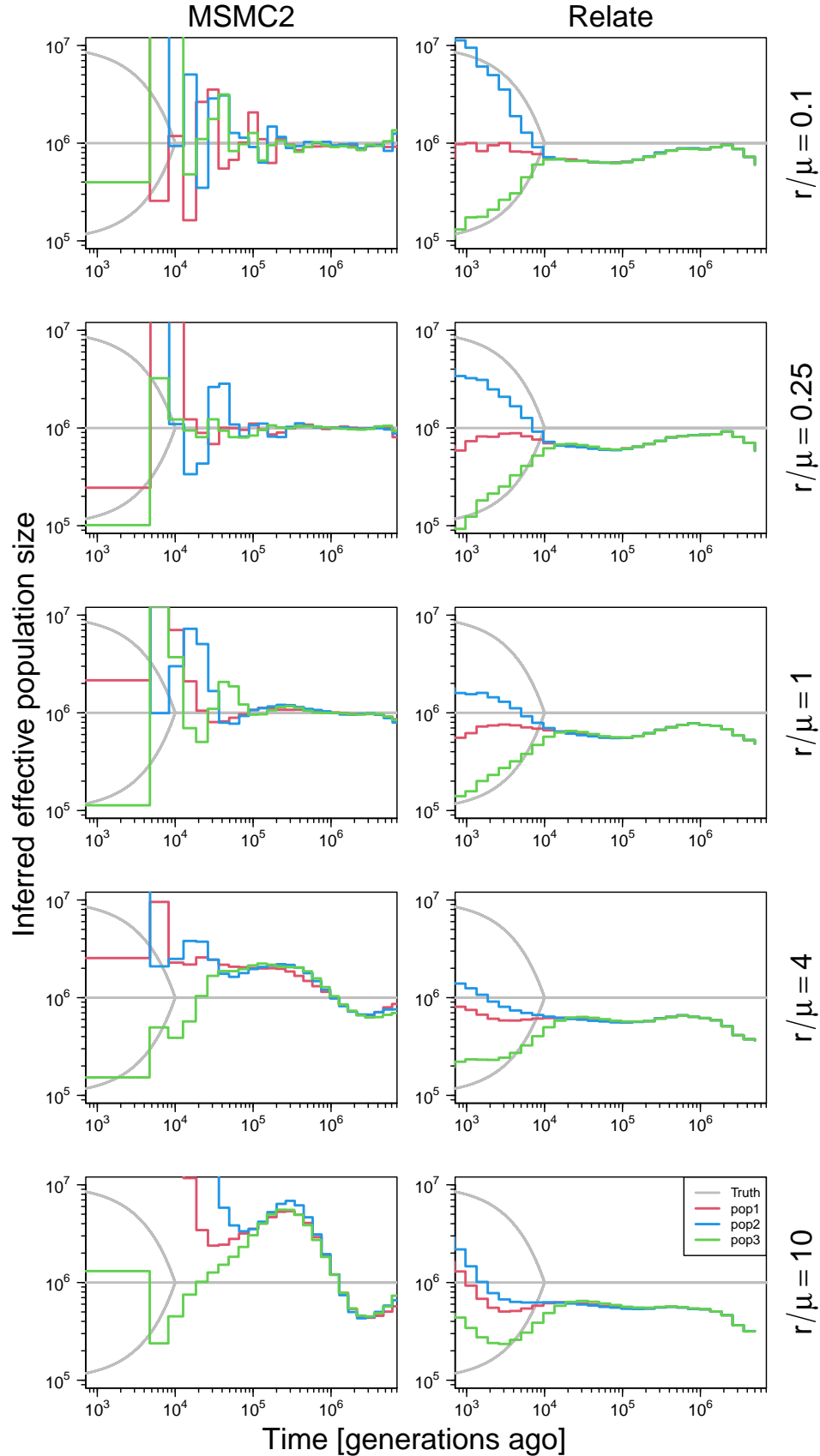


Supplementary Figure 4: Inference of genealogies by Relate is affected specifically within high-recombining regions. Time to the final coalescence (tree height) of genealogies of 300 sequences (50 diploids per population) were compared between the simulated truth (x axis) and inference by Relate (y axis). Top row: two 3-Mb intervals in both ends of the simulated chromosome with elevated recombination rates. Middle row: a 6-Mb intervals in the centre of the chromosome with recombination rate 1/10 of mutation rate. Bottom row: both two 3-Mb ends and 6-Mb middle intervals. n is the number of genomic intervals whose boundaries are defined by either a true or inferred genealogy. ρ is the Spearman's coefficient of correlation.

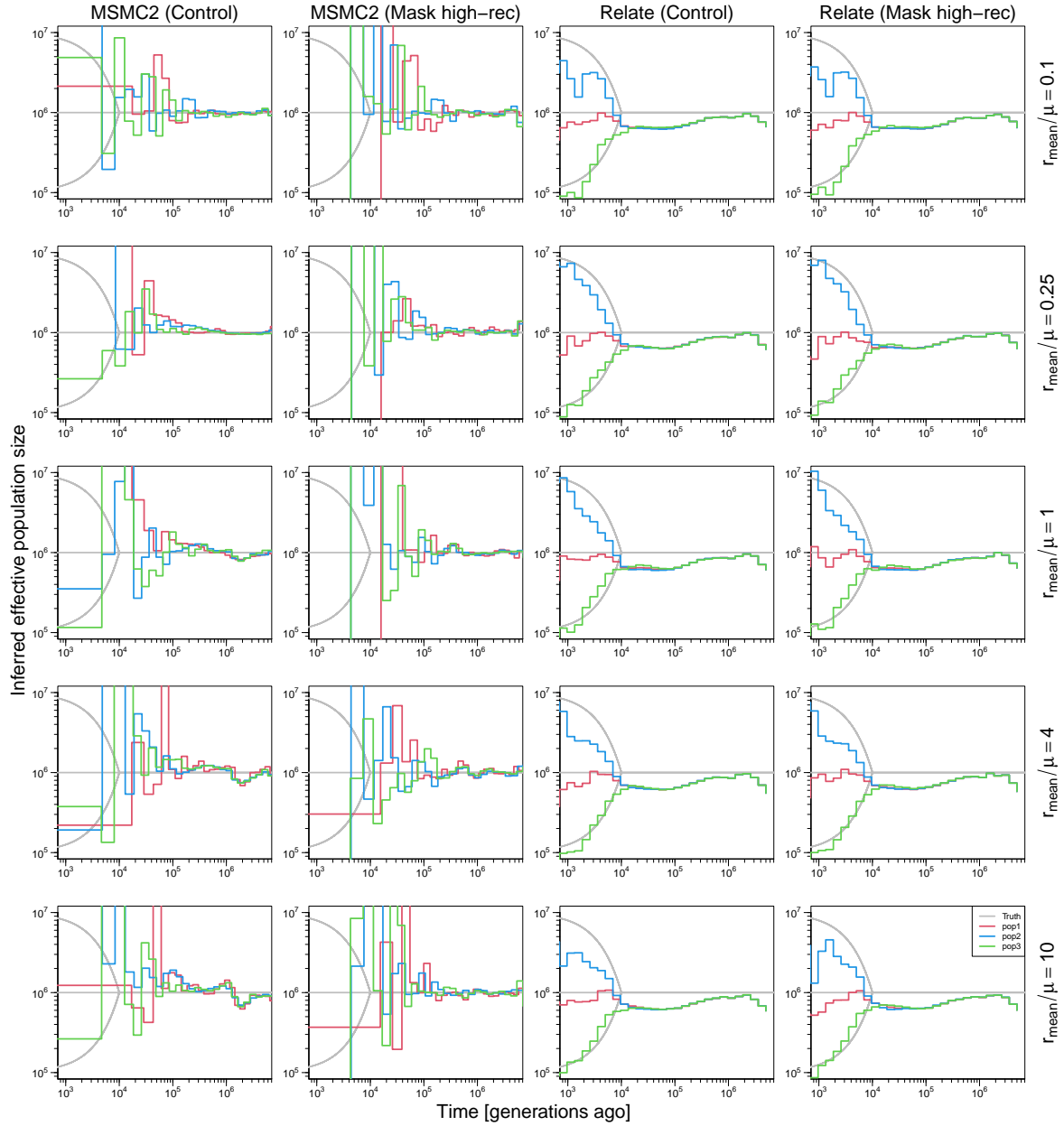


Supplementary Figure 5: Two scenarios with different sets of recombination landscapes.

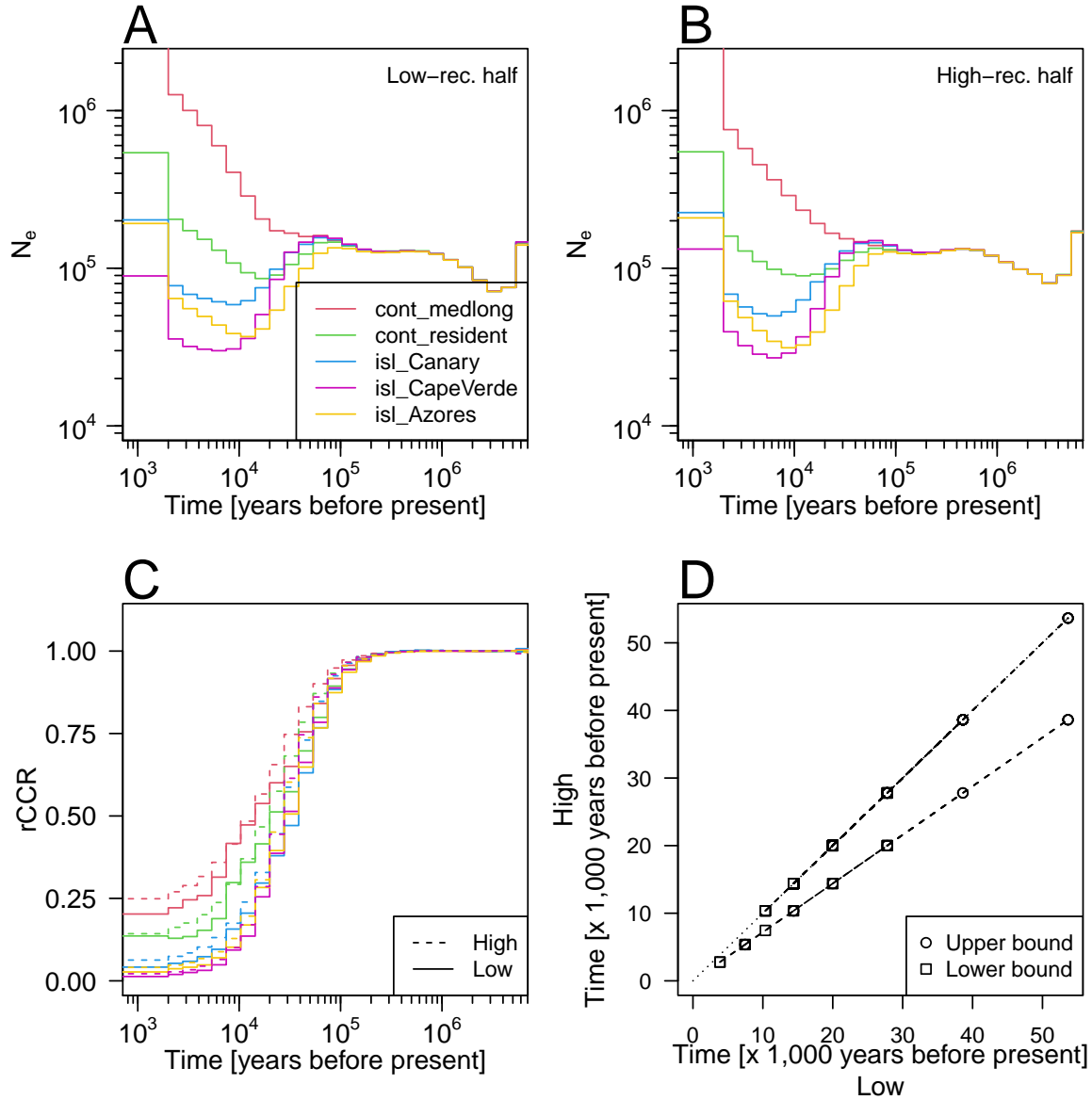
A. Recombination maps of the “narrow high-rec.” scenarios. **B.** Recombination maps of the “uniform” scenarios **C.** Two settings of demography inference masking different parts of the chromosomes for the narrow high-rec scenario (Yellow shades depict genomic regions used in demography inference. Gray shades depict regions masked from demography inference). We asked whether the presence of the high-recombining region (i.e. in the middle of the chromosome) affects demography inference and whether masking them improves demography inference. We applied methods of demography inference on the simulated data using different parts of the chromosome: either including the high-recombining regions (“control”, top) or masking the 1 Mb of high-recombining regions (bottom). To control for the amount of sequences used in the inferences, we applied 1 Mb mask outside the high-recombining regions in the first setting (top).



Supplementary Figure 6: Inference of effective population size by MSMC2 and Relate under the uniform recombination landscape scenarios. The effect of recombination rate is qualitatively consistent with the results with stepwise recombination landscapes (Fig. 3, Sup. Fig. 1) but more pronounced.)



Supplementary Figure 7: Inference of effective population size by MSMC2 and Relate under the recombination landscape scenarios with a single narrow high-recombining region. In MSMC2, the effect of the high-recombining region is qualitatively consistent with the results with stepwise recombination landscapes (Fig. 3, Sup. Fig. 1) but less pronounced.) **Relate**, is robust to the narrow high-recombining region.



Supplementary Figure 8: Demography inference by Relate with lower- and higher-recombining halves of blackcap genomes. **A, B.** Inference of historical effective population size. **C.** Inference of relative cross-coalescence rate (rCCR) between Azores population and each of all other four populations in **A** and **B** using the lower (solid lines) and the higher (dotted lines) half of the genome based on local recombination rates. **D.** Comparison of split times inferred by Relate using the lower higher halves of the genome based on recombination rates. Segments represent inference between 45 pairs of 10 populations. Two ends of a segment represent the lower and upper boundaries of two consecutive discretised epochs between which rCCR crosses the threshold of 0.5.

4

Shifting Balancing Selection on a Chromosomal Inversion in Island Populations

“Doctor, you have yourself shut in the room for fifteen years, haven’t you?” Moe remembered the questions she had stored away in her head. “What changes have you seen in your fifteen years of being in a place with no seasons, no night and day? What changes have occurred to you because of the death of your parents all at once?”

“First of all, let me assure you at the outset that I am not in this room of my own free will from the beginning. Therefore, any change in my thinking about my current particular environment cannot be a positive one. However, many things have become independent in me. It has, in a way, stabilized me and anchored me in reality.” Ms. Magata answered. “I wonder how that question relates to your life?”

– Hiroshi Mori, *The Perfect Insider* (1996)

Shifting balancing selection on a chromosomal inversion in island populations

Jun Ishigohoka^{1,*}

Miriam Liedvogel^{1,2,3,*}

¹MPRG Behavioural Genomics, Max Planck Institute for Evolutionary Biology, 24306 Plön, Germany

²Institute of Avian Research, An der Vogelwarte 21, 26386 Wilhelmshaven, Germany

³Department of Biology and Environmental Sciences, Carl von Ossietzky Universität Oldenburg, Ammerländer Heerstraße 114-118, 26129 Oldenburg, Germany

* Correspondence: [Jun Ishigohoka <ishigohoka@evolbio.mpg.de>](mailto:ishigohoka@evolbio.mpg.de), [Miriam Liedvogel <liedvogel@evolbio.mpg.de>](mailto:liedvogel@evolbio.mpg.de)

Abstract

Chromosomal inversions often underlie local adaptation and differentiation between populations. However, little is known about how selection acting on a balanced inversion shifts in different environments upon demographic events. Here, using population genomics with extensive simulations, we show that split events of island populations shifted a parameter of balancing selection on a polymorphic inversion. In Eurasian blackcaps (*Sylvia atricapilla*), an 8 Mb-long inversion has been maintained polymorphic in most populations by long-term balancing selection. The frequency of this inversion is consistently lower in island and continental resident populations compared to behaviourally ancestral continental migrant populations. Inference of population history shows that at least four groups of resident populations, including one continental population and three groups of populations on different island systems, originate from independent and simultaneous split events from an ancestral population of most modern populations. This indicates that the consistent reduction in the inversion frequency among these resident populations is unlikely due to shared selectively neutral demographic events. Approximate Bayesian computation (ABC) applied to simulations of balancing selection under the blackcap demography indicates that optimal frequency of the inversion in the regime of negative frequency-dependent selection, a type of balancing selection, shifted downwards in island populations. These results highlight how a shift in selection parameters upon demographic events with parallel shift in environment can contribute to genetic differentiation among populations at inversion loci.

Introduction

Chromosomal inversions, a structural mutation with a reversed chromosomal segment, play major roles in adaptation. Since the pioneering work by Dobzhansky (1947) in *Drosophila melanogaster*, inversion polymorphisms in multiple systems have been shown to be distributed with environmental gradient called “clines” (Ayala et al., 2013; Hager et al., 2022; Kapun et al., 2016; Lowry & Willis, 2010; Nosil et al., 2023). This spatial structure of inversion frequency has been considered to be the result of spatially varying selection (Ayala et al., 2013; Hager et al., 2022; Kapun et al., 2016; Kirkpatrick & Barton, 2006). Indeed, some traits under spatially varying selection are shown to be associated with genotype of inversions with a clinal distribution (Hager et al., 2022; Huang et al., 2020; Kapun et al., 2016; Sanchez-Donoso et al., 2021; Todesco et al., 2020). Additionally, a number of characterised inversion loci are under some form of balancing selection and have been maintained polymorphic over a long period of time, and they are associated with large (often discrete) phenotypic variation within species (Chouteau et al., 2017; Hager et al., 2022; Jay et al., 2018; Knief et al., 2016; Küpper et al., 2016; Matschiner et al., 2022; Sanchez-Donoso et al., 2021; Tuttle et al., 2016).

Despite the widely recognised evolutionary importance of inversion polymorphisms, identification of the mode of selection acting on inversions — spatially varying divergent selection with gene flow, overdominance (heterozygote advantage), and negative frequency-dependent selection — and measurement of parameter values in controlled conditions or natural populations are still limited (Ayala et al., 2013; Hager et al., 2022; Nosil et al., 2023). Furthermore, it is largely unknown in empirical systems how inversion clines are formed when populations expand and/or split from the ancestral range to novel environments. One common challenge addressing these questions is the confounding by demographic history. Disentangling the selectively neutral effect of demography on a clinal pattern from selection on inversions requires modelling of the underlying demography finely tuned to the study system.

In this study, we investigate the evolutionary basis of geographically structured frequencies of a polymorphic inversion in the Eurasian blackcap *Sylvia atricapilla*. Blackcaps are common and widespread in Europe, and their breeding populations (Fig. 1A) are characterised with different phenotypes of seasonal migration (Berthold, 1991; Delmore et al., 2020; Shirihai et al.,

2010). We previously identified an 8 Mb-long polymorphic inversion in blackcap chromosome 12 (inv_12_3) through genome-scan of local genetic structure (Fig. 1A, Ishigohoka et al. (2024)). Inv_12_3 contains mutations differentiated between the two haplotypes (Fig. 1C), indicating that the polymorphism has been maintained for a long time by balancing selection (Ishigohoka et al., 2021). Inv_12_3 is segregated at different frequencies among populations with an apparent cline between the continental and island (or migratory and resident) populations (Fig. 1D) (Ishigohoka et al., 2024). Using this inversion system in blackcaps, we address how selection acting on the inversion changed in different populations split from the ancestral population.

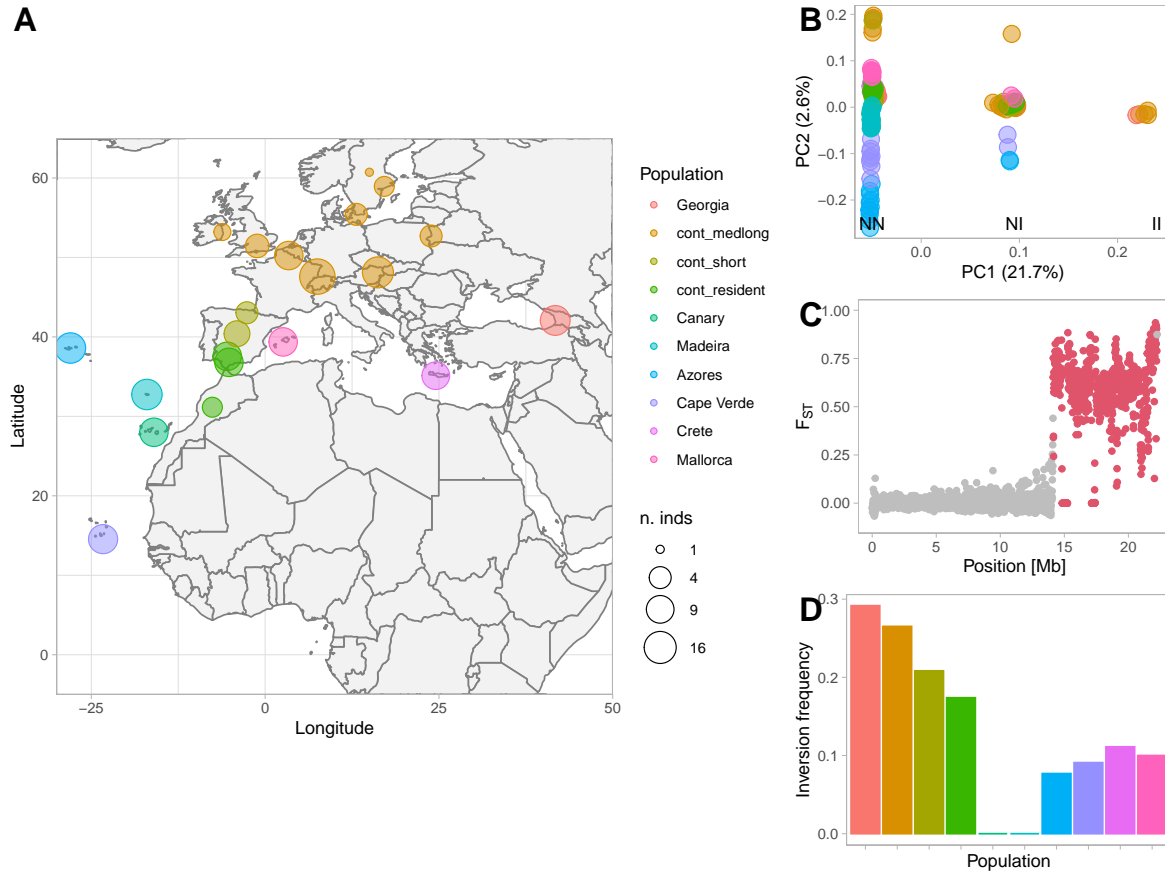


Figure 1: Inversion in blackcaps is under balancing selection **A.** Geographic locations of blackcaps samples. **B.** Local population structure within the 8 Mb-long inversion of chromosome 12 based on PCA. The three clusters of individuals correspond to genotype at a putative inversion (NN: normal/normal, NI: normal:inverted, II: inverted/inverted). **C.** F_{ST} in 10 kb windows between NN and II along chromosome 12. Red points depict windows within inv_12_3. **D.** The frequency of the inversion among the blackcap population.

Results

The study consists of two steps. First, we inferred the demographic history of blackcap populations using whole-genome SNPs. This inference of neutral demography included identification of a demography model and estimation of demography parameters, which allowed simulation of balancing selection under the blackcap population history in the second step. Second, we characterised shifting balancing selection using simulation and observed inversion frequencies. We focused on two types of balancing selection: overdominance and negative frequency-dependent selection (NFDS). We excluded the possibility of divergent selection across the cline, because the frequency of *inv_12_3* stays lower than 0.5 throughout our sampled populations (Fig. 1A, D) which covers most of the species breeding range (Shirihai et al., 2010). We identified a model from neutrality, overdominance, and NFDS, and estimated parameters.

Demography inference reveal simultaneous and independent split of populations with lower inversion frequency

To characterise demographic history of blackcap populations, we used whole-genome resequencing data of 179 blackcaps covering their breeding range (Delmore et al., 2020; Ishigohoka et al., 2024). We first used three “model-free” methods for demography inference: **Stairway plot 2** (Liu & Fu, 2020), **MSMC2** (Malaspinas et al., 2016; Schiffels & Durbin, 2014; Schiffels & Wang, 2020), and **Relate** (Speidel et al., 2019). **Stairway plot 2** infers piecewise effective population size (N_e) over time for a population based on the site-frequency spectrum and is robust to high recombination rates. **MSMC2** approximates the ancestral process along the genome in a structure called ancestral recombination graph (ARG) by sequentially Markovian coalescent (SMC) (Malaspinas et al., 2016; McVean & Cardin, 2005; Schiffels & Durbin, 2014; Schiffels & Wang, 2020). It estimates piecewise coalescence rate over time between multiple pairs of sequences from a population or from a pair of populations, which are used to obtain piece-wise N_e for each population and relative cross-coalescence rate (rCCR) between the population pair over time. **Relate** estimates the underlying ARG as a series of marginal trees (“genome-wide genealogies”) based on local distance matrices (Speidel et al., 2019), which

are constructed by modelling observed haplotypes and ancestral haplotypes using a hidden Markov model (“chromosome painting”, Li & Stephens (2003)). Piecewise coalescence rate over time epochs between all pairs of haplotypes are estimated from the inferred genealogies, which can be used to obtain N_e and rCCR over time as in **MSMC2**. **MSMC2** and **Relate** are sensitive to the presence of wide high-recombining regions in the genome, which is prominent in birds including blackcaps (Ishigohoka & Liedvogel, 2024). **Stairway plot 2** was run using folded SFS of each blackcap population. **MSMC2** was run using a low-recombining half of the genome of at most four individuals per population. **Relate** was run using a low-recombining half of the genome using all individuals. The inferences were qualitatively similar (Fig. 2A, B, Sup. Fig. 1) with consistency in one important aspect of the demography: all resident populations started to split simultaneously.

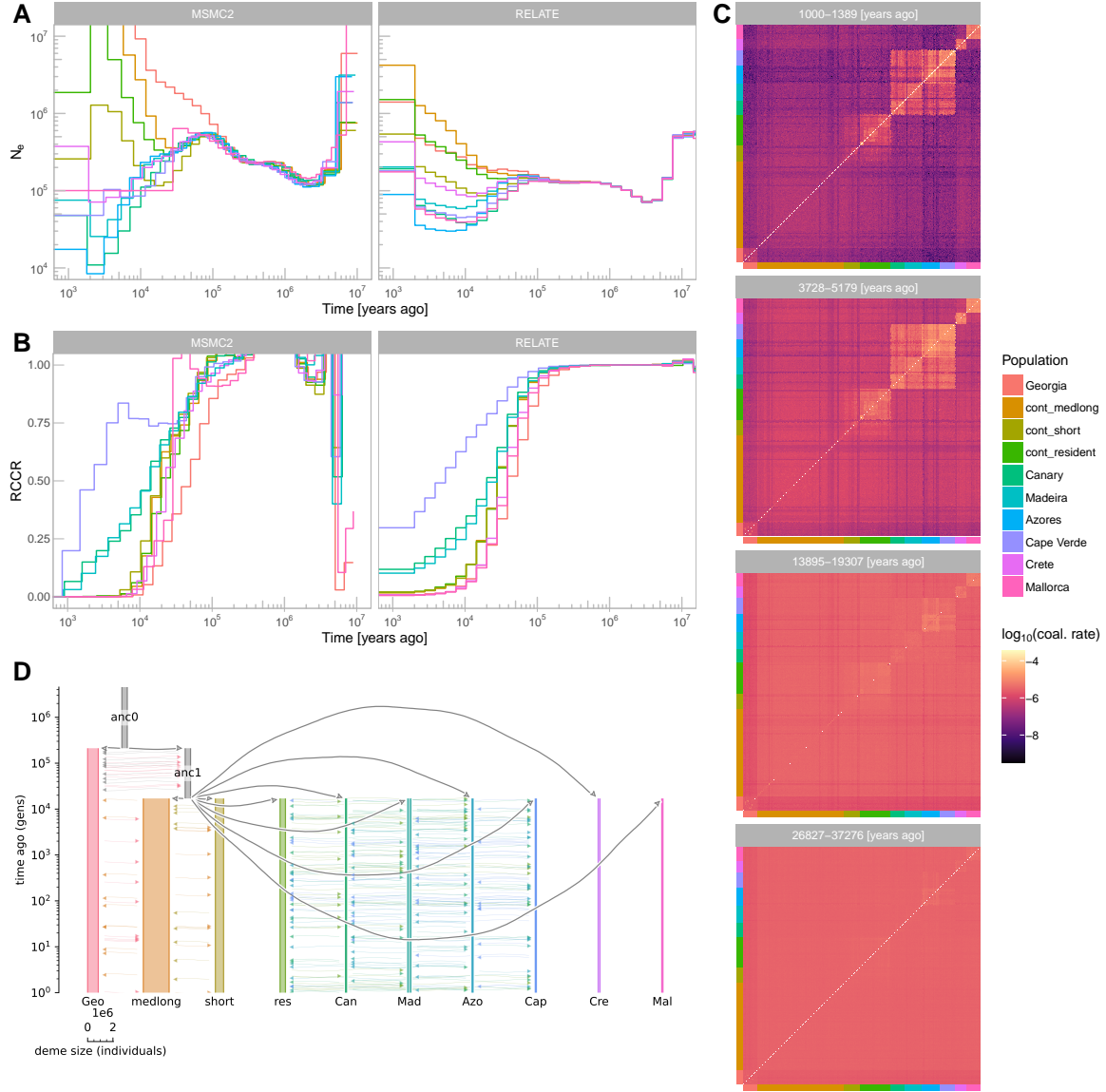


Figure 2: Demography inference. **A.** Historical effective population size (N_e) of blackcap populations inferred with **MSMC2** and **Relate**. **B.** Relative cross-coalescence rate (RCCR) inferred with **MSMC2** and **Relate**. Nine lines show RCCR between Azores and the other nine populations. **C.** Historical coalescence rate inferred with **Relate** shows multiple independent isolation events resident populations of island systems. The heatmaps show coalescence rate between all pairs of haplotypes at a focal epoch. **D.** Demography model inferred through approximate Bayesian computation (ABC) with ABC-RF. Parts of A and B were reproduced from Ishigohoka & Liedvogel (2024).

To further investigate this aspect of population history (independent and simultaneous splits), we summarised how coalescence rate changed over time (from present to past) for all pairs of haplotypes using genealogies inferred by **Relate**. We observed elevated coalescence rates in four distinct clusters of individuals (Fig. 2C): continental resident population; four

Macaronesian island populations; Mallorca island resident population; and Crete island resident population. These clusters do not merge with each other until the signals disappear (backwards in time). This pattern, in addition to N_e and rCCR, indicates that at least four independent split events occurred simultaneously to form both continental and island resident populations. Crucially, all populations in these four groups show reduced frequency of *inv_12_3* (Fig. 1D). Such consistent shifts in frequency to the same direction is unlikely to be explained purely by demography, indicating that the parameters of balancing selection on *inv_12_3* shifted in a consistent manner across all islands and southern end of the continental distribution range (inhabited by continental residents).

We also observed inconsistency among demography inferences by the three methods in the following three aspects. First, the split of the ancestral population to the current Georgian population was inferred to be older than that of the ancestral population of other modern populations based on **Stairway plot 2** (Sup. Fig. 1) and **MSMC2** (Fig. 2A, B, left column), whereas **Relate** inferred that all populations split around the same time (Fig. 2A, B, right column). Second, N_e of the continental resident population was consistent across the split event according to **Stairway plot 2** (Sup. Fig. 1), whereas **MSMC2** and **Relate** inferred an increase in N_e (Fig. 2A). Lastly, the estimated values of N_e and time were different among these three methods.

To select a demography model from these inconsistencies and to estimate parameters, we performed approximate Bayesian computation (ABC) using simulations for eight different models, consisting of combinations of three binary factors. The first factor was whether the ancestral population of the current Georgian population split older than the population ancestral to other modern populations. The second factor was whether the continental resident population increased in N_e after the split. The last factor was whether gene flow should be included in the model between some pairs of populations. We included symmetrical gene flow between Macaronesian island resident populations and between continental populations based on rCCR (Fig. 2B) and historical coalescence rate (Fig. 2C). By setting parameter ranges covering quantitative differences in N_e and time among inferences by **Stairway plot 2**, **MSMC2** and **Relate**, we covered the space of models and parameters as large as necessary

and as small as possible. Each of these eight models were simulated using `ms` (Hudson, 2002) over 1 million times with randomly sampled parameters. We used `abcrf`, an implementation of ABC with random forest (Raynal et al., 2019), for model selection. The model with older Georgian split, constant N_e for the continental resident population and gene flow was selected over other models with a posterior probability of 0.698 (Sup. Table 1). Parameter inference using `abcrf` revealed that the ancestral population of the current Georgian population split first ~424,000 years ago (assuming a generation time of two years), and other populations split ~34,000 years ago (Sup. Table 2).

Negative frequency-dependent selection shifted concomitantly in independent island populations

We hypothesised that parameters of balancing selection shifted in some populations (island populations or resident populations) by unknown common environmental factors. We tested this hypothesis by addressing two layers of questions. In the first layer, we asked what type of balancing selection is acting on `inv_12_3` (we term them “models”). Specifically, we asked whether it is overdominance (heterozygote advantage, Fig. 3A) or negative frequency-dependent selection (NFDS, Fig. 3B), and we included a neutral scenario as a control. In the second layer, we asked in what populations the parameters shifted (Fig. 3C, D. We term them “scenarios”). Specifically, we asked whether parameters shifted in resident populations (scenario 2), in island resident populations (scenario 3), or differently in all populations (scenario 4), in addition to a scenario where parameters do not change (scenario 1).

To select models and scenarios, and to estimate parameters, we simulated selection on a locus for each scenario of each model over one million times in `SLiM` under the estimated blackcap demography, and performed ABC using `abcrf`. For each model, we sampled two parameters for simulation: selection coefficient (s) and dominance (h) for model 1 (overdominance); and selection coefficient (s) and optimal inversion frequency (p_{opt}) for model 2 (NFDS). The two layers of questions (models and scenarios) were tested sequentially by two steps of model selection of ABC. For the first layer, the model for NFDS was selected over the other models with a posterior probability of 0.727 (Fig. 3E, Sup. Table 3). For the second layer, scenario 3

(parameters shifted in island populations) was selected over the other scenarios with a posterior probability of 0.619 (Fig. 3F, Sup. Table 4). Parameter inference revealed that the optimal frequency p_{opt} reduced in island populations to 0.086 from 0.266 in continental populations (Fig. 3G, Sup. Table 5). This result indicates that the frequency of `inv_12_3` reduced in some populations because the optimal frequency of NFDS reduced in island populations.

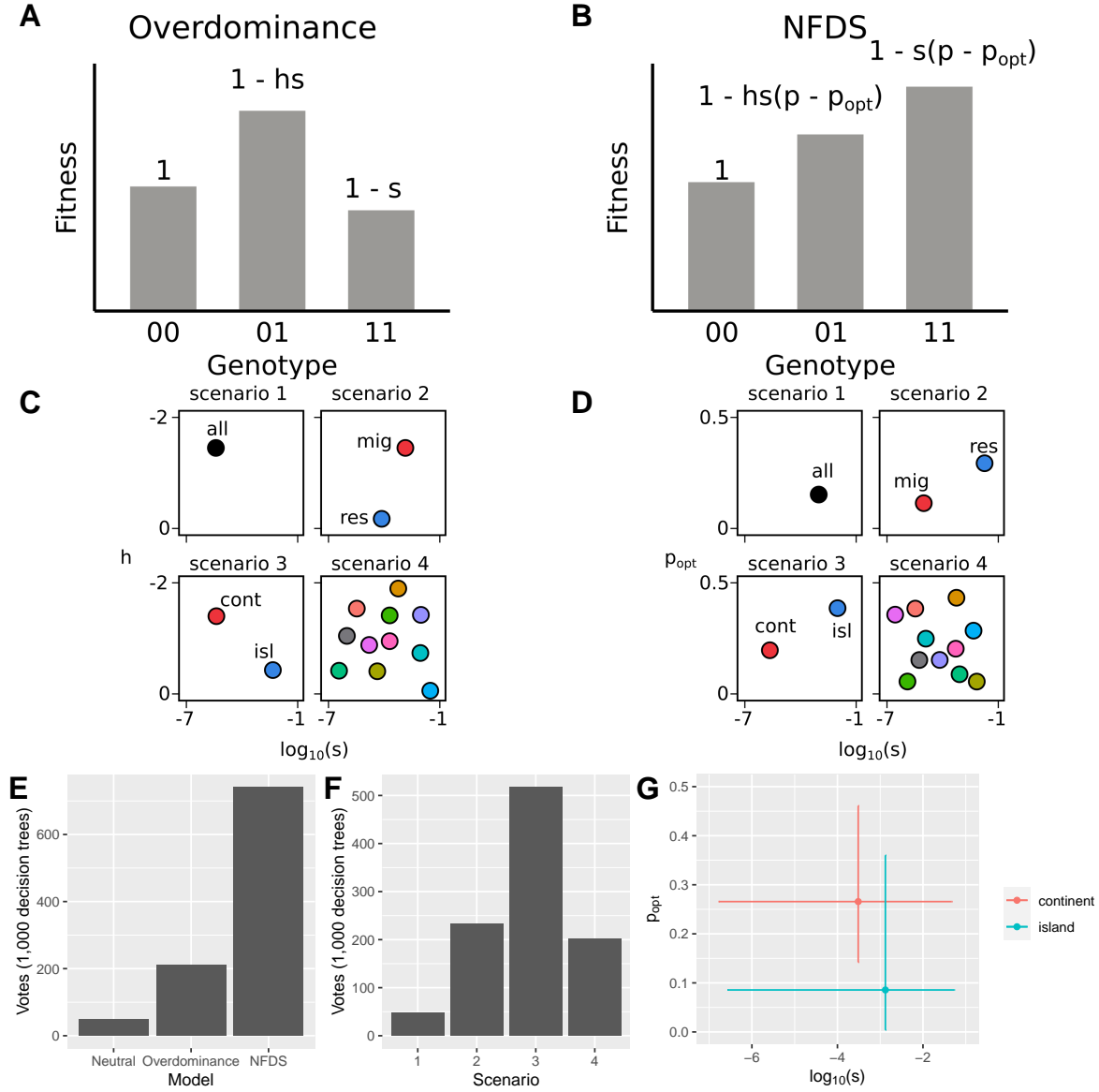


Figure 3: Shifting balancing selection. **A, B.** Two candidate models of balancing selection operating on the blackcap inversion. In the overdominance (heterozygote advantage) model (**A**), heterozygotes have higher fitness than homozygotes by the combination of two parameters, dominance (h) and selection (s) coefficients. In the negative frequency-dependent selection (NFDS) model (**B**), the fitness of the inversion depends on the difference between the inversion frequency p and the optimal frequency (p_{opt}). We hypothesise that the lower frequency of the inversion on islands can be explained by different parameters of balancing selection (h and s in overdominance or p_{opt} and s in NFDS). **C, D.** Four scenarios of population difference in overdominance (**C**) or NFDS (**D**). In scenario 1, all populations share the same parameter value. In scenario 2, migratory (cont_medlong, cont_short, and ancestral population) and resident populations (cont_resident and all island populations) have different parameter values. In scenario 3, continental and island populations have different parameter values. In scenario 4, all populations have different parameter values. **E.** Model selection among neutral, overdominance, and NFDS with ABC-RF. **F.** Selection among four scenarios of NFDS with ABC-RF. **G** Parameter inference with ABC-RF. Points show the expectation, and error bars show 95% credibility interval.

Discussion

Using approximate Bayesian computation (ABC) on simulated shifting balancing selection under the blackcap demography, we identified that the optimal frequency of negative frequency-dependent selection (NFDS) acting on a segregating inversion *inv_12_3* shifted downwards in island populations, resulting in different frequency of the inversion among populations. In our simulation, we implemented scenarios in which parameters for balancing selection shifts in a discrete manner. However, this discrete shift may not be close enough to the underlying phenomena. Although the frequency of *inv_12_3* is lower in island resident populations than continental populations, spatial pattern of this inversion exists also among the continental populations, reducing in frequency from northeast to southwest (Fig. 1D). In other words, the frequency of *inv_12_3* follows a wide cline covering the entire breeding range of the species. The parameter values of balancing selection therefore may be shifting continuously along this axis. Although we aimed to capture this difference within continental populations in one scenario (scenario 2) considering different values of parameters in migrant and resident populations, an additional scenario (for both overdominance and NFDS) in which the focal parameter is expressed as a monotonic function of the location of populations along the cline axis should be carried out in a future study.

The target traits under balancing selection associated with the genotype of *inv_12_3* were not identified in this study. One possibility is that *inv_12_3* may harbour immune-related genes under balancing selection and they may have a different optimal frequency in island populations due to reduced parasite prevalence (Nieberding et al., 2006). Traits associated with inversions under selection may be identified after the finding of balanced polymorphism. For example, one inversion in the zebra finch was not associated with morphological traits or fitness components measured in the initial study (Knief et al., 2016), but was later identified to have an overdominance effect on sperm morphology and motility (Kim et al., 2017; Knief et al., 2017). Although quantifying morphological, behavioural, and fitness traits, including parasite prevalence, in wild-caught animals is not trivial, characterising the phenotypic and fitness effects of the inversion will be essential to understand the ultimate cause of the observed cline.

Inversions with clines in other systems are often associated with traits under spatially-

varying selection (Ayala et al., 2013; Durmaz et al., 2018; Hager et al., 2022; Kapun et al., 2016; Kapun & Flatt, 2019; Kirkpatrick & Barton, 2006; Koch et al., 2021, 2022; Nosil et al., 2023). For example, an inversion in deer mice *Peromyscus maniculatus*, which is associated with forest and prairie ecotypes with different tail length (associated with climbing performance) and coat colour (crypticity in matching environment), is under divergent selection (Hager et al., 2022). Inversions in marine snails *Littorina saxatilis* are associated with weight, colour, and aperture size, which are diverged between ecotypes adapted to neighbouring intertidal habitats with opposing levels of pressure between crab predation and wave action (Koch et al., 2021, 2022). Inversions with latitudinal clines in *Drosophila melanogaster* are associated with multiple survival traits and are under selection by climatic factors (Durmaz et al., 2018; Kapun et al., 2016; Kapun & Flatt, 2019). An inversion in stick insects *Timema knulli* is under overall overdominance consisting of opposing effects of adaptation to a challenging host plant and survival (Nosil et al., 2023). In most of these inversions, the frequency difference between two sides of a narrow cline is so large that major allele switches across the cline. On the contrary to these opposing fitness effects across clines, *inv_12_3* in blackcaps is maintained as a minor allele along the wide cline. This may represent a less extreme but more general type of spatially varying balancing selection that does not involve flipping of the beneficial allele or genotype with the highest fitness.

Materials and Methods

Data and historical population structure

We used phased whole-genome resequencing (WGR) data of 179 blackcaps from (Ishigohoka et al., 2024). We revisited demography inference with *MSMC2* using low-recombining half of blackcap genomes in (Ishigohoka & Liedvogel, 2024). We used genome-wide genealogies of blackcaps inferred by *Relate* using low-recombining half of the blackcap genomes in (Ishigohoka & Liedvogel, 2024). Historical population structure was estimated from genome-wide genealogies using the *RelateCoalescenceRate* module of *Relate*.

Demography inference with ABC

To select a demography model and estimate demography parameters, we performed approximate Bayesian computation (ABC) with random forest using `abcrf` (Raynal et al., 2019), using `ms` (Hudson, 2002) as a simulator. We simulated eight scenarios consisting of the three binary factors:

1. Population ancestral to modern Georgian population split earlier than other modern populations (1) or it split with other populations simultaneously (2)
2. N_e of continental resident population was constant from the ancestral population (1) or it increased (2)
3. There is no gene flow after population splits (1) or gene flow between some pairs of populations are included (2)

The prior distributions for parameters were: a log uniform between 1×10^5 and 1×10^6 for ancestral N_e ; a log uniform between 1 and 100 for the fold change in N_e in Georgian population, medium and long distance migrant population, and short distance migrant population (and continental resident for models with increase in N_e in continental resident); a log uniform between 0.01 and 1 for fold change in N_e in island populations; a log uniform between 1×10^4 and 1×10^5 (generations) for split time of all population (but Georgian population for model with earlier split of Georgian population); a log uniform between the sampled split time of modern populations and 4×10^5 (generations) for split time of Georgian population in models with earlier split of Georgian population. The prior distribution for gene flow (symmetric migration rate) was a log uniform between 1×10^{-9} and 1×10^{-3} (except for within Macaronesian islands), and seven (for models without earlier split of Georgian population) or eight (for models with earlier split of Georgian population) values of gene flow were sampled: between Georgian population and population ancestral to all other populations; between Georgian and `cont_medlong`; between `cont_medlong` and `cont_short`; between `cont_short` and `cont_resident`; between Azores/Cape Verde and Canary/Madeira (“`mig_mac`”); a log uniform from 1×10^{-9} to `mig_mac` between `cont_resident` and Macaronesian island populations; a log uniform from `mig_mac` to 1×10^{-3} between Azores and Cape Verde and between Canary and Madeira. Sampling of parameters and writing of `ms` commands with sampled parameters for

different models were done in custom AWK scripts. In `ms` simulation, 1,000 independent loci with one mutation each were simulated, and the same numbers of individuals as the empirical data set were sampled from populations. The `ms` output was directly piped into an AWK script to compute 75 summary statistics: mean pairwise nucleotide difference π and Watterson's θ for each population, and Weir and Cockerham's estimator of F_{ST} for all pairs of populations. This simulation was performed 1,000,000 times for each of eight models. For the empirical data, we randomly sampled 1,000 SNPs from autosomes and computed the summary statistics using the same script.

To perform model selection, a random forest was constructed using `abcrf` function of `abcrf` package. Model selection was performed using `predict` method of the random forest. Cross validation was performed using `err.abcrf` function of `abcrf` package. Goodness of fit was visualised using `gfitpca` function of `abc` package (Csilléry et al., 2012).

To estimate parameters, a regression random forest was constructed using `regAbcrf` function of `abcrf` with a random forest of 1,000 trees. Parameters were estimated using `predict` method of the regression random forest.

Selection inference

To select a model of selection on `inv_12_3`, we performed ABC with random forest using `abcrf` using SLiM version 4.1 (Haller & Messer, 2022) as a simulator. We simulated one neutral model, one model for overdominance, and one model for NFDS. For the overdominance and NFDS models, we included four scenarios. In scenario 1, where all populations have the same parameters, a pair of parameters were sampled (s and h for overdominance and s and p_{opt} for NFDS). In scenario 2, where parameters differ between migrant and resident populations, two pairs of parameters were sampled and assigned to migrant and resident populations. In scenario 3, where parameters differ between continent and islands, two pairs of parameters were sampled and assigned to continental and island populations. In scenario 4, ten pairs of parameters were sampled, and they were assigned to different populations. For both overdominance and NFDS models, s was sampled from a log uniform distribution between 1×10^{-7} and 1×10^{-1} . For the overdominance model, h was sampled from a uniform

distribution between 0 and -2 (corresponding to expected inversion frequencies from 0 to 0.4). For the NFDS model, p_{opt} was sampled from a uniform distribution between 0 and 0.5. Sampling of parameters was done using custom AWK scripts.

We simulated a 1-bp locus representing `inv_12_3` in SLiM version 4.0.1. We scaled the population size and time by a factor of 1,000. Assuming that the inversion was at the equilibrium frequency in the ancestral population, we introduced a marker mutation at the equilibrium frequency in the ancestral population (based on sampled h or p_{opt} for the ancestral population) in the initial generation. For the neutral model, we followed the same procedure as the overdominance model with $s = 0$. This leads to unrealistically high initial frequency for a neutral locus, hence the posterior probability for the neutral model can be overestimated. We implemented a rescaled version of the blackcap population history, and population-specific fitness effects were implemented within `mutationEffect` callback based on the genotype of the individual. At the final generation, we sampled the same numbers of individuals as our empirical data set, and recorded the inversion frequency. We ran 1,000,000 replicates of simulations per scenario.

We first selected a model (from neutral, overdominance, and NFDS), then selected a scenario (from scenarios 1-4) using `abcrf` package. For both steps, `abcrf` function was used to construct a random forest. A model and a scenario was selected using `predict` method of the random forests. Cross validation was performed using `err.abcrf` function of `abcrf` package. Goodness of fit was visualised using `gfitpca` function of `abc` package.

To estimate parameters, a regression random forest was constructed using `regAbcrf` function of `abcrf` with a random forest of 1,000 trees. Parameters were estimated using `predict` method of the regression random forest.

Acknowledgments

This work was supported by the Max Planck Society (Max Planck Research Group grant MFFALIMN0001 to ML), and the DFG (project Nav05 within SFB 1372 – Magnetoreception and Navigation in Vertebrates (395940726) to ML). We thank Demetris Taliadoros for feedback

on the study design and Alexander Jacobsen for helping implementation of simulation.

References

- Ayala, D., Guerrero, R. F., & Kirkpatrick, M. (2013). Reproductive Isolation and Local Adaptation Quantified for a Chromosome Inversion in a Malaria Mosquito. *Evolution*, 67(4), 946–958. <https://doi.org/10.1111/j.1558-5646.2012.01836.x>
- Berthold, P. (1991). Genetic control of migratory behaviour in birds. *Trends in Ecology and Evolution*, 6(8), 254–257. [https://doi.org/10.1016/0169-5347\(91\)90072-6](https://doi.org/10.1016/0169-5347(91)90072-6)
- Chouteau, M., Llaurens, V., Piron-Prunier, F., & Joron, M. (2017). Polymorphism at a mimicry supergene maintained by opposing frequency-dependent selection pressures. *Proceedings of the National Academy of Sciences*, 114(31), 8325–8329. <https://doi.org/10.1073/pnas.1702482114>
- Csilléry, K., François, O., & Blum, M. G. B. (2012). Abc: An R package for approximate Bayesian computation (ABC). *Methods in Ecology and Evolution*, 3(3), 475–479. <https://doi.org/10.1111/j.2041-210X.2011.00179.x>
- Delmore, K., Illera, J. C., Pérez-Tris, J., Segelbacher, G., Lugo Ramos, J. S., Durieux, G., Ishigohoka, J., & Liedvogel, M. (2020). The evolutionary history and genomics of European blackcap migration. *eLife*, 9, e54462. <https://doi.org/10.7554/eLife.54462>
- Dobzhansky, T. (1947). Adaptive Changes Induced by Natural Selection in Wild Populations of *Drosophila*. *Evolution*, 1(1-2), 1–16. <https://doi.org/10.1111/j.1558-5646.1947.tb02709.x>
- Durmaz, E., Benson, C., Kapun, M., Schmidt, P., & Flatt, T. (2018). An inversion supergene in *Drosophila* underpins latitudinal clines in survival traits. *Journal of Evolutionary Biology*, 31(9), 1354–1364. <https://doi.org/10.1111/jeb.13310>
- Hager, E. R., Harringmeyer, O. S., Wooldridge, T. B., Theingi, S., Gable, J. T., McFadden, S., Neugeboren, B., Turner, K. M., Jensen, J. D., & Hoekstra, H. E. (2022). A chromosomal inversion contributes to divergence in multiple traits between deer mouse ecotypes. *Science*, 377(6604), 399–405. <https://doi.org/10.1126/science.abg0718>
- Haller, B. C., & Messer, P. W. (2022). SLiM 4: Multispecies Eco-Evolutionary Modeling. *The American Naturalist*, E000–E000. <https://doi.org/10.1086/723601>
- Huang, K., Andrew, R. L., Owens, G. L., Ostevik, K. L., & Rieseberg, L. H. (2020). Multiple chromosomal inversions contribute to adaptive divergence of a dune sunflower ecotype. *Molecular Ecology*, 29(14), 2535–2549. <https://doi.org/10.1111/mec.15428>
- Hudson, R. R. (2002). Generating samples under a Wright–Fisher neutral model of genetic variation. *Bioinformatics*, 18(2), 337–338. <https://doi.org/10.1093/bioinformatics/18.2.337>
- Ishigohoka, J., Bascón-Cardozo, K., Bours, A., Fuß, J., Rhie, A., Mountcastle, J., Haase, B., Chow, W., Collins, J., Howe, K., Uliano-Silva, M., Fedrigo, O., Jarvis, E. D., Pérez-Tris, J., Illera, J. C., & Liedvogel, M. (2021, December 23). *Recombination suppression and selection affect local ancestries in genomes of a migratory songbird*. <https://doi.org/10.1101/2021.12.22.473882>

- Ishigohoka, J., Bascón-Cardozo, K., Bours, A., Fuß, J., Rhie, A., Mountcastle, J., Haase, B., Chow, W., Collins, J., Howe, K., Uliano-Silva, M., Fedrigo, O., Jarvis, E. D., Pérez-Tris, J., Illera, J. C., & Liedvogel, M. (2024, February 16). *Distinct patterns of genetic variation at low-recombining genomic regions represent haplotype structure*. <https://doi.org/10.1101/2021.12.22.473882>
- Ishigohoka, J., & Liedvogel, M. (2024, February 8). *High-recombining genomic regions affect demography inference*. <https://doi.org/10.1101/2024.02.05.579015>
- Jay, P., Whibley, A., Frézal, L., María Ángeles Rodríguez de Cara, de Cara, M., Nowell, R. W., Mallet, J., Dasmahapatra, K. K., & Joron, M. (2018). Supergene Evolution Triggered by the Introgression of a Chromosomal Inversion. *Current Biology*, 28(11), 1839. <https://doi.org/10.1016/j.cub.2018.04.072>
- Kapun, M., Fabian, D. K., Goudet, J., & Flatt, T. (2016). Genomic Evidence for Adaptive Inversion Clines in *Drosophila melanogaster*. *Molecular Biology and Evolution*, 33(5), 1317–1336. <https://doi.org/10.1093/molbev/msw016>
- Kapun, M., & Flatt, T. (2019). The adaptive significance of chromosomal inversion polymorphisms in *Drosophila melanogaster*. *Molecular Ecology*, 28(6), 1263–1282. <https://doi.org/10.1111/mec.14871>
- Kim, K.-W., Bennison, C., Hemmings, N., Brookes, L., Hurley, L. L., Griffith, S. C., Burke, T., Birkhead, T. R., & Slate, J. (2017). A sex-linked supergene controls sperm morphology and swimming speed in a songbird. *Nature Ecology & Evolution*, 1(8), 1168–1176. <https://doi.org/10.1038/s41559-017-0235-2>
- Kirkpatrick, M., & Barton, N. (2006). Chromosome Inversions, Local Adaptation and Speciation. *Genetics*, 173(1), 419–434. <https://doi.org/10.1534/genetics.105.047985>
- Knief, U., Forstmeier, W., Pei, Y., Ihle, M., Wang, D., Martin, K., Opatová, P., Albrechtová, J., Wittig, M., Franke, A., Albrecht, T., & Kempnaers, B. (2017). A sex-chromosome inversion causes strong overdominance for sperm traits that affect siring success. *Nature Ecology & Evolution*, 1(8, 8), 1177–1184. <https://doi.org/10.1038/s41559-017-0236-1>
- Knief, U., Hemmrich-Stanisak, G., Wittig, M., Franke, A., Griffith, S. C., Kempnaers, B., & Forstmeier, W. (2016). Fitness consequences of polymorphic inversions in the zebra finch genome. *Genome Biology*, 17(1), 199. <https://doi.org/10.1186/s13059-016-1056-3>
- Koch, E. L., Morales, H. E., Larsson, J., Westram, A. M., Faria, R., Lemmon, A. R., Lemmon, E. M., Johannesson, K., & Butlin, R. K. (2021). Genetic variation for adaptive traits is associated with polymorphic inversions in *Littorina saxatilis*. *Evolution Letters*, 5(3), 196–213. <https://doi.org/10.1002/evl3.227>
- Koch, E. L., Ravinet, M., Westram, A. M., Johannesson, K., & Butlin, R. K. (2022). Genetic architecture of repeated phenotypic divergence in *Littorina saxatilis* ecotype evolution. *Evolution*, 76(10), 2332–2346. <https://doi.org/10.1111/evo.14602>
- Küpper, C., Stocks, M., Risse, J. E., dos Remedios, N., Farrell, L. L., McRae, S. B., Morgan, T. C., Karlionova, N., Pinchuk, P., Verkuil, Y. I., Kitaysky, A. S., Wingfield, J. C., Piersma, T., Zeng, K., Slate, J., Blaxter, M., Lank, D. B., & Burke, T. (2016). A supergene determines highly divergent male reproductive morphs in the ruff. *Nature*

- Genetics*, 48(1), 79–83. <https://doi.org/10.1038/ng.3443>
- Li, N., & Stephens, M. (2003). Modeling Linkage Disequilibrium and Identifying Recombination Hotspots Using Single-Nucleotide Polymorphism Data. *Genetics*, 165(4), 2213–2233. <https://www.genetics.org/content/165/4/2213>
- Liu, X., & Fu, Y.-X. (2020). Stairway Plot 2: Demographic history inference with folded SNP frequency spectra. *Genome Biology*, 21(1), 280. <https://doi.org/10.1186/s13059-020-02196-9>
- Lowry, D. B., & Willis, J. H. (2010). A Widespread Chromosomal Inversion Polymorphism Contributes to a Major Life-History Transition, Local Adaptation, and Reproductive Isolation. *PLOS Biology*, 8(9), e1000500. <https://doi.org/10.1371/journal.pbio.1000500>
- Malaspinas, A.-S., Westaway, M. C., Muller, C., Sousa, V. C., Lao, O., Alves, I., Bergström, A., Athanasiadis, G., Cheng, J. Y., Crawford, J. E., Heupink, T. H., Macholdt, E., Peischl, S., Rasmussen, S., Schiffels, S., Subramanian, S., Wright, J. L., Albrechtsen, A., Barbieri, C., et al. (2016). A genomic history of Aboriginal Australia. *Nature*, 538(7624), 207–214. <https://doi.org/10.1038/nature18299>
- Matschiner, M., Barth, J. M. I., Tørresen, O. K., Star, B., Baalsrud, H. T., Briec, M. S. O., Pampoulie, C., Bradbury, I., Jakobsen, K. S., & Jentoft, S. (2022). Supergene origin and maintenance in Atlantic cod. *Nature Ecology & Evolution*, 1–13. <https://doi.org/10.1038/s41559-022-01661-x>
- McVean, G. A. T., & Cardin, N. J. (2005). Approximating the coalescent with recombination. *Philosophical Transactions of the Royal Society B: Biological Sciences*, 360(1459), 1387–1393. <https://doi.org/10.1098/rstb.2005.1673>
- Nieberding, C., Morand, S., Libois, R., & Michaux, J. R. (2006). Parasites and the island syndrome: The colonization of the western Mediterranean islands by *Heligmosomoides polygyrus* (Dujardin, 1845). *Journal of Biogeography*, 33(7), 1212–1222. <https://doi.org/10.1111/j.1365-2699.2006.01503.x>
- Nosil, P., Soria-Carrasco, V., Villoutreix, R., De-la-Mora, M., de Carvalho, C., Parchman, T., Feder, J. L., & Gompert, Z. (2023). Complex evolutionary processes maintain an ancient chromosomal inversion. *Proceedings of the National Academy of Sciences of the United States of America*, 120(25), e2300673120. <https://doi.org/10.1073/pnas.2300673120>
- Raynal, L., Marin, J.-M., Pudlo, P., Ribatet, M., Robert, C. P., & Estoup, A. (2019). ABC random forests for Bayesian parameter inference. *Bioinformatics*, 35(10), 1720–1728. <https://doi.org/10.1093/bioinformatics/bty867>
- Sanchez-Donoso, I., Ravagni, S., Rodríguez-Teijeiro, J. D., Christmas, M. J., Huang, Y., Maldonado-Linares, A., Puigcerver, M., Jiménez-Blasco, I., Andrade, P., Gonçalves, D., Friis, G., Roig, I., Webster, M. T., Leonard, J. A., & Vilà, C. (2021). Massive genome inversion drives coexistence of divergent morphs in common quails. *Current Biology*, 32. <https://doi.org/10.1016/j.cub.2021.11.019>
- Schiffels, S., & Durbin, R. (2014). Inferring human population size and separation history from multiple genome sequences. *Nature Genetics*, 46(8), 919–925. <https://doi.org/10.1038/ng.3015>

- Schiffels, S., & Wang, K. (2020). MSMC and MSMC2: The Multiple Sequentially Markovian Coalescent. In J. Y. Dutheil (Ed.), *Statistical Population Genomics* (pp. 147–166). Springer US. https://doi.org/10.1007/978-1-0716-0199-0_7
- Shirihai, H., Gargallo, G., & Helbig, A. (2010). *Sylvia Warblers: Identification, taxonomy and phylogeny of the genus Sylvia*. Bloomsbury Publishing.
- Speidel, L., Forest, M., Shi, S., & Myers, S. R. (2019). A method for genome-wide genealogy estimation for thousands of samples. *Nature Genetics*, 51(9), 1321–1329. <https://doi.org/10.1038/s41588-019-0484-x>
- Todesco, M., Owens, G. L., Bercovich, N., L  gar  , J.-S., Soudi, S., Burge, D. O., Huang, K., Ostevik, K. L., Drummond, E. B. M., Imerovski, I., Lande, K., Pascual-Robles, M. A., Nanavati, M., Jahani, M., Cheung, W., Staton, S. E., Mu  os, S., Nielsen, R., Donovan, L. A., et al. (2020). Massive haplotypes underlie ecotypic differentiation in sunflowers. *Nature*, 584(7822, 7822), 602–607. <https://doi.org/10.1038/s41586-020-2467-6>
- Tuttle, E. M., Bergland, A. O., Korody, M. L., Brewer, M. S., Newhouse, D. J., Minx, P., Stager, M., Betuel, A. M., Cheviron, Z. A., Warren, W. C., Gonser, R. A., & Balakrishnan, C. N. (2016). Divergence and Functional Degradation of a Sex Chromosome-like Supergene. *Current Biology*, 26(3), 344–350. <https://doi.org/10.1016/j.cub.2015.11.069>

Supplementary Information

Shifting balancing selection on a chromosomal inversion in island populations

Jun Ishigohoka^{1,*}

Miriam Liedvogel^{1,2,3,*}

¹MPRG Behavioural Genomics, Max Planck Institute for Evolutionary Biology, 24306 Plön, Germany

²Institute of Avian Research, An der Vogelwarte 21, 26386 Wilhelmshaven, Germany

³Department of Biology and Environmental Sciences, Carl von Ossietzky Universität Oldenburg, Ammerländer Heerstraße 114-118, 26129 Oldenburg, Germany

* Correspondence: [Jun Ishigohoka <ishigohoka@evolbio.mpg.de>](mailto:ishigohoka@evolbio.mpg.de), [Miriam Liedvogel <liedvogel@evolbio.mpg.de>](mailto:liedvogel@evolbio.mpg.de)

Supplementary Table 1: Model selection of demography models by ABC-RF.

model	votes
1_1_1	3
1_1_2	52
1_2_1	0
1_2_2	25
2_1_1	45
2_1_2	600
2_2_1	35
2_2_2	240

Supplementary Table 2: Parameter estimation of demography by ABC-RF. N_{anc} is N_e of the ancestral population of all populations. N_{N0_i} ($i \in \{1, 2, 3, 5, 6, 7, 8, 9, 10\}$) is N_e of population i relative to N_{anc} . T_{geo} is the splitting time of Georgian population from the ancestral population. T_{split} is the splitting time of all other populations. mig_{i_j} ($((i, j) | i \neq j) \in \{1, 2, 3, 5, 6, 7, 8, 9, 10\}$) is the symmetrical migration rate (gene flow) between population i and j . 1 = Georgia. 2 = cont_medlong. 3 = cont_short. 5 = Canary. 6 = Madeira. 7 = Azores. 8 = Cape Verde. 9 = Mallorca. 10 = Crete.

parameter	expectation	median	q2.5	q97.5
N_{anc}	4.081e+05	4.253e+05	1.414e+05	9.495e+05
N_{N0_1}	2.137e+00	1.981e+00	1.033e+00	6.521e+00
N_{N0_2}	5.229e+00	4.799e+00	1.174e+00	3.750e+01
N_{N0_3}	1.364e+01	1.530e+01	1.240e+00	9.178e+01
N_{N0_5}	1.927e-01	1.964e-01	3.971e-02	8.624e-01
N_{N0_6}	5.200e-01	5.824e-01	1.603e-01	9.733e-01
N_{N0_7}	1.230e-01	1.193e-01	2.308e-02	7.256e-01
N_{N0_8}	2.064e-01	2.068e-01	4.244e-02	8.786e-01
N_{N0_9}	3.649e-01	3.553e-01	1.464e-01	8.920e-01
$N_{\text{N0}_{10}}$	2.385e-01	2.350e-01	9.489e-02	6.078e-01
T_{geo}	1.891e+05	2.120e+05	4.145e+04	3.907e+05
T_{split}	1.854e+04	1.704e+04	1.018e+04	5.056e+04
mig_{0_1}	1.174e-07	1.008e-07	1.239e-09	3.968e-05
mig_{1_0}	1.174e-07	1.139e-07	1.207e-09	3.340e-05
mig_{1_2}	1.823e-07	1.983e-07	1.270e-09	2.736e-05
mig_{2_1}	1.358e-07	1.334e-07	1.224e-09	2.815e-05
mig_{2_3}	5.528e-07	5.222e-07	1.304e-09	4.767e-04
mig_{3_2}	4.610e-07	4.181e-07	1.380e-09	4.518e-04
mig_{3_4}	2.046e-07	2.224e-07	1.275e-09	2.805e-05
mig_{4_3}	1.910e-07	2.068e-07	1.202e-09	2.663e-05
mig_{4_5}	4.489e-08	3.384e-08	1.159e-09	5.060e-06
mig_{4_6}	4.345e-08	3.441e-08	1.113e-09	5.193e-06
mig_{4_7}	4.629e-08	3.886e-08	1.098e-09	5.039e-06
mig_{4_8}	5.322e-08	4.937e-08	1.138e-09	4.884e-06
mig_{5_4}	5.647e-08	4.891e-08	1.151e-09	5.407e-06
mig_{5_6}	2.984e-05	3.510e-05	9.701e-07	2.091e-04
mig_{5_7}	3.252e-06	6.232e-06	3.634e-09	4.391e-05

parameter	expectation	median	q2.5	q97.5
mig_5_8	3.692e-06	7.108e-06	4.741e-09	4.214e-05
mig_6_4	5.918e-08	5.366e-08	1.157e-09	5.152e-06
mig_6_5	3.014e-05	3.599e-05	1.868e-06	1.909e-04
mig_6_7	3.557e-06	6.487e-06	4.653e-09	4.166e-05
mig_6_8	3.702e-06	6.704e-06	4.478e-09	4.285e-05
mig_7_4	4.997e-08	4.405e-08	1.127e-09	4.590e-06
mig_7_5	3.482e-06	5.910e-06	8.183e-09	4.399e-05
mig_7_6	3.561e-06	6.312e-06	5.950e-09	4.234e-05
mig_7_8	3.547e-05	4.116e-05	2.353e-06	1.978e-04

Supplementary Table 3: Model selection of balancing selection models by ABC-RF.

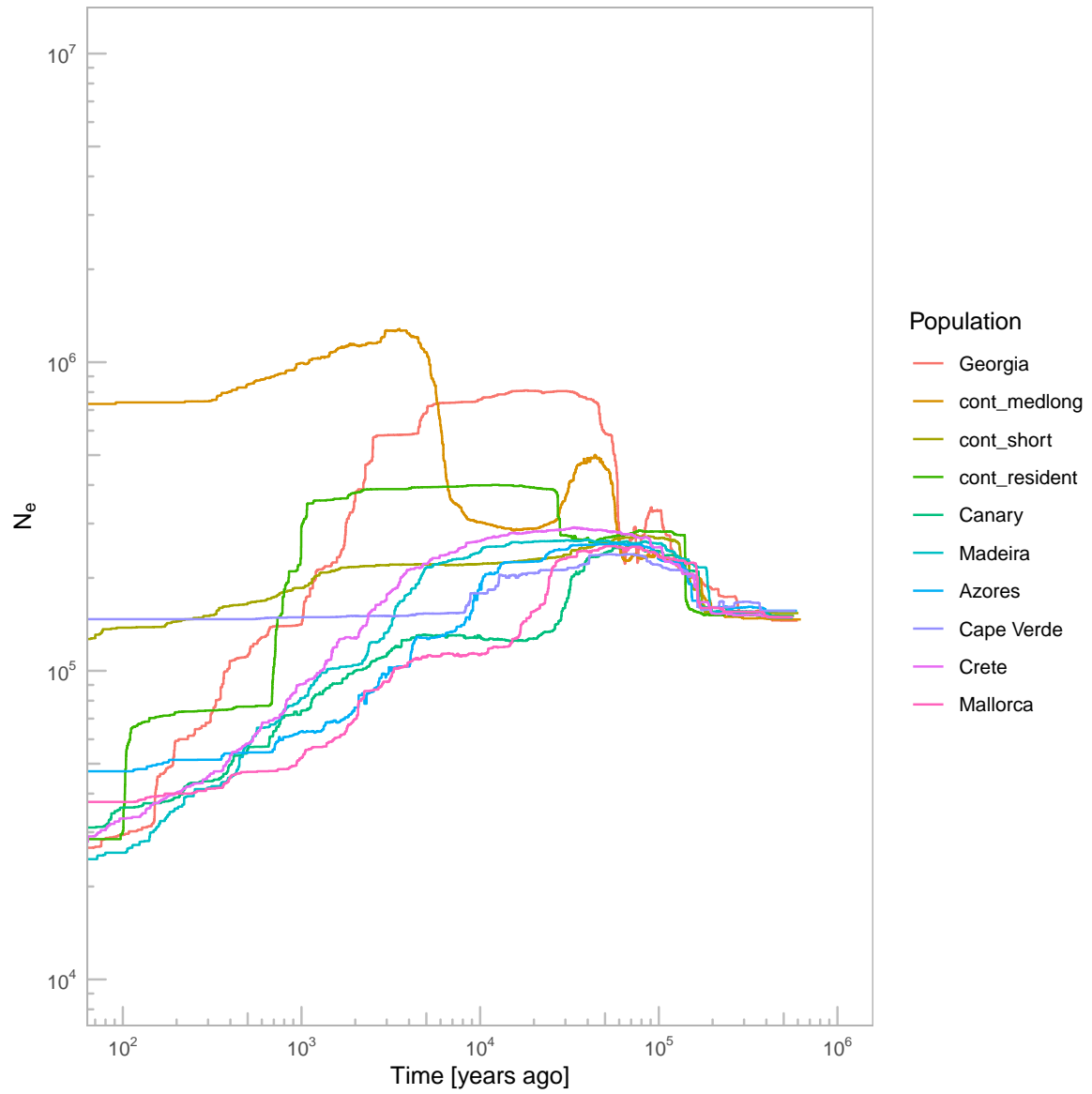
model	votes
neutral	48
OD	210
NFDS	742

Supplementary Table 4: Model selection of shifting NFDS scenarios by ABC-RF.

scenario	votes
scenario_1	48
scenario_2	232
scenario_3	518
scenario_4	202

Supplementary Table 5: Parameter estimation of shifting NFDS by ABC-RF.

parameter	expectation	median	q2.5	q97.5
s_cont	3.061e-04	5.283e-04	1.670e-07	4.693e-02
s_isl	1.321e-03	3.009e-03	2.669e-07	5.369e-02
p_opt_cont	2.657e-01	2.520e-01	1.420e-01	4.610e-01
p_opt_isl	8.560e-02	6.800e-02	4.000e-03	3.600e-01



Supplementary Figure 1: Demography inference with Stairway plot 2.

5

Differential Epigenetic Regulation Underlies Evolutionary Transition of Seasonal Migration

Space, and time. She was disconnected from both.

– Hiroshi Mori, *The Four Seasons - Green Spring* (2003)

Differential epigenetic regulation underlies evolutionary transition of seasonal migration

Jun Ishigohoka^{1,*}

Juan Sebastian Lugo Ramos^{1,4}

Gillian Durieux¹

Miriam Liedvogel^{1,2,3,*}

¹MPRG Behavioural Genomics, Max Planck Institute for Evolutionary Biology, Plön, Germany

²Institute of Avian Research, An der Vogelwarte 21, Wilhelmshaven, Germany

³Department of Biology and Environmental Sciences, Carl von Ossietzky Universität Oldenburg, Oldenburg, Germany

⁴Francis Crick Institute, Croydon, UK

* Correspondence: [Jun Ishigohoka <ishigohoka@evolbio.mpg.de>](mailto:ishigohoka@evolbio.mpg.de), [Miriam Liedvogel <liedvogel@evolbio.mpg.de>](mailto:liedvogel@evolbio.mpg.de)

Abstract

Seasonal migration is an ecologically and evolutionarily important behaviour found in various groups across the animal kingdom. Aspects of migratory behaviour, including propensity to migrate, can vary between and even within species. However, it is still unknown what evolutionary changes in cellular and molecular regulation underlie the divergence in the propensity to migrate. In vertebrates, the hypothalamus regulates physiology and behaviour by integrating the internal and environmental conditions, which makes it a strong candidate structure for seasonal regulation of the propensity to migrate. The hypothalamus consists of multiple nuclei, and different cell types within and across these nuclei regulate different physiology and behaviour. To understand the cell type-specific molecular regulation in the hypothalamus underlying diverged propensity to migrate between populations, we use the Eurasian blackcap (*Sylvia atricapilla*) system in Spain consisting of ancestral migrant and derived resident populations. These two populations are ideal to study differential epigenetic regulation because they remain hardly differentiated at the genomic level. Using single cell assay for transposase-accessible chromatin sequencing (scATAC-seq), we compare open chromatin regions of the genome between spring migratory and wintering (control) seasons as well as between populations at the single cell resolution. Seasonal changes in chromatin accessibility was reduced in the resident population in multiple cell types. The genomic positions of these regions are different between cell types. These results indicate that the evolution of reduced propensity to migrate in residents from ancestral migrants involves cell type-specific reduction of seasonal change in epigenetic states, which extends the threshold model of seasonal migration in the light of single cell epigenetics.

Introduction

Migration is a ubiquitous behavioural adaptation to shifting environmental conditions between seasons involving timed and oriented movement of animals (Dingle, 2014; Hansson & Åkesson, 2014; Liedvogel et al., 2011; Newton & Brockie, 2008). Migratory behaviour consists of multiple components, such as orientation and trajectory, distance and propensity, and timing of onset and offset, which vary between and even within species (Berthold, 1993, 1996; Dingle, 2014; Hansson & Åkesson, 2014; Liedvogel et al., 2011; Newton & Brockie, 2008). In Eurasian blackcaps (*Sylvia atricapilla*), multiple resident populations split from an ancestral migrant population as recent as 34,000 years ago (Chapter 4; Delmore et al., 2020; Ishigohoka & Liedvogel, 2024). Resident populations show much lower migratory propensity measured as the amount of nocturnal restlessness compared to migrants (Fig. 1B. Berthold & Querner, 1981; Berthold, 1993). Quantitative genetics and behavioural experiments show that this difference in migratory propensity has both genetic and environmental components (Berthold, 2003; Pulido et al., 1996; Pulido, 2011). However, the molecular and cellular mechanisms underlying this microevolutionary transition from migrants to residents are unknown.

The hypothalamus, with conserved anatomy and physiological functions across vertebrates (Fong et al., 2023), is a major candidate brain region regulating differential migratory propensity between migrants and residents during migratory season (Berthold, 1996; Dingle, 2014; Majumdar et al., 2021; Newton & Brockie, 2008; Rastogi et al., 2013; Sharma et al., 2021; Singh et al., 2020, 2020; Stevenson & Kumar, 2017). Multiple neuroendocrine systems are associated with regulation of physiology and behaviour relevant for migration, and they are centrally regulated at hypothalamic nuclei. First, migrants are characterised with elevated food intake associated with migration (“hyperphagia”) and migratory fattening (Berthold, 1993, 1996; Newton & Brockie, 2008; Ramenofsky, 1990; Wingfield et al., 1990), which can be regulated in the hypothalamus (Fong et al., 2023; Rastogi et al., 2013; Wingfield et al., 1990). Food intake is regulated by the balance between two types of neurons in the ARH (arcuate nucleus of hypothalamus), POMC neurons (expressing pro-opiomelanocortin) releasing α -MSH (α -melanocyte-stimulating hormone) and AgRP neurons (expressing agouti-related protein) releasing orexigenic neuropeptides (AgRP and NPY (neuropeptide Y)) and the inhibitory

neurotransmitter GABA (γ -aminobutyric acid) (Luo, 2016). Both POMC and AgRP neurons express leptin receptor and are regulated by circulating leptin from the adipose tissue (Luo, 2016). POMC and AgRP neurons project on target neurons in the PVH (paraventricular nucleus of hypothalamus) expressing MC4R, the receptor for α -MSH (Luo, 2016). Second, the timing of migratory behaviour in a year and a day are respectively regulated by circannual and circadian clocks (Bartell & Gwinner, 2005; Gwinner, 1990; Gwinner & Helm, 2003). In birds, the SCH (suprachiasmatic nucleus of hypothalamus) and the pineal gland are known circadian oscillators (Ebihara & Kawamura, 1981; Takahashi & Menaker, 1982). The circannual clock is entrained by the photoperiod (Gwinner, 1990). In mammals, a long-day photoperiod induces more heterogeneous phases of circadian activity among SCH neurons by spatial gradient in chloride ion channel activity among SCH neurons, causing some neurons to show ESPS (excitatory post-synaptic potentiation), instead of ISPS (inhibitory post-synaptic potentiation) by GABA (Farajnia et al., 2014; Myung et al., 2015; VanderLeest et al., 2007). Cell types switch between seasons in the PVH, causing seasonal difference in behaviour (Dulcis et al., 2013). Third, nocturnal migratory restlessness involves wakefulness and behavioural activity (Berthold, 1993, 1996). Wakefulness is regulated by orexin(hypocretin)-expressing neurons in the LHA (lateral hypothalamic area) projecting onto different regions in the brain in mammals (Luo, 2016; Sakurai, 2007), which is also known to regulate food intake, and somatostatin(Sst)-expressing neurons in the LHA induce behavioural activity (Mickelsen et al., 2019). Seasonal change in the environment may trigger the onset of migration through the stress response regulated along the hypothalamus-pituitary-adrenal axis (Hill et al., 2012). These functions of the hypothalamus can be differentially regulated between migrant and resident populations of blackcaps and between migratory and non-migratory seasons.

In this study, using a common-garden experiment, we characterise differential epigenetic regulation underlying different migratory propensity between migrant and resident blackcaps to understand regulatory mechanisms underlying evolutionary transition from migrants to residents. Importantly, the hypothalamus consists of multiple nuclei, each with different composition of cell types whose functions are specific to cell types and the nucleus (Fong et al., 2023; Luo, 2016). Because of this heterogeneity, we conduct molecular dissection of differential

regulation in the hypothalamus using a single cell epigenetics method.

Results

Study design

To investigate the mechanism of different levels of propensity to migrate between migrant and resident populations of blackcaps, a common-garden experiment was conducted using first-year juveniles caught in San Mames and Tarifa in Spain representing migrant and resident populations (Fig. 1A). Birds were kept singly in the aviary in Plön, Germany, where the light-dark cycle was simulated to reflect the seasonal change. Blackcaps showed diurnal behavioural activity outside the migratory season (“control”, Fig. 1B, Sup. Fig. 1), while migrants showed elevated nocturnal activity known as Zugunruhe (migratory restlessness) during spring migratory season (Fig. 1B, Sup. Fig. 1). In the control and migratory seasons, hypothalamus samples were micro-dissected and flash frozen (Fig. 1C). Nuclei were extracted from the frozen samples and scATAC-seq (single cell assay for transposase-accessible chromatin sequencing) was performed.

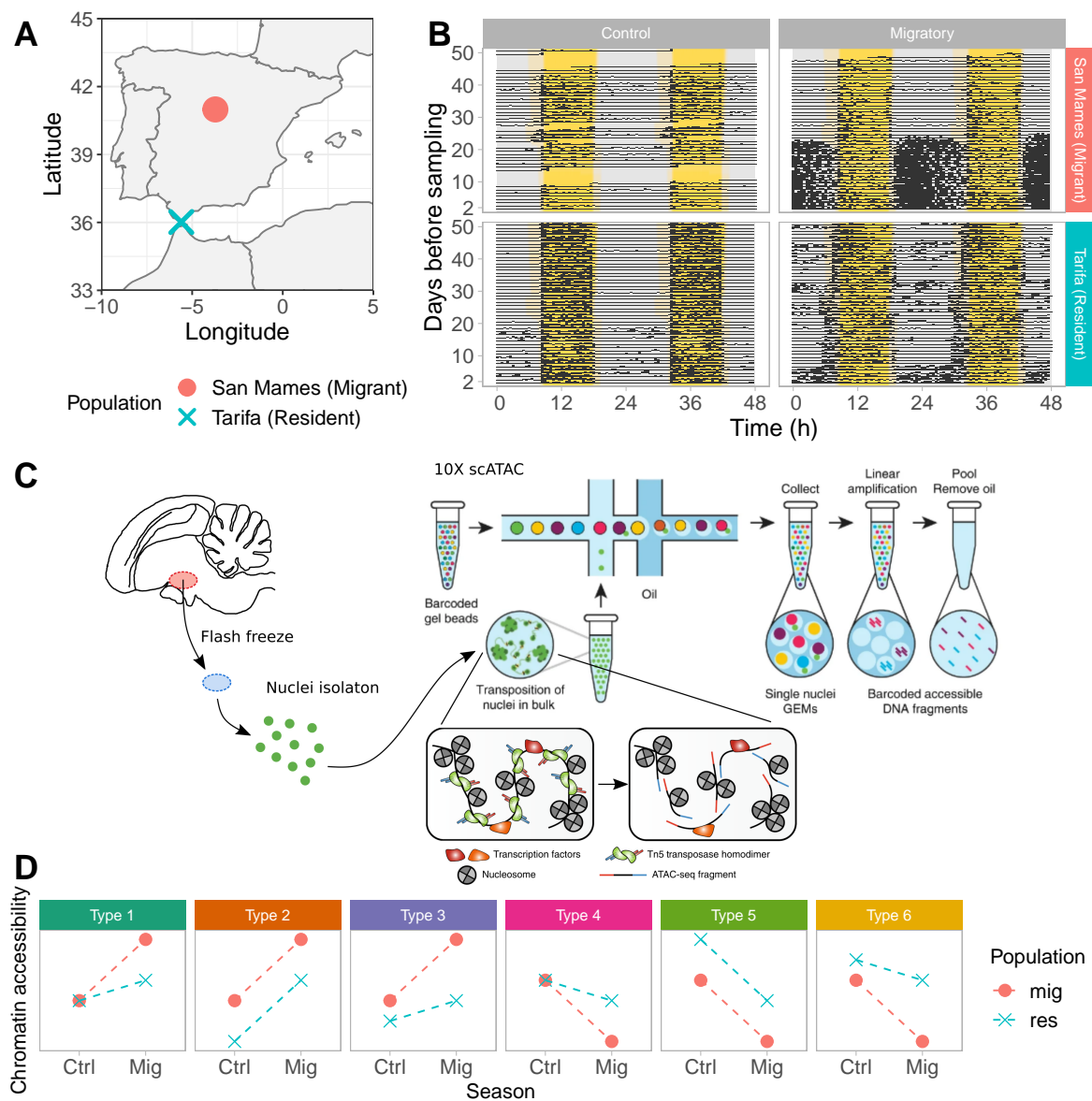


Figure 1: Experimental design. **A.** Geographic locations of migrant and resident blackcap populations used in this study. **B.** Double-plot actograms of blackcaps over 50 days until hypothalamus sampling. Two rows correspond to two populations. Two columns correspond to two seasons (control (the first winter) and migratory (the first spring)). Each panel exemplifies one individual representing one of the four conditions. In each panel, x-axis shows the time of two consecutive days (48 hours) and rows from top to bottom show consecutive days. Black bars show behavioural activity. The background colours from yellow to grey show light intensity (i.e. light-dark cycle). The migrant individual shows increased nocturnal activity (migratory restlessness: “Zugunruhe”) in the migratory season. **C.** Workflow of the experiment. Hypothalamus was micro-dissected and flash frozen. Nuclei were extracted from the frozen hypothalamus samples, and 10x scATAC was performed. **D.** Six types of differential regulation of chromatin accessibility between seasons and between populations focally evaluated in this study. Expression of migratory behaviour is assumed to depend on chromatin accessibility above (type 1-3) or below (type 4-6) a threshold (grey). In types 1-3, seasonal in the reference (migrant) population is positive, while it is negative in types 4-6. Types 1 and 4 have population-specific seasonal effects but no population effects in the reference (i.e. control) season. Types 2 and 5 have population effects in the control season without population-specific seasonal effects. Types 3 and 5 have both population effects in the control season and population-specific seasonal effects. Diagrams of 10x Chromium and tagmentation in **C** are adapted respectively from Satpathy et al. (2019) and Grandi et al. (2022).

scATAC-seq identifies major hypothalamic cell types

We identified 15 cell types in the scATAC-seq data. We initially called a total of 129,513 cells from ten samples (mean and SD per sample of 12,951.3 and 4517.0 cells) using **cellranger-atac** version 2.1.0 (10x Genomics), of which we kept 18,520 cells from nine samples for further analysis. Using a merged set of 98,934 peaks called by **cellranger-atac** for each sample, we first performed dimensionality reduction and clustering to identify 14 cell clusters (Sup. Fig. 2) using **Signac** (Stuart et al., 2021) and **Seurat** (Hao et al., 2021, 2024; Satija et al., 2015) with batch correction with **Harmony** (Korsunsky et al., 2019). We repeated the dimensionality and clustering using a new merged set of 149,005 peaks called by **MACS** (Zhang et al., 2008) for each cell cluster. This resulted in 15 cell clusters consisting of neurons (at least three clusters of glutamatergic (excitatory) and five GABAergic (inhibitory) neurons with one unclear type), astrocytes/adult neural stem cells, oligodendrocytes, oligodendrocyte precursor cells (OPC), microglia, and endothelial cells (Fig. 2, Table 1). Samples from the four groups were well mixed in each cell cluster allowing comparison between seasons and populations, except for clusters 3 and 4 (Sup. Fig. 3).

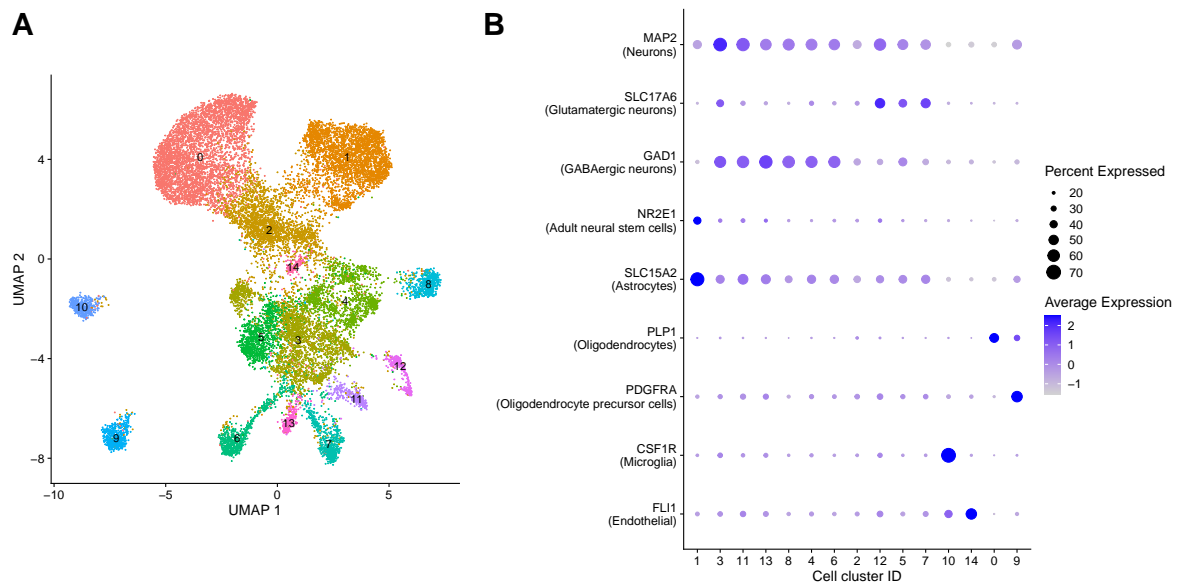


Figure 2: scATAC-seq identifies major cell types in blackcap hypothalamus. **A.** UMAP of scATAC-seq data (peak-by-cell matrix) of blackcap hypothalamus. Colours represent clusters of cells identified by a shared nearest neighbour (SNN) modularity optimization based on the SLM algorithm. **B.** Predicted expression of known cell type marker genes based on the sum of scATAC counts in pseudobulk per cell cluster.

Table 1: Cell type annotation based on predicted marker gene activity.

Index	Cell type
0	Oligodendrocyte
1	Astrocyte
2	Low-quality cells
3	Neuron (GABA)
4	Neuron (GABA)
5	Neuron (Glutamate)
6	Neuron (GABA)
7	Neuron (Glutamate)
8	Neuron (GABA)
9	Oligodendrocyte precursor cell
10	Microglia
11	Neuron (GABA)
12	Neuron (Glutamate)
13	Neuron (GABA)
14	Endothelial cell

Reduced seasonal change in cell type-specific chromatin accessibility in resident population

To assess differential regulation of chromatin accessibility in *cis* regulatory elements, we fitted the peak-by-cell count matrix for each cell type to a negative binomial generalised linear mixed-effect model (GLMM) using **Nebula** (He et al., 2021). Based on the sign of the coefficients depicting the effect of season (β_s), population (β_p) and interaction between season and population (β_{sp}), we assessed in each cell type whether a focal peak falls into one of the six types of differential regulation depicted in Fig. 1D. The seasonal change in chromatin accessibility between the control and migratory seasons was reduced in residents compared to migrants. We found a total of 33 peaks of type 1 differential accessibility in 9 cell types and

12 peaks of type 4 differential accessibility in 4 cell types (Fig. 3, Sup. Fig. 4). We did not find peaks of types 2, 3, 5, or 6 differential regulation in any cell types.

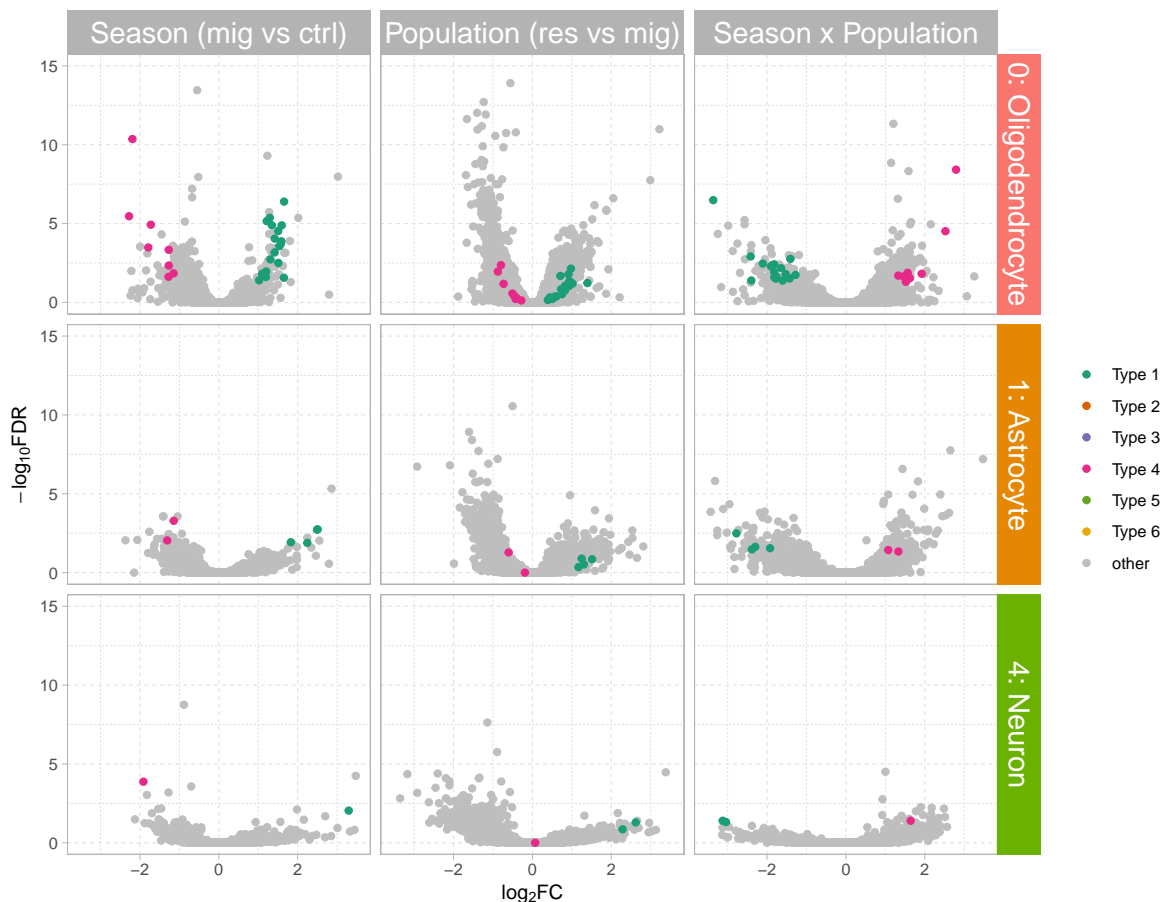


Figure 3: Reduced seasonal change in chromatin accessibility in resident *cis*-regulatory elements. Volcano plots showing effect of seasons, populations, and their interaction between seasons and populations (columns) on chromatin accessibility in three exemplified cell types (rows). In each panel, data points depict peaks of accessible chromatin (Tn5 integration events) corresponding to individual *cis* regulatory elements in a focal cell cluster. Peaks with differential regulation of type 1 and type 4 but not other types are found among the scATAC peaks.

To assess differential regulation of chromatin accessibility within sets of jointly regulated *cis* elements, we repeated negative binomial GLMM on *cis*-co-accessible networks (hereafter “domains”) of different cell types. Using Cicero, we identified on average 2286.2 *cis*-co-accessible domains per cell type (SD = 423.9) (Fig. 4A). We generated a domain-by-cell count matrix for each cell type based on the peak-by-cell matrix and the sets of constituent peaks of domains, and fitted it to a negative binomial generalised linear mixed-effect model (GLMM) using Nebula. We found 28 domains of type 1 differential regulation in two cell types (Fig. 4B).

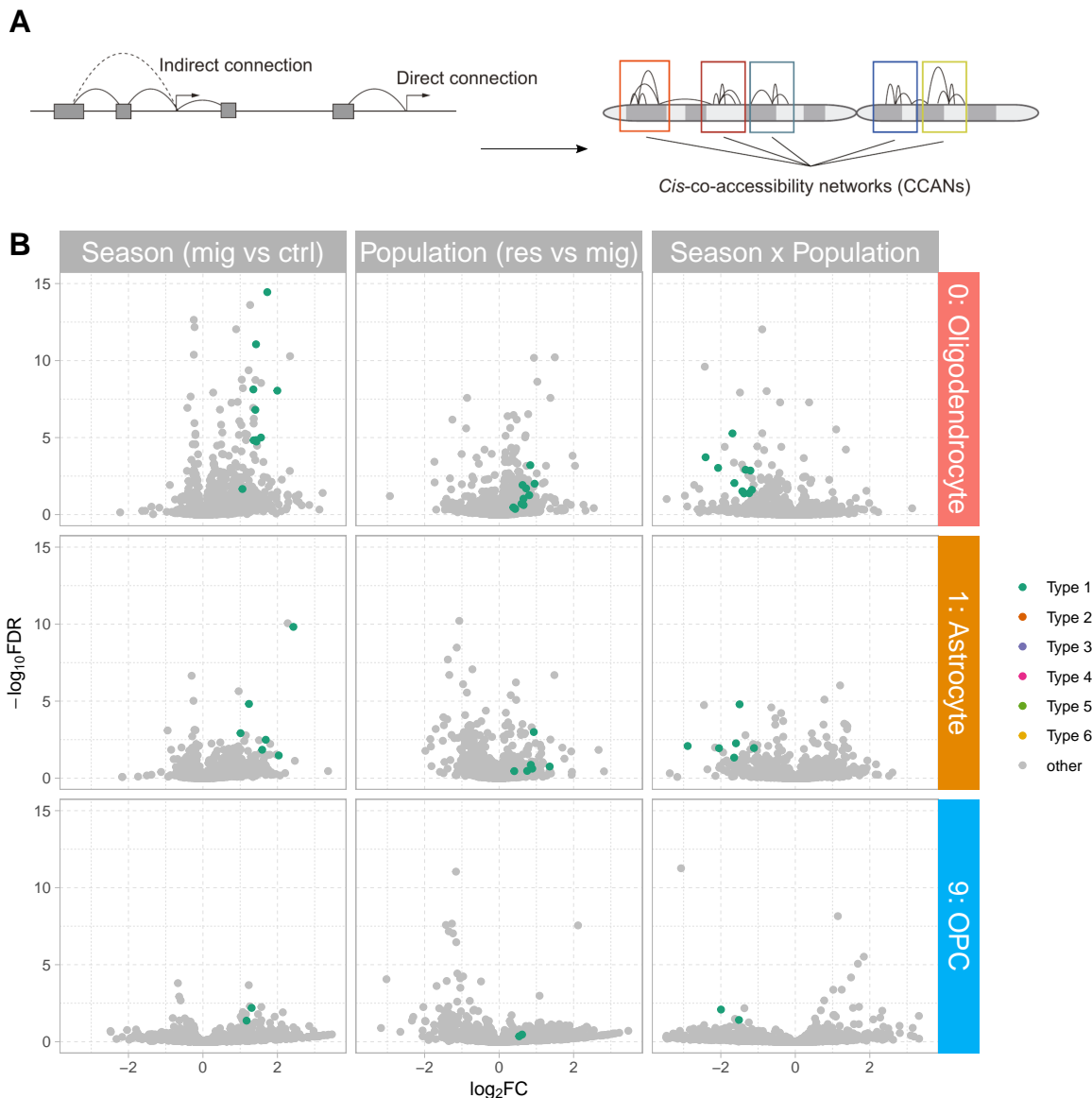


Figure 4: Reduced seasonal change in chromatin accessibility in resident *cis*-regulatory domains. **A.** Co-accessibility domains (a.k.a *cis*-co-accessibility networks (CCANs)) were identified for each cell cluster from the scATAC peak-by-cell matrix using *Cicero*. **B.** Volcano plots showing effect of seasons, populations, and their interaction (columns) on chromatin accessibility in three exemplified cell clusters (rows). In each panel, data points depict total accessibility (Tn5 integration events) within co-accessibility domains in a focal cell cluster. Domains with type 1 regulations but not other types are found among the scATAC peaks.

Differential regulation types of individual *cis* elements and joint *cis*-co-accessibility domains are inconsistent

To test whether individual *cis* elements of type 1 differential regulation are responsible for type 1 domains, we computed the proportion of type 1 peaks covered by type 1 domains for

each cell type. The overlap proportions were low (1.2% (cluster 0 oligodendrocytes), 10.2% (cluster 5 neurons), 4.2% (cluster 9 OPC)), and none were significant (Fisher’s exact tests, p values = 1). This result indicates that the differential regulation types of *cis*-coaccessibility domains are inconsistent with those of *cis*-regulatory elements.

Differential transcription factor footprinting analysis with cell type-specific pseudobulk data lack statistical power

To understand differential regulation of transcription factor (TF) binding, we performed transcription factor footprinting analysis. By modifying Bentsen et al. (2020), we quantified cell type-specific TF footprinting score for genomic positions of known TF motifs in each sample, treating all cells of a focal cell type from an individual as a pseudobulk ATAC-seq data (Fig. 5A). For each cell type of each sample, the local TF footprinting scores were quantified for every occurrence of motifs along the genome based on Tn5 bias-corrected accessibility (Fig. 5A). To estimate the effects of seasons, populations, and the interaction between seasons and populations, the footprint scores for each cell type were fitted to a linear mixed-effects model. For all cell types, no significant motifs were found. FDR of most motifs were 1, indicating this approach lacks statistical power.

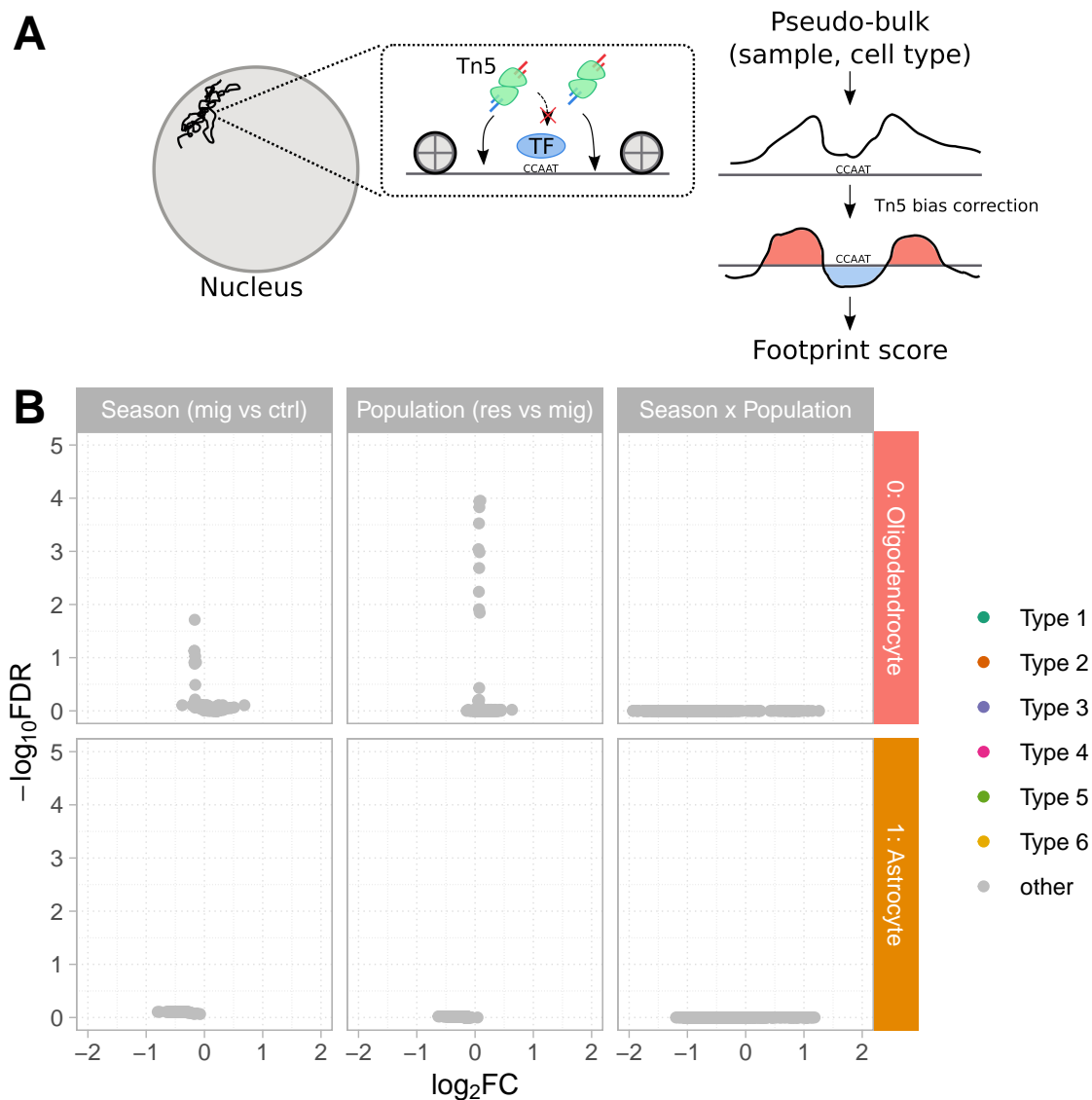


Figure 5: Differential transcription factor footprinting analysis. **A.** Schematics of transcription factor footprinting. **B.** Volcano plots showing effect of seasons, populations, and their interaction term (columns) on chromatin accessibility in two exemplified cell clusters (rows). Data points depict transcription factor binding motifs known in vertebrates.

Discussion

Extending the threshold model: Chromatin accessibility as a layer of liability complex of seasonal migration

By investigating single cell epigenomics of the hypothalamus of migrant and resident blackcaps in a common garden experiment, we found that seasonal change in chromatin accessibility

reduced in residents compared to migrants in a cell type-specific manner. Here, we will extend an evolutionary and quantitative genetic model of seasonal migration based on our findings.

Principal mechanisms underlying plastic expression of migratory behaviour have been explained by the polygenic threshold model of quantitative genetics (Pulido et al., 1996; Pulido, 2011). This model assumes an underlying continuously distributed latent variable (“liability”), and the threshold trait (such as migratory behaviour) is expressed in individuals whose liability exceeds a threshold value along the liability scale. Variation in liability among individuals consists of both genetic and environmental components, as well as their interaction term. The threshold model was first applied in migration research by Pulido et al. (1996) to understand the genetic basis of behavioural heterogeneity in a partial migrant population of blackcaps, in which individuals expressing migratory behaviour coexist with those not expressing it. In partial migrant populations, due to the genetic makeup of the population and the environment, the threshold is overlapped by the distribution of liability, leading to the variation in expression of migratory behaviour among individuals.

Reid & Acker (2022) combined the quantitative genetics of threshold traits with evolutionary theory of plastic traits, aligning evolutionary change in threshold traits with seasonal switches in phenotypes along the same liability scale. Reid & Acker (2022) explained variation in reversible and repeatable change in traits, such as seasonal migration, by the relationship between the reaction norm of liability (as a function of environment) and the threshold value along the liability scale. Individuals have reaction norms of liability of migration (due to genetic and environmental factors) differing in the intercept (e.g. liability in the “reference” season) and slope (e.g. amount to seasonal change in the liability). Within this framework, reaction norms of individuals from a resident population are below the threshold for all seasons, while reaction norms of liability in individuals from a migrant population cross the threshold line.

We propose that the liability of migration consists of multiple layers of biological processes — subcellular (epigenetic modifications, transcription, post-transcriptional regulation, translation, protein folding, protein localisation etc), physiological (endocrine and electrophysiological regulation), and behavioural (food intake, sleep, locomotor activity etc) aspects— collectively

representing a high-dimensional state of liability, which we term “liability complex”. Our finding of chromatin accessibility of *cis*-regulatory elements with types 1 and 4 differential regulation (both characterised with resident-specific reduction in seasonal change) and no elements with other types of differential regulation indicates that the evolution of migratory behaviour involves modification of the reaction norm (more specifically, the slope of the reaction norm) of the low-level liability of migration (Fig. 6). This interpretation is in line with the fact that the behavioural activity is not different between migrants and residents during the control season.

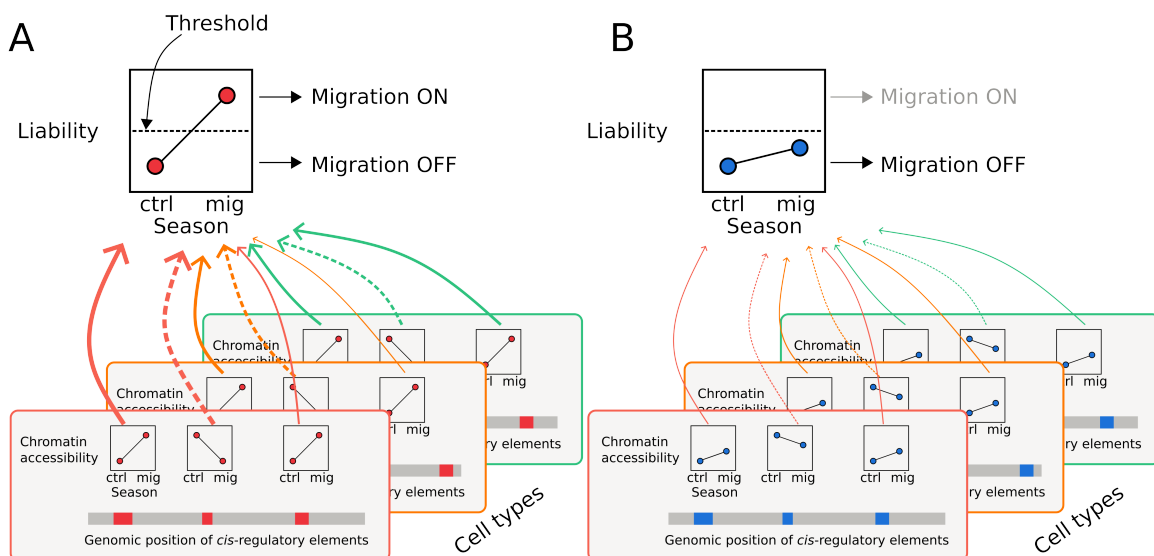


Figure 6: Modification of reaction norm underlying evolutionary change from migrants and residents. In migrants (**A**), chromatin at *cis*-regulatory elements/domains are differentially accessible between seasons in a cell type-specific manner (bottom). Each *cis*-regulatory element/domain contributes to the overall reaction norm of liability crossing the threshold (top). This results in expression of migratory behaviour during the migratory season. In residents (**B**), seasonal changes in chromatin accessibility at these genomic regions are reduced (bottom). As a result, the overall reaction norm of liability is below the threshold line in both control and migratory seasons, manifested as residency.

How do the evolution of reaction norms at the epigenetic level translate to those at higher levels? We expect that evolution of the reaction norm at the epigenetic level will relatively directly influence the reaction norm at the transcription level. This is because transcriptional activity is regulated by the local epigenetic states (Castro et al., 2019; Perino & Veenstra, 2016). However, the effect on the reaction norms at higher levels, even within the same cell (e.g. post-transcriptional regulation, translation, protein folding, and subcellular localisation),

is difficult to predict, because of complex interactions. Another related question is whether the effect of evolution of a reaction norm at a lower level (e.g. chromatin accessibility) gets amplified in a reaction norm at the higher level. Between the epigenetic and transcription levels, we suspect this is the case, because transcription of a gene is jointly regulated by multiple *cis*-regulatory elements, and the range of transcription level is much larger than that of chromatin accessibility. These questions should be studied in better controlled conditions using classical model systems for molecular genetics and epigenetics (e.g. *Drosophila melanogaster* or cell culture systems).

Different targets with shared rules

Multiple cell types, both neurons and glia, had *cis*-regulatory elements with population-specific reduction in seasonal change of chromatin accessibility. Genomic regions with this differential regulation were not shared across cell types. Based on this pattern, we postulate that different *cis*-regulatory elements may be differentially regulated among cell types following a shared rule. For example, a receptor of a hormone expressed in multiple cell types may be involved in this differential regulation. Although the downstream signalling pathway, including the target *cis*-regulatory elements, are differently wired between cell types, they respond similarly to differential regulation of the common ligand. Alternatively, the cells with shared type of differential regulation, including neurons and a subset of glia, may be located in a specific hypothalamic nuclei or a subregion of a nucleus, and they may be under correlated regulation via local cell-cell communication with a series of paracrine signalling. However, even if such a mechanism were to be found, it will be an open question how expression of the mechanism is differentially regulated in either case. Once a few important candidate mechanisms, such as ligands, are listed, more fine-tuned molecular and epigenetic study will be necessary to understand the molecular mechanism of the master regulators of differential regulation.

Redundancy may explain inconsistency in regulatory patterns between individual *cis*-regulatory elements and *cis*-coaccessibility domains

Individual *cis*-regulatory elements with types 1 and 4 differential regulation did not represent *cis*-coaccessibility domains with type 1 and 4 differential regulation. Although this could

be due to false negatives by small sample size, multiple *cis*-regulatory elements may have undetectable effects of differential regulation which collectively become detectable as a domain, and conversely, effects of individual *cis*-regulatory elements may be diluted out by undetectable levels of effects of other elements of the same domain. Multiple *cis*-regulatory elements jointly regulate expression of target genes (Frankel et al., 2011), and redundancy among *cis*-regulatory elements allows robustness of the expression of target genes (Osterwalder et al., 2018). Such effects of regulatory redundancy on developmental robustness have been focally studied in the context of mutational perturbation (Frankel et al., 2011; Osterwalder et al., 2018) and the same pattern can be extended to the epigenetic level. Co-regulation of some, but not necessarily all, of *cis*-regulatory elements may be important for regulation of target genes, and there may be some levels of freedom in the exact combination of *cis*-regulatory elements to be co-regulated. This freedom would cause variation in the combination of accessible *cis*-regulatory elements among cells for stable accessibility at the domain level.

Limitations

Our study suffers from the small sample size, leading both type 1 (false positive) and type 2 (false negative) errors. Adding more samples will be necessary to deal with this issue. However, the power analysis of the negative binomial GLMM used in this study (He et al., 2021) indicates that at least sample size of $n = 30$ is necessary to minimise the false positive rates for a simple differential analysis of two groups (compared to our design with two factors (seasons and populations) and their interaction term). Because of the limited availability of samples (both costs of running scATAC and the number of birds used for the common garden experiment), this problem cannot be solved within the practical ranges of sample size. Corroborating the scATAC-seq analysis with other experiments, such as scRNA-seq (Shafer et al., 2022; Wen et al., 2020) and sciHi-C (Stevens et al., 2017) will provide more holistic view of differential epigenetic and transcription regulation.

Our analysis of chromatin footprinting lacked statistical power. This is because all cells of a focal cell type in a focal individual were treated as a pseudobulk. As a possible solution, fewer cells could be downsampled to treat as smaller pseudobulks. This approach has been

utilised to account for batch effects by **Cicero** (Pliner et al., 2018), and could be implemented for the differential footprinting analysis.

Conclusion

By investigating epigenomic states of hypothalamic cells in migrant and resident birds in a common garden experiment, we found that seasonal change in chromatin accessibility reduced in residents compared to migrants in a cell type-specific manner. This evolutionary change in the reaction norm at the epigenetic level canalised the liability of migration at the epigenetic level, manifested as the lack of migratory propensity during migratory season. Shared pattern of differential regulation of different *cis*-regulatory elements and domains among multiple cell types indicates season-specific differential regulation of master regulator with different targets among cell types in the resident population. Such change in cell type-specific reaction norm of liability at the molecular level in the hypothalamus may be a common process underlying microevolution of seasonal behaviour.

Materials and Methods

Animals and housing

Juvenile blackcaps were caught in August 2017 in San Mames (migrants, $n = 26$ males) and Tarifa (residents, $n = 25$ males and $n = 5$ females) using mist nets before their first autumn migration season. These migration-naïve birds were transported to Max Planck Institute for Evolutionary Biology in Plön, Germany, where they were individually housed under controlled conditions of food and light-dark cycles of simulated photoperiod changing according to the time of the year.

Behavioural phenotyping and brain sampling

The behavioural activity of each individual was measured using motion sensors mounted in the cages. Sampling of individuals used for the scATAC-seq experiment was conducted in two seasons: control season (between 2018-01-24 and 2018-02-19) and migratory season (between 2018-04-02 and 2018-05-06). In both seasons, birds were sacrificed 1-3 hours after the

light-off. In the control season, lack of migratory restlessness was confirmed before sampling. In the migratory season, migratory restlessness was confirmed three consecutive nights before sampling. They were sacrificed by decapitation and the whole brain was immediately extracted.

The right hemisphere of the brain was placed on a tissue slicer (Stoeling) with Vetbond 3M tissue adhesive and the medial part of the brain facing the blade. Sagittal sections of 400 μm were obtained and placed in a clockwise fashion on a Petri dish with ice-cold PBS with complete proteinase inhibitor cocktail. From the most medial sections, the hypothalamus except for the anteroventral portion was obtained. The tissue samples were placed in separate Eppendorf tubes, and immediately flash frozen in dry ice. The samples were stored at $-70\text{ }^{\circ}\text{C}$ until ATAC-seq procedure.

Actograms were visualised using **zeitgebr** and **ggetho** packages from **Rethomics** platform (Geissmann et al., 2019). Based on the behaviour, recorded time of sampling, and visual inspection of tissue size, a total of 16 individuals (four samples per condition) were selected for scATAC-seq experiment.

scATAC-seq

Nuclei were extracted from frozen hypothalamus samples following 10x Genomics “Nuclei Isolation from Mouse Brain Tissue for Single Cell ATAC Sequencing” (document number CG000212 Rev C), and extracted nuclei were resuspended in 250 μL 1x wash buffer (10 mM Tris-HCl (pH 7.4), 10 mM NaCl, 3 mM MgCl_2 , 1% BSA, 0.1% Tween-20). To remove debris, nuclei in 250 μL of 1x wash buffer were mixed with 250 μL of 1.2 M sucrose (in 10 mM Tris-HCl (pH 7.4), 10 mM NaCl, 3 mM MgCl_2 , 1% BSA), and layered on 450 μL of 1.2 M sucrose, and the sucrose gradient was centrifuged at $7,000 \times g$ for 45 minutes at 4°C . The nuclei pellet was resuspended in 260 μL of 1x wash buffer, of which 10 μL was used for nuclei counting using haemocytometer with trypan blue. The nuclei resuspension in 1x wash buffer was centrifuged at $500 \times g$ for 10 minutes, then resuspended in 15 μL of 0.1x nuclei buffer (10x Genomics). Transposition, GEM generation and barcoding, post-GEM cleanup, and library construction were performed following 10x Genomics “Chromium Next GEM Single Cell ATAC Reagent Kits v2” (document number CG000496 Rev B). After quality check using

Qubit fluorometer, libraries of 10 samples were sequenced using Illumina NovaSeq 6000 at IKMB Institute of Clinical Molecular Biology Kiel.

Preparation of data

Alignment of reads to the blackcap reference (GenBank: GCA_009819655.1) and calling of cells and peaks were performed using 10x Genomics `cellranger-atac` (version 2.1.0) per sample. Using `Signac` (version 1.11.0) (Stuart et al., 2021) and `Seurat` (version 5.0.1) (Hao et al., 2021, 2024; Satija et al., 2015), and low-quality cells were removed keeping cells with the following criteria.

$$\log_{10}(\text{nCount_ATAC}) < \text{mean}(\log_{10}(\text{nCount_ATAC})) + 2\text{SD}(\log_{10}(\text{nCount_ATAC}))$$

$$\text{nCount_ATAC} > 1750$$

$$\log_{10}(\text{nFeature_ATAC}) < \text{mean}(\log_{10}(\text{nFeature_ATAC})) + 2\text{SD}(\log_{10}(\text{nFeature_ATAC}))$$

$$\log_{10}(\text{nFeature_ATAC}) > \text{mean}(\log_{10}(\text{nFeature_ATAC})) - 2\text{SD}(\log_{10}(\text{nFeature_ATAC}))$$

$$\text{TSS.enrichment} < \text{mean}(\text{TSS.enrichment}) + 2\text{SD}(\text{TSS.enrichment})$$

$$\text{TSS.enrichment} > \text{mean}(\text{TSS.enrichment}) + 2\text{SD}(\text{TSS.enrichment})$$

$$\text{nucleosome_signal} < \text{mean}(\text{nucleosome_signal}) + 2\text{SD}(\text{nucleosome_signal})$$

$$\text{nucleosome_signal} > \text{mean}(\text{nucleosome_signal}) - 2\text{SD}(\text{nucleosome_signal})$$

Latent semantic indexing (LSI) was performed using `RunTFIDF`, `FindTopFeatures`, and `RunSVD` functions. Batch effect in LSI was removed with `RunHarmony` function of `Harmony` (version 1.1.0) (Korsunsky et al., 2019). Using batch-corrected dimensions of LSI, non-linear dimensionality reduction and clustering were performed with `RunUMAP` (using 2nd to 30th LSI components), `FindNeighbors` (using 2nd to 30th LSI components), and `FindCluster` (with the smart local moving (SLM) algorithm and the resolution parameter of 0.5) functions of `Seurat`. To separate cell types with a small number of cells better in UMAP embedding, peaks were called again for each of 14 cell clusters using `CallPeaks` function of `Signac`, which wraps `MACS2` (Zhang et

al., 2008). Merged peak set and filtered cells were used to repeat the same process of merging, dimensionality reduction, embedding, and clustering. This yielded 15 cell clusters (Fig. 2A).

To identify which cell types the clusters correspond to, we computed predicted gene activity per cell based on accessibility within genes and their 2 kb upstreams using **GeneActivity** function of **Signac**, and normalised the predicted gene activity by the number of Tn5 integration events per cell (nCount_ATAC) and the length of genes (+ 2 kb upstream). Based on these normalised predictions of activity, we visualised gene activity of cell type markers (the same markers as used in (Colquitt et al., 2021)) across cell clusters using **DotPlot** function of **Seurat** (Fig. 2B).

Differentially accessible peaks

To characterise the effect at the level of peaks by seasons, populations and the interaction on chromatin accessibility in hypothalamus cell types accounting for random effects by samples and cells and heterogeneity in total Tn5 integration events per cell, we modelled the single cell accessibility data in peak-by-cell count matrix to negative binomial generalised linear mixed-effect models (NB-GLMM). Briefly, we focus on one cell type at a time, and we modelled accessibility score $y_{i,j,k}$ at peak i in cell j of sample k as

$$y_{i,j,k} \sim NB(\mu_i, d_i)$$

$$\ln(\mu_i) = \alpha_i + \ln(c_j) + \beta_{ssn,i}ssn + \beta_{pop,i}pop + \beta_{ssn,pop,i}ssn \times pop + a_j + a_k$$

$$a_j \sim N(0, \sigma_{a(cell)}^2)$$

$$a_k \sim N(0, \sigma_{a(sample)}^2)$$

where ssn denotes season (0 for control and 1 for migratory), pop denotes population (0 for migrant and 1 for resident), α_i denotes intercept (i.e. accessibility in control season in migrant), $\beta_{ssn,i}$ denotes the season effect of peak i , $\beta_{pop,i}$ denotes population effect of peak i , $\beta_{ssn,pop,i}$ denotes population-specific season effect at peak i , and c_j denotes the offset term (total accessibility) of cell j . a_j and a_k denote random effects of cell j and individual k , which

are distributed normally around 0 with variances $\sigma_{a(cell)}^2$ and $\sigma_{a(sample)}^2$.

We fitted the data to this model using **Nebula**. For each population, season, and interaction terms of each peak in each cell type, we applied thresholds of fold change > 2 or fold change $< \frac{1}{2}$ and FDR < 0.05 to designate significance. Based on three possible signs of population, season, and interaction terms (positive, negative, non-significant), we assigned six types of differential regulation (Fig. 1D) out of $3^3 = 27$ possible patterns of differential accessibility.

Differentially accessible domains

To characterise differentially accessibility at the level of *cis*-coaccessibility domains in each cell type, we first identified *cis*-coaccessibility domains. Briefly, a peak-by-cell count matrix was made for each cell type using `write10xCounts` function of **DropletUtils** package (Griffiths et al., 2018). We performed UMAP using `reduce_dimensions` function of **Cicero** with `reduction_method = 'UMAP'` and `preprocess_method = 'LSI'`. *Cis*-coaccessibility matrix was computed through downsampling based on the UMAP using `run_cicero` function of **Cicero**. *Cis*-coaccessibility domains were assigned to sets of peaks using `generate_ccan` function of **Cicero**. We created a domain-by-cell count matrix by summing accessibility counts for all peaks belonging to the same *cis*-coaccessibility domain for each cell. We performed negative binomial generalised linear mixed-effect models and identified domains with one of the six focal types of differential regulation the same way as above based on the domain-by-cell matrix using **Nebula**.

Differential transcription factor footprinting

To characterise differential binding of transcription factors by season, population, and their interaction in each cell type, we performed differential transcription factor footprinting analysis. We extended the approach of pairwise differential footprinting implemented in **TOBIAS** (Bentsen et al., 2020) to allow a mixed-effect model for characterisation of the effects of season, population, and their interaction accounting for random effects by samples in each cell type.

Briefly, we treated the alignment in each cell type of each sample as a pseudo-bulk,

measured footprinting score, and fitted a linear mixed-effect model. To generate pseudo-bulk data, we split an alignment file per sample in BAM format by cell types and samples using 10x Genomics `subset-bam` (version 1.1.0, <https://github.com/10xGenomics/subset-bam>). We identified motifs within the ATAC peaks by applying MOODS (Korhonen et al., 2009) with the JASPAR database for motifs known in vertebrates (version 2024. Rauluseviciute et al., 2024) on FASTA files containing sequences of ATAC peaks generated using `samtools faidx` (Danecek et al., 2021). We corrected for Tn5 integration bias using TOBIAS `ATACorrect`. We measured footprint score at each motif position of a peak for each sample with an algorithm modified from TOBIAS `ScoreBigWig`.

In TOBIAS `ScoreBigWig`, footprint score $F_{i,j}^*$ at position $x_{i,j}$ for the j -th instance out of n_i copies of the i -th motif M_i is defined as the maximum value of footprint scores $F_{i,j}(w_{f,\gamma}, w_{b,\delta})$ for all possible combinations of $w_{f,\gamma}$ base pair-wide foreground around position $x_{i,j}$ and $w_{b,\delta}$ base pair-wide background (flanking sequences) taken from pre-defined sets of widths ($w_{f,\gamma} \in W_f$ and $w_{b,\delta} \in W_b$)

$$F_{i,j}^* = \max_{\gamma, \delta} (F_{i,j}(w_{f,\gamma}, w_{b,\delta}))$$

The footprint score $F_{i,j}(w_{f,\gamma}, w_{b,\delta})$ for a pair of $w_{f,\gamma}$ and $w_{b,\delta}$ values is defined as the difference between excess of corrected accessibility in background $\bar{c}_b(x_{i,j}; w_{f,\gamma}, w_{b,\delta})$ and depletion (i.e. negative values) of corrected accessibility within the foreground $\bar{c}_f(x_{i,j}; w_{f,\gamma}, w_{b,\delta})$

$$F_{i,j}(w_{f,\gamma}, w_{b,\delta}) = \bar{c}_b(x_{i,j}; w_{f,\gamma}, w_{b,\delta}) - \bar{c}_f(x_{i,j}; w_{f,\gamma}, w_{b,\delta})$$

where the excess in the background and depletion in the foreground are computed by focusing on positive or negative corrected accessibility

$$\bar{c}_f(x_{i,j}; w_{f,\gamma}) = \frac{\sum_{w=0}^{w_{f,\gamma}} c_f(x_{i,j} + w)}{w_{f,\gamma}}$$

$$\bar{c}_b(x_{i,j}; w_{f,\gamma}, w_{b,\delta}) = \frac{\sum_{w=0}^{w_{b,\delta}} (c_b(x_{i,j} - w) + c_b(x_{i,j} + w_{f,\gamma} + w))}{2w_{b,\delta}}$$

$$c_b(x) = \begin{cases} c(x), & \text{if } c(x) > 0 \\ 0, & \text{otherwise} \end{cases}$$

$$c_f(x) = \begin{cases} c(x), & \text{if } c(x) > 0 \\ 0, & \text{otherwise} \end{cases}$$

where $c(x)$ denotes the corrected accessibility count at position x .

This approach in **TOBIAS** ignores positive corrected accessibility in the foreground and negative corrected accessibility in the background, potentially leading to an erroneous signals in regions with highly variable accessibility even with the mean of 0. To account for this, we simply modified the definitions of $c_b(x)$ and $c_f(x)$

$$c_b(x) = c_f(x) = c(x)$$

For each position $x_{i,j}$ of all motifs M_i ($1 \leq i \leq 879$) in JASPAR database for vertebrates (version 2024), footprint score $F_{i,j}^*$ was computed with $w_{f,\gamma} \in W_f = \{10, 20, 30, 40\}$ and $w_{b,\delta} \in W_b = \{10, 15, 20, 25, 30\}$ in each cell type in each sample using a custom python script. The computed set of footprint scores $F_i^* = \{F_{i,1}^*, F_{i,2}^*, \dots, F_{i,n_i}^*\}$ for motif M_i were fitted to the following linear mixed-effect model using **lme** function of **lme4** (Bates et al., 2015)

$$F_i^* \sim N(\mu_i, \sigma_i^2)$$

$$\mu_i = \alpha_i + \beta_{ssn,i}ssn + \beta_{pop,i}pop + \beta_{ssn,pop,i}ssn \times pop + a_k$$

$$a_k \sim N(0, \sigma_{a(sample)}^2)$$

where ssn denotes season (0 for control and 1 for migratory), pop denotes population (0 for migrant and 1 for resident), α_i denotes intercept (i.e. corrected footprint score in control season in migrant), $\beta_{ssn,i}$ denotes the season effect of motif M_i , $\beta_{pop,i}$ denotes population effect of motif M_i , $\beta_{ssn,pop,i}$ denotes population-specific season effect at motif M_i . a_k denotes random

effects of individual k , which is distributed normally around 0 with variance $\sigma_{a(sample)}^2$.

Acknowledgments

We thank Susanne Reinsch for field work for catching birds and transferring and taking care of them. We thank Kira Delmore for the field work, transfer of birds and helping animal care taking and tissue sampling. We thank Javier Pérez-Tris and Juan Carlos Illera for the field work. We thank Julien Dutheil for input on scATAC-seq design and sharing 10x Chromium. We thank Markéta Kaucká and Andrea Patricia Murillo Rincon for input on the design and technical support on scATAC-seq and providing us with reagents. We thank Diethard Tautz for sharing materials and IKMB for sequencing.

References

- Bartell, P. A., & Gwinner, E. (2005). A Separate Circadian Oscillator Controls Nocturnal Migratory Restlessness in the Songbird *Sylvia borin*. *Journal of Biological Rhythms*, 20(6), 538–549. <https://doi.org/10.1177/0748730405281826>
- Bates, D., Mächler, M., Bolker, B., & Walker, S. (2015). Fitting Linear Mixed-Effects Models Using lme4. *Journal of Statistical Software*, 67, 1–48. <https://doi.org/10.18637/jss.v067.i01>
- Bentsen, M., Goymann, P., Schultheis, H., Klee, K., Petrova, A., Wiegandt, R., Fust, A., Preussner, J., Kuenne, C., Braun, T., Kim, J., & Looso, M. (2020). ATAC-seq footprinting unravels kinetics of transcription factor binding during zygotic genome activation. *Nature Communications*, 11(1, 1), 4267. <https://doi.org/10.1038/s41467-020-18035-1>
- Berthold, P. (1993). *Bird Migration: A General Survey* (1st ed.). Oxford University Press.
- Berthold, P. (1996). *Control of Bird Migration*. Chapman & Hall.
- Berthold, P. (2003). Genetic Basis and Evolutionary Aspects of Bird Migration. In *Advances in the Study of Behavior* (Vol. 33, pp. 175–229). Academic Press. [https://doi.org/10.1016/S0065-3454\(03\)33004-9](https://doi.org/10.1016/S0065-3454(03)33004-9)
- Berthold, P., & Querner, U. (1981). Genetic Basis of Migratory Behavior in European Warblers. *Science*, 212(4490), 77–79. <https://doi.org/10.1126/science.212.4490.77>
- Castro, J. P., Yancoskie, M. N., Marchini, M., Belohlavy, S., Hiramatsu, L., Kučka, M., Beluch, W. H., Naumann, R., Skuplik, I., Cobb, J., Barton, N. H., Rolian, C., & Chan, Y. F. (2019). An integrative genomic analysis of the Longshanks selection experiment for longer limbs in mice. *eLife*, 8, e42014. <https://doi.org/10.7554/eLife.42014>
- Colquitt, B. M., Merullo, D. P., Konopka, G., Roberts, T. F., & Brainard, M. S. (2021). Cellular transcriptomics reveals evolutionary identities of songbird vocal circuits. *Science*, 371(6530), eabd9704. <https://doi.org/10.1126/science.abd9704>
- Danecek, P., Bonfield, J. K., Liddle, J., Marshall, J., Ohan, V., Pollard, M. O., Whitwham, A., Keane, T., McCarthy, S. A., Davies, R. M., & Li, H. (2021). Twelve years of SAMtools and BCFtools. *GigaScience*, 10(giab008). <https://doi.org/10.1093/gigascience/giab008>
- Delmore, K., Illera, J. C., Pérez-Tris, J., Segelbacher, G., Lugo Ramos, J. S., Durieux, G., Ishigohoka, J., & Liedvogel, M. (2020). The evolutionary history and genomics of European blackcap migration. *eLife*, 9, e54462. <https://doi.org/10.7554/eLife.54462>
- Dingle, H. (2014). *Migration: The Biology of Life on the Move* (2nd ed.). Oxford University Press.
- Dulcis, D., Jamshidi, P., Leutgeb, S., & Spitzer, N. C. (2013). Neurotransmitter Switching in the Adult Brain Regulates Behavior. *Science*. <https://doi.org/10.1126/science.1234152>
- Ebihara, S., & Kawamura, H. (1981). The role of the pineal organ and the suprachiasmatic nucleus in the control of circadian locomotor rhythms in the Java sparrow, Padda

- oryzivora. *Journal of Comparative Physiology*, 141(2), 207–214. <https://doi.org/10.1007/BF01342667>
- Farajnia, S., Westering, T. van, Meijer, J. H., & Michel, S. (2014). Seasonal induction of GABAergic excitation in the central mammalian clock. *Proceedings of the National Academy of Sciences*, 111(26), 9627–9632. <https://doi.org/10.1073/pnas.1319820111>
- Fong, H., Zheng, J., & Kurrasch, D. (2023). The structural and functional complexity of the integrative hypothalamus. *Science*, 382(6669), 388–394. <https://doi.org/10.1126/science.adh8488>
- Frankel, N. S., Erezylmaz, D. F., McGregor, A. P., Wang, S., Payre, F., & Stern, D. L. (2011). Morphological evolution caused by many subtle-effect substitutions in regulatory DNA. *Nature*, 474(7353), 598–603. <https://doi.org/10.1038/nature10200>
- Geissmann, Q., Rodriguez, L. G., Beckwith, E. J., & Gilestro, G. F. (2019). Rethomics: An R framework to analyse high-throughput behavioural data. *PLOS ONE*, 14(1), e0209331. <https://doi.org/10.1371/journal.pone.0209331>
- Grandi, F. C., Modi, H., Kampman, L., & Corces, M. R. (2022). Chromatin accessibility profiling by ATAC-seq. *Nature Protocols*, 17(6, 6), 1518–1552. <https://doi.org/10.1038/s41596-022-00692-9>
- Griffiths, J. A., Richard, A. C., Bach, K., Lun, A. T. L., & Marioni, J. C. (2018). Detection and removal of barcode swapping in single-cell RNA-seq data. *Nature Communications*, 9(1), 2667. <https://doi.org/10.1038/s41467-018-05083-x>
- Gwinner, E. (1990). Circannual Rhythms in Bird Migration: Control of Temporal Patterns and Interactions with Photoperiod. In *Bird Migration: Physiology and Ecophysiology*. Springer-Verlag.
- Gwinner, E., & Helm, B. (2003). Circannual and Circadian Contributions to the Timing of Avian Migration. In P. Berthold, E. Gwinner, & E. Sonnenschein (Eds.), *Avian Migration* (pp. 81–95). Springer. https://doi.org/10.1007/978-3-662-05957-9_5
- Hansson, L. A., & Åkesson, S. (Eds.). (2014). *Animal Movement Across Scales*. Oxford University Press.
- Hao, Y., Hao, S., Andersen-Nissen, E., Mauck, W. M., Zheng, S., Butler, A., Lee, M. J., Wilk, A. J., Darby, C., Zager, M., Hoffman, P., Stoeckius, M., Papalexi, E., Mimitou, E. P., Jain, J., Srivastava, A., Stuart, T., Fleming, L. M., Yeung, B., et al. (2021). Integrated analysis of multimodal single-cell data. *Cell*, 184(13), 3573–3587.e29. <https://doi.org/10.1016/j.cell.2021.04.048>
- Hao, Y., Stuart, T., Kowalski, M. H., Choudhary, S., Hoffman, P., Hartman, A., Srivastava, A., Molla, G., Madad, S., Fernandez-Granda, C., & Satija, R. (2024). Dictionary learning for integrative, multimodal and scalable single-cell analysis. *Nature Biotechnology*, 42(2), 293–304. <https://doi.org/10.1038/s41587-023-01767-y>
- He, L., Davila-Velderrain, J., Sumida, T. S., Hafler, D. A., Kellis, M., & Kulminski, A. M. (2021). NEBULA is a fast negative binomial mixed model for differential or co-expression analysis of large-scale multi-subject single-cell data. *Communications Biology*, 4(1, 1), 1–17. <https://doi.org/10.1038/s42003-021-02146-6>

- Hill, R. W., Wyse, G. A., & Anderson, M. (2012). *Animal Physiology* (3rd ed.). Sinauer Associates, Inc. Publishers.
- Ishigohoka, J., & Liedvogel, M. (2024, February 8). *High-recombining genomic regions affect demography inference*. <https://doi.org/10.1101/2024.02.05.579015>
- Korhonen, J., Martinmäki, P., Pizzi, C., Rastas, P., & Ukkonen, E. (2009). MOODS: Fast search for position weight matrix matches in DNA sequences. *Bioinformatics*, *25*(23), 3181–3182. <https://doi.org/10.1093/bioinformatics/btp554>
- Korsunsky, I., Millard, N., Fan, J., Slowikowski, K., Zhang, F., Wei, K., Baglaenko, Y., Brenner, M., Loh, P.-r., & Raychaudhuri, S. (2019). Fast, sensitive and accurate integration of single-cell data with Harmony. *Nature Methods*, *16*(12), 1289–1296. <https://doi.org/10.1038/s41592-019-0619-0>
- Liedvogel, M., Åkesson, S., & Bensch, S. (2011). The genetics of migration on the move. *Trends in Ecology and Evolution*, *26*(11), 561–569. <https://doi.org/10.1016/j.tree.2011.07.009>
- Luo, L. (2016). *Principles of neurobiology*. Garland Science.
- Majumdar, G., Yadav, G., Malik, S., Rani, S., Balthazart, J., & Kumar, V. (2021). Hypothalamic plasticity in response to changes in photoperiod and food quality: An adaptation to support pre-migratory fattening in songbirds? *European Journal of Neuroscience*, *53*(2), 430–448. <https://doi.org/10.1111/ejn.14994>
- Mickelsen, L. E., Bolisetty, M., Chimileski, B. R., Fujita, A., Beltrami, E. J., Costanzo, J. T., Naparstek, J. R., Robson, P., & Jackson, A. C. (2019). Single-cell transcriptomic analysis of the lateral hypothalamic area reveals molecularly distinct populations of inhibitory and excitatory neurons. *Nature Neuroscience*, *22*(4, 4), 642–656. <https://doi.org/10.1038/s41593-019-0349-8>
- Myung, J., Hong, S., DeWoskin, D., Schutter, E. D., Forger, D. B., & Takumi, T. (2015). GABA-mediated repulsive coupling between circadian clock neurons in the SCN encodes seasonal time. *Proceedings of the National Academy of Sciences*, *112*(29), E3920–E3929. <https://doi.org/10.1073/pnas.1421200112>
- Newton, I., & Brockie, K. (2008). *The Migration Ecology of Birds*. Academic Press.
- Osterwalder, M., Barozzi, I., Tissi eres, V., Fukuda-Yuzawa, Y., Mannion, B. J., Afzal, S. Y., Lee, E. A., Zhu, Y., Plajzer-Frick, I., Pickle, C. S., Kato, M., Garvin, T. H., Pham, Q. T., Harrington, A. N., Akiyama, J. A., Afzal, V., Lopez-Rios, J., Dickel, D. E., Visel, A., & Pennacchio, L. A. (2018). Enhancer redundancy provides phenotypic robustness in mammalian development. *Nature*, *554*(7691), 239–243. <https://doi.org/10.1038/nature25461>
- Perino, M., & Veenstra, G. J. C. (2016). Chromatin Control of Developmental Dynamics and Plasticity. *Developmental Cell*, *38*(6), 610–620. <https://doi.org/10.1016/j.devcel.2016.08.004>
- Pliner, H. A., Packer, J. S., McFaline-Figueroa, J. L., Cusanovich, D. A., Daza, R. M., Aghamirzaie, D., Srivatsan, S., Qiu, X., Jackson, D., Minkina, A., Adey, A. C., Steemers, F. J., Shendure, J., & Trapnell, C. (2018). Cicero Predicts cis-Regulatory DNA

- Interactions from Single-Cell Chromatin Accessibility Data. *Molecular Cell*, 71(5), 858–871.e8. <https://doi.org/10.1016/j.molcel.2018.06.044>
- Pulido, F. (2011). Evolutionary genetics of partial migration – the threshold model of migration revisited. *Oikos*, 120(12), 1776–1783. <https://doi.org/10.1111/j.1600-0706.2011.19844.x>
- Pulido, F., Berthold, P., & van Noordwijk, A. (1996). Frequency of migrants and migratory activity are genetically correlated in a bird population: Evolutionary implications. *Proceedings of the National Academy of Sciences*, 93(25), 14642–14647. <https://doi.org/10.1073/pnas.93.25.14642>
- Ramenofsky, M. (1990). Fat Storage and Fat Metabolism in Relation to Migration. In E. Gwinner (Ed.), *Bird Migration* (pp. 214–231). Springer. https://doi.org/10.1007/978-3-642-74542-3_15
- Rastogi, A., Kumari, Y., Rani, S., & Kumar, V. (2013). Neural Correlates of Migration: Activation of Hypothalamic Clock(s) in and out of Migratory State in the Blackheaded Bunting (*Emberiza melanocephala*). *PLoS ONE*, 8(10), 1–12. <https://doi.org/10.1371/journal.pone.0070065>
- Rauluseviciute, I., Riudavets-Puig, R., Blanc-Mathieu, R., Castro-Mondragon, J. A., Ferenc, K., Kumar, V., Lemma, R. B., Lucas, J., Chèneby, J., Baranasic, D., Khan, A., Fornes, O., Gundersen, S., Johansen, M., Hovig, E., Lenhard, B., Sandelin, A., Wasserman, W. W., Parcy, F., & Mathelier, A. (2024). JASPAR 2024: 20th anniversary of the open-access database of transcription factor binding profiles. *Nucleic Acids Research*, 52(D1), D174–D182. <https://doi.org/10.1093/nar/gkad1059>
- Reid, J. M., & Acker, P. (2022). Properties of phenotypic plasticity in discrete threshold traits. *Evolution*, 76(2), 190–206. <https://doi.org/10.1111/evo.14408>
- Sakurai, T. (2007). The neural circuit of orexin (hypocretin): Maintaining sleep and wakefulness. *Nature Reviews Neuroscience*, 8(3), 171–181. <https://doi.org/10.1038/nrn2092>
- Satija, R., Farrell, J. A., Gennert, D., Schier, A. F., & Regev, A. (2015). Spatial reconstruction of single-cell gene expression data. *Nature Biotechnology*, 33(5), 495–502. <https://doi.org/10.1038/nbt.3192>
- Satpathy, A. T., Granja, J. M., Yost, K. E., Qi, Y., Meschi, F., McDermott, G. P., Olsen, B. N., Mumbach, M. R., Pierce, S. E., Corces, M. R., Shah, P., Bell, J. C., Jhuttu, D., Nemec, C. M., Wang, J., Wang, L., Yin, Y., Giresi, P. G., Chang, A. L. S., et al. (2019). Massively parallel single-cell chromatin landscapes of human immune cell development and intratumoral T cell exhaustion. *Nature Biotechnology*, 37(8), 925–936. <https://doi.org/10.1038/s41587-019-0206-z>
- Shafer, M. E. R., Sawh, A. N., & Schier, A. F. (2022). Gene family evolution underlies cell-type diversification in the hypothalamus of teleosts. *Nature Ecology & Evolution*, 6(1), 63–76. <https://doi.org/10.1038/s41559-021-01580-3>
- Sharma, A., Das, S., Sur, S., Tiwari, J., Chaturvedi, K., Agarwal, N., Malik, S., Rani, S., & Kumar, V. (2021). Photoperiodically driven transcriptome-wide changes in the

- hypothalamus reveal transcriptional differences between physiologically contrasting seasonal life-history states in migratory songbirds. *Scientific Reports*, 11(1, 1), 12823. <https://doi.org/10.1038/s41598-021-91951-4>
- Singh, O., Agarwal, N., Yadav, A., Basu, S., Malik, S., Rani, S., Kumar, V., & Singru, P. S. (2020). Concurrent changes in photoperiod-induced seasonal phenotypes and hypothalamic CART peptide-containing systems in night-migratory redheaded buntings. *Brain Structure and Function*, 225(9), 2775–2798. <https://doi.org/10.1007/s00429-020-02154-y>
- Stevens, T. J., Lando, D., Basu, S., Atkinson, L. P., Cao, Y., Lee, S. F., Leeb, M., Wohlfahrt, K. J., Boucher, W., O’Shaughnessy-Kirwan, A., Cramard, J., Faure, A. J., Ralser, M., Blanco, E., Morey, L., Sansó, M., Palayret, M. G. S., Lehner, B., Di Croce, L., et al. (2017). 3D structures of individual mammalian genomes studied by single-cell Hi-C. *Nature*, 544(7648), 59–64. <https://doi.org/10.1038/nature21429>
- Stevenson, T. J., & Kumar, V. (2017). Neural control of daily and seasonal timing of songbird migration. *Journal of Comparative Physiology A*, 203(6), 399–409. <https://doi.org/10.1007/s00359-017-1193-5>
- Stuart, T., Srivastava, A., Madad, S., Lareau, C. A., & Satija, R. (2021). Single-cell chromatin state analysis with Signac. *Nature Methods*, 18(11, 11), 1333–1341. <https://doi.org/10.1038/s41592-021-01282-5>
- Takahashi, J. S., & Menaker, M. (1982). Role of the suprachiasmatic nuclei in the circadian system of the house sparrow, *Passer domesticus*. *Journal of Neuroscience*, 2(6), 815–828. <https://doi.org/10.1523/JNEUROSCI.02-06-00815.1982>
- VanderLeest, H. T., Houben, T., Michel, S., Deboer, T., Albus, H., Vansteensel, M. J., Block, G. D., & Meijer, J. H. (2007). Seasonal Encoding by the Circadian Pacemaker of the SCN. *Current Biology*, 17(5), 468–473. <https://doi.org/10.1016/j.cub.2007.01.048>
- Wen, S., Ma, D., Zhao, M., Xie, L., Wu, Q., Gou, L., Zhu, C., Fan, Y., Wang, H., & Yan, J. (2020). Spatiotemporal single-cell analysis of gene expression in the mouse suprachiasmatic nucleus. *Nature Neuroscience*, 23(3, 3), 456–467. <https://doi.org/10.1038/s41593-020-0586-x>
- Wingfield, J. C., Schwabl, H., & Mattocks, P. W. (1990). Endocrine Mechanisms of Migration. In E. Gwinner (Ed.), *Bird Migration* (pp. 232–256). Springer. https://doi.org/10.1007/978-3-642-74542-3_16
- Zhang, Y., Liu, T., Meyer, C. A., Eeckhoutte, J., Johnson, D. S., Bernstein, B. E., Nusbaum, C., Myers, R. M., Brown, M., Li, W., & Liu, X. S. (2008). Model-based Analysis of ChIP-Seq (MACS). *Genome Biology*, 9(9), R137. <https://doi.org/10.1186/gb-2008-9-9-r137>

Supplementary Information

Differential epigenetic regulation underlies evolutionary transition of seasonal migration

Jun Ishigohoka^{1,*}

Juan Sebastian Lugo Ramos^{1,4}

Gillian Durieux¹

Miriam Liedvogel^{1,2,3,*}

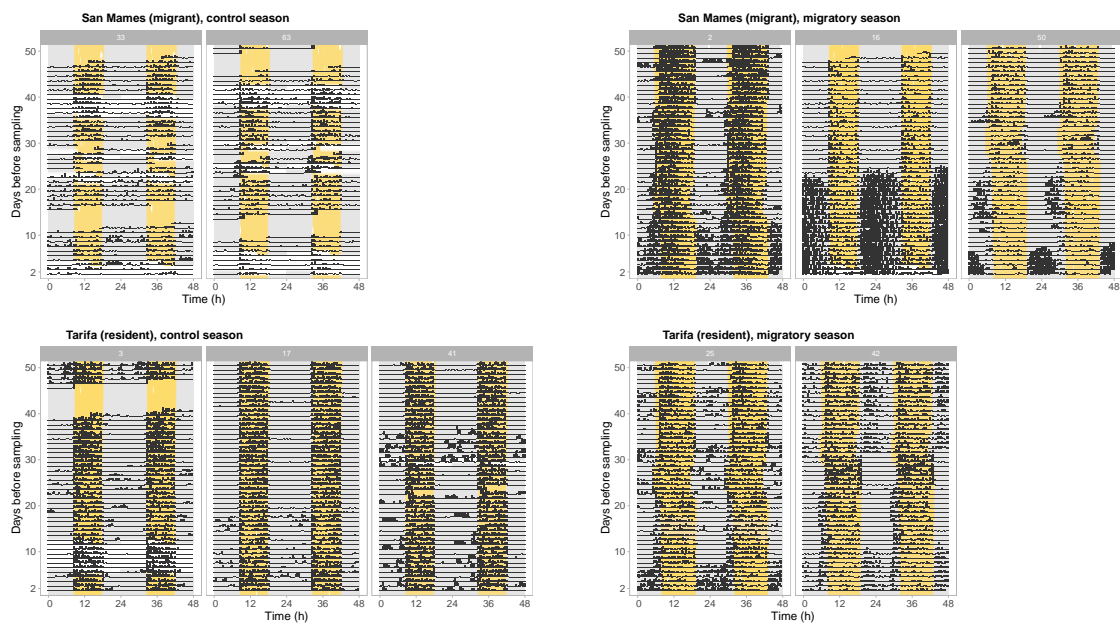
¹MPRG Behavioural Genomics, Max Planck Institute for Evolutionary Biology, Plön, Germany

²Institute of Avian Research, An der Vogelwarte 21, Wilhelmshaven, Germany

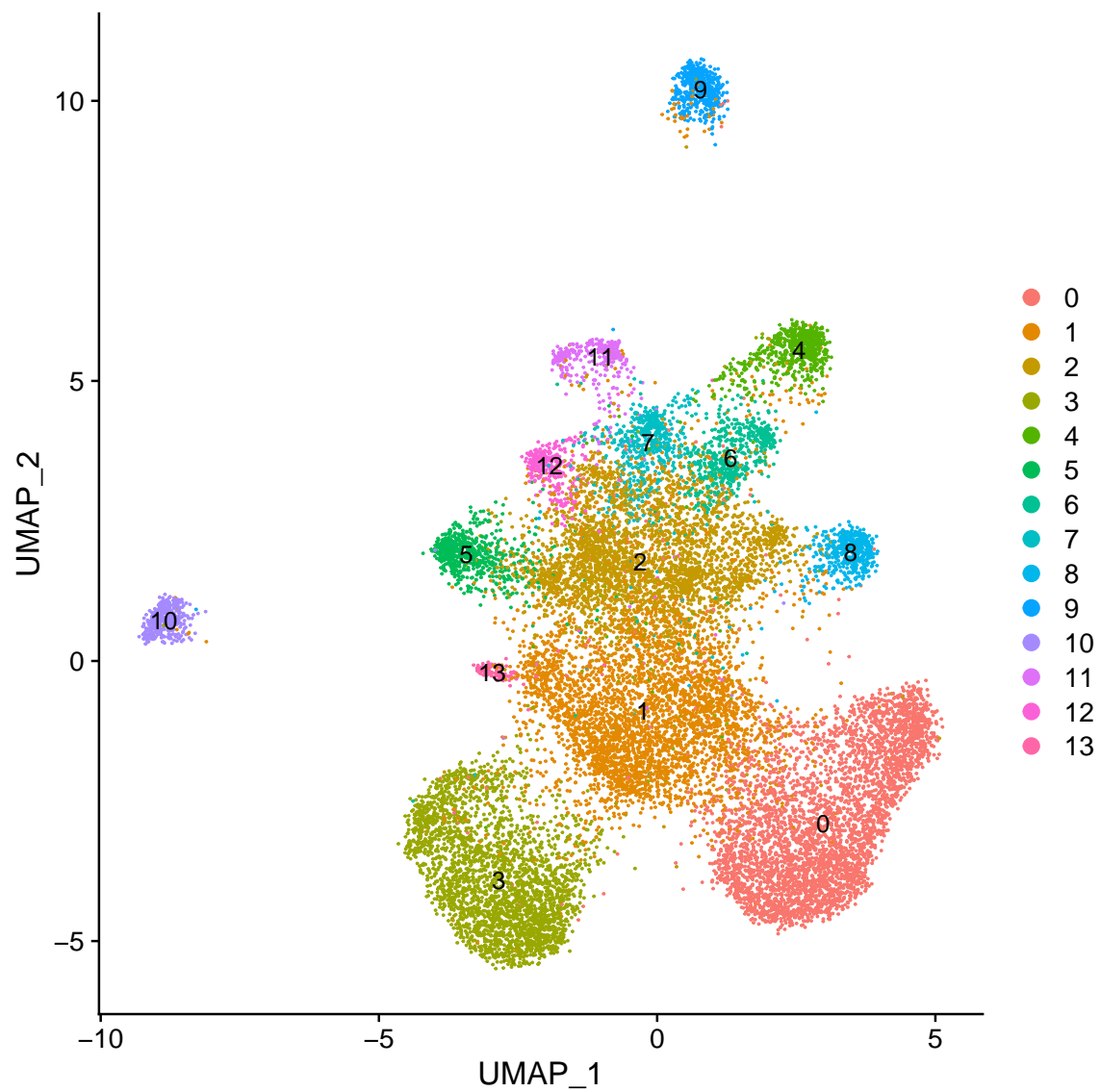
³Department of Biology and Environmental Sciences, Carl von Ossietzky Universität Oldenburg, Oldenburg, Germany

⁴Francis Crick Institute, Croydon, UK

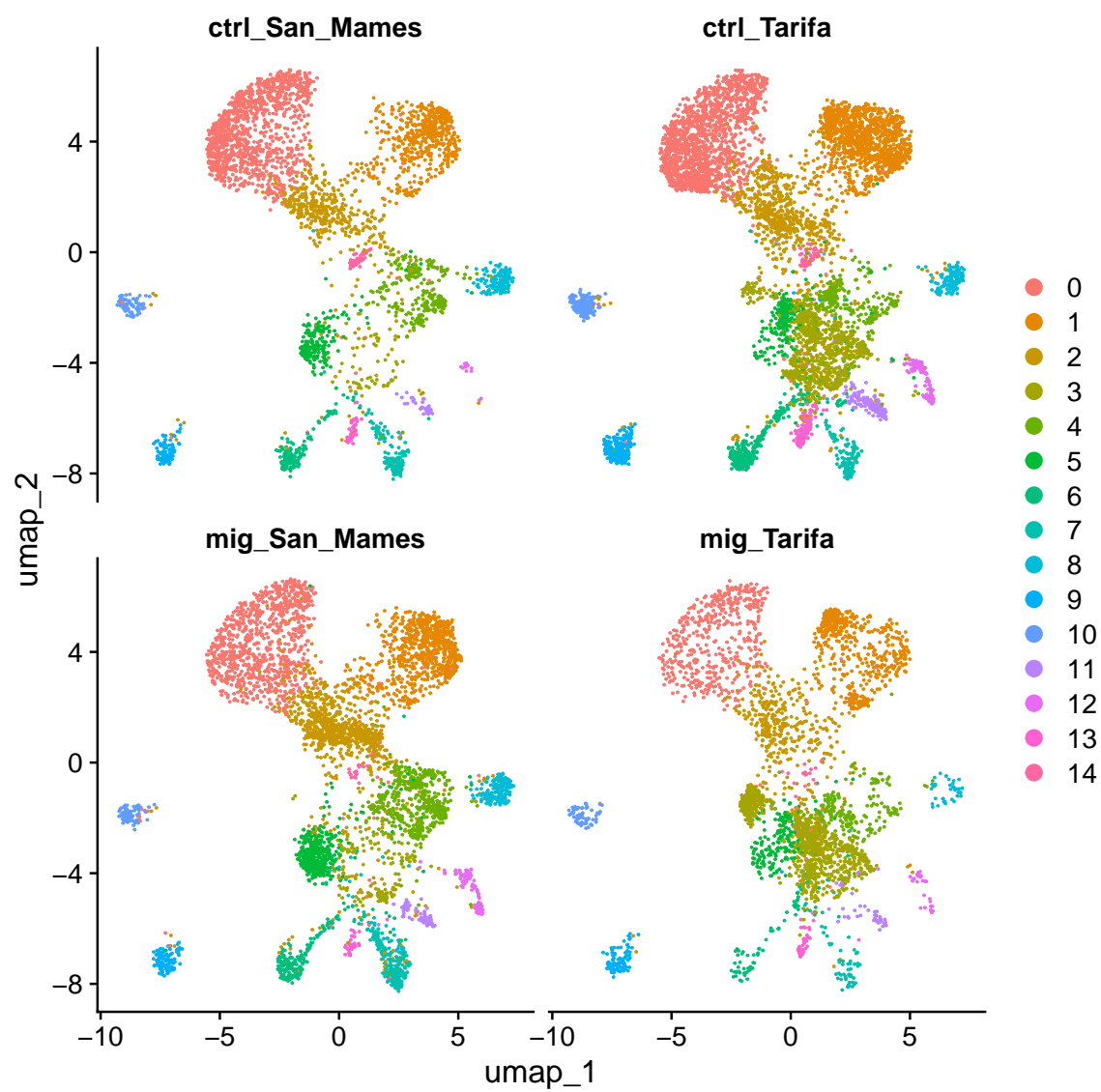
* Correspondence: [Jun Ishigohoka <ishigohoka@evolbio.mpg.de>](mailto:Jun.Ishigohoka@evolbio.mpg.de), [Miriam Liedvogel <liedvogel@evolbio.mpg.de>](mailto:Miriam.Liedvogel@evolbio.mpg.de)



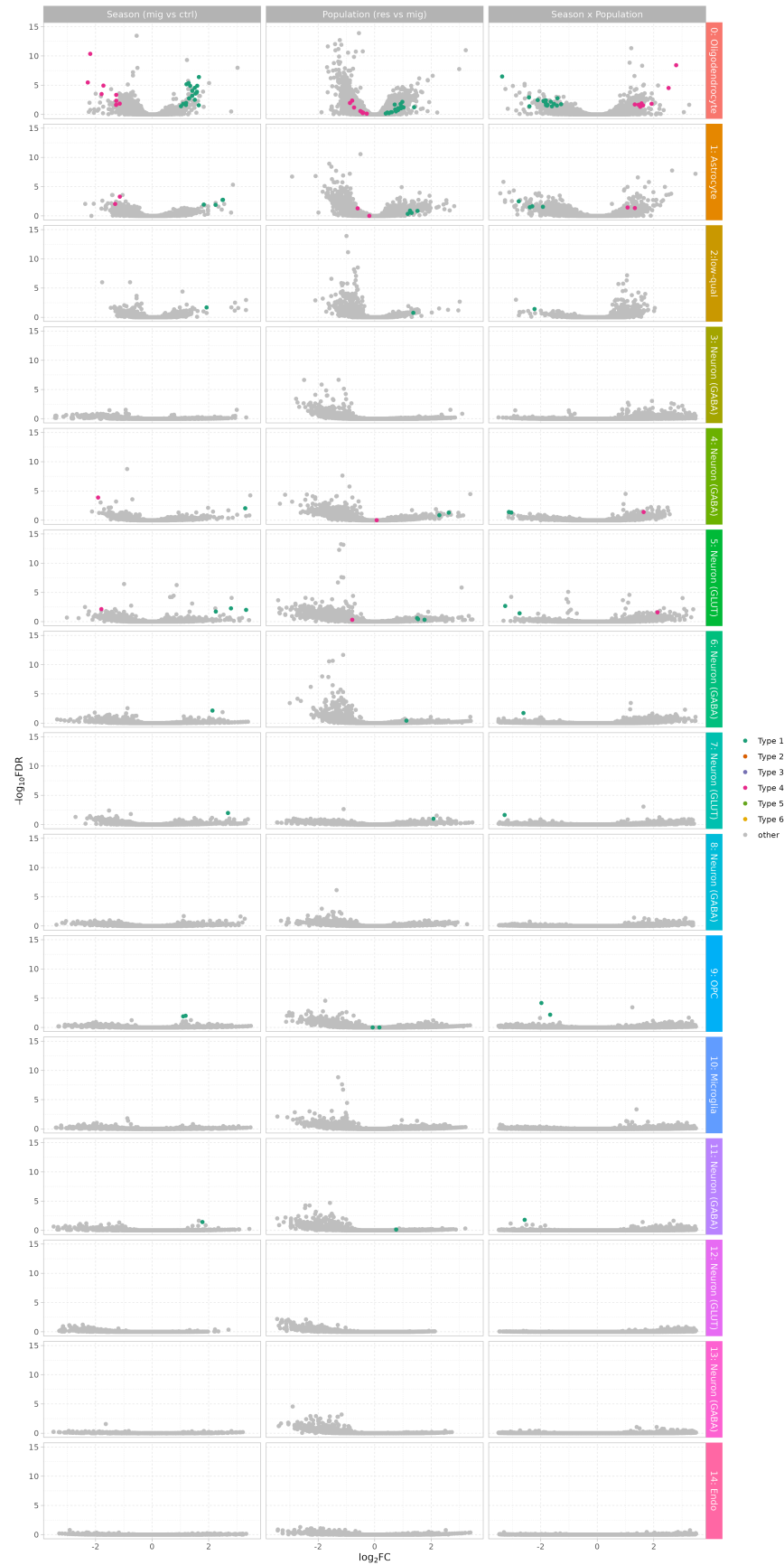
Supplementary Figure 1: Double-plotted actograms of all individuals included in the scATAC analysis.



Supplementary Figure 2: Initial UMAP of scATAC data based on peaks called by `cellranger-atac` for each sample.



Supplementary Figure 3: UMAP of scATAC data based on peaks split by season and population.



Supplementary Figure 4: Volcano plots showing effect of seasons, populations, and their interaction term (columns) on chromatin accessibility in all 15 cell clusters

6

Discussion

Changes of instinct may sometimes be facilitated by the same species having different instincts at different periods of life, or at different seasons of the year, or when placed under different circumstances, etc.; in which case either one or the other instinct might be preserved by natural selection. And such instances of diversity of instinct in the same species can be shown to occur in nature.

– Charles Darwin, *On the Origin of Species by Means of Natural Selection* (1859)

Overview

The goal of this thesis was to understand how seasonal migration behaviour evolves in a micro-evolutionary time scale. In Chapter 2, I showed that outliers in genome scans of local genetic variation, which are often interpreted as signatures of selective processes acting on target genomic regions, can represent haplotype structure due to low recombination rate instead of selection. Within empirical analysis in this Chapter, I identified an 8 Mb-long polymorphic inversion segregated in most blackcap populations. In Chapter 3, I showed that the presence of high-recombining regions in the genome affects demography inference methods based on ancestral recombination graphs (ARGs). As a validation of the concept, I inferred the population history of blackcaps. In Chapter 4, I found that the inversion identified in Chapter 2 is under spatially varying negative frequency-dependent selection with lower optimal frequency in island resident populations compared to continental populations. In this chapter, to enable simulation of selection on the inversion, I refined the demography inference done in Chapter 3, revealing two split events among blackcap populations. The older split was around 420,000 years ago which resulted in isolation between eastern (ancestral to current Georgian migrant population) and western (ancestral to populations spanning from Macaronesian and Mediterranean islands and Iberia to Poland) populations, and a subsequently at around 34,000 years ago, different populations within the western ancestral population started to split into current populations. It was this second split event when residency emerged in multiple populations. In Chapter 5, characterising differential chromatin accessibility in the hypothalamus, I revealed that the transition from migrants to residents is associated with a reduced amount of seasonal change in chromatin accessibility in some different sets of genomic regions specific to cell types.

In this chapter, I discuss the empirical results presented in Chapters 4 and 5. I will integrate my findings of evolutionary history of blackcap populations and differential molecular regulation to build a holistic model of how seasonal migration evolves.

Where were the ancestors and what were they doing?

Recurrent patterns of historical biogeography in Europe are attributed to isolation of populations in separate glacial refugia formed by glacial cycles in the Pleistocene (Hewitt, 2000; Petit et al., 2003; Taberlet et al., 1998). By comparing historical biogeography in ten taxa, Taberlet et al. (1998) concluded that there were three main refugia in Europe – Iberia, Italy, and the Balkan (Fig. 1)– leading to the concordant pattern of current phylogeography. Despite the general concordant pattern, Taberlet et al. (1998) also emphasised inconsistency in phylogeography among taxa. This inconsistency is now interpreted to be due to complex history of isolation and admixture events by repeated cycles of advance and retreat of glacier during the Pleistocene and cryptic refugia besides the three (Marková et al., 2020; Nogueras & Ortego, 2022; Pedreschi et al., 2019; Petit et al., 2003; Provan & Bennett, 2008). After the last glacial maximum (LGM), the Holocene glacial retreat initiated around 18,000 years ago, during which post-glacial expansions from the refugia occurred in multiple organisms, following expanding temperate areas (Hewitt, 2000; Taberlet et al., 1998). Current geographic distribution of multiple taxa are formed from expanded populations from different refugia, resulting in complex genetic ancestries due to gene flow between once-isolated populations at contact zones (Nogueras & Ortego, 2022).

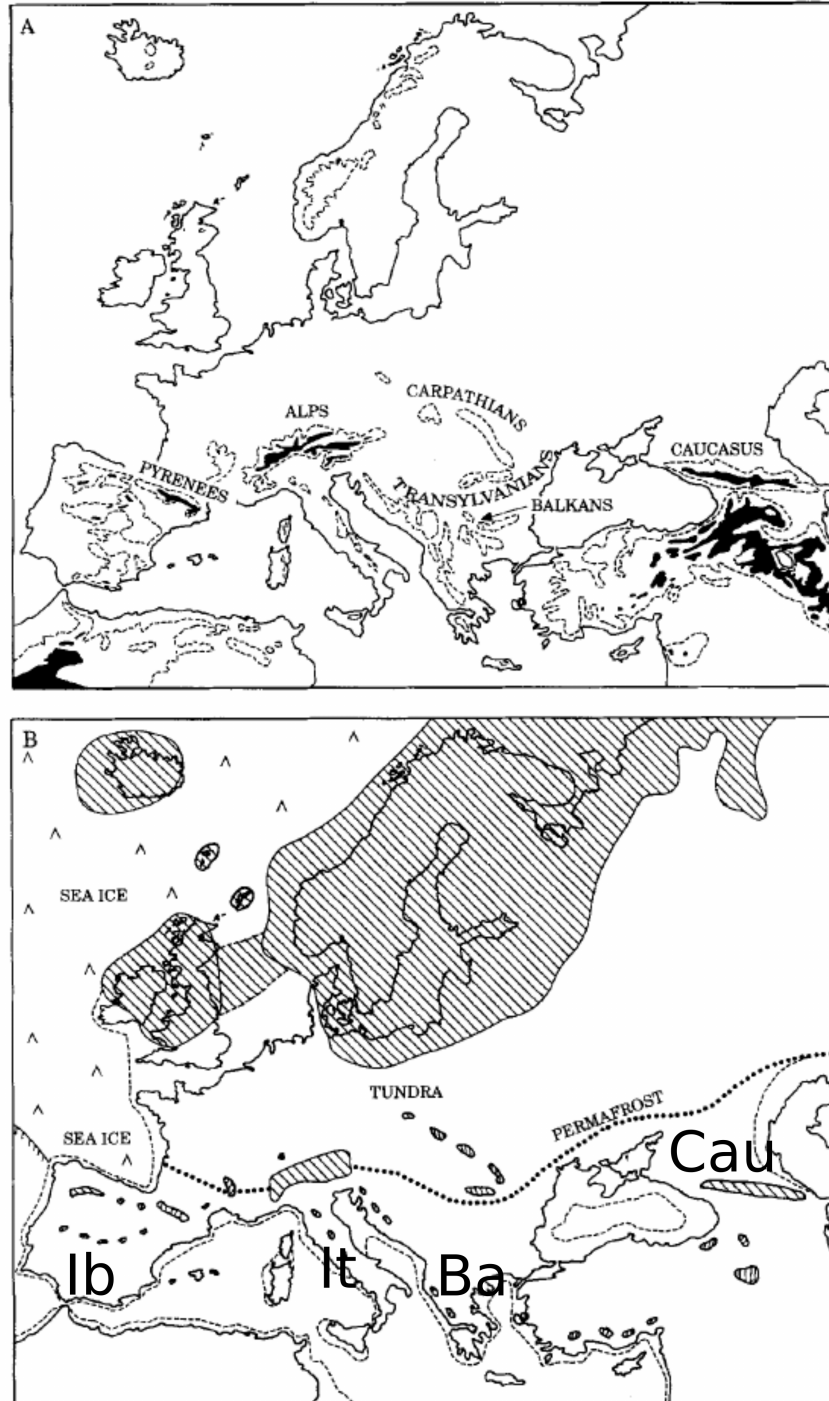


Figure 1: Western and Caucasus refugia. A. Physical geography of Europe, showing the predominance of mountains in the south running east-west potentially working as geographic barriers. Black regions = over 2000 m, dashed line = over 1000m altitude. B. Ice cover (hatched) and extent of permafrost at the end of last ice age (18,000 years ago). Main refugia are marked (Ib = Iberia; It = Italy; Ba = Balkan; Cau = Caucasus). Based on Hewitt (1999) with information from Hewitt (2000) and Taberlet et al. (1998).

The estimated history of blackcap populations matches well with this refugia model. The split of the eastern and western populations at 430,000 years ago indicates that they became isolated in two refugia in one of the Pleistocene glacial periods prior to the LGM. The eastern refugium likely corresponds to one refugium in the Caucasus region. This separation of Caucasus refugium and western refugia (including Iberia, Italy and Balkan) is common (Hewitt, 2000; Neiber & Hausdorf, 2015; Taberlet et al., 1998). It is not clear whether there are other refugia populations of blackcaps besides Iberia e.g. in Italy and Balkan due to the lack of samples. Compared to other animals which are subdivided into the western refugia (Hewitt, 2000; Neiber & Hausdorf, 2015; Nogueras & Ortego, 2022; Taberlet et al., 1998), birds have greater dispersal ability and Iberia, Italy, and Balkan refugia were less isolated from each other (Drovetski et al., 2018; Perktas et al., 2015). The lack of ancestral substructure among the western blackcaps, including ancestors of the Crete population, is in line with this pattern. The effective absence of ancestral structure within the western refugium translates as the lack of structured diversification in migratory phenotypes (at least among the ancestors of the contemporary populations), because such behavioural diversification in seasonal migration¹, which is expected to directly affect prezygotic reproductive isolation, would have resulted in further substructure within each refugium. Substructure within the Caucasus refugium is inconclusive. However, the apparent increase in effective population size after the split shown in Chapter 4, despite the glaciation, may be due to cryptic ancestral substructure within the Caucasus refugium. Such substructure in this region has been reported in other systems (Neiber & Hausdorf, 2015; Seddon et al., 2002; Tarkhnishvili et al., 2000). Deeper characterisation of both genetic and behavioural variation in eastern populations will allow evolutionary history of blackcaps through the Pleistocene glacial period.

The eastern and western refugia populations remained isolated until the Holocene retreat. I argue that this long-term separation is not due to different migratory phenotypes, because such separation was also the case for the green woodpecker, which is resident, and non-flying animals (Hewitt, 2000; Orth et al., 2002; Perktas et al., 2015; Taberlet et al., 1998). The fact that migratory birds (the blackcap (presented in this thesis) and the dunnoek (Drovetski et al.,

¹Note that divergence by different migratory phenotypes is unlikely, yet variation in migratory behaviour could have existed.

2018)) also follow the same pattern indicates strong isolation by geographic barriers between the western and eastern refugia: the permafrost to the north of Balkan and highland regions of Anatolia and Caucasus (Fig. 1).

These ancestral migrant populations in the two main refugia expanded during the Holocene retreat. This is especially evident in the western refugium population splitting into multiple contemporary populations with different migratory phenotypes, including multiple transitions from migrants to residents in islands and southern Iberia, and variation in migratory distance, from short to medium and long distance migrants. It is unclear how the eastern refugium population split and expanded because we have only one contemporary population from Georgia representing the descendant of this refugium in the data set.

This postglacial expansion model expects reduced genetic diversity in non-relict populations due to founder events at the edge of the range (“leading edge”) (Hewitt, 2000; Milá et al., 2007; Petit et al., 2003). However, this pattern is not the case in blackcap populations. Genetic diversity in non-relict populations (i.e. medium and long distance migrants breeding in regions north of Alps) are no lower than short distance migrants in Iberia, which presumably represents (one/part of) the western relict population(s). There are three possible explanations to this pattern, which are not mutually exclusive. First, these migrant populations increased in effective population size after the split as revealed by demography inference. This may have counteracted founder effects. Second, as in other species (Marková et al., 2020; Petit et al., 2003; Provan & Bennett, 2008), populations which expanded from the eastern and western (and other) refugia populations may have admixed in the central Europe, which is covered by the current breeding range of medium and long distance migrants. Such admixture events are expected to increase genetic diversity. In support of this possibility, continental individuals are sorted along PC3 of genome-wide PCA by the longitude (i.e. from Georgia to medium/long distance migrants, short distance migrants, and continental residents). This pattern is difficult to explain without assuming admixture, because separation between eastern (Georgia) and western populations, and substructure among western populations by the postglacial expansion would be represented in separate PC axes. Third, the expansion of migrant populations may not be only at the leading edge of the range. In other words, individuals far from the front line

of expansion may have colonised northern regions. Although we do not have direct evidence of this possibility, we know that such change in migratory behaviour in individuals from different regions is possible based on *de novo* evolution of migratory phenotype. In the past few decades, some blackcaps have started to migrate northwest and winter in the British Isles (Berthold et al., 1992). Tracking by light level geolocators revealed that these individuals originate from and breed in different places in Europe from Spain to Poland (Delmore et al., 2020). Different restrictions may exist in spring migration (as opposed to novel autumn migration phenotypes underlying the northwest migrants) at both proximate and ultimate levels, yet if such evolution of new migration phenotypes occurred during the postglacial expansion, individuals from different places in the original distribution could have contributed to expanded population, counteracting loss of genetic diversity. Comparative approaches including multiple species with different biogeography of migratory phenotypes (including fully resident species) will help discern these possibilities.

How and when did transition from migrants to residents occur?

The last glacial retreat is characterised by change in abiotic (e.g. temperature) and biotic (e.g. vegetation) environments (Hewitt, 2000). As a result, the high-latitude area of the refugia and some parts of the wintering areas in low latitude, which had been not suitable for breeding during the glacial period, became available for blackcaps to breed in summer. The former areas were filled by medium and long distance migrants in the breeding season. In the latter areas, some individuals switched from migrants to residents, and became reproductively isolated from other migrants.

How did this transition from migrants to residents occur? The phenotypic variation in migratory propensity, such as in a partial migrant population, has been explained by the threshold model (Pulido et al., 1996; Pulido, 2011; Reid & Acker, 2022). The same framework is also useful for this question. The migration liability, a polygenic latent trait underlying migratory propensity, is assumed to be normally distributed in a population. The variation in liability within the population can be partitioned into genetic variation (G), environmental variation (E), and the interaction (termed genotype-by-environment or GxE) (Reid & Acker,

2022). The distribution of migratory liability shifts between seasons, because the environment changes between seasons (Reid & Acker, 2022). This seasonal difference in migratory liability can be attributed to the environmental contribution by seasonal change E_{ssn} and interaction between genotype and environment $G \times E_{ssn}$, as the genotypes do not change between seasons. In the ancestral migrant population, this seasonal change is so large that all individuals cross the liability threshold, above which migratory behaviour is expressed (Fig. 2A). Importantly, due to genetic variation contributing to $G \times E_{ssn}$, some individuals must have had smaller seasonal change in liability than others in the ancestral migrant population.

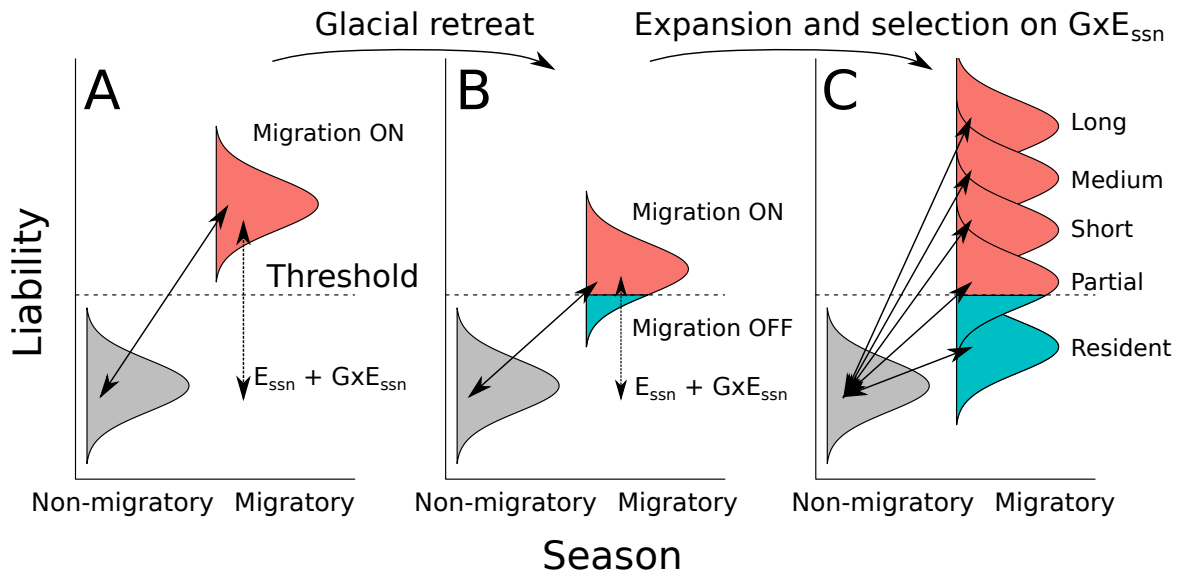


Figure 2: Model of emergence of resident population. During the glacial period (A), the distribution of migratory liability crosses the liability threshold between non-migratory and migratory seasons. This seasonal difference in liability can be expressed as the sum of environmental factors (between seasons) and the interaction between genotype and environment ($G \times E$). During the glacial retreat (B), the environmental contribution changed, leading to smaller seasonal change in liability in the population. As a result, some individuals in the population stopped expressing migratory behaviour during the migratory season (blue), which split the breeding range between migrants and residents. Breeding in wintering grounds was too costly during the glacial period but not any more after the glacial retreat, allowing establishment of resident populations.

In Chapter 5, I showed that the amount of seasonal change in epigenetic states in hypothalamic cells is smaller in residents compared to migrants. This result, in the light of the threshold model, indicates that resident populations originate from individuals with low seasonal change in liability (Fig. 2B, C). These individuals did not express migratory behaviour in migratory seasons after the glacial retreat because the environmental effect between seasons

shifted compared to the glacial period (Fig. 2A, B). The same evolutionary response is expected in multiple locations with similar environmental change (which is the case for the glacial retreat), as long as variation in $G \times E_{\text{ssn}}$ exists in the population. I propose that this is how the multiple simultaneous transitions from migrants to residents were initiated by the glacial retreat.

Due to the fitness benefit after the glacial retreat by breeding in what used to be wintering areas, the genetic variation for lower migratory propensity (i.e. lower seasonal change in liability) was likely selected for. This can be viewed as a natural experiment of selection for reduced phenotypic plasticity, termed “genetic compensation²”. Because the selected phenotype (residency) contributes to prezygotic isolation, this can also be regarded as reinforcement from the speciation perspective. Therefore, the transition from migrants to residents in multiple blackcap populations is an interesting case of parallel reinforcement by selection on reduced phenotypic plasticity initiated by the glacial retreat.

Future directions

So far I mostly focused on the transition from migrants to residents, but the same principle can be extended to evolution of medium and long distance migrants from presumably ancestral short distance migrants. Individuals with the highest migratory propensity in the population, associated with longer distance of migration (Berthold, 1993, 1996), may have benefited from breeding in unoccupied new temperate areas in high latitude, and the genetic bases for greater seasonal change in liability (via e.g. greater seasonal change in epigenetic states) may have been selected for to establish medium and long distance migrant populations. I propose that different levels of seasonal change in migratory liability, from subthreshold to the highest liability in migratory season, were differentially selected along a latitudinal gradient resulting in latitudinal distribution from resident to long distance migrant populations (Fig. 2C). Because the phenotype, selection gradient and geographic distribution are all continuous, the boundary

²Little consensus exists among terms regarding evolution of phenotypic plasticity (collectively “genetic accommodation” (Crispo, 2007)). Here I use “genetic compensation” (Grether, 2005) to refer to evolution of canalised loss of an initially environmentally-induced phenotype to differentiate from “genetic assimilation” (Waddington, 1961), which refers to evolution of canalised expression of an initially environmentally-induced phenotype.

among populations — from resident to long distance migrants through short and medium distance migrants — may not even exist, and the process of migratory divergence may be more parapatric than allopatric.

Spatially varying selection studied in Chapter 4 is a particularly attractive mode of selection with this respect. As discussed within Chapter 4, consideration of spatial gradient may reveal effects of the polymorphic inversion *inv_12_3* on evolution of migratory propensity and distance, and other genetic factors collectively contributing to variation in migratory phenotypes in a polygenic manner.

In addition to the geographic spatial information of population genetic parameters, I argue that inclusion of heterogeneity in parameters across different stages of individuals' life is important. Simplification is necessary to model evolutionary history, yet timing, distance, and orientation of migration can directly influence the survival, reproductive success, and isolation. Selection can act on a specific season, or even the mode or direction of selection can differ between seasons. Dobzhansky (1973) famously stated that “Nothing in biology makes sense except in the light of evolution”, and I argue that nothing in behavioural evolution makes sense except in the light of life history and surrounding environments. For example, expressing migratory behaviour during non-migratory season would be obviously disadvantageous thus it is under stabilising selection, while high migratory liability during migratory season could be under directional selection in high-latitude areas (Fig. 2). This spatiotemporal heterogeneity in selection pressure can play an important role in the evolutionary change in seasonal migration. The forward simulation used in Chapter 4 is so flexible that complex life history with spatiotemporal models can be implemented. Combining inference methods based on high-throughput sequencing and exhaustive simulations of complex life history may provide novel and more holistic insights into the general principle of evolution of seasonal migration.

References

- Berthold, P. (1993). *Bird Migration: A General Survey* (1st ed.). Oxford University Press.
- Berthold, P. (1996). *Control of Bird Migration*. Chapman & Hall.
- Berthold, P., Helbig, A. J., Mohr, G., & Querner, U. (1992). Rapid microevolution of migratory behaviour in a wild bird species. *Nature*, 360(6405, 6405), 668–670. <https://doi.org/10.1038/360668a0>
- Crispo, E. (2007). The Baldwin effect and genetic assimilation: Revisiting two mechanisms of evolutionary change mediated by phenotypic plasticity. *Evolution*, 61(11), 2469–2479. <https://doi.org/10.1111/j.1558-5646.2007.00203.x>
- Delmore, K. E., Van Doren, B. M., Conway, G. J., Curk, T., Garrido-Garduño, T., Germain, R. R., Hasselmann, T., Hiemer, D., van der Jeugd, H., Justen, H., Lugo Ramos, J. S., Maggini, I., Meyer, B. S., Phillips, R. J., Remisiewicz, M., Roberts, G. C. M., Sheldon, B. C., Vogl, W., & Liedvogel, M. (2020). Individual variability and versatility in an eco-evolutionary model of avian migration. *Proceedings of the Royal Society B: Biological Sciences*, 287(1938), 20201339. <https://doi.org/10.1098/rspb.2020.1339>
- Dobzhansky, T. (1973). Nothing in Biology Makes Sense except in the Light of Evolution. *The American Biology Teacher*, 35(3), 125–129. <https://doi.org/10.2307/4444260>
- Drovetski, S. V., Fadeev, I. V., Raković, M., Lopes, R. J., Boano, G., Pavia, M., Koblik, E. A., Lohman, Y. V., Red'kin, Y. A., Aghayan, S. A., Reis, S., Drovetskaya, S. S., & Voelker, G. (2018). A test of the European Pleistocene refugial paradigm, using a Western Palaearctic endemic bird species. *Proceedings of the Royal Society B: Biological Sciences*, 285(1889), 20181606. <https://doi.org/10.1098/rspb.2018.1606>
- Grether, G. F. (2005). Environmental Change, Phenotypic Plasticity, and Genetic Compensation. *The American Naturalist*, 166(4), E115–E123. <https://doi.org/10.1086/432023>
- Hewitt, G. (1999). Post-glacial re-colonization of European biota. *Biological Journal of the Linnean Society*, 68(1-2), 87–112. <https://doi.org/10.1111/j.1095-8312.1999.tb01160.x>
- Hewitt, G. (2000). The genetic legacy of the Quaternary ice ages. *Nature*, 405(6789), 907–913. <https://doi.org/10.1038/35016000>
- Marková, S., Horníková, M., Lanier, H. C., Henttonen, H., Searle, J. B., Weider, L. J., & Kotlík, P. (2020). High genomic diversity in the bank vole at the northern apex of a range expansion: The role of multiple colonizations and end-glacial refugia. *Molecular Ecology*, 29(9), 1730–1744. <https://doi.org/10.1111/mec.15427>
- Milá, B., McCormack, J. E., Castañeda, G., Wayne, R. K., & Smith, T. B. (2007). Recent postglacial range expansion drives the rapid diversification of a songbird lineage in the genus Junco. *Proceedings of the Royal Society B: Biological Sciences*, 274(1626), 2653–2660. <https://doi.org/10.1098/rspb.2007.0852>
- Neiber, M. T., & Hausdorf, B. (2015). Phylogeography of the land snail genus *Circassina* (Gastropoda: Hygromiidae) implies multiple Pleistocene refugia in the western Caucasus

- region. *Molecular Phylogenetics and Evolution*, 93, 129–142. <https://doi.org/10.1016/j.ympev.2015.07.012>
- Noguerales, V., & Ortego, J. (2022). Genomic evidence of speciation by fusion in a recent radiation of grasshoppers. *Evolution*, 76(11), 2618–2633. <https://doi.org/10.1111/evo.14508>
- Orth, A., Auffray, J.-C., & Bonhomme, F. (2002). Two deeply divergent mitochondrial clades in the wild mouse *Mus macedonicus* reveal multiple glacial refuges south of Caucasus. *Heredity*, 89(5), 353–357. <https://doi.org/10.1038/sj.hdy.6800147>
- Pedreschi, D., García-Rodríguez, O., Yannic, G., Cantarello, E., Diaz, A., Golicher, D., Korstjens, A. H., Heckel, G., Searle, J. B., Gillingham, P., Hardouin, E. A., & Stewart, J. R. (2019). Challenging the European southern refugium hypothesis: Species-specific structures versus general patterns of genetic diversity and differentiation among small mammals. *Global Ecology and Biogeography*, 28(2), 262–274. <https://doi.org/10.1111/geb.12828>
- Perktaş, U., Gür, H., & Ada, E. (2015). Historical demography of the Eurasian green woodpecker: Integrating phylogeography and ecological niche modelling to test glacial refugia hypothesis. *Folia Zoologica*, 64(3), 284–295. <https://doi.org/10.25225/fozo.v64.i3.a9.2015>
- Petit, R. J., Aguinagalde, I., de Beaulieu, J.-L., Bittkau, C., Brewer, S., Cheddadi, R., Ennos, R., Fineschi, S., Grivet, D., Lascoux, M., Mohanty, A., Müller-Starck, G., Demesure-Musch, B., Palmé, A., Martín, J. P., Rendell, S., & Vendramin, G. G. (2003). Glacial Refugia: Hotspots But Not Melting Pots of Genetic Diversity. *Science*, 300(5625), 1563–1565. <https://doi.org/10.1126/science.1083264>
- Provan, J., & Bennett, K. D. (2008). Phylogeographic insights into cryptic glacial refugia. *Trends in Ecology & Evolution*, 23(10), 564–571. <https://doi.org/10.1016/j.tree.2008.06.010>
- Pulido, F. (2011). Evolutionary genetics of partial migration – the threshold model of migration revisited. *Oikos*, 120(12), 1776–1783. <https://doi.org/10.1111/j.1600-0706.2011.19844.x>
- Pulido, F., Berthold, P., & van Noordwijk, A. (1996). Frequency of migrants and migratory activity are genetically correlated in a bird population: Evolutionary implications. *Proceedings of the National Academy of Sciences*, 93(25), 14642–14647. <https://doi.org/10.1073/pnas.93.25.14642>
- Reid, J. M., & Acker, P. (2022). Properties of phenotypic plasticity in discrete threshold traits. *Evolution*, 76(2), 190–206. <https://doi.org/10.1111/evo.14408>
- Seddon, J. M., Santucci, F., Reeve, N., & Hewitt, G. M. (2002). Caucasus Mountains divide postulated postglacial colonization routes in the white-breasted hedgehog, *Erinaceus concolor*. *Journal of Evolutionary Biology*, 15(3), 463–467. <https://doi.org/10.1046/j.1420-9101.2002.00408.x>
- Taberlet, P., Fumagalli, L., Wust-Saucy, A.-G., & Cosson, J.-F. (1998). Comparative phylogeography and postglacial colonization routes in Europe. *Molecular Ecology*, 7(4),

453–464. <https://doi.org/10.1046/j.1365-294x.1998.00289.x>

- Tarkhnishvili, D. N., Thorpe, R. S., & Arntzen, J. W. (2000). Pre-Pleistocene Refugia and Differentiation between Populations of the Caucasian Salamander (*Mertensiella caucasica*). *Molecular Phylogenetics and Evolution*, 14(3), 414–422. <https://doi.org/10.1006/mpev.1999.0718>
- Waddington, C. H. (1961). Genetic Assimilation. In E. W. Caspari & J. M. Thoday (Eds.), *Advances in Genetics* (Vol. 10, pp. 257–293). Academic Press. [https://doi.org/10.1016/S0065-2660\(08\)60119-4](https://doi.org/10.1016/S0065-2660(08)60119-4)

List of Manuscripts

Chapter 2

Ishigohoka, J., Bascón-Cardozo, K., Bours, A., Fuß, J., Rhie, A., Mountcastle, J., Haase, B., Chow, W., Collins, J., Howe, K., Uliano-Silva, M., Fedrigo, O., Jarvis, E. D., Pérez-Tris, J., Illera, J. C., & Liedvogel, M. (2024). Distinct patterns of genetic variation at low-recombining genomic regions represent haplotype structure (p. 2021.12.22.473882). bioRxiv. <https://doi.org/10.1101/2021.12.22.473882>

Peer-reviewed and recommended by Peer Community in Evolutionary Biology

Fumagalli, M. (2024) Discerning the causes of local deviations in genetic variation: the effect of low-recombination regions. Peer Community in Evolutionary Biology, [100711.10.24072/pci.evolbiol.100711](https://doi.org/10.24072/pci.evolbiol.100711)

Chapter 3

Ishigohoka, J., & Liedvogel, M. (2024). High-recombining genomic regions affect demography inference (p. 2024.02.05.579015). bioRxiv. <https://doi.org/10.1101/2024.02.05.579015>

Submitted to Genetics and in the process of first revision as of 2024-05-03

Author Contributions

Chapter 1

Jun Ishigohoka wrote the chapter.

Chapter 2

Authors: Jun Ishigohoka, Karen Bascón-Cardozo, Andrea Bours, Janina Fuß, Arang Rhie, Jacquelyn Mountcastle, Bettina Haase, William Chow, Joanna Collins, Kerstin Howe, Marcela Uliano-Silva, Olivier Fedrigo, Erich D. Jarvis, Javier Pérez-Tris, Juan Carlos Illera, Miriam Liedvogel

Contributions: **JI** and **ML** designed the study. Reference genome was generated by **JF**, **AR**, **JM**, **BH**, **WC**, **JC**, **KH**, **MU**, **OF**, and **EDJ**. **JP-T** and **JCI** collected samples for resequencing. **AB** performed read mapping, variant calling, and data filtration. **KB-C** inferred recombination maps. **JI** conducted haplotype inference, population genomics analyses, simulations, sequence analyses, statistical modelling, and data visualisation. **JI** and **ML** wrote the manuscript with inputs from other authors.

Chapter 3

Authors: Jun Ishigohoka, Miriam Liedvogel

Contributions: **JI** conceptualised and conducted the study. **JI** wrote the manuscript with inputs from **ML**.

Chapter 4

Authors: Jun Ishigohoka, Miriam Liedvogel

Contributions: **JI** conceptualised and conducted the study. **JI** wrote the manuscript with inputs from **ML**.

Chapter 5

Authors: Jun Ishigohoka, Juan Sebastian Lugo Ramos, Gillian Durieux, Miriam Liedvogel

Contributions: **ML** conceptualised the study. **JSLR**, **GD** and **ML** conducted animal sampling, conducted the common-garden experiment and collected tissues. **JI** conducted the molecular experiment and data analysis. **JI** interpreted data and wrote the manuscript with inputs from **ML**.

Chapter 6

Jun Ishigohoka wrote the chapter.



Jun Ishigohoka




Miriam Liedvogel

Declaration / Affidavit

I hereby declare that:

- i. Apart from my supervisor's guidance, the content and design of this thesis is the product of my own work. The co-authors' contributions are listed in the dedicated section;
- ii. This thesis has not been already submitted either partially or wholly as part of a doctoral degree to another examination body, and no other materials are published or submitted for publication than indicated in the thesis;
- iii. The preparation of the thesis has been subjected to the Rules of Good Scientific Practice of the German Research Foundation;
- iv. Prior to this thesis, I have not attempted and failed to obtain a doctoral degree.

Plön, 3 May, 2024



Jun Ishigohoka